The Effects of Hypomorphic STAT3 on Lymphocyte Function and Intestinal Immune Regulation

Scott Steward-Tharp

Balliol College

The Sir William Dunn School of Pathology

University of Oxford

Lymphocyte Cell Biology Section/NIAMS

National Institutes of Health

A thesis submitted in partial fulfillment of the requirements for degree of Doctor of Philosophy, Trinity Term 2012

The Effects of Hypomorphic STAT3 on Lymphocyte Function and Intestinal Immune Regulation

Scott Steward-Tharp

Balliol College, University of Oxford

A thesis submitted in partial fulfillment of the requirements for degree of Doctor of Philosophy, Trinity Term 2012

Abstract:

Dominant-negative mutations in signal transducer and activator of transcription 3 (*STAT3*) underlie the human primary immunodeficiency autosomal dominant hyper IgE syndrome (HIES). A number of aspects of this disease, including the eponymous elevated serum IgE, remain poorly understood. Additionally, work from numerous animal models has suggested STAT3 plays a critical role in the development, regulation and resolution of intestinal inflammation. Human genetic studies have associated this pleiotropic transcription factor with inflammatory bowel disease (IBD), but elucidation of the overall role of STAT3 in intestinal homeostasis has been hindered by the lethality associated with germline deletion. To better understand STAT3 function in both intestinal homeostasis and IgE regulation, we generated bacterial artificial chromosome (BAC)-transgenic mice that expressed a HIES-associated STAT3 allele. Transgenic cells exhibited normal tyrosine phosphorylation of STAT3 following acute cytokine stimuli, but marked inhibition in DNA-binding activity. The mice recapitulated important aspects of HIES, including elevated serum IgE. We identified an intrinsic bias towards IgE class switch recombination (CSR) in transgenic B cells, and a possible role for STAT3 in directly regulating both the immunoglobulin heavy chain locus and key regulators of CSR, such as Id2, an inhibitor of μ-ε switching. The partial loss of STAT3 signaling also led to important changes in intestinal responses, with transgenic mice showing enhanced susceptibility to both dextran sodium sulfate (DSS) and *Citrobacter rodentium* induced colitis. Following *C. rodentium* infection, we observed defects in both the early production of certain antimicrobial peptides such as RegIIIγ and resolution of inflammation in late infection, where the bacterial burden was decreasing. Transgenic myeloid cells were hyporesponsive to IL-10, suggesting that hypomorphic STAT3 activity within the intestine destabilizes the system: predisposing to infection and hindering the IL-10 regulatory pathway's ability to keep inflammatory responses in check. Therefore, our data suggest that STAT3 plays key roles in both CSR and the maintenance of intestinal homeostasis.

Abbreviations Listing:

A/E, attaching and effacing

AD, autosomal dominant

AHR, aryl hydrocarbon receptor

AID, activation-induced cytidine-deaminase

AMP, antimicrobial peptide

APC, antigen presenting cell

AR, autosomal recessive

BAC, bacterial artificial chromosome

BAFF, B cell activating factor of the TNF family

BCR, B cell receptor

BM, bone marrow

BrdU, Bromodeoxyuridine

CD, Crohn's disease

CFSE, carboxyfuorescein succinimidyl ester

CFU, colony-forming units

CIS, cytokine-induced SH2-domain containing protein

CLP, common lymphoid progenitor

CSR, class switch recombination

CTLA-4, cytotoxic T-lymphocyte antigen 4

DC-PCR, digestion-circularization PCR

DC, dendritic cell

DN, double negative

Dock8, dedicator of cytogenesis 8 protein

DP, double positive

DSB, double-stranded break

DSS, dextran sodium sulfate

E, enhancer

EAE, experimental autoimmune encephalomyelitis

EtBr, ethidium bromide

FDC, follicular dendritic cell

FO, follicular

Foxp3, forkhead box P3

FSC, forward scatter

GALT, gut-associated lymphoid tissue

GC, germinal center

GL, germline

GLT, germline transcript

GM-CSF, granulocyte-macrophage colony-stimulating factor

H3Ac, acetylated histone 3

H3K4me3, histone h3 lysine 4 trimethylation

HIES, Hyper IgE syndrome

IBD, inflammatory bowel disease

Id2, inhibitor of DNA-binding protein 2

IEC, intestinal epithelial cell

Ig, Immunoglobulin

IHC, immunohistochemistry

IL, Interleukin

ILC, innate lymphoid cell

ILF, isolated lymphoid follicle

IFN, Interferon

iNKT, invariant natural killer T cells

IRF, interferon regulatory factor

iTreg, induced T regulatory cell

JAK, Janus kinase

KIR, kinase inhibitory region

LCMV, lymphocytic choriomeningitis virus

LIF, leukemia inhibitory factor

LP, lamina propria

LPL, lamina propria leukocyte

LPS, lipopolysaccharide

Lti, lymphoid tissue inducer cell

MCS, multiple-cloning site

MFI, mean fluorescence intensity

MHC, major histocompatibility complex

MLN, mesenteric lymph node

MZ, marginal zone

NK, natural killer

nTreg, natural T regulatory cell

PIAS, protein inhibitors of activated STATs

Ptip, Pax-interacting protein 1

pLN, peripheral lymph node

PMA, phorbol 12-myristate 13-acetate

PNA, peanut agglutinin

PP, peyer's patch

PRR, pattern recognition receptor

PTB, phosphotyrosine-binding

PTPB1, protein tyrosine phosphotase B1

RA, retinoic acid

RBC, red blood cell

Rec A, recombinase A

ROR, retinoic acid-related orphan receptor

RTq PCR, real-time quantitative PCR

Runx, runt-related transcription factor

S, switch

SCID, severe combined immunodeficiency

SEA, Schistosoma mansoni soluble egg antigen

SH2, Src homology 2

SHP, SH2-containing phosphotase

SOCS, suppressors of cytokine signaling

SP, single positive

SSB, single–stranded break

SSC, side scatter

STAT, signal transducer and activator of transcription

SUMO, small ubiquitin-like modifier

TCR, T cell receptor

Tfh, follicular helper T cell

Th, helper T cell

TNF, tumor necrosis factor

Treg, regulatory T cell

UC, ulcerative colitis

UNG, uracil DNA glycosylases

WT, wild type

γC, common gamma chain

Contents:

1. General Introduction

1.1. The Immune System……1

1.2. Cytokines……2

1.2.1. Type I and Type II Cytokines……2

1.3. JAK-STAT Signaling……3

1.3.1. JAKs……4

1.3.2. STATs……5

1.3.2.1. Negative Regulation of STATs……6

1.4. STAT3……10

1.4.1. Growth Development and Cancer……10

1.4.2. STAT3 in Myeloid Cells……11

1.4.3. STAT3 in Lymphoid Cells……12

1.4.4. STAT3 in Autosomal Dominant Hyper IgE Syndrome……13

1.5. The Innate Immune System……15

1.6. The Adaptive Immune System……15

1.6.1. B Cells……15

1.6.1.1. B Cell Development……16

1.6.1.2. Mature B Cell Subsets……16

1.6.1.3. B Cell Activation……17

1.6.1.4. Plasma Cells……18

1.6.1.5. The Germinal Center Reaction……19

1.6.1.6. Antibody Class Switch Recombination……20

1.6.1.6.1. Regulation of Class Switch Recombination……23

1.6.1.6.2. Histone Modifications in Class Switch Recombination……25

1.6.2. $CD4^+$ T Cells……25

1.6.2.1. T Cell Development……26

1.6.2.2. $CD4^+$ T Cell Differentiation……27

1.6.2.2.1. Th1 Cells……29

1.6.2.2.2. Th2 Cells……29

1.6.2.2.3. Th17 Cells……31

1.6.2.2.4. Tregs……..…….32
1.6.2.2.5. Tfh Cells…….35
1.6.2.3. Plasticity of CD4$^+$ T Cell Subsets……...36
1.7. The Intestinal Immune System……..…37
1.7.1. Intestinal Epithelial Cells……..…38
1.7.2. Innate Lymphoid Cells……..39
1.7.3. Myeloid Cells and the Adaptive Arm of Intestinal Immunity……..41
1.8. Experimental Models of Colitis……..45
1.8.1. Dextran Sodium Sulfate Induced Colitis……...45
1.8.2. *Citrobacter rodentium* Induced Typholocolitis……..45
1.9. Aims……...46
2. Materials and Methods……..…48
2.1. Mice……48
2.1.1. Generation of the *Stat3ΔV463* BAC-Transgenic Mouse Line……48
2.1.2. Genotyping……49
2.2. Cell Isolation……..…50
2.2.1. Thymus, Spleen, MLN and pLN……50
2.2.2. Colonic Lamina Propria Leukocyte (LPL) Isolation……50
2.2.3. B Cell Isolation……..52
2.2.4. CD4$^+$ T Cell Enrichment……..52
2.2.5. CD11c$^+$ Cell Enrichment……..52
2.2.6. Purification of Naïve T cells……...…53
2.3. Flow Cytometry and Antibodies……53
2.3.1. Restimulation for Intracellular Cytokine Staining……53
2.3.2. Surface Staining……...…54
2.3.3. Intracellular Staining……..…54
2.3.4. Phosflow……55
2.3.5. Antibodies……...…56
2.4. *In Vitro* Cell Cultures……59
2.4.1. CD4$^+$ T Cell Polarization……59
2.4.2. B Cell CSR……59

2.4.3. Immunoblotting……..…60
2.4.4. STAT3 Transcription Factor ELISA……..….61
2.4.5. Transgene Expression and Germline Transcripts……...…61
2.4.6. Digestion-Circularization-PCR (DC-PCR)……..…62
2.4.7. Proliferation Using CFSE……63
2.4.8. Retroviral Transduction of B Cells……..…63
2.5. *In Vivo* Studies……..…64
2.5.1. Immunizations……...64
2.5.1.1. Foot Pad Immunization……..…64
2.5.1.2. SEA Immunization……..…64
2.5.2. Induction of Intestinal Inflammation……...65
2.5.2.1. Dextran Sodium Sulfate (DSS) Induced Colitis……...65
2.5.2.2. *Citrobacter rodentium* Culture……...65
2.5.2.3. Induction of *C. rodentium* Colitis……....66
2.5.2.4. Generation of Bone Marrow Chimeras……..…66
2.5.2.5. Histological Assessment of Colitiis……67
2.5.2.6. Evaluation of *C. rodentium* Colonization……...…69
2.5.3. Endotoxic Shock……...69
2.6. ELISA……..…69
2.7. RNA Extraction……...70
2.8. Real-Time Quantitative PCR Analysis……...71
2.9. Microarray……...71
2.10. mRNA-Seq……...…72
2.11. ChIP-Seq……..73
2.12. Statistics……...74
3. Generation of the STAT3ΔV463 Mouse Model of HIES……75
3.1. Introduction……75
3.2. Results……...77
3.2.1. Selection of Mutation and Targeting Strategy for AD-HIES Mouse Model……..77
3.2.2. Generation of the *Stat3ΔV463* Recombination Cassette……...84

3.2.3. Homologous Recombination Leads to *Stat3ΔV463* BAC Construct……90

3.2.4. Generation of *Stat3ΔV463* BAC-Transgenic Mice……..…97

3.2.5. Mut-*Stat3* Mice Recapitulate Biochemical and Immunological AD-HIES Phenotype……..103

3.3. Discussion……...108

4. Hypomorphic STAT3ΔV463 in T and B Cell Biology……..…113

4.1. Introduction……..113

4.2. Results…….…….114

4.2.1. STAT3ΔV463's Effects in T Cell Homeostasis……...114

4.2.2. STAT3ΔV463's Effects in T Cell Differentiation…….……..117

4.2.3. STAT3ΔV463 Does Not Alter B Cell Development……....120

4.2.4. Interrogation of Germinal Center Responses in mut-*Stat3* Mice……125

4.2.5. Mut-*Stat3* Mice Mount IgE Skewed Antibody Response……127

4.2.6. Intrinsic Defects in mut-*Stat3* B Cells Lead to Enhanced Igε CSR…...129

4.2.7. Probing the Ability of mut-*Stat3* B Cells to Secrete Igs……137

4.2.8. STAT3 Regulates Expression of the Igε CSR Inhibitor Id2…….139

4.2.9. Reconstitution of mut-*Stat3* B Cells with Id2 Restores IgE Regulation……..146

4.3. Discussion……...…149

5. Hypomorphic STAT3ΔV463 in Intestinal Immune Homeostasis……..157

5.1. Introduction……..…157

5.2. Results…….....159

5.2.1. Steady-State Characterization of Intestinal Lymphoid Subsets in mut-*Stat3* Mice……..…159

5.2.2. Mut-*Stat3* Mice Show Increased Susceptibility to DSS Colitis……163

5.2.3. Mut-*Stat3* Mice Show Increased Susceptibility to *C. rodentium*…….165

5.2.4. Interrogation of the Adaptive Immune Response to *C. rodentium* in mut-*Stat3* Mice……..……170

5.2.5. Reduced IL-22 and Antimicrobial Peptide Production in Early *C. rodentium* Infection of mut-*Stat3* Mice……..176

5.2.6. Mut-*Stat3* Mice Exhibit Elevated Intestinal Pathology, Despite Declining *C. rodentium* Colonization, Post 1-Week Infection……..181

5.2.7. IL-10 Signals Dampened in mut-*Stat3* Mice……..185

5.2.8. Both Hematopoietic and Non-Hematopoietic Compartments Contribute to *C. rodentium* Phenotype of mut-*Stat3* Mice……..189

5.3. Discussion……...193

6. General Discussion……199

6.1. A BAC-Transgenic Approach for the AD-HIES Mouse Model……199

6.2. STAT3ΔV463 in B Cell CSR and the Humoral Immune Response…….....203

6.3. STAT3ΔV463 in Intestinal Immune Homeostasis……206

6.4. Conclusions……211

7. Bibliography……214

1. Chapter 1: General Introduction.

1.1. The Immune System.

The immune system is composed of a network of specialized organs, tissues and cells that function in concert to serve as the body's primary means of defense against invading pathogens. As a consequence, the immune system has evolved numerous mechanisms to recognize and eliminate infected cells or microbes while ensuring tolerance to host tissues. Firstly, the immune system is compartmentalized among specialized lymphoid organs which function to promote the development, maturation and activation of immune cells via antigen uptake/sampling and the facilitation of information transferring cellular interactions. Secondly, lymphatic vessels and the vasculature facilitate transportation of antigens from sites of infection, such as the skin, gastrointestinal tract and respiratory tract, to the draining lymph nodes and spleen, respectively, to allow for both local and systemic responses. Thirdly, the immune response is orchestrated by both an innate and adaptive arm which allow for both a rapid and appropriate response to be generated for each specific offending pathogen. The innate immune system, consisting of the epithelial barrier, monocytes, tissue macrophages, granulocytes (neutrophils, basophils, eosinophils), dendritic cells (DCs), mast cells, NK cells and complement factors in the blood forms the first line of defense against foreign invaders and is capable of rapid, non-specific responses to infections. A network of DCs can instruct the adaptive immune system by direct presentation of antigens and secretion of cytokines. B and T

lymphocytes of the adaptive immune system orchestrate more specific responses to infections and are able to “remember” the invading pathogen so that if reencountered, they can respond more rapidly during subsequent infections. Importantly, the adaptive immune system ensures that recognition of self-antigens elicits a non-reactive or tolerant response to prevent unnecessary damage to its own tissues. Thus an effective immune system requires a careful balance of protective and tolerogenic responses.

1.2. Cytokines.

Cytokines are secreted proteins that mediate a diverse array of biological functions including cell growth, survival, proliferation and differentiation. In the immune system, cytokines serve as important chemical messengers involved in orchestrating both host protective and tolerant immune responses. Cytokines function in recruitment of immune cells and directing protective responses to eradicate harmful pathogens. In addition, cytokines are actively involved in suppressing inflammatory immune responses and returning the tissues to homeostasis. Thus, controlled cytokine expression and activity are paramount for mounting appropriate and specific immunity, while avoiding unnecessary responses that can lead to chronic inflammatory and autoimmune diseases.

1.2.1. Type I and Type II Cytokines.

Cytokines can be divided into two broad families based on their structural homology and the receptors they bind to. Type I cytokines, including hormones, the colony stimulating factors and most of the interleukin (IL) members, all have a characteristic four-α-helical structure and bind to transmembrane receptors containing two cysteine residues and a tryptophan-serine-X-tryptophan-serine (WSXWS) motif in their extracellular domains (*1*). Meanwhile, Type II cytokines include type I and type II interferons and the IL-10 family cytokines, and these bind to structurally related receptors but with extracellular domains that lack the WSXWS motif (*1*). Type I/II cytokine receptors are heteromeric and consist of both a ligand-binding polypeptide chain and one or more signal-transducing chains. An important feature of Type I/II cytokines is that they are further classified into subfamilies based on their shared receptor chains. For instance, IL-2, IL-4, IL-7, IL-9, IL-15, and IL-21 all share the common gamma chain (γc) which couples to ligand specific receptor subunits and this could help to explain functional specificity and redundancy among these cytokines. Importantly, a major pathway activated by type I/II cytokine receptors is the Janus kinase (JAK)-signal transducers and activators of transcription (STAT) pathway and this plays an important role in translating the chemical signal from the cytokine into a functional outcome (*2*, *3*).

1.3. JAK-STAT Signaling.

When cytokines bind their cognate receptors, they activate intracellular signaling cascades that ultimately lead to regulated gene transcription and

expression. For Type I and Type II cytokines, the major pathway activated is the JAK-STAT pathway (*2*, *3*). Signaling is transduced from the cytokine receptor to the nucleus by a series of tyrosine phosphorylation events, beginning with the JAKs and culminating with the STATs, which can then bind to DNA and regulate gene expression. Importantly, specificity of signaling is achieved at the level of the cytokine receptor and the preferential activation of a particular STAT. However, how cytokines sharing the same receptor (ie. γc cytokines) and activating the same STATs are able to induce different functional outcomes remains unclear.

1.3.1. JAKs.

The JAK family of tyrosine kinases is composed of four members in mammals, designated JAK1, JAK2, JAK3 and TYK2 (*4*). The primary function of the JAKs is to mediate transduction of cytokine signals from the receptor to the nucleus. JAKs are constitutively associated with the intracellular domains of cytokine receptors via their N-terminal domain. When a cytokine binds to its receptor, oligomerization of the receptor subunits occurs and the associated JAKs become activated through either trans- or auto-phosphorylation. Importantly, the JAKs appear to be interdependent for their activation and loss of one JAK can interfere with the activation of the other JAK in the dimer pair (*5*, *6*). The activated JAKs then phosphorylate specific tyrosine residues in the intracellular domain of cytokine receptors, which serve as docking sites for src homology 2 (SH2) or phosphotyrosine-binding (PTB) domain containing proteins, most importantly the STATs. The bound STATs subsequently are

phosphorylated by the JAKs, leading to their activation and downstream signaling activity, which will be discussed further below.

1.3.2. STATs.

The STATs are the major family of SH2-domain containing cytosolic proteins activated by JAKs in response to Type I and Type II cytokine signals (*7*). The STAT family is made up of seven members in mammals (STAT1, STAT2, STAT3, STAT4, STAT5a, STAT5b and STAT6) and each contains a unique SH2 domain, which binds a specific phosphotyrosine residue within the intracellular domain of a cytokine receptor (*8*, *9*). As such, the STATs are capable of imparting specificity of cytokine signaling and downstream transcriptional regulation. Structurally, the STATs share homologous features including a coil-coil interaction domain, a DNA binding domain, a linker domain, an SH2 domain, a transactivation domain and a conserved tyrosine around residue 700 (*8*).

When a STAT binds to a phosphorylated tyrosine residue on the cytokine receptor, it in turn is tyrosine phosphorylated by a JAK, leading to its activation (*8*). Activated STATs can then dimerize via an SH2 domain-phosphotyrosine interaction (*10*, *11*). Whether homo or heterodimerization occurs is based on the specificity of SH2 domains and on the nature of the phosphorylated tyrosine. STAT1, STAT3, STAT4, STAT5 and STAT6 all form homodimers while STAT1 and STAT2 and STAT1 and STAT3 can also form heterodimers (*8*). Following dimerization, STATs translocate to the nucleus

with the help of molecular chaperones like the importins and regulate gene expression (*12*).

In the nucleus, STAT dimers recognize and bind to DNA at specific motifs called IFN-γ activated sequences (GAS), which contain the semipalindromic sequence $TTCN_{3-4}GAA$ (*13*). The number of amino acids in the central core of the motif is specific to the STAT combination and corresponds to the DNA binding domain of the STAT. STATs generally act as transcriptional activators and have been shown to interact with other transcription factors (c-Jun, c-Fos, C/EBP), co-activators (Sp1, MCM5) and histone acetyltransferases (HATs: p300/CBP) through their transactivation domains (*14-19*). Transcriptional activity of certain STATs is enhanced by serine phosphorylation as well as post-translational modifications like arginine methylation and acetylation (*20*, *21*). Finally, STAT dimers can interact with one another on tandem DNA sites to form tetramers through interactions between their amino termini (*13*, *22*). Importantly, the exact mechanisms of how STATs and other transcriptional machinery interact to induce transcription are incompletely understood. STATs appear on gene promoters at the time of transcriptional activation, however, it is possible that this requires coordination with many other factors (*23*). Nonetheless, the ability of STATs to recruit co-factors could provide important clues about how the same STAT molecule induces unique effects in response to different cytokines.

1.3.2.1. Negative Regulation of STATs.

Constitutive activation of STATs is associated with malignant transformation and chronic inflammation in a number of diseases (*24-26*). Therefore, a number of negative regulatory mechanisms are in place to attenuate STAT-mediated signals to prevent prolonged activation. Cytoplasmic tyrosine phosphatases like SH2-containing phosphatase (SHP-1), SHP-2 and protein tyrosine phosphatase B1 (PTPB1) have been shown to dephosphorylate the STATs, the JAKs, or the cytokine receptors to inhibit signaling (*27-30*). The protein inhibitors of activated STATs (PIAS) are nuclear proteins that act as E3 ligases for small ubiquitin-like modifier (SUMO) (*29*). PIAS1 and PIAS3 can also directly bind to STAT1 and STAT3, respectively, to prevent their binding to DNA (*29*).

The suppressors of cytokine signaling (SOCS) proteins are a group of inhibitors that get induced by cytokines and growth factors and attenuate JAK-STAT signal transduction (*31-33*). There are eight family members, SOCS1-7 and cytokine-induced SH2 domain containing protein (CIS), each containing a central SH2 domain and a c-terminal SOCS box (*34*). The SOCs box interacts with a complex containing elongin b, elongin c, cullin-5, RING box-2 and E2 ligase (*35*, *36*). Thus, SOCS proteins are thought to mediate degradation of their targets through E3 ubiquitin ligase activity (*34*). SOCS1, SOCS2, SOCS3, and CIS all bind directly to phosphtyrosine residues on cytokine receptors via their SH2 domains (*32*). SOCS3 binds tyrosines in the gp130 receptor and the IL-12Rβ2 chains, while SOCS1 binds tyrosines on the IFNαR and IFNγR chains and inhibits signaling events downstream of these

receptors (*37*, *38*). Both SOCS1 and SOCS3 also contain a kinase inhibitory region (KIR), which allows them to directly inhibit JAK catalytic activity (*34*). Likewise, SOCS1 has been reported to bind directly to the activation loop of JAKs via its SH2 and KIR domains (*39*). *Socs* deficiency in mice is associated with dysregulated immune responses, emphasising the important inhibitory roles these proteins play in cytokine signaling pathways (*32*). Figure 1.1 illustrates some of the different mechanisms by which the JAK-STAT signaling pathway is regulated.

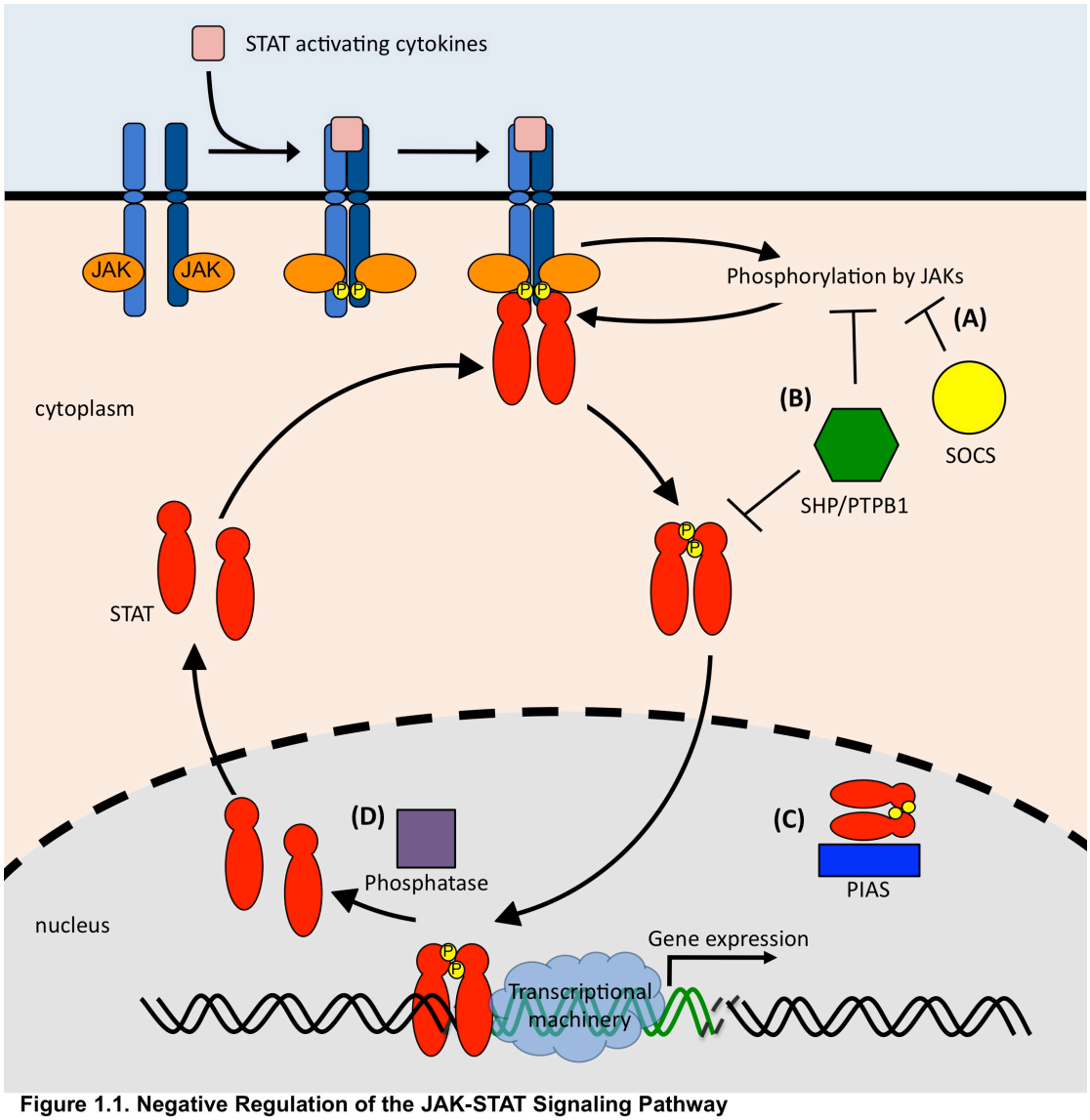

Figure 1.1. Negative Regulation of the JAK-STAT Signaling Pathway

Ligand binding to cytokine receptors results in a conformational change that activates associated JAK molecules. JAKs phosphorylate the cytoplasmic portions of cytokine receptors, creating binding sites for STAT proteins. Bound STATs are subsequently phosphorylated by JAKs and dimerize via SH2 domain:phospho-tyrosine interactions. Active dimers translocate to the nucleus, bind to promoters, and activate transcription through recruitment of the RNA polymerase II machinery. The signal-transduction pathway is regulated at a number of levels:

(A) SOCs proteins inhibit JAK mediated phosphorylation of STATs by targeting the cytokine receptor complex for degradation and by binding activated JAKs and inhibiting their activity.

(B) Cytoplasmic phosphatases dephosphorylate the cytokine receptor complexes, JAKs, and STATs.

(C) PIAS sequesters activated STAT dimers in the nucleus and promotes their degradation.

(D) Nuclear phosphatases terminate the STAT signaling cycle by dephosphorylating activated STAT proteins.

1.4. STAT3.

The STATs were first discovered in the course of studies examining the specificity of signaling pathways from IFN receptors (*3*). Since that time, they have been identified as important regulators of numerous other processes (*40*). The importance of a particular STAT member to biological functions is directly related to the type and breadth of factors that activate and utilize it for signaling. The initial *Stat* gene-targeting studies in mice suggested a high degree of specificity for the various STAT proteins in individual signaling pathways, with the important exception of STAT3.

STAT3 was first identified as the acute phase response factor (APRF) activated by IL-6 in the liver (*41-43*). Since then, STAT3 has been shown to be activated by numerous other ligands including cytokines like IL-10, IL-22, IL-23, and the gp130 family members [IL-6, IL-11, IL-27, oncostatin-M, CNTF, leukaemia inhibitory factor (LIF), cardiotrophin-1, cardiotrophin-like cytokine, and neuropoietin], as well as growth factors (G-CSF, EGF), hormones (leptin) and interferons (IFNs) (*44*). Thus, uniquely among STATs, STAT3 appears to be involved in mediating signals from diverse pathways and as a result is important for various aspects of growth and development, as well as immunity.

1.4.1. Growth, Development and Cancer.

Germline deletion of *Stat3* in mice resulted in embryonic lethality before embryonic day 8.5, possibly due to defects in placental implantation and the

loss of LIF signaling (*45*, *46*). Therefore mice have been generated with tissue-specific deletion of *Stat3* using the Cre-*Loxp* recombination system and these have provided further clues into STAT3's diverse functions. In keratinocytes, for instance, STAT3 is involved in skin remodeling, would healing and hair recycling (*47*). While in epithelial cells, STAT3 inhibits apoptosis through induction of insulin-like growth factor binding protein 5 and regulates mammary gland involution (*48*). In addition, STAT3 mediates protective IL-22 signaling into colonic epithelial cells to promote wound healing (*49*).

In contrast to these beneficial aspects of STAT3 signaling, constitutive activation of STAT3 is associated with malignancy and tumor progression in a variety of cancers and is a marker of inflammation in chronic inflammatory diseases. In keratinocytes, hyperactivated STAT3 is associated with skin carcinogenesis and psoriasis (*50*, *51*). STAT3 is also constitutively expressed by immune cells in the tumor microenvironment and may further support tumor progression by promoting production of immunosuppressive factors (*52*).

1.4.2. STAT3 in Myeloid Cells.

In addition to its functions in development, STAT3 also has important roles in the immune system. Mice with selective deletion of *Stat3* in myeloid cells, including macrophages and neutrophils, were highly susceptible to LPS-

induced endotoxic shock and produced heightened levels of inflammatory cytokines like tumor necrosis factor (TNF)-α, IFN-γ and IL-1 (*53*). These mice also developed a spontaneous, T helper 1 (Th1) mediated enterocolitis, similar to that which has been documented in IL-$10^{-/-}$ mice, and this was attributed to a loss of IL-10 suppressive signals (*53*-*55*). Deletion of *Stat3* in BM cells using the *Tie2*-Cre promoter also led to the development of a lethal intestinal inflammation in mice as early as 4-6 weeks of age (*56*). Furthermore, STAT3 was shown to negatively regulate granulopoiesis and deletion of *Stat3* in hematopoietic cells caused neutrophilia in mice due to enhanced G-CSF signaling (*57*). STAT3 is also an important mediator of Flt3l signaling and commitment of hematopoietic stem cells to differentiate into DCs (*56*). Thus, STAT3 is centrally involved in both developmental and inflammatory aspects of the innate immune system.

1.4.3. STAT3 in Lymphoid Cells.

In lymphoid tissues, STAT3 expression in thymic epithelial cells was found to be important for the maintenance of thymic architecture and survival of thymocytes (*58*). However, selective deletion of *Stat3* in T cells using the *Lck*-Cre recombinase did not result in any overt developmental deficits (*59*). Although *Stat3* deficient T cells had impaired proliferation in response to IL-6 and reduced expression of the IL-2Rα (CD25), T cell populations in the thymus and spleen were normal (*59*, *60*). More recently, STAT3 has been implicated in the differentiation of effector $CD4^+$ T cells, including the induced

regulatory T cells (iTreg), T helper 17 (Th17) cells and T follicular helper (Tfh) cells (*61*).

Previous studies looking at *Stat3* deficiency in B cells provided conflicting results. On the one hand, *CD19*-Cre mediated deletion of *Stat3flox/flox* alleles resulted in defective plasma cell terminal differentiation but otherwise normal B cell ontogeny (*62*). On the other hand, mice where *Stat3flox/flox* were conditionally ablated via *Mx*-Cre displayed developmental defects in early BM B cell progenitors (*63*). Peripheral *Stat3* deletion by *Mx*-Cre however was incomplete and no defects were reported in the mature B cell compartment of these mice (*63*).

1.4.4. STAT3 in Autosomal Dominant Hyper IgE Syndrome.

Autosomal dominant (AD) Hyper IgE Syndrome (HIES) is a rare primary immunodeficiency first described in 1966 as Job's syndrome and characterized by the clinical triad of eosinophilia, eczematoid dermatitis, and recurrent skin and pulmonary infections (*64*). IgE was recognized as a cardinal feature in 1972 and the name hyper IgE syndrome was proposed (*65*). AD-HIES is now recognized as a multi-system disorder as patients with this syndrome exhibit a variety of skeletal, dental and soft-tissue defects, including: abnormal healing of pneumonias leading to pneumatoceles and bronchiectasis, scoliosis, retained primary teeth, minimal trauma fractures, hyperextensibility and coronary artery aneurysms and tortuosity (*66-69*). In

2007, mutations in *STAT3* were identified in a number of patients with this disease. These heterozygous mutations appear to function in a dominant-negative manor and are primarily focused in the DNA binding and SH2 domain regions of *STAT3*. A number of mutation “hotspots”, with several unrelated patients exhibiting the same mutations, have been identified within these two regions. *STAT3* mutations now account for the vast majority of HIES cases and have been found in diverse ethnic groups (*70*-*72*). The less prevalent autosomal recessive variant of HIES has been primarily associated with mutations in dedicator of cytogenesis 8 protein (*Dock8*) (*73*, *74*).

The discovery of *STAT3* mutations in patients has led to a number of advances in the mechanistic understanding of AD-HIES. Recent work has implicated deficiency in Th17 cells as an important aspect of the host defense defects noted in this disorder (*72*, *75*-*78*). Additionally, defects in the formation of central memory T cells have been associated with latent virus reactivation. However, a number of aspects of this disease, including the eponymous hyper IgE, remain poorly understood. In some respects, it is equally intriguing to consider what AD-HIES patients do not exhibit clinically. Indeed, the severe phenotypes associated with *Stat3* deficiency in myeloid populations, begs the question why colitis and other autoinflammatory diseases have not been linked with AD-HIES.

1.5. The Innate Immune System.

The innate immune system responds rapidly to infection or tissue damage and its primary functions include the phagocytic removal of pathogens or damaged cells, the production of inflammatory mediators and the induction of acquired immunity. Further discussion of this system will be done in the context of the intestinal immune system (1.7).

1.6. The Adaptive Immune System.

The major effector cells of the adaptive immune system are the B and T lymphocytes. Preexisting diversity in the B and T cell antigen receptor repertoire allows them to promote specific immunity to a myriad of pathogens. Following antigen encounter, these cell types are uniquely responsible for the formation of immunological memory to promote more rapid immune responses following subsequent re-exposure to pathogens. Additionally, the adaptive immune system plays a critical role in tolerance or non-reactivity to self-antigens and is thus important for the prevention of autoimmune disease.

1.6.1. B Cells.

B cells are a critical component of the adaptive immune system, providing both specific and long-lasting protection from a tremendously diverse range of potential pathogens. In addition to driving the humoral immune response through their production of antibodies, they also serve important functions as

antigen presenting cells (APCs) and modulate immune responses through the production of cytokines.

1.6.1.1. B Cell Development.

B lymphocytes mature from lymphoid progenitor cells in the bone marrow (BM) and the fetal liver. Cytokines such as IL-7 and B cell activating factor of the TNF family (BAFF) are essential to the maturation process, which is marked by pre-pro-B, pro-B, pre-B and immature-B cell stages. During the pro-B cell stage recombinase activating genes RAG1 and RAG2 mediate V(D)J rearrangement of the immunoglobulin (Ig) heavy chain. This results in the generation and surface expression of the pre-B-cell receptor (pre-BCR) with surrogate light chains. Subsequent rearrangement of the Ig light chain results in the formation of a mature BCR that is capable of binding antigen. At this immature stage of development, B cells undergo both receptor editing and clonal deletion processes to prevent any escape of self-reactive cells to the periphery. Cells successfully completing this checkpoint leave the BM as transitional B cells, initially expressing surface Ig solely of the IgM class. The maturation process is completed by surface expression of IgD as well.

1.6.1.2. Mature B Cell Subsets.

The majority of naïve mature B cells enter lymphoid follicles in the spleen. These follicular B cells freely recirculate and thus comprise >95% of the B cells in peripheral lymph nodes. Importantly, follicular (FO) B cells require

CD40-CD40 ligand dependent T cell help to promote effective primary immune responses, CSR, and to establish high-affinity B cell memory (*79*). Present in fewer numbers than FO B cells, marginal zone (MZ) B cells localize in a distinct anatomical region of the spleen that represents the major antigen-filtering center. They express a limited BCR repertoire, and mediate early T-dependent and likely T-independent responses (*80*-*82*). MZ B cells appear to have very similar antigen specificity to a third population of mature antibody producing cells: the B1 cells. B1 cells are present in low numbers in the spleen but enriched in the peritoneal and pleural cavities. They participate in T-independent responses and are thought to function in clearance of dead or dying cells and to provide initial protection against common bacterial or viral pathogens (*83*-*85*). As such, B1 cells are thought to play a significant role in mucosal immunity.

1.6.1.3. B Cell Activation.

The initial antibody response against pathogens is largely mediated by a rapid T cell independent expansion of MZ and B1 cells and their subsequent differentiation into short-lived plasma cells. These acute responses are initiated through either polyclonal activation or cross-linking of the BCR via multivalent antigens. Slower to form are T cell dependent antibody responses which arise from a multi-step process including: BCR recognition of monovalent antigens, subsequent endocytosis and degradation of antigen into peptide fragments, expression of class II major histocompatibility complex (MHC) loaded peptides on the B cell surface, relocation to the T/B cell

interface of secondary lymphoid organs, recognition by CD4 T cells which provide B cell activation via expression of CD40 ligand and various cytokines. Importantly, cognate T cell help is required for high titer antibody responses and the development of B cell memory. There is increasing evidence that T cell help is provided by a specialized CD4 population marked by CXCR5 expression and termed follicular helper (Tfh) cells; these will be discussed in greater detail later.

1.6.1.4. Plasma Cells.

B cell activation results in expansion and commitment to either short-lived plasma cell (PC) development and antibody secretion or entry into the germinal center (GC) reaction that leads to high-affinity memory B cell development. PC development occurs via an intermediate plasmablast stage and is marked by reduced expression of a number of cell surface molecules including MHC II, B220, CD19 and CD21. Proteoglycan syndecan-1 (CD138) is a unique marker of PCs and is frequently used for their identification *in vivo*. Short-lived PCs have half-lives of 3 to 5 days, express germline-encoded antigen-specific antibodies and are important for acute protective responses (*86*-*88*). By contrast, long-lived PCs provide long-lasting humoral immunity. They are thought to predominantly arise from the GC response and thus express affinity matured antibodies. However, recent data suggests that non GC B cells can also differentiate to long-lived plasma cells (*89*, *90*). PC differentiation is strongly regulated by the transcriptional repressor Blimp-1 (encoded by *Prdm1*) (*91*). B cells lacking Blimp-1 do not differentiate into

short- or long-lived PCs, and correspondingly show severely diminished T independent and dependent antibody responses *in vivo* (*92*). Blimp-1 controls many genes important for plasma cell differentiation (*93*, *94*). Blimp-1 directly represses genes involved in cellular proliferation, such as *Myc* and *Bcl6*, to allow terminal differentiation of plasma cells into a post-mitotic state (*95*, *96*).

1.6.1.5. The Germinal Center Reaction.

GCs are initiated by an expansion of antigen-primed B cells within the lymphoid follicle. These secondary follicles subsequently polarize into dark and light zones, which consist of B cells undergoing somatic hypermutation to improve their antigen binding capability and clonal selection of mutants that produce high affinity antibody, respectively. Antigen expressing follicular dendritic cells (FDC) direct this process, with low numbers of GC Th cells also being present (*97*). The selection process is dependent on survival of only those clones with high affinity for the antigen so GC B cells show downregulation of prosurvival factors such as Bcl-2 and elevated expression of apoptotic markers like Fas (*98-100*). The net process results in the formation of both high affinity long-lived plasma cells and memory B cells.

The GC response involves substantial amounts of DNA damage due to affinity maturation and class switch recombination (CSR). The transcriptional repressor Bcl-6 is a crucial inhibitor of the DNA-damage response and is necessary for GC formation (*101*). Bcl-6 deficient mice have an absence of

germinal center B cells and affinity maturation (*102*, *103*). Notably, Bcl-6 can bind to *Prdm1* and directly repress Blimp-1 expression, just as Blimp-1 can regulate *Bcl6* (*96*, *104*, *105*). This reciprocal regulation is of particular interest as both genes are STAT3 targets (*106*-*110*).

1.6.1.6. Antibody Class Switch Recombination.

Antibody class, or isotype, is determined by the heavy chain constant (C_H) region expressed downstream of the rearranged heavy chain V(D)J gene, and is important in imparting specific antibody effector functions. Additionally, the membrane-bound forms of the various isotypes differ in their intracytoplasmic carboxy termini and ability to associate with intracellular signaling molecules, suggesting a role for CSR in defining BCR signals (*111*-*113*). Mice have 8 C_H regions all oriented in the same 5'-3' direction: μ, δ, γ3, γ1, γ2b, γ2a, ε, α (corresponding to IgM, IgD, IgG3, IgG1, IgG2b, IgG2a, IgE, and IgA respectively).

CSR involves a deletional recombination event between specialized switch (S) regions that are located upstream of each C_H gene (with the exception of δ, IgD expression occurs by alternative transcription termination/splicing of the μ-δ genes) and results in a change from IgM and IgD expression by naïve B cells to expression of one of the downstream isotypes (Figure 1.2). S regions are made of short-G rich tandem repeat sequences that are unique for each isotype. Despite these repeats, recombination is not limited to any particular

site within a given S region; recombination events can even occur outside of S regions (*114*, *115*). CSR can occur sequentially to different isotypes and even between chromosomes (*116*).

CSR is dependent on activation-induced cytidine deaminase (AID), which converts multiple deoxycytosines in S regions to deoxyuracils by deamination (*117-122*). The subsequent removal of dU residues by one of the uracil DNA glycosylases (UNG) results in single-strand DNA breaks (SSBs). SSBs can spontaneously form double-strand breaks (DSBs) if they are near each other on opposite DNA strands. Alternatively, error-prone translesion polymerases can repair nicks but introduce mismatch mutations of their own. Subsequent mismatch repair processes can also lead to DSBs. DSBs within the donor Sμ region and acceptor Sx regions initiates the DNA recombination process. Repair and ligation through nonhomologous end joining completes the process and results in the looping-out and replacement of Cμ with other downstream C_H genes. CSR requires multiple rounds of cell division in the target cell, possibly due to cell division-related regulation of AID expression (*87*, *123-126*).

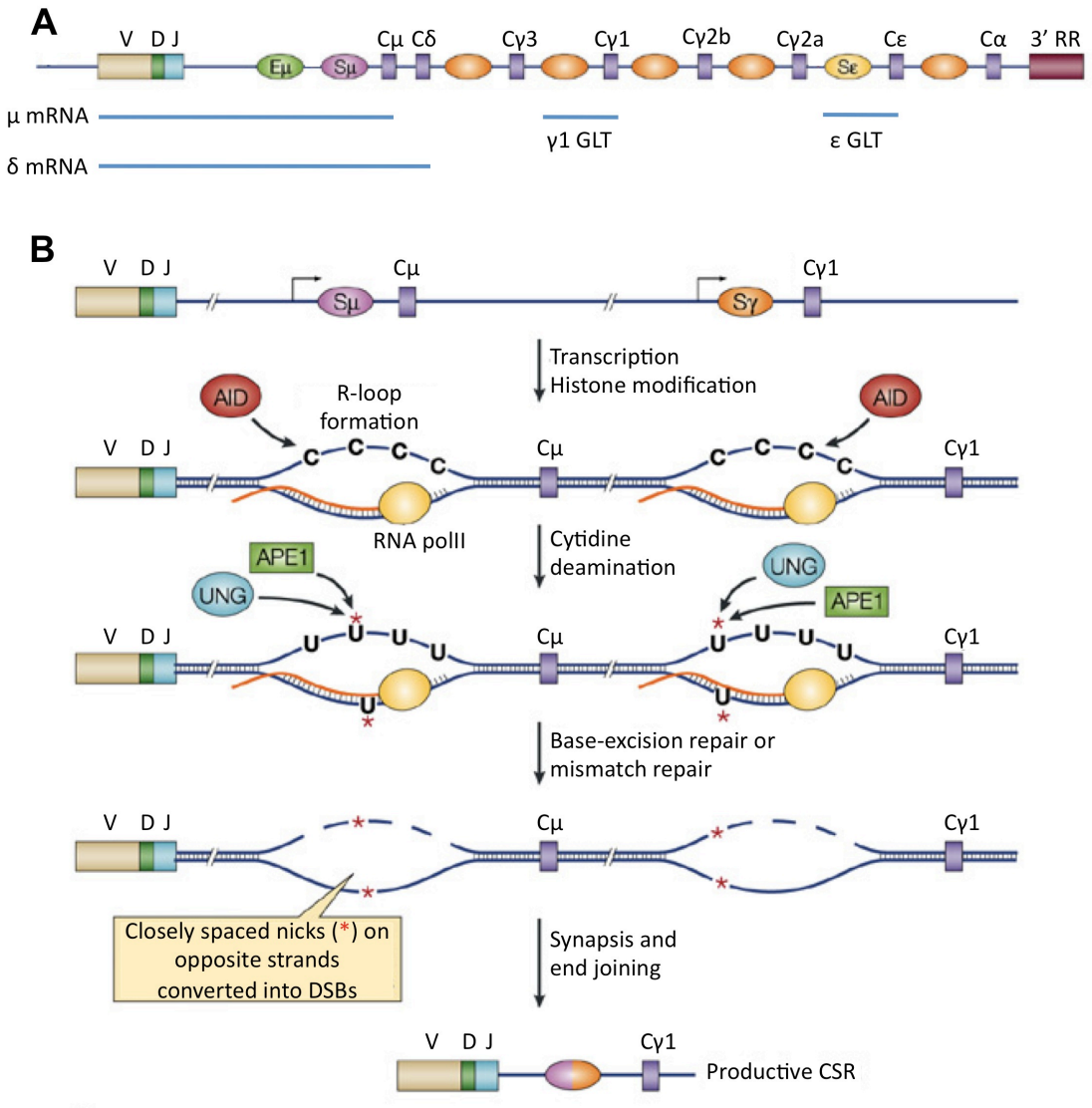

Figure 1.2. Class Switch Recombination

(A) Diagram of the mouse IgH locus in B cells expressing IgM and IgD (by alternative RNA transcription/ processing). The μ intron enhancer (Eμ) and 3' IgH enhancers (3'RR), along with IgH promoters, regulate the expression of germline transcripts (GLT).

(B) Transcription through switch (S) regions and associated histone modifications allow greater accessibility of activation-induced cytidine deaminase (AID). Transcription generates single-stranded DNA substrates for AID, which deaminates dC residues in the top and bottom strands of S regions. During the repair process, the activities of uracil-DNA glycosylase (UNG) and apurinic/apyrimidinic endonuclease 1 (APE1) introduce a high density of nicks (*) which can lead to double-stranded breaks (DSBs) in the S regions. The breaks are synapsed and class switch recombination (CSR) is completed by fusion of two S region DSBs. CSR to IgG1 is shown.

Figure modifed from (*132*)

1.6.1.6.1. Regulation of Class Switch Recombination.

Signaling through CD40 and toll-like receptors (TLRs) provides essential activation of B cells to undergo CSR. However, T and DC derived cytokines direct this process through promoting transcription across target S regions, initiating just upstream at the I_H exon. These RNA transcripts, referred to as "sterile" or germline", extend through the target C region and are spliced to join the I_H exon to the first coding exon of the C region. Donor S regions are constitutively transcribed. The function of germline (GL) transcription appears to be to direct AID action to specific S regions. GL transcription promotes this process in several ways: making intronic S regions more accessible to AID through histone modifications (*127-130*), separating the DNA strands at both the transcriptional bubble and through the formation of RNA:DNA hybrids or R-loops (AID only targets ssDNA) (*131*, *132*), direct recruitment of AID to the RNA polymerase II complex, allowing deamination of deoxycytosines to occur as the complex travels along the DNA (*133-137*).

Thus, secondary stimuli such as IL-4, TGF-β1 and IFN-γ adapt antibody effector functions to different environmental milieus; for example, IgA is induced in the mucosae, where TGF-β1 is produced at high levels (*138*). Cytokine mediated switch specificity is thought to be largely due to cytokine-responsive elements in GL I_H promoters. IL-4 promotes CSR to IgG1 and IgE through activation of STAT6, which binds to the Iγ1 and Iε promoters to initiate GL transcription of these loci. TGF-β1 activates SMAD3, SMAD4 and/or RUNX proteins to promote transcription proceeding through Sγ2b and Sα for

class switching to IgG2b and IgA, respectively. In mice, IFN-γ activates T-bet, STAT1 and/or STAT2, which promote GL transcription of the γ2a locus to promote IgG2a CSR (*139*). Competition between different I_H promoters for the transcriptional machinery enhances isotype selection (*140*).

In addition to I region promoters, sterile transcription and isotype switching are also regulated by two IgH enhancer regions, which are primarily activated by NF-κB, HOXC4, OCT1 and/or OCT2 downstream of BCR, TLR and CD40 stimuli (*141*). The μ intron enhancer is situated just 5′ to the Sμ region and four enhancers are spread over 30 Kb 3′ to the Cα gene in mice. The mouse 3′ IgH enhancers are labeled hs3A, hs1,2, hs3B, and hs4 (from 5′ to 3′). Deletion of hs3A or hs1,2 has no effect on CSR but joint deletion of hs3b and hs4 resulted in significant reductions in both germline transcription and switching to all isotypes, with the important exception of IgG1 (*142*, *143*). Selective deletion of the μ enhancer in B and T cells (using the RAG complementation approach (*144*) resulted in decreased total CSR levels (*145*). The region just 5′ to Sγ1 also has enhancer activity for γ1 transcription, perhaps explaining the independence of IgG1 from the 3' IgH enhancers (*146*, *147*). The combination of primary (BCR, TLR, CD40) and secondary (cytokines) stimuli also regulate CSR through induction of AID; the *Aicda* locus has STAT6, SMAD, NF-κB, HOXC4 and OCT1 binding sites (*148-152*).

1.6.1.6.2. Histone Modifications in Class Switch Recombination.

S regions are highly enriched in histone modifications compared to I_H promoters in activated B cells. This is in stark contrast to the rest of the genome, where promoters carry the bulk of activating histone marks (113, zhou). Upon B cell activation, S regions lose repressive histone modifications, such as trimethylation of histone H3 lysine 27 (H3K27me3), and acquire permissive histone modifications, such as H3K4me3 (60,83,86,88,109–112). It remains unclear whether histone modifications allow for initiation of GL transcription or whether GL transcription leads to histone modifications. At present, the two processes seem to take place simultaneously, suggesting that the transcription factors that activate GL transcription downstream of both primary and secondary CSR stimuli also recruit histone modifiers. In support of such a model, a recent study showed that PAX-interacting protein 1 (PTIP) was necessary for both GL transcription and H3K4me3 of the γ1 locus(*130*). Elucidation of additional transcription factors capable of driving histone modifications of C_H loci will be very valuable for future study.

1.6.2. $CD4^+$ T Cells.

T cells are a major component of the adaptive immune system and have essential functions in orchestrating immune responses. In particular, the $CD4^+$ or “helper” T cells produce cytokines to instruct macrophage killing of phagocytosed microbes and also enhance cytolytic functions of $CD8^+$ T cells and NK cells during cell-mediated immune responses. $CD4^+$ T cells also provide help to B cells as part of the humoral response.

1.6.2.1. T Cell Development.

T cells are thought to derive from the same subset of common lymphoid progenitors (CLPs) in the BM as B cells, NK cells and some DCs (*153*). Expression of the transcription factors Notch-1 and GATA-3 in CLPs drives commitment towards the T cell lineage (*154-157*). Following commitment to T cell differentiation, CLPs circulate to the thymus, where a productive T cell receptor (TCR) is produced following V(D)J recombination (*158*). V(D)J rearrangement of the TCRβ chain progresses through a series of steps within the double negative (DN) stage of development, where thymocytes lack expression of the heterodimeric TCR, associated CD3 and TCRζ chains, and the CD4 or CD8 co-receptors (*159*). Once a productive rearrangement of the TCRβ chain has occurred, the CD4 and CD8 co-receptors are upregulated to generate double positive (DP) thymocytes (*160*). Subsequent V(D)J rearrangement of the TCRα gene results in expression of a mature heterodimeric TCR$\alpha\beta$ complex which can interact with self-MHC molecules expressed on cortical thymic epithelial cells (*161*). This allows for a positive selection process by which MHC Class I/II restriction occurs, leading to downregulation of the irrelevant co-receptor and generation of single positive (SP) $CD4^+$ or $CD8^+$ T cells (*162*). By comparison, productive rearrangement of the TCRγ and TCRδ genes commits thymocytes to the $\gamma\delta$ T cell lineage. Subsequent negative selection processes delete autoreactive T cell clones (*162*).

1.6.2.2. $CD4^+$ T Cell Differentiation.

Selected T cells exit into the bloodstream and recirculate through secondary lymphoid tissues (*163*). Recirculating T cells can be activated in secondary lymphoid organs by antigen recognition, leading to TCR activation. However, T cells are only fully activated in the presence of co-stimulatory signals on activated APCs (*164*), such as CD80 and CD86, which interact with CD28 on T cells (*164*). Activated $CD4^+$ T cells differentiate into T helper cells, which have been classified into different subsets according to their cytokine effector profiles and the expression of specific transcription factors. The first studies described Th1 and Th2 cells as distinct lineages of effector T cells, defined by their ability to generate immune responses to different types of pathogens (*165-169*). More recently the Th17, Treg and Tfh cells have been described as distinct effector subsets, requiring different cytokines and transcription factors for their development and functions (Figure 1.3) (*170-175*). STATs play a central role in dictating $CD4^+$ T cell differentiation by mediating cytokine-induced gene expression that drives specific effector responses. Although the T helper subset paradigm provides a very useful framework to define T cell function and biology, it is important to note that these subsets are often heterogeneous and the different T helper subsets can cooperate against infection (*176-178*).

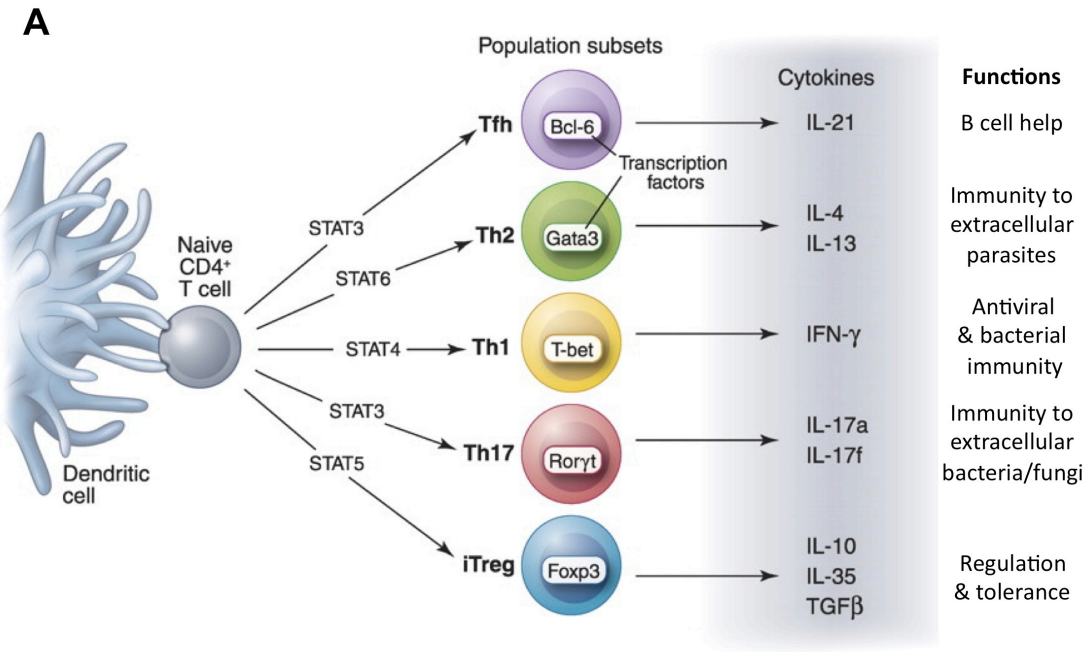

Figure 1.3. CD4⁺ T cell Differentiation

(A) Upon encounter of pathogens or inflammatory stimuli, innate immune cells produce factors that drive the differentiation of naïve CD4⁺ T cells to alternate effector fates: Th1, Th2, Th17, iTreg and Tfh. Th1, Th2 and Th17 cells are each important in protection against certain classes of pathogens while Tfh cells provide help to B cells and Treg cells dampen immune responses. The classic view, diagrammed here, is one in which each "lineage" produces a unique assortment of effector cytokines that are tailored for the specific functions of that cell-type. Differentiation takes place in a linear process whereby the cytokine milieu present at the time of TCR engagement activates one of a number of alternate STAT signaling pathways. This leads to the subsequent induction of a transcriptional "master regulator" that is sufficient to impart selective effector functions. Recent studies have demonstrated the system to be far more flexible, with CD4⁺ T cells being able to switch from production of one class of cytokines to another upon exposure to a new pathogen or microenvironment. Additionally, CD4⁺ cells can express lineage-defining transcription factors only transiently or even express multiple ones simultaneously.

(B) Figure modifed from (*286*)

1.6.2.2.1. Th1 Cells.

The Th1 subset is characterized by the production of the cytokines IFN-γ and lymphotoxin and by the expression of the transcription factor T-bet (*179*, *180*). Although the strength of TCR stimulation can shape T cell responses, the cytokine milieu is the major determinant of T helper subsets differentiation. For Th1 cells, T-bet expression is induced by IFN-γ, IL-12 and IL-27, through the activation of STAT1 (*165*, *181*, *182*). T-bet activation promotes Th1 differentiation by activating the *Ifng* locus (*183-185*) and by silencing the locus for the key Th2 transcription factor GATA-3 (*186*, *187*). Moreover, T-bet activation leads to up-regulation of the β2 chain of the IL-12 receptor (IL-12Rβ2). As IL-12 promotes Th1 expansion in a STAT4 dependant way, this process helps stabilize the commitment to the Th1 lineage (*188*). Both *Tbx21*$^{-/-}$ mice, which lack T-bet, and *Stat4*$^{-/-}$ mice show impaired Th1 differentiation, and are more susceptible to intracellular pathogens (*189-193*). Th1 cell protective activities are mainly attributed to the production of IFN-γ, which activates cellular immunity, especially macrophage activation (*179*). However, excessive Th1 responses have also been implicated in the development of inflammatory pathologies, such as type 1 diabetes and inflammatory bowel disease (IBD) (*194-196*).

1.6.2.2.2. Th2 Cells.

Th2 cells are defined by the expression of GATA-3 and by the production of IL-4, IL-5 and IL-13 (*179*). Th2 differentiation in vitro requires both IL-4 and

IL-2, as they promote GATA-3 expression and stabilization through STAT6 and STAT5, respectively; recent data also suggests a role for STAT3 in this process (*179*, *197*). Moreover, other transcription factors, such as NFAT, TCF-1 and c-Maf contribute to Th2 differentiation. Molecular mechanisms involved in Th2 differentiation repress the differentiation of Th1 cells, as GATA-3 represses IL-12Rβ2 expression and TCF-1 inhibits the expression of IFN-γ (*198*, *199*). Th2 responses play a key part in the response against extracellular infectious agents, such as intestinal nematodes, by coordinating a complex immune response, including recruitment of eosinophils, mast cells and basophils, IgE production, increased mucus secretion by goblet cells and increased intestinal contractility (*200*). However, aberrant Th2 responses are implicated in the development of atopic diseases, such as asthma and allergy (*201*). Traditionally, IL-9 was considered a Th2 cytokine, as it promotes mast cell function and IL-13 production, contributing to allergic inflammation. However, naïve $CD4^+$ T cells differentiated in the presence of TGF-β1 and IL-4 produce high levels of IL-9 and IL-10, but no other Th2 cytokines and do not express any defining transcription factor (*202*, *203*). These have been termed Th9 cells and promote immune responses to intestinal helminthes and asthma (*204*). However, as yet no specific transcription factor has been associated with Th9 differentiation and it is not clear whether they truly are a separate T cell lineage.

1.6.2.2.3. Th17 Cells.

In mice, Th17 cells are characterized by the production of IL-17A, IL-17F, IL-17E, IL-21 and IL-22 and they typically express the surface molecules CCR6 and the IL-23R (*205*). In mouse and human, Th17 cells differentiate in response to TGF-β1 stimulation in the presence of the STAT3 activating cytokines IL-6 or IL-21 (*206-209*), although TGF-β1 independent Th17 differentiation has been described (*210*). IL-1β also contributes to early Th17 differentiation (*211*, *212*), while IL-23 plays an essential role in sustaining Th17 differentiation and promoting survival of Th17 cells (*213*, *214*). IL-17A itself, mainly produced at mucosal surfaces by γδ T cells, may also promote the differentiation of $CD4^+$ Th17 cells (*215*, *216*). The main transcription factors implicated in Th17 differentiation are RORγt and RORα, members of the retinoic acid-related orphan nuclear hormone receptor family with redundant functions in Th17 differentiation (*179*, *205*). RORγt and RORα expression is dependent on STAT3 activation (*217-219*) Other transcription factors can also contribute to Th17 differentiation and expansion, such as interferon regulatory factor 4 (IRF4) (*220*), c-MAF, basic leucine zipper transcription factor, ATF-like (Batf) (*221*), runt-related transcription factor 1 (RUNX-1), and the aryl hydrocarbon receptor (AHR) (*222*, *223*). However, their relative contribution to Th17 cell differentiation remains largely unresolved.

Th17 cells are enriched at mucosal surfaces and they are thought to play a central role in the defense against extracellular bacteria and fungi. Infection of mice with pathogens like *Candida albicans*, *Pneumocystis carinii*, *Mycobacterium tuberculosis* and *Klbesiella pneumonia* all induce heightened expression of IL-17A from $CD4^+$ T cells, suggesting that Th17 cells play an important role in their clearance (*224-226*). Additionally, Th17 cell-associated cytokines IL-17A and IL-17F have been shown to promote neutrophil recruitment, activation, and host defense to bacterial infection, particularly in mucosal tissues like the lungs (*227-229*). IL-17A and IL-17F can also induce proinflammatory cytokine, chemokine and prostaglandin expression by stromal cells, keratinocytes, and macrophages (*230-236*). Furthermore, IL-22 has been shown to induce production of anti-microbial peptides, like β-defensins, by intestinal epithelial, liver, and skin cells and has been implicated in epithelial cell wound-healing (*237-239*). Conversely, excessive Th17 responses are believed to contribute to numerous chronic inflammatory and autoimmune conditions (*240*). In mice, Th17 cell responses are enhanced in experimental models of colitis, psoriasis, uveitis, scleritis, experimental autoimmune encephalomyelitis (EAE) and pneumonitis, and suppression of these responses is correlated with prevention of disease (*241-244*).

1.6.2.2.4. Tregs.

Although many cell types can be immunosuppressive in specific settings, Tregs represent a specialized subset of T cells whose main function is to mediate tolerance by suppressing immune responses (*245*). Although many

early studies showed that a population of memory $CD4^+$ T cells expressing the IL-2 receptor α chain (CD25) was able to suppress immune responses both *in vitro* and *in vivo* (*246-251*), the formal classification of regulatory T cells as a separate lineage was facilitated by the identification of the transcription factor required for their development, forkhead box P3 (Foxp3) (*252-255*). Foxp3 was identified in an effort to define the cause of a severe human autoimmune disorder, the IPEX syndrome (immune dysregulation, polyendocrinopathy, enteropathy, X-linked), a disease phenotype that is recapitulated by the scurfy mouse. Both IPEX patients and scurfy mice bear loss of function mutations of Foxp3, resulting in a severe early-onset lymphoproliferative disorder affecting multiple systems (*252-255*).

Two main types of $CD4^+$ $Foxp3^+$ Tregs have been described, possibly sharing similar functions *in vivo*: natural Tregs (nTreg) that differentiate into fully functional $Foxp3^+$ Tregs in the thymus; and induced Tregs (iTreg) that differentiate from naïve $CD4^+$ T cells in the periphery (*245*). nTreg generation in the thymus is dependent on high affinity recognition of self antigens (*245*). TCR stimulation results in up-regulation of CD25 and IL-2 signaling leads to the induction of Foxp3 by STAT5 (*256*, *257*). Other signals, such as stimulation by the γc cytokines IL-7 and IL-15 and costimulation through CD28 are important for the development of nTregs (*258-261*). These signals result in the activation of a complex transcriptional program, including the activation of the NF-κB pathway and of other transcription factors, including NFAT and AP-1 (*262*). However, Foxp3 expression is crucial to maintain the

Treg pool, as loss or attenuation of Foxp3 expression in Tregs results in severe autoimmune pathology (*263*, *264*).

Treg cells have been shown to exert their suppressive function on a plethora of immune cell types *in vitro* and *in vivo*, including monocytes, macrophages, DCs, granulocytes, T and B cells and NK cells (*265*). *In vivo*, Tregs are likely to suppress effector T cell activation by directly interacting with DCs, rather than with T cells (*266*, *267*). Tregs can strongly down-modulate the pro-inflammatory functions of DCs by blocking co-stimulatory molecules through the expression of CTLA-4 (Cytotoxic T Lymphocyte Antigen 4) and by promoting IL-10 production (*268*, *269*). Tregs also mediate immune-suppression by producing soluble factors, such as IL-10, TGF-β1 and IL-35 (*270*, *271*). Moreover, Tregs can dampen immune responses by depleting the microenvironment of growth factors, such as IL-2, or proinflammatory molecules, such as extracellular ATP, thereby limiting the activation of other immune cells (*272*, *273*). Other regulatory T cell populations have been described, but are as yet poorly characterized. In particular, $Foxp3^-$ Tr1 cells may be potent sources of IL-10 and can play an important role in modulating immune responses against infection at mucosal surfaces (*274-276*).

1.6.2.2.5. Tfh Cells.

Follicular helper T cells (Tfh) reside in secondary lymphoid organs and provide B cells with the help necessary to differentiate into high affinity plasma cells (*277*). Tfh cells are characterized by high expression of CXCR5, ICOS, PD-1 and CD40L, and produce high levels of IL-21 (*278-282*). Principally, they are involved in GC formation; they additionally promote class switch and survival in GC B cells (*279*). STAT3 activating cytokines (IL-6 and IL-21) are thought be the primary drivers of Tfh differentiation (*283*); although, STAT3 independent pathways have also been demonstrated *in vivo* (*284*). Notably, Tfh differentiation has been suggested to arise from active transcriptional repression of other helper T lymphocyte lineages via Bcl6 (*174*). Complicating this hypothesis is the finding of significant co-expression of "lineage defining" cytokines (IFN-γ, IL-4 and IL-17A) within Bcl6 expressing, supposed Tfh cells (*279*). With a slightly different spin on a similar theme, a recent study has suggested that hybrid Th1/Tfh cells represent a transitional step in Th1 differentiation and that even "fully differentiated" Th1 cells exhibit epigenetic evidence for plasticity in *Bcl6* expression (*285*). Suffice it to say, the evidence to date is insufficient to definitively place Tfh cells as either an exclusive and separate lineage or a transitional/inducible change within the traditional T helper cell subsets.

1.6.2.3. Plasticity of $CD4^+$ T Cell Subsets.

Recent evidence suggests that $CD4^+$ T helper effector cell phenotypes are not completely fixed, as committed T helper cells can produce different cytokines from those determined by their differentiation status (*286*). For instance, Th17

cells can produce IFN-γ *in vivo* (*243*, *287*), Th1 cells can make IL-13 (*288*) and Th2 clones can produce IFN-γ (*289*). In addition the concept of transcriptional "master regulators" has been challenged by the finding that many of these transcription factors can be co-expressed and do not always antagonize each other but can also cooperate in shaping T helper cell effector function. Similarly, co-expression of Foxp3 with classically defined lineage specific transcription factors (T-bet, GATA-3, IRF-4, Bcl6 and STAT3) has been reported and may be essential in tailoring Treg responses to individual immune responses (*290-295*). Pro-inflammatory cytokine production and loss of *Foxp3* expression has been shown in Treg cells, even to the point of pathogenic, unchecked, immune-mediated damage (*296*, *297*). Such However, loss of Foxp3 expression is not always associated with pathology as Foxp3$^+$ Treg cells have also been shown to convert into Tfh cells in the peyer's patches of the small intestine and promote GC formation and IgA production in the gut (*298*). Functional plasticity is not restricted to Foxp3$^+$ Treg cells. Epigenetic analyses have revealed that Th17 cells are inherently unstable and that the loci for *Tbx21* and *Ifng* are associated with permissive histone modifications in Th17 cells suggesting that Th17 cells are "poised" to express T-bet and IFN-γ (*299*, *300*). Indeed the cytokines IL-12 and IL-23 have been shown to promote conversion of established Th17 cells into Th1-like cells *in vitro* (*300*) and populations of IL-17A$^+$IFN-γ$^+$ cells arise at sites of inflammation in both mice and humans (*301-304*). Similarly, infection with the lymphocytic choriomeningitis virus (LCMV) was shown to reprogram committed GATA-3$^+$ Th2 cells into GATA-3$^+$T-bet$^+$ T cells in an IL-12 and IFN dependent manner (*305*). Thus considerable heterogeneity exists among T

helper subsets and a new model is forming in which $CD4^+$ T cells are not fully committed, but can fine-tune their effector functions in response to changing environmental stimuli.

1.7. The Intestinal Immune System.

Extending over 100m^2 in humans, the intestinal epithelium is the largest mucosal surface in the body (*306*). It is covered with a single layer of intestinal epithelial cells (IECs), which allow swift absorption of nutrients, but also represents a major entry route for invading pathogens (*307*). As the gut is heavily colonized by commensal bacteria, distinct anatomical features have evolved to allow the intestinal immune system to rapidly react against invading pathogens whilst avoiding inflammatory responses against beneficial commensal bacteria and food antigens.

The gut associated lymphoid tissue (GALT) comprises both effector sites, such as the intestinal epithelium and lamina propria (LP), and secondary lymphoid structures, including the mesenteric lymph nodes (MLNs), the Peyer's patches (PPs) of the small intestine and isolated lymphoid follicles (ILF) and cryptopatches (CPs) that are distributed throughout the intestine (*308*). Secondary lymphoid structures are essential for the induction of adaptive immune responses and the development of tolerance to food antigens (*307*). Moreover, MLNs allow the compartmentalization of the intestinal immune response, as antigen-loaded intestinal DCs usually do not

penetrate further than these structures into systemic secondary lymphoid organs (*309*). Antigen presentation in the MLN results in the expression of gut homing receptors on lymphocytes, such as $\alpha4\beta7$ and CCR9 in T lymphocytes, that promote their recirculation to the intestinal mucosa (*307*). The intestinal LP and epithelium are rich in innate and adaptive leukocytes, which are briefly discussed below.

1.7.1. Intestinal Epithelial Cells.

The gut epithelium comprises 5 different intestinal epithelial cell lineages: absorptive enterocytes, goblet cells, paneth cells, enteroendocrine cells and M cells, all of which contribute to epithelial barrier function. The gut epithelium is continuously renewed; epithelial stem cells that are present in the crypts constantly generate new epithelial cells that migrate progressively to the tip of the intestinal villi and eventually undergo apoptosis and exfoliate into the lumen (*310*, *311*). IECs are strongly polarized, as their apical side is rich in microvilli (forming the typical “brush border”) and the IEC layer is held together by paracellular tight junctions that prevent diffusion of fluids and particles present in the lumen (*306*). Goblet cells further enhance the epithelial barrier by secreting gel-forming mucins, such as MUC2, which form a thick layer of mucous on the surface of the epithelium, thus excluding most bacteria from the epithelial surfaces (*312*). Paneth cells are specialized secretory cells found at the base of the intestinal crypts in the small intestine. Paneth cells are characterized by large secretory granules, mainly containing antimicrobial peptides (AMP), such as defensins, cathelicidins and

calprotectins (*313*). Paneth cells release the content of their granules into the intestinal lumen, preventing bacterial invasion of the crypts (*314*). Enteroendocrine cells are also situated at the base of the intestinal crypts, where they sense luminal signals and transmit these signals to enteric neurons by secreting different bioactive products across the basolateral membrane (*315*). M cells play a strategic role in monitoring the luminal environment. They are found within the follicle-associated epithelium that overlies the PP and ILF, lack a brush border and are not covered in mucous. M cells sample antigens from the lumen and transport them to the subepithelial dome, an area of the PP that is rich in DCs (*316*), allowing transfer of luminal antigen to APCs and representing an important portal into the intestinal immune system.

1.7.2. Innate Lymphoid Cells.

Lymphoid tissue inducer cells (LTis) are essential for the formation of lymph nodes and PPs in the fetus (*317*). LTis don't express lineage markers specific for T cells, B cells or myeloid cells (lin^-), but are defined by the expression of CD4, lymphotoxin-α (LT-α) and LT-β, CD127 (IL-7Rα), c-kit, RANK-L and the transcription factor RORγt (*318*). LTis originate from the fetal liver and migrate to the lymph nodes and PP in response to chemotactic signals (*319*, *320*). Here, they interact with stromal cells through activation of the LT-β receptor, inducing the secretion of different cytokines, which in turn recruit hematopoietic cells to the nascent lymph node (*321*). LTis also play important roles later in life as they contribute to the formation of ILFs in the gut (*322*-

324) and to tissue remodeling, as they are essential for the re-establishment of normal lymph node structure following damage induced by acute viral infection (*325*). LTi cells can produce IL-17A and IL-22, key players in intestinal homeostasis and immunity (*317*, *326*), and sustain T cell-independent production of IgA by B cells (*327*).

Recent advances in the field suggest that LTi cells are part of a broader family of innate lymphoid cells (ILCs) that play a central role in modulating immune responses, especially in the gut (*317*). One recently described population of ILCs share some surface markers with natural killer (NK) cells, produce IL-22, and have been designated as NK22, NCR22, or ILC22 cells (*317*, *328*, *329*). In mice, NK22 cells are NKp46^{+}, but do not express the conventional NK marker NK1.1 (*328*, *330*, *331*). Moreover, they differ from NK cells as they don't have cytotoxic capacity, they lack the expression of inhibitory receptors and they produce very little IFN-γ (*332*). The development of NK22 cells is dependent on the transcription factor RORγt and on the presence of the intestinal microflora (*328*, *331*). Another subset of ILCs, which is able to produce IL-17A, IFN-γ and IL-22 during intestinal inflammation has recently been described (*333*). This population, which differs from both LTi and NK22 cells by lacking expression of c-kit and NKp46, plays a central role in promoting innate immune inflammation during *Helicobacer hepaticus*-induced colitis (*333*). ILCs have also been described in Th2 immunity in the gut (*334-337*). These lin^{-} cells can respond to type-2 cytokines like IL-25 and IL-33

by producing IL-13, IL-4, IL-5 and IL-6 (*338*), promoting Th2 responses, especially in the context of helminth infections (*338*). Further work is required to identify the relationship between these different ILC subtypes but it is becoming increasingly clear that, despite being present in small numbers, they play a substantial role in both the initial response against invading pathogens and in shaping the subsequent adaptive immune response through rapid production of cytokines.

1.7.3. Myeloid Cells and the Adapitve Arm of Intestinal Immunity.

Myeloid APCs of the intestine are a heterogeneous population consisting of DCs and macrophages and can broadly be distinguished by their expression of CD103 and CX3CR1 (*339*, *340*). Intestinal macrophages are highly phagocytic cells with potent bacteriocidal activity. Crucial for the maintenance of homeostasis, engulfment of microbes by these cells does not induce pro-inflammatory cytokine release (*339*). APCs are endowed with the unique capacity to prime naïve $CD4^+$ T cells and intestinal DCs can acquire antigen in the intestine and migrate to the MLN where they prime the activation of T cells (*341-344*). $CD103^+$ DCs represent a unique population of intestinal DCs that appear especially endowed to promote tolerance in the intestine. Indeed, $CD103^+$ DCs in the intestine are potent inducers of $Foxp3^+$ Tregs through TGF-β1 and retinoic acid (RA) dependent mechanisms (*345*, *346*). Furthermore, resident $CX3CR1^+$ APCs are important for promoting local proliferation of Tregs in the lamina propria (*347*) and might also contribute to the maintenance of Foxp3 expression by Treg cells (*348*).

Conditioning of intestinal DCs through factors produced locally in the intestine such as TSLP and PGE2, which can be produced by IECs, help to maintain the tolerogenic state of intestinal DCs in the face of a vast microbiota (*349*, *350*). However not all APCs in the intestine are tolerogenic and they can also prime effector $CD4^+$ T cell responses (*351-353*). APCs express a variety of patern recognition receptors (PRRs) which allow them to respond to microbial stimulation and integrate this information to instruct the immune decision making process (*344*). Indeed $CX3CR1^+CD70^{high}$ APCs in the lamina propria express high levels of the pro-inflammatory cytokines IL-23 and IL-6, which are important for the generation of T helper 17 cells (*353*). Th17 cells are abundant in the intestinal lamina propria (*170*) and although Th17 cells are essential for host protective immunity against extracellular bacteria and fungi they are also implicated as major drivers of chronic intestinal inflammation (*240*). Furthermore $CD103^+$ DCs isolated from an inflamed environment can favor the induction of effector T cells rather than Tregs highlighting their capacity to respond to cues in the intestine and prime the appropriate immune response (*354*).

Intestinal homeostasis depends on complex interactions between the microbiota, the intestinal epithelium and the host immune system (Figure 1.4). Diverse regulatory mechanisms cooperate to maintain intestinal homeostasis, and a breakdown in these pathways may precipitate the accumulation of pathogenic effector T cells in the intestine and reductions in Tregs, which

drives chronic inflammatory responses. The colitogenic potential of intestinal effector T cells is revealed in experimental systems when regulatory pathways such as IL-10 (*55*, *355*) and TGF-β1 (*356*, *357*) are blocked. Thus, there is a delicate balance of pro- and anti-inflammatory responses in the intestine and although breakdown of this balance is remarkably infrequent perturbation results in chronic intestinal inflammation and immune system mediated damage to the host (*358*).

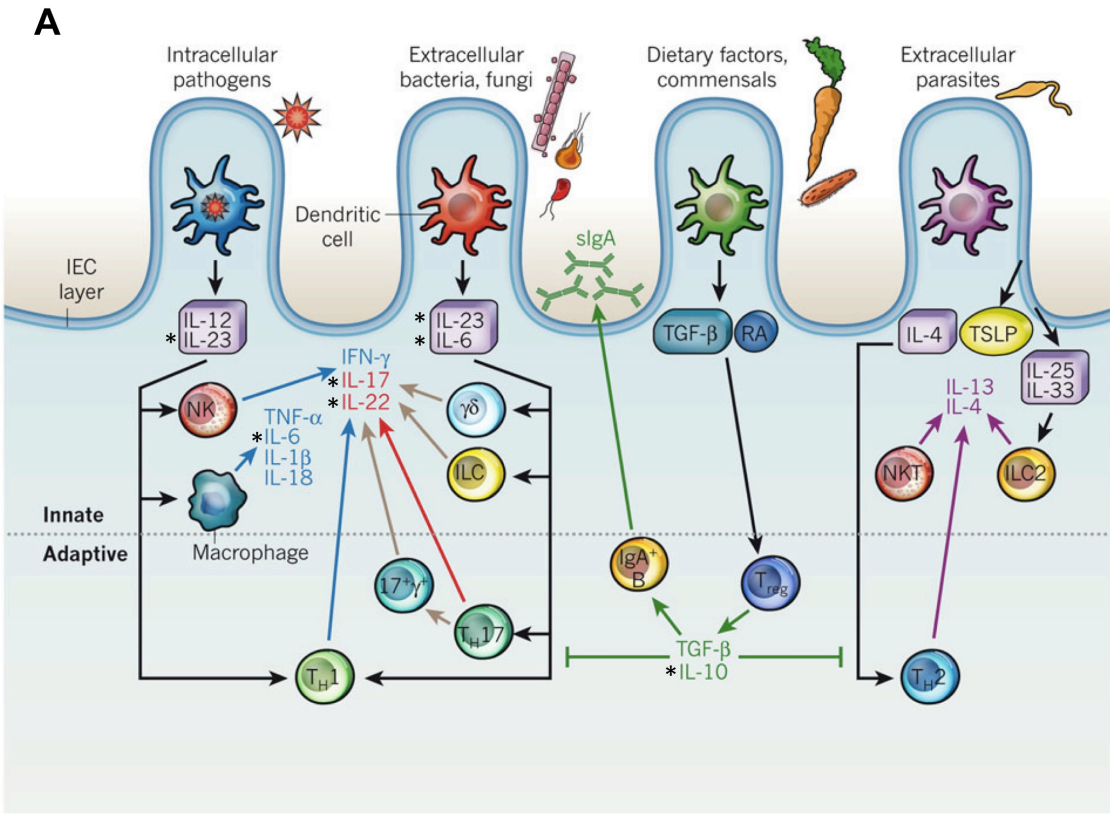

Figure 1.4. Innate and Adaptive Immune Responses in Intestinal Homeostasis

(A) A single layer of epithelial cells separates the intestinal lamina propria from the lumen. A thick mucus layer coating, rich in antimicrobial peptides and secreted immunoglobulins, provides the primary barrier between host and microbes. Intestinal epithelial cells (IECs) and dendritic cells continually sample the intestinal microenvironment and subsequently direct specific effector responses (black arrows) through the production of both pro-inflammatory (IL-12, IL-23) and tolerogenic (TGF-β, RA) factors. Local innate leukocyte populations (NK cells, ILCs, myeloid cells) are an important early source of effector cytokines upon pathogen invasion and serve to contain the infection until specific adaptive responses can form in the secondary lymphoid tissues. Cells and molecules associated with distinct effector profiles are color-coded; Th1 type (blue), Th17 type (red), mixed Th1 and Th17 (brown), Th2 type (purple). Treg responses (green) limit these distinct effector modules and thus prevent the formation of a chronic inflammatory state. Importantly, STAT3 is involved in both the development of effector and regulatory responses. Cytokines that either signal via STAT3 or that are dependant on STAT3 for their induction are labeled with a (*).

Figure modifed from (*358*)

1.8. Experimental Models of Colitis.

1.8.1. Dextran Sodium Sulphate Induced Colitis.

Dextran sodium sulphate (DSS) is thought to be toxic to gut epithelial cells (*359*), and upon DSS polymer administration in drinking water, mice suffer from acute colitis that has been shown to induce bloody diarrhea, ulcerations, and infiltration with granulocytes (*360*). The adaptive immune system does not seem to play a role in the acute phase of this model as mice lacking T and B cells also suffer from severe intestinal inflammation (*361*). STAT3 phosphorylation has been shown to be elevated in the colon of DSS treated mice (*362*) and mice with *Stat3* deficient IECs are more susceptible (*49*). Therefore, this model is ideal for probing epithelial and innate immune responses to intestinal injury.

1.8.2. *Citrobacter rodentium* Induced Typholocolitis.

Enteropathogenic *E. coli* (EPEC), enterohemorrhagic *E. coli* (EHEC), and *Citrobacter rodentium* are Gram negative attaching and effacing (A/E) pathogens that cause intestinal inflammation and diarrhea in their respective hosts. While EPEC and EHEC infect humans, they colonize poorly in mice. Therefore, much of our knowledge about how hosts control infection by A/E pathogens comes from experimental studies with *C. rodentium*, a naturally occurring pathogen in mice (*363*).

A/E pathogens colonize the intestinal epithelial cells by localized destruction of brush-border microvilli and intimate attachment of bacteria to the host plasma membrane. This process leads to acute intestinal inflammation of the cecum and colon, mucosal hyperplasia and diarrhea (*364*). Both IECs and immune cells are crucial in host defense against A/E pathogens. IECs form the barrier against bacterial influx through their tight junctions and AMP production (*365*, *366*), while $CD4^+$ T cells, B cells and *C. rodentium*–specific antibody responses are all essential components of adaptive immunity used for containing and eradicating the infection (*367*, *368*). Many cytokines from lymphocytes, including IL-17A, IL-17F, IFN-γ and IL-22 have been suggested to play an important in this process. Additionally, ILCs have recently been shown to be major players in the early response against *C. rodentium* and a significant source of IL-22 (*369-372*). Therefore the collective roles of IECs, innate and adaptive immune responses in host defense against *C. rodentium, make this* an ideal model to interrogate intestinal immune function.

1.9. Aims.

Selective inactivation of *Stat3* in various adult mouse tissues has led to many advances in our understanding of this transcription factor's function within the immune system (*44*). However, as STAT3 appears to control seemingly conflicting pathways in different cell types, much is left to learn about STAT3 function at the organism level. The discovery of dominant-negative *STAT3* mutations in AD-HIES patients presented a unique opportunity for further

understanding of both the pathogenesis of this disease and of the interplay of STAT3 function from various cell and tissue types (*70*, *71*).

Therefore, the primary aims of this thesis were:

1) To generate a mouse model of AD-HIES that would recapitulate important aspects of the human disease and serve as a tool for gaining a further understanding of both disease pathogenesis and STAT3 function in the immune system.

2) To probe the effects of hypomorphic STAT3 activity on B and T cell responses, with an aim towards gaining mechanistic insight into why serum IgE might be increased in AD-HIES patients.

3) To examine the effects of hypomorphic STAT3 signaling on the intestinal immune system.

2. Chapter 2: Materials and Methods.

2.1. Mice.

C57BL/6 (B6) fertilized mouse eggs were used for pronuclear microinjection of the *Stat3ΔV463* BAC construct. Microinjection and initial screening for BAC integration were carried out at the National Cancer Institute (Frederick, USA). B6.*Stat3ΔV463* (mut-*Stat3*) mice and wild-type (WT) littermate controls were maintained in individually ventilated cages in specific pathogen-free (SPF) animal facilities at the 9C127 ACRF Animal Facility, Building 10, National Institutes of Health (Bethesda, USA) and Biomedical Services Facility, John Radcliffe Hospital, University of Oxford. All experiments carried out at the NIH were in accordance with the guidelines of the NIH Animal Care and Use Committee and conducted under approved NIAMS Animal Study Protocols (ASPs). Experiments performed at the University of Oxford were in accord with the UK Animal Procedures Act of 1986 and approved by a project license from the UK Home Office.

2.1.1. Generation of the *Stat3ΔV463* BAC-Transgenic Mouse Line.

Generation of the *Stat3ΔV463* BAC construct and mut-*Stat3* mice is discussed in detail in chapter 3. Select experimental details and primer sequences are discussed in this section. Unless otherwise noted, all polymerase chain reactions (PCR) were performed following previously published conditions and using 1 U of Taq polymerase (Roche) (*373*). All DNA

extractions were performed using Qiagen kits with the exception of the final isolation of the modified BAC. BAC isolation was performed using the NucleoBond BAC 100 kit (Clontech). Restriction enzymes were purchased from New England BioLabs and used per the manufacturer's instructions. Bacterial plates and media were prepared as previously described (*374*). Primer sequences are listed below:

HIES0: 5'- CTTCCTGTGTGTCTGTGTTTGTG-3'

HIES1: 5'- AATTGTCGACTATGGTCGCACATGTGCGATG-3'

HIES2: 5'- GACCACAGGGAGAGAATGTGTCTCTAGGTCAATCTTGAGGCCTTG-3'

HIES3: 5'- ACACATTCTCTCCCTGTGGTCATCTCCAACATCTGTCAGATGCCAAATG-3'

HIES4: 5'- AATTGTCGACAACCTGGTCCTGGCATGGTG-3'

HIES5: 5'- GAAACATGCTCTTCAAACACACTTAG-3'

HIES3': 5'- GACCACAGGGAGAGAATGTGT-3'

HIES5': 5'- ACACATTCTCTCCCTGTGGTC-3'

116: 5'-GTCAAACATGAGA-ATTAGCTTGCATG-3'

117 5'- ATGACAGAATCAACATCCCGTCGC-3'

2.1.2. Genotyping.

Genomic DNA was obtained by digesting tail or ear biopsies in proteinase K followed by isopropanol precipitation. A section of genomic DNA specific to the *Stat3ΔV463* mutant construct was amplified using primers HIES5 and HIES5'. Standard PCR conditions were used and a single 580 bp band was

amplified with the following conditions: 35 cycles at 94°C for 30 seconds, 60°C for 30 seconds, 72°C for 45 seconds. Samples were visualised on a 2 % agarose gel. Only mut-*Stat3* DNA yielded an amplified product.

2.2. Cell Isolation.

2.2.1. Thymus, Spleen, MLN and pLN.

Single cell suspensions were prepared in PBS (Gibco) supplemented with 0.1% BSA (Sigma Aldrich) by passing individual spleens, thymi, MLNs and pLNs through 70 μm cell strainers (BD Biosciences). Following centrifugation at 1500 rpm for 5 minutes, spleen cell pellets were resuspended in ACK lysis buffer (150 mM NH_4CL, 10 mM, $KHCO_3$, 0.1 mM NA_2.EDTA, pH 7.2-7.4) and incubated for 1-3 minutes at RT to lyse red blood cells. Thereafter 10 volumes of PBS/0.1% BSA was added and cells were refiltered through a 70 μm cell strainer. Cells were washed once to remove residual ACK lysis buffer, resuspended in PBS/0.1% BSA, and put on ice.

2.2.2. Colonic Lamina Propria Leukocyte (LPL) Isolation.

Luminal contents were removed and each colon was first cut longitudinally with scissors. Colons were then cut into approx. 0.5 cm pieces with a scalpel and placed in a 50 mL tube (BD Biosciences) containing ice-cold 10mL PBS/0.1% BSA. Tubes were inverted several times and the supernatants aspirated or poured off to remove any residual luminal contents. 10 mL pre-warmed (37°C) complete RPMI 1640 mouse media [RPMI 1640 (Sigma

Aldrich), 10% FCS (Gibco), 100 Units penicillin/streptomycin (PAA), 1% glutamine, .05 mM 2-mercaptoethanol, 10 mM HEPES (PAA)] containing 5mM EDTA (VWR) was added to each sample. Samples were incubated for 40 minutes at 37°C in a shaking incubator at 200 rpm to release epithelial cells. Supernatant was discarded and tissue was incubated in complete RPMI 1640 + EDTA for a further 20 minutes at 37°C in a shaking incubator at 200 rpm. The supernatant was discarded and samples were incubated in 20mL pre-warmed (37°C) compete RPMI 1640 containing 15 mM HEPES for 10 minutes at RT. This step served to neutralize EDTA, which would otherwise inhibit collagenase activity in the following step. Supernatants were then aspirated and 10mL of RPMI 1640 containing 15mM HEPES and 0.4-0.6 mg/mL type VIII collagenase (Sigma Aldrich) was added to each sample. Samples were incubated for 1 hour at 37°C while shaking at 200 rpm. Supernatants were filtered through a 70 μm cell strainer and washed in cold PBS/0.1% BSA. Percoll (GE) gradients consisting of a bottom layer of 3 mL 75% Percoll solution in PBS (P75) and a middle layer of 4 ml 40% Percoll solution in RPMI 1640 (P40) were prepared in a 50 mL tube. Cells released from the colon tissue by digestion were resuspended in 3 ml of 30% Percoll solution in PBS (P30) and gently placed on top of the 40% Percoll layer. Gradients were then centrifuged at 1800 rpm without brake for 20 minutes. The P30/P40 layer was aspirated and the colonic lamina propria leukocytes isolated from the P40/P75 interface. Cells were washed in PBS/0.1% BSA to remove excess Percoll and cell suspensions were resuspended in cold PBS/0.1% BSA and kept on ice.

2.2.3. B Cell Isolation.

Spleens were harvested from mut-*Stat3* and littermate control (WT) mice and single cell suspensions were prepared as described in 2.2.1. Cells were resuspended in complete RPMI 1640 supplemented with 1 mM EDTA for B cell enrichment. B cells were isolated by negative selection using CD43 MACS beads and LS columns (Miltenyi biotec) according to the manufacturers instructions.

2.2.4. $CD4^+$ T Cell Enrichment.

Spleens and peripheral lymph nodes were harvested from mut-*Stat3* and littermate control (WT) mice and single cell suspensions were prepared as described in 2.2.1. Cells were resuspended in PBS/0.01% BSA supplemented with 1 mM EDTA. $CD4^+$ cells were isolated using a $CD4^+$ T cell isolation kit and LS columns (Miltenyi biotec) according to the manufacturers instructions.

2.2.5. $CD11c^+$ Cell Enrichment.

Spleens were harvested from mut-*Stat3* and littermate control (WT) mice and single cell suspensions were prepared as described in 2.2.1. Cells were resuspended in PBS/0.01% BSA supplemented with 1 mM EDTA. $CD11c^+$ cells were isolated using CD11c microbeads and MS columns (Miltenyi biotec) according to the manufacturers instructions.

2.2.6. Purification of Naïve T Cells.

Spleen and peripheral lymph nodes were isolated and single cell suspensions were prepared as described in 2.2.1. $CD4^+$ T cell enrichment was completed as described in 2.2.4. Cells were then surface stained as described in 2.3.2., resuspended in 1xPBS/2% FCS supplemented with 1 mM EDTA and purified by cell sorting (Moflo, Dako Cytomation or FACS Aria, BD Biosciences). Naïve T cells were purified as $CD4^+CD44^{hi}CD62^{low}CD25^-$. To-Pro-3 (Invitrogen) or DAPI (Sigma-Aldrich) were used to exclude dead cells. Cell purity was >99% by cell sorting.

2.3. Flow Cytometry and Antibodies.

2.3.1. Restimulation for Intracellular Cytokine Staining.

Cell suspensions ($1*10^6$ cells/well) were restimulated in a 96 well round bottom plates (Corning) for 3.5-4 hours at 37°C in 200 μL complete IMDM mouse media [IMDM (Gibco), 10% FCS, 100 Units penicillin/streptomycin, 1% glutamine, .05 mM 2-mercaptoethanol, 10 mM Hepes] supplemented with 0.1 μg/mL phorbol 12-myristate 13-acetate (PMA) and 1 μg/mL ionomycin (both Sigma Aldrich) and Brefeldin A (eBioscience or GolgiPlug:BD Biosciences) or Monensin (GolgiStop:BD Biosciences). Monensin was used for intracellular staining panels involving IL-5, IL-10 and IL-13. Thereafter, cells were washed at least twice in 200 μL PBS and centrifuged at 1500 rpm for 5 minutes.

2.3.2. Surface Staining.

Cell suspensions ($1*10^6$ cells/well) were stained with anti-CD16/32 (eBioscience) and Fixable Viability Dye e780 or e450 (eBioscience) simultaneously in PBS for 10 minutes at RT in a V bottom 96 well plate (Corning). Cells were washed twice in PBS and spun down at 1500 rpm for 5 minutes. Thereafter all incubations were performed in 50 μL PBS supplemented with 0.1% BSA. Cells were washed at least twice by addition of 200 μl PBS/0.1% BSA and centrifugation at 1500rpm for 5 minutes. Cells were then incubated with the relevant antibodies for 15 minutes on ice in the dark. Biotinylated primary antibodies were detected by secondary staining using fluorescently labelled streptavidin conjugates. Samples were washed at least twice in 200 μl PBS/0.1% BSA and centrifuged at 1500 rpm for 5 minutes. Stained samples were resuspended in 200 μl PBS/0.1% BSA for analysis or fixed in 100 μl PBS/2% PFA for 10 minutes on ice, washed twice and resuspended in 200 μl PBS/0.1% BSA. Fixed samples were analyzed no later than 3 days following staining.

2.3.3. Intracellular Staining.

Following cell surface staining, cell suspensions were resuspended in 100 μL fixation/permeabilisation buffer (BD Biosciences or eBioscience) and incubated for 30 minutes in the dark at 4°C. 100 μL cell permeabilisation buffer (BD Biosciences or eBioscience) was added and cells were centrifuged at 1500 rpm for 5 minutes. Cells were resuspended in 50 μL of the relevant

antibodies prepared in permeabilisation buffer and incubated at 4°C for 30-45 minutes in the dark. Cells were washed three times by the addition of 100-200 μL of permeabilisation buffer and centrifuged at 15000 rpm for 5 minutes. After the final wash, cells were resuspended in 200 μL PBS/0.1% BSA for analysis.

2.3.4. Phosflow.

Freshly isolated splenic B cells were surface stained as described in 2.3.2. $2*10^6$ cells were resuspended in 500 μL complete RPMI media in a 12 well flat bottom plate (Corning) and placed at 37°C. After 10 minutes 250 μL pre-warmed complete RPMI media alone or supplemented with IL-6, IL-10 or IL-21 was added. Following 30 minutes, cells were rapidly fixed by adding an equal volume of pre-warmed fixation buffer (BD Biosciences) and rapidly pipetting up and down. Cells were incubated at 37°C for 10–12 min and transferred to eppendorf tubes. Cells were centrifuged at 6000 rpm for 1 min and washed twice with ice-cold PBS/0.1% BSA. Cells were permeabilized in 1 mL of pre-chilled permeabilization buffer III (BD Biosciences) for 15-30 minutes on ice. Cells were washed twice in PBS/0.1% BSA and stained with the relevant antibodies in 50 μL PBS/0.1% BSA at RT for 30-60 minutes in the dark. Cells were washed twice in PBS/0.1% BSA and resuspended in 200 μL PBS/0.1% BSA for analysis.

2.3.5. Antibodies.

The following anti-mouse antibodies were used in this study for *in vitro* stimulation and flow cytometry:

Specificity	**Clone**	**Source**	**Fluorochrome**	**Concentration**
***In vitro* stimulation**				
CD3 (agonistic)	1-45-2C11	eBioscience	N/A	5 μg/ml
CD28 (agonistic)	37.51	eBioscience	N/A	5 μg/ml
anti-IFN-g□□blocking)	XMG1.2	BioXCell	N/A	10 μg/ml
anti-IL-4 (blocking)	11B11	BioXCell	N/A	10 μg/ml
anti-IL-6 (blocking)	MP5-20F3	eBioscience	N/A	10 μg/ml
anti-IL-10 (blocking)	JES5-2A5	eBioscience	N/A	10 μg/ml
Surface Staining				
Fc Block (CD16/32)	93	eBioscience	N/A	5 μg/ml
B220	RA3-6B2	BD Bioscience	APC/PE/FITC/PerCP-Cy5.5	0.5 μg/ml
CD3	17A2	BD Bioscience	PerCP-Cy5.5	1 μg/ml
CD4	GK1.5	eBioscience	PE	1 μg/ml
CD4	RM4-5	eBioscience	PerCP-Cy5.5	1 μg/ml
CD4	RM4-5	Invitrogen	Qdot 605	0.5 μg/ml
CD8a	53-6.7	eBioscience	APC	1 ug/mL
CD11b	M1/70	eBioscience	PerCP-Cy5.5	1 μg/ml
CD11c	N418	eBioscience	PerCP-Cy5.5	
CD19	1D3	BD Bioscience	APC/PE/FITC	0.4 μg/ml
CD21/35	7G6	BD Bioscience	PE	0.2 μg/ml
CD25	7D4	BD Bioscience	FITC	1 μg/ml
CD43	S7	BD Bioscience	PE/FITC	1 μg/ml

CD44	KM114	BD Bioscience	APC	1 µg/ml
CD45.2	104	eBioscience	PerCP-Cy5.5/PE	1 µg/ml
CD62L	MEL-14	BD Bioscience	PE	1 µg/ml
CD95	JO2	BD Bioscience	PE	2 µg/ml
CD127 (IL-7Rα)	A20	eBioscience	PE	2 µg/ml
CD138	2M1-2	BD Bioscience	PE	2 µg/ml
CXCR5	2G8	BD Bioscience	Biotin	1 µg/ml
GR1	RB6-8C5	eBioscience	APC	0.5 µg/ml
ICOS	7E.17G9	BD Pharmingen	PE	1 µg/ml
IgM	715-095-020	Jackson	APC	1 µg/ml
IgD	11-26c.2a	BD Bioscience	PE	2 µg/ml
IgG1	A85-1	BD Bioscience	PE	0.1 µg/ml
IgG2a	R19-15	BD Bioscience	FITC	2 µg/ml
IgG3	R40-82	BD Bioscience	Biotin	2 µg/ml
NK1.1	PK136	eBioscience	PE	2 µg/ml
NKp46	29A1.4	BD Bioscience	V450	1 µg/ml
Siglec-F	E50-2440	BD Bioscience	PE	1 µg/ml
TCR-β	H57-597	eBioscience	APC/PE/PerCP-Cy5.5	1 µg/ml
Thy1.2	30-H12	Biolegend	PE-Cy7	1 µg/ml
Fixable Viability Dye	N/A	eBioscience	e450/e780	N/A
Streptavidin	N/A	BD Bioscience	PE/APC	0.5 µg/ml
Intracellular Staining				
IFN-γ	XMG1.2	eBioscience	FITC/APC/e450	2 µg/ml
IL-5	TRFK5	BD Bioscience	PE	2µg/ml
IL-10	JES5-16E3	eBioscience	PE/APC	2µg/ml
IL-13	Ebio13A	eBioscience	Alexa 647	2µg/ml

IL-17A	ebio17B7	eBioscience	PE/FITC/APC	2 µg/ml
IL-17F	9D3.1C8	Biolegend	PE/ Alexa 647	2µg/ml
IL-22	1H8PWSR	eBioscience	PE	2µg/ml
GM-CSF	MP-122E9	BD Bioscience	PE	2µg/ml
TNF-α	MP6-XT22	eBioscience	e450	2µg/ml
Foxp3	FJK-16S	eBioscience	FITC/APC	2 µg/ml
pTyr705 STAT3	4/P-STAT3	BD Bioscience	PE/APC	1:10
pTyr694 STAT5	47	BD Bioscience	PE/APC	1:10
Isotype Controls				
IgG1	R3-34	BD Bioscience or eBioscience	FITC/PE/APC	2-5 µg/ml
IgG1	A110-1	BD Bioscience or eBioscience	APC, Alexa 647	5 µg/ml
IgG2a	R35-95	BD Bioscience or eBioscience	FITC/PE/APC	2 µg/ml
IgG2a	MOPC-173	BD Bioscience	PE/APC	1:10
IgG2b	A95-1	BD Bioscience or eBioscience	PE, e450	5 µg/ml

Stained cells were acquired on a Dako CyAn, BD FACS Calibur or BD FACS LSRII flow cytometer and analysed using FlowJo software (TreeStar Inc.).

2.4. *In Vitro* Cell Cultures.

2.4.1. $CD4^+$ T Cell Polarization.

FACS sorted naïve $CD4^+$ T cells were obtained from spleens and pLNs as detailed in 2.2. In a 96 well flat bottom plate (Corning) $2*10^5$ T cells in 200 μL complete IMDM media were activated with plate-bound anti-CD3/anti-CD28 (5 μg/mL each, eBioscience). Treatment conditions were the following: Th1 [10 ng/mL IL-12 (R&D Systems) + 10 μg/mL anti-IL-4 (BioXcell)], Th2 [10 ng/mL IL-4 (Peprotech) + 10 μg/mL anti-IFN-γ (BioXcell)], Th17 [5 ng/mL TGF-β1 (R&D Systems) + 10 ng/mL IL-6 (Peprotech) + 10 μg/mL anti-IFN-γ + 10 μg/mL anti-IL-4], Treg [10 ng/mL TGF-β1 (R&D Systems) + 100 units IL-2 (Peprotech) + 10 μg/mL anti-IFN-γ + 10 μg/mL anti-IL-4]. Cells were incubated at 37°C for 72 hours prior to being restimulated and stained as described in 2.3.

2.4.2. B Cell CSR.

Splenic B cells were obtained as detailed in 2.2. In a 6 well flat bottom plate (Corning), $1.5*10^6$ B cells were cultured in 5 mL complete RPMI media supplemented with factors to promote CSR. B cells were activated for 24-96 hours at 37°C in the presence of 25 μg/mL LPS (Escherichia coli 0111:B4; Sigma-Aldrich) and 5 ng/ml IL-4 to induce CSR to IgG1/IgE, LPS and 2 ng/mL IFN-γ (PeproTech) to induce IgG2a CSR, or LPS and anti-δ-dextran to induce IgG3 CSR. Cells were analyzed for surface immunoglobulin expression by FACS at 96 hours and cell culture supernatants were analyzed by ELISA as

described below.

2.4.3. Immunoblotting.

MACS enriched $CD4^+$ T cells were activated in compete IMDM media in 48 well flat bottom plates (Corning) with plate-bound anti-CD3/CD28 for 3 days at 37°C. Cells were subsequently removed from plates, washed twice in complete media and resuspended in complete media supplemented with 100 units IL-2. Cells were expanded for 2 days in uncoated 24 well plates at 37°C. Cells were washed twice, resuspended in fresh media and rested for 2 hours at 37°C. Cells were subsequently restimulated for 5-45 minutes with 100 ng/mL IL-21. Cells were pelleted and lysed in Triton detergent buffer containing Complete Mini Protease Inhibitors Cocktail (Roche). Lysates were heated with Laemelli sample buffer at a 1:1 ratio at 85º C for 10 minutes before loading and resolving proteins in 4-20% pre-cast SDS-polyacrylamide gradient gels (BioRad). Gels were transferred onto nitrocellulose membranes (Amersham). Membranes were blocked with 5% powdered non-fat milk (Safeway/Vons) for 30 minutes, immunoblotted with anti-pTyr705-STAT3 or anti-STAT3 antibodies (Cell Signaling) diluted according to manufacturer recommendations, and then membranes were incubated with a horseradish peroxidase conjugated secondary antibody (Cell Signaling). Bands were visualised using an enhanced chemiluminescence detection kit (Amersham).

2.4.4. STAT3 Transcription Factor ELISA.

MACS enriched $CD4^+$ T cells were activated as for immunoblotting and restimulated for 15 minutes with 100 ng/mL IL-6. Freshly MACS enriched splenic B or $CD11c^+$ cells were stimulated with 100 ng/mL IL-6 for 15 minutes. STAT3 binding to a candidate oligonucleotide was assayed using the TransAm STAT3 assay kit (Active Motif) according to the manufacturer's instructions. 2 mg of whole cell lysate from stimulated or unstimulated cells was used for each assay.

2.4.5. Transgene Expression and Germline Transcripts.

To detect WT *Stat3*, *Stat3ΔV463*, and GL transcript expression levels, MACS selected B cells from mut-*Stat3* or littermate control mice were cultured in the presence of LPS plus IL-4 for 48 hours. RNA was extracted and processed as described in 2.7. and 2.8. The primer pairs used are listed below:

IgG1 GLT: 5'-ATCGAGAAGCCTGAGGAATGTG-3'
5'-GGCCAGTGGATAGACAGATG-3'

IgE GLT: 5'-GTTCTGAACTCAAGGTCACCAC-3'
5'-GTCGCAGGATGAATGGAGTAG-3'

Mature IgE: 5'-GACCAGGCTGCTGCTGGGTAG-3'
5'-CAGTGCCTTTACAGGGCTTC-3'

2.4.6. Digestion–Circularization-PCR (DC-PCR).

B cells from mut-*Stat3* or littermate controls were cultured in the presence of LPS + IL-4 for 96 hours. Dead cells were removed with a Ficol gradient and genomic DNA was isolated using a Purgene DNA isolation kit (Gentra) according to the manufacturer's instructions. 1 μg DNA was digested with EcoRI (New England Biolabs, Inc.) for 6 hours and 65 ng was ligated overnight with T4 DNA ligase in a volume of 100 μL (New England Biolabs, Inc.). Ligated DNA was concentrated using a Microcon YM-30 (Millipore) according to the manufacturer's instructions. Switch-junctions were amplified by PCR using primer pairs for Sμ–Sγ1, Sμ–Sε, and an internal control nicotinic acetylcholine receptor (nAChR).

The primers used are listed below.

Sμ–Sγ1:	5'- TTACAGGTCAAGACTGAGTAGAATC -3',
	5'-CTGTAAATGCTTCGGGTATTGG -3'
Sμ–Sε:	5'-CGGGTATTGGAAAATAATTGAATG-3',
	5'-GCAGAGCATCCTCACATACA-3'
nAChR,	5'-ACCTTGTCTCACACACAACCTTATTC-3'
	5'-AAGTTGGGATGTAGCTTCCATTATG-3'

Amplification conditions were:

Sμ–Sγ1:	30 cycles at 94°C for 1 minute, 59.5°C for 45 seconds, 72°C for 2 minutes
Sμ–Sε:	35 cycles at 94°C for 1 minute, 55°C for 1.5 minutes, 72°C for 2 minutes
nAChR:	30 cycles at 94°C for 1 minute, 63°C for 45 seconds, 72°C for 2 minutes.

2.4.7. Proliferation Using CFSE.

For assessment of *in vitro* proliferation, mut-*Stat3* or littermate control (WT) B cells were MACS purifed as described in 2.2. Cells were then labelled with 1 μM carboxyfuorescein succinimidyl ester (CFSE; Invitrogen) according to the manufacturer's instructions. Labeled cells were activated for 48 hours with LPS and IL-4 as described above. Following culture, cells were washed and counted using a hemacytometer slide under a light microscope. CFSE dilution was examined by FACS.

2.4.8. Retroviral Transduction of B Cells.

The murine stem cell virus (MSCV)–based retroviral vectors MSCV-IRES-GFP & MSCVId2-IRES-GFP were graciously provided by Dr Jonathan Keller, National Cancer Institute (Frederick, MD, USA) (*375*). Vectors were transfected into PlatE packaging cells by Lipofectamine 2000 (Invitrogen). Viral supernatants were collected every 24 hours for 3 days post-transfection

and used to infect cells in the presence of 4 μg/mL Polybrene (Sigma-Aldrich). Briefly, freshly MACS isolated B cells were stimulated with LPS for 12 hours, then infected with MSCV-Id2-IRES-GFP or MSCV-IRES-GFP twice over the subsequent 24 hours in the presence of LPS and IL-4. Transduction efficiency and cell surface expression of immunoglobulin subtypes were assessed by FACS at 72 hours after infection; supernatants for ELISA were also taken at this time. GL transcripts were assessed 48 hours post-infection.

2.5. *In Vivo* Studies.

2.5.1. Immunizations.

2.5.1.1. Foot Pad Immunization.

Six to eight week old mut-*Stat3* and littermate control mice were immunized in the hind foot pads with 100 g NP25-CGG precipitated in Alum (Thermo Fisher Scientific). The draining lymph nodes were harvested for further processing on day 7.

2.5.1.2. SEA Immunization.

Extracts from Schistosoma mansoni eggs were prepared as described84. The water soluble fraction was injected intraperitoneally (50 μg) two times a week for 2 weeks into mut-*Stat3* or control mice. Following an additional three-week rest period sera were collected.

2.5.2. Induction of Intestinal Inflammation.

2.5.2.1. Dextran Sodium Sulfate (DSS) Induced Colitis.

Colitis was induced in mice using DSS (molecular weight = 36,000–50,000; MP Biomedicals) dissolved in the drinking water at a concentration of 2.0% (m/v). Mice were exposed to DSS for 7 days, followed by a recovery period without DSS. Mice were monitored daily for weight loss and sacrificed when weight loss approached 20% of the original body weight at the start of the experiment.

2.5.2.2. *Citrobacter rodentium* Culture.

C. rodentium (ICC169; a gift from Professor Gadi Frankel) was grown at 37°C in Luria Broth (LB) supplemented with 50 μg/mL nalidixic acid (Sigma Aldrich) for a maximum of 18 hours. Liquid cultures were kept in vented Erlenmeyer flasks (Corning) in a shaking incubator set to 175 rpm. Bacteria were pelleted by ultracentrifugation at 6000 rpm for 10 minutes and concentrated 10 fold in PBS. The bacterial suspension was placed on ice and used to infect mice within 2 hours. Serial dilutions of the bacterial suspension were plated in triplicate on LB agar plates supplemented with nalidixic acid (50 μg/mL) to calculate the effective dose that mice were fed.

2.5.2.3. Induction of *C. rodentium* Colitis.

Adult mice (>8 weeks) were fed 4-5*10^9 cfu *C. rodentium* in PBS by oral gavage with a 22G curved needle on day 0 of the experiment. Mice were weighed and monitored for clinical signs of disease daily. Mice were sacrificed at the indicated time points. Blood was collected by cardiac puncture and serum was isolated by centrifugation in a serum separator tube. The colon and cecum were washed in PBS/0.1% BSA and sections taken for RNA extraction, bacterial colonization and histology. Spleens were weighed and sections of both the liver and spleen taken for analysis of bacterial colonization.

2.5.2.4. Generation of Bone Marrow Chimeras.

Recipient mice were γ-irradiated (2 × 550 RADs, with a 4 hour interval between each dose) and injected intravenously with single cell suspensions of 1*10^7 donor BM cells. Single cell suspensions of BM were prepared by flushing the femurs and tibias of mice with PBS/0.1% BSA. Bone marrow cells were passed through a 100 μm cell strainer and centrifuged at 1500 rpm for 5 minutes. Red blood cells were removed via ACK lysis followed by two washes in PBS/0.1% BSA. Mice were allowed to rest for at least 8 weeks to allow for full reconstitution of the hematopoietic system. Colitis was induced by infection with *C. rodentium* as described above.

2.5.2.5. Histological Assessment of Colitis.

Cecums and colons were extracted from *C. rodentium* infected mut-*Stat3* or littermate control mice and washed in PBS/0.1% BSA. Then sections of distal colon and cecum were fixed in buffered 10% formalin. After >2 weeks, sections (4.0 μm) were prepared from fixed tissue samples using a microtome and stained with haematoxylin and eosin. Scoring was performed by two researchers in a blinded fashion according to the criteria described below. Cecum and distal colon sections were calculated independently (Max = 15).

C. rodentium pathology scoring system:

A.	EPITHELIUM	HYPERPLASIA and/or	GOBLET CELL DEPLETION and/or	DAMAGE
	0	None	None	None
	1	Mild (1.5x)	Mild (25%)	Mild
	2	Moderate (2-3x)	Marked (25-50%)	Marked
	3	Severe (>3x)	Substantial (>50%)	Substantial
B.	INFLAMMATION IN LAMINA PROPRIA			
	0	None - few leucocytes		
	1	Mild - some increase in leucos at tips of crypts OR many lymphoid follicles		
	2	Moderate - marked infiltrate (notable broadening of crypt)		
	3	Severe - dense infiltrate throughout		
C.	SUBMUCOSA	EDEMA	INFILTRATION	Follicle
	0	None	None	None
	1	Mild	Mild	Enlarged
	2	Marked	Marked	-
	3	Both marked edema and marked infiltration		-
D.	AREA AFFECTED	(% of section)		
	0	None		
	1	up to 25%		
	2	25-50%		
	3	>50%		
E.	SEVERE	BLEEDING and/or	CRYPT ABSCESSES and/or	NECROSIS/ULCERS
	0	None	None	None
	1	Some	Few	-
	2	Marked	Many	Few/Small
	3	-	-	Large/Many

2.5.2.6. Evaluation of *C. rodentium* Colonization.

C. rodentium colonization levels were calculated by serially diluting tissue homogenates in PBS and plating them in duplicate on LB agar supplemented with nalidixic acid (50 μg/mL). *C. rodentium* colonies were identified as large colonies following 12-18 hours of incubation at 37°C. Tissue sections (0.2 cm pieces of cecum, distal colon, spleen and liver) were washed in PBS/0.1% BSA and weighed prior to homogenization. Tissue was homogenised in PBS in Lysing Matrix D Tubes (MP Biomedicals) at 2x 6.0 m/s for 10s in a FastPrep™ 24 homogeniser (MP Biomedicals).

2.5.3. Endotoxic Shock.

Mice were injected intraperitoneally with 250 μg LPS (*Escherichia coli* 0111:B4; Sigma-Aldrich) dissolved in 200 μL of PBS. Approximately 1.5 hours following injection, 50 μL of blood was collected from the tail vein. Serum was isolated via centrifugation in a microcapillary tube and serum cytokine levels were measured using a cytometric bead array (CBA) kit (BD Bioscieces) according to the manufacturers instructions. Animals were monitored every two hours for the first twelve and three additional times in the following twelve.

2.6. ELISA.

Serum immunoglobulin levels were measured from 8-12 week old mice by ELISA (Bethyl), using 3,3',5,5'-tetramethylbenzidine (Pierce) as a developing substrate. Levels of SEA specific antibody were determined by ELISA as

described previously (*376*). Serum immunoglobulin levels were measured from *C. rodentium* infected mice using a FlowCytomix Multiplex kit (eBioscience) according to the manufacturers instructions. Samples were acquired on a LSRFortessa. *C. rodentium* specific immunoglobulins were assessed as per the SEA protocol. Briefly, 96-well round-bottom plates (Fisher Scientific) were coated with heat killed *C. rodentium*. Serum samples from infected mice were serially diluted in 1% milk and added to coated or uncoated (to determine background) wells. Plates were incubated with HRP-conjugated goat anti-mouse IgM, IgG3 or IgA (Southern Biotechnology Associates), developed with Peroxidase Substrate and Stop Solution (KPL), and measured for absorbance at 450 nm.

2.7. RNA Extraction.

RNA from single cell suspensions was extracted using either the RNAqueous-Micro kit (Applied Biosystems/ABI) or the RNeasy Mini kit (Qiagen) according to the manufacturers' protocol. One or more DNAase steps were always included to minimize genomic DNA contamination. For RNA extraction from whole tissue, 0.25 cm pieces of cecum and distal colon were snap frozen in liquid nitrogen and stored at -80°C. Tissue was homogenised in TRI Reagent (Ambion) in Lysing Matrix D Tubes (MP Biomedicals) at 6.5 m/s for 15s in a FastPrep™ 24 homogeniser (MP Biomedicals). Total RNA was then extracted using the RiboPure™ Kit (Ambion) according to the manufacturers' protocol. RNA was quantified using a NanoDrop (Thermo Scientific). RNA was snap frozen on dry ice and stored at -80°C immediately.

2.8. Real-Time Quantitative PCR Analysis.

cDNA was synthesised using 1-5 μg of total RNA with Superscript III reverse transcriptase (Invitrogen) and oligo dT primers or random hexamers (Invitrogen or ABI), according to the manufacturer's instructions. RT-qPCR reactions were performed using TaqMan Gene Expression Assays or SYBR-green Master Mix (ABI). All probes were labeled with FAM/TAMRA. RNA that was not reverse transcribed was used as a negative control to assess DNA contamination. Samples were assayed in triplicate in a final reaction volume of 20μl using the Bio-Rad CFX96 RT-qPCR machine or an ABI 7500 Fast Real- Time PCR System. Gene expression levels for each individual sample were normalized to GAPDH, HPRT, or Actin. Mean relative gene expression was determined and expressed as $2^{-\Delta C(t)}$ ($\Delta C(t)=C(t)$gene of interest-$C(t)$control).

2.9. MIcroarray.

For microarray analysis, $CD11c^+$ cells MACS selected from mut-*Stat3* or littermate control spleens were activated with 25 μg/mL LPS (Escherichia coli 0111:B4; Sigma-Aldrich) or LPS and IL-10 (10 ng/mL; R&D Systems) for 18-24 hours in the presence of IFN-γ (10 ng/mL; Peprotech) and IL-4 (10 ng/mL; Peprotech). To minimize variability in the groups, autocrine IL-6 production was blocked with 10 μg/mL anti-IL-6 (eBioscience) in all conditions and IL-10 was blocked in the LPS alone condition using 10 μg/mL anti-IL-10

(eBioscience). RNA was purified using the MirVana miRNA isolation kit from Ambion according to the kit protocol. RNA purity and quantity were determined using the Nanodrop spectrophotometer. RNA was reverse transcribed, biotinylated and amplified using the MessageAMP™ II-Biotin Enhanced Single Round aRNA amplification kit (ABI) according to the manufacturer's instructions. 10 μg of biotinylated aRNA was fragmented and hybridized to GeneChip Mouse Genome 430 2.0 arrays from Affimetrix according to the manufacturer's protocols. Gene expression levels were determined using GeneChip Operating Software (GCOS; v1.1.1) and analysis was performed with GeneSpring software GX 12.1 (Agilent Technologies).

2.10. mRNA-Seq.

mRNA-Seq experiments and data processing were performed as previously described (*377*). Briefly, mRNA from LPS + IL-4 stimulated B cells was purified, fragmented and reverse transcribed. The DNA fragments were blunt-end ligated to the Illumina adaptors, amplified and sequenced using the Illumina Genome Analyzer II (Illumina). The Solexa GA pipeline (Version 1.0) was used to perform image analysis and base calling of the 36 nucleotide reads. Reads truncated to 30 nucleotides were then aligned with Tophat 1.0.8 (*378*) against mouse assembly NCBI build 37 (mm9) using splice junctions annotated in ENSEMBL release 54. Tophat was used to calculate expression estimates for each gene as reads per kb per million reads aligned to gene models (RPKM). Further analysis was carried out with GeneSpring software GX 7.3.1 (Agilent Technologies).

2.11. ChIP-Seq.

ChIP-Seq experiments and data processing were performed as previously described (*377*). Briefly, B cells ($2*10^7$) were treated with MNase to generate mononucleosome fractions to analyze histone modifications using the following antibodies (anti-H3K4me3, ab8580, Abcam; anti-acetyl-H3, 06-599, Millipore). For all non-histone ChIP experiments, cells were chemically cross-linked and sonicated to generate fractionated genomic DNA and immunoprecipitated with anti-STAT3 (14-6727, eBiosciences), anti-phospho-STAT3 (Ser727) (9134, Cell Signaling), anti-STAT6 (sc981, Santa Cruz), anti-p300 (C-20) (sc585,Santa Cruz), anti-H3K4me1 (ab8895, Abcam), or anti-H3K4me3 (ab8580, Abcam). DNA fragments were blunt-end ligated to the Illumina adaptors, amplified and sequenced using the Illumina Genome Analyzer II (Illumina). Sequenced reads of 36 bp were obtained using the Illumina Analysis Pipeline. All reads were mapped to the mouse genome (mm9) and only uniquely matching reads were retained. Those unique tags were mapped into non-overlapping 200 bps windows of the genome. Significant peaks (islands) were identified based on window tag-count threshold determined from a P value of 0.05 (defined by Poisson background model).

2.12. Statistics.

Non-parametric tests were used for all statistical analyses and calculated using Prism (Graphpad). Data is depicted as the mean ± standard error of the mean (SEM) and the statistical tests used are detailed in the figure legends. Differences were considered to be statistically significant when $p<0.05$.

3. Chapter 3: Generation of the STAT3ΔV463 Mouse Model of HIES.

3.1. Introduction.

The STAT family of DNA-binding proteins comprise a small, but critical subset of proteins involved in growth, development and homeostasis (*44*, *379*). These transcription factors are particularly important for transmitting cytokine signals and in this respect are essential for normal hematopoiesis, host defense, and immunoregulation (*380*). Each STAT family member exhibits distinct functions and is preferentially phosphorylated in response to select cytokines. Once phosphorylated, STAT molecules dimerize and accumulate in the nucleus where they regulate transcription (*44*). Among the 7 STAT family members, STAT4 and STAT6 have very discrete functions, whereas others like STAT5A, STAT5B and STAT3 have broader functions in multiple cells and tissues (*2*).

The essential role of STAT3 is highlighted by the fact that, in contrast to all other STATs, its germline deletion results in embryonic lethality (*45*). This is primarily due to STAT3's role in leukemia inhibitory factor (LIF) signaling and placental integrity. However, selective inactivation of *Stat3* in various adult mouse tissues also leads to a wide spectrum of defects (*44*). Within the immune system alone, *Stat3* deficiency results in impaired $CD4^+$ T cell differentiation, defective dendritic cell maturation, and altered neutrophil homeostasis (*53*, *56*, *57*, *218*, *381-384*). Furthermore, *Stat3-/-* myeloid cells are hyperactive and promote fatal autoimmunity and inflammatory bowel

disease (IBD). In humans, STAT3 can serve as an important driver of malignant transformation, and constitutive STAT3 activation is linked to a number of cancers (*25*). Conversely, dominant-negative mutations in *STAT3* have been shown to be causative for the multi-system disorder hyper IgE or Job's syndrome (*70*, *71*).

AD-HIES is characterized by high incidence of cutaneous and sinopulmonary infections, as well as elevated serum IgE (*65*, *385*). Consistent with the broad functions of STAT3, patients with this syndrome also exhibit a variety of skeletal, dental and soft-tissue defects, and have increased incidence of lymphoma (*386*). Recent work has implicated deficiency in Th17 cells as an important aspect of the host defense defects noted in this disorder (*72*, *75-78*). STAT3 directly regulates a number of genes involved in differentiation of Th17 cells (*219*), which are critical for protection against extracellular bacteria and fungi that typically infect AD-HIES patients (*387-390*). However, the mechanisms responsible for various other aspects of the disease, including the cardinal feature of elevated IgE levels, have not been elucidated. Furthermore, it remains unclear whether phenotypic differences between human AD-HIES and mouse knockouts reflect species-specific discrepancies in STAT3 function, or incomplete STAT3 inactivation in AD-HIES patients. Tissue specific deletions of *Stat3* have been greatly informative in defining specific functions of this important transcription factor, yet provide an incomplete picture of STAT3 function in the immune system. Indeed, STAT3 has been shown to regulate opposing pro- and anti-inflammatory networks, but the net role of STAT3 in an immune response has been impossible to

elucidate. To resolve these issues and to obtain a clearer picture of STAT3's function as it relates to both AD-HIES and immune homeostasis, we decided to generate a murine model of this disease.

3.2. Results.

3.2.1. Selection of Mutation and Targeting Strategy for AD-HIES Mouse Model.

Eighty-two unique heterozygous *STAT3* mutations have been identified in patients with AD-HIES. The majority of these are focused in the DNA-binding and SH2 domains and can be roughly broken into three classes: point mutations, duplications or deletions, and mutations within non-coding regions that affect RNA splicing (Figure 3.1.A). Five hot spots, or regions of common mutation in multiple patient cohorts, have been identified: R382, F384, R423, V463 and V637 (*70*-*72*). Within these regions, four mutations are particularly recurrent, with R382W, R382Q, V463del, and V637M being identified in 21%, 11%, 7%, and 14.5% of patients, respectively, accounting for more than 53% of the mutations identified to date (*70*-*72*, *391*-*396*).

The heterozygous mutations work in a dominant-negative fashion, with mutant STAT3 proteins being thought to form inactive dimers with wild-type (WT) STAT molecules (*71*). JAK-mediated phosphorylation of STAT3 in response to cytokine signals thus results in a net hypomorphic DNA-binding activity within the nucleus of cells carrying the mutations (Figure 3.2.A). We

hypothesized that, in such a system, the net transactivation potential of STAT3 would be solely dependent on the ratio rather than the absolute number of WT and mutant STAT3 proteins. Thus, insertion of mutant *Stat3* copies into WT mice, without replacement of endogenous *Stat3* sequences, would be able to reproduce the reduced DNA-binding potential of STAT3 observed in AD-HIES patients (*75*). Usage of such an insertional strategy, as oppose to a standard gene knock-in approach, would allow us to look at immunologic responses in the context of a gradient of STAT3 activity (depending on the number of mutant copies inserted).

Bacterial artificial chromosome (BAC) vectors, can accommodate large genomic intervals, making them ideal for use in systems where expression of a gene from endogenous promoters and enhancers, which can be located tens of kilobase pairs up- or down-stream of the gene coding sequence, is required. As transgenes, BACs generally offer stable integration and show a linear relationship between copy number and the level of expression of integrated genes. In addition, the use of homologous recombination in *E. coli* to modify BACs prior to microinjection has been well established (*374*, *397-404*). Therefore, we chose to insert a AD-HIES mutation into a *Stat3* competent BAC and subsequently use this vector for generation of a BAC-transgenic murine model of AD-HIES.

BAC RP24-236G5, which carried the complete *Stat3* gene as well as ~ 60 Kb regions up- and downstream, was selected as the template for generation of

the modified construct. BAC modification by homologous recombination requires long segments of DNA both up and downstream of the targeted change so *Stat3*'s location in the middle of BAC RP24-236G5 made it ideal for targeting. Additionally, with 60 Kb both up- and downstream present, we were quite confident that regulatory elements necessary for endogenous-like expression patterns were included. In the mouse, *Stat3*, *Stat5a*, and *Stat5b* lie next to one another in the genome, likely due to a genetic duplication in an early mammalian ancestor (*405*). As a result, the complete *Stat5a* gene and promoter were encoded by BAC RP24-236G5 and were thus included in the construct. However, only the proximal portion of *Stat5b* was present.

Of the eighty-two *Stat3* mutations identified in AD-HIES, we chose to delete valine 463 of the DNA-binding domain in the mouse model. Our rationale was three-fold. Firstly, mutations of the *Stat3* DNA-binding domain are both the most prevalent and well characterized functionally. Secondly, *Stat3ΔV463* is one of the most common mutations in this disease (7% of all reported cases). Thirdly, BAC modification by homologous recombination works most efficiently when large rather than small modifications are made, and the positioning of valine 463 allowed the deletion of an adjacent intron to be incorporated into the targeting strategy.

The V463 deletion was incorporated into BAC RP24-236G5 using a slight modification of the technique first described by Misulovin and colleagues (*373*). A recombination cassette consisting of two ~500 bp regions of

homology, which flanked the desired V463 and intron deletion, was inserted into the multiple cloning site (MCS) of the low copy shuttle vector pSV1-RecA. The shuttle vector carried the bacterial recombinase RecA and was transfected into RP24-236G5 competent *E. coli*. RecA-mediated homologous recombination between the *Stat3*∆V463 recombination cassette and unaltered BAC yielded BAC clones carrying the *Stat3*∆V463 mutation (Figure 3.3.A). Purification, linearization and subsequent pronuclear injection of the modified BAC into C57BL/6 zygotes yielded transgenic mice carrying mutant *Stat3* copies (Figure 3.3.B).

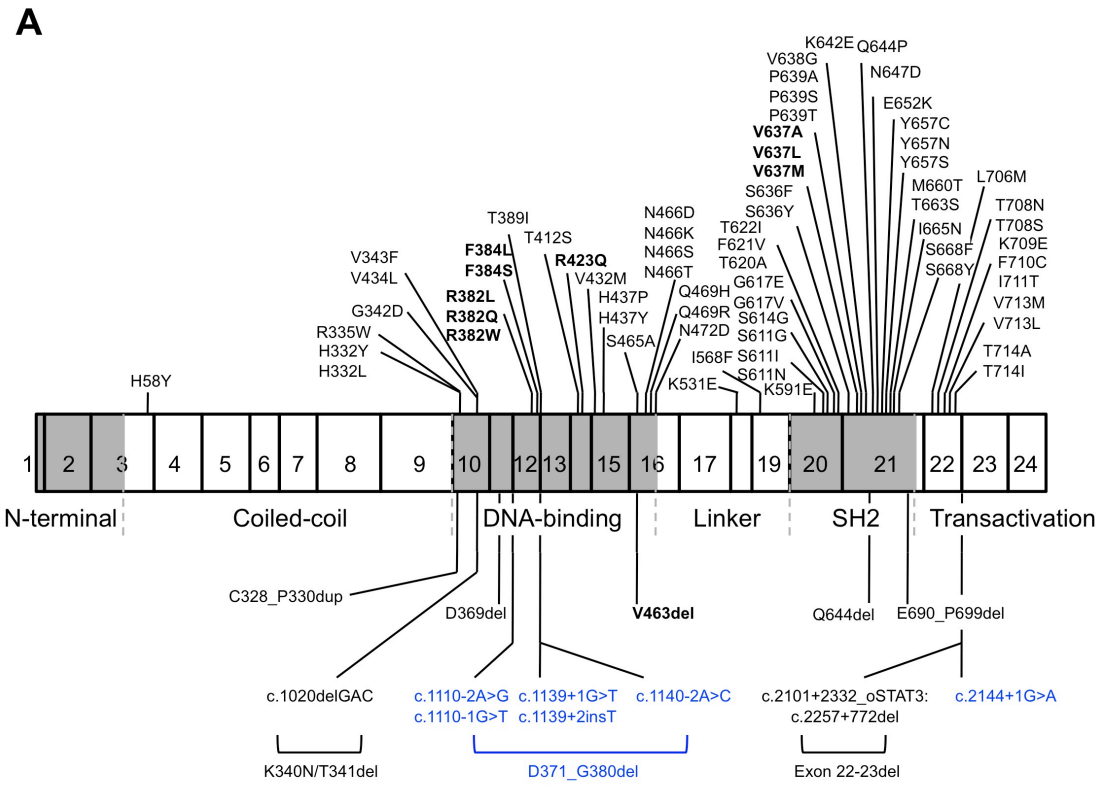

Figure 3.1. Schematic of *STAT3* showing mutations linked to autosomal dominant hyper-IgE syndrome (HIES)

(A) *STAT3* is made up of 24 exons and 6 domains. 82 unique *STAT3* mutations have been identified in patients with HIES. The majority of these are focused in the DNA binding and Src homology 2 (SH2) domains and can be roughly broken into three classes: point mutations (top half of the figure), duplications and deletions (bottom half of the figure), and mutations in introns that affect RNA splicing (shown in blue). Mutations have been identified in a number of studies and distinct patient pools, but 5 "hot spots", or regions of common mutation, (shown in bold) have been identified: arginine 382, phenylalanine 384, arginine 423, valine 463 in the DNA-binding domain and valine 637 in the SH2 domain. The positions of all known mutations are indicated in amino acid nomenclature with the exception of those starting with c., which are shown in nucleotide nomenclature.

(B) Figure modified from (*426*).

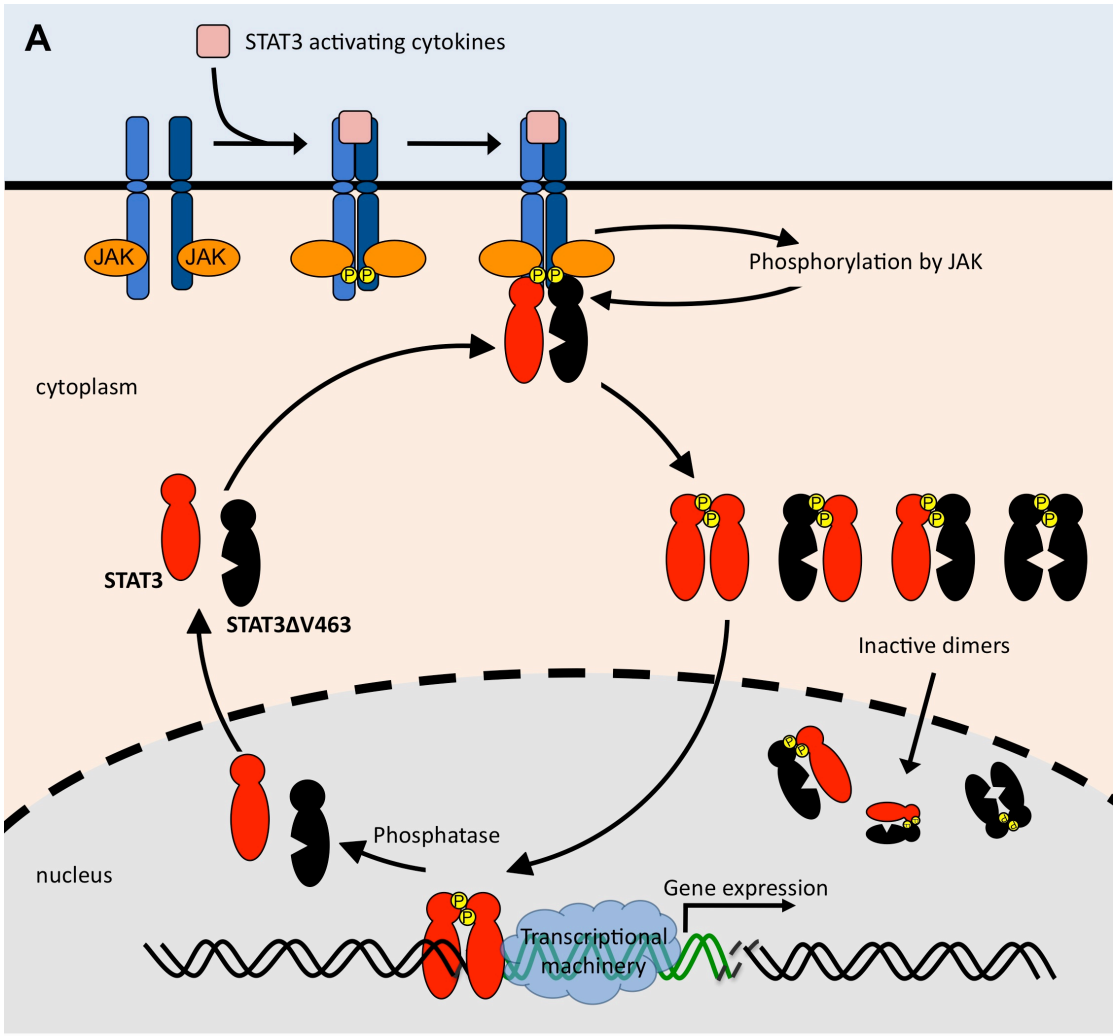

Figure 3.2. STAT3 mutations in the JAK-STAT signalling pathway

(A) Ligand binding to cytokine receptors results in a conformational change that activates associated Janus kinase (JAK) molecules. JAKs phosphorylate the cytoplasmic portions of cytokine receptors, creating binding sites for STAT proteins. Bound STATs are subsequently phosphorylated by JAKs and dimerize via SH2 domain:phospho-tyrosine interactions. Active dimers translocate to the nucleus, bind to promoters, and activate transcription through recruitment of the RNA polymerase II machinery. The signal-transduction cycle is terminated by dephosphorylation of activated STAT proteins by nuclear phosphatases. Mutant STAT proteins, such as STAT3ΔV463, are incapable of binding DNA but still interact with wild-type and mutant STAT proteins, resulting in nonproductive dimers that can accumulate in the nucleus and have a dominant negative effect on STAT function.

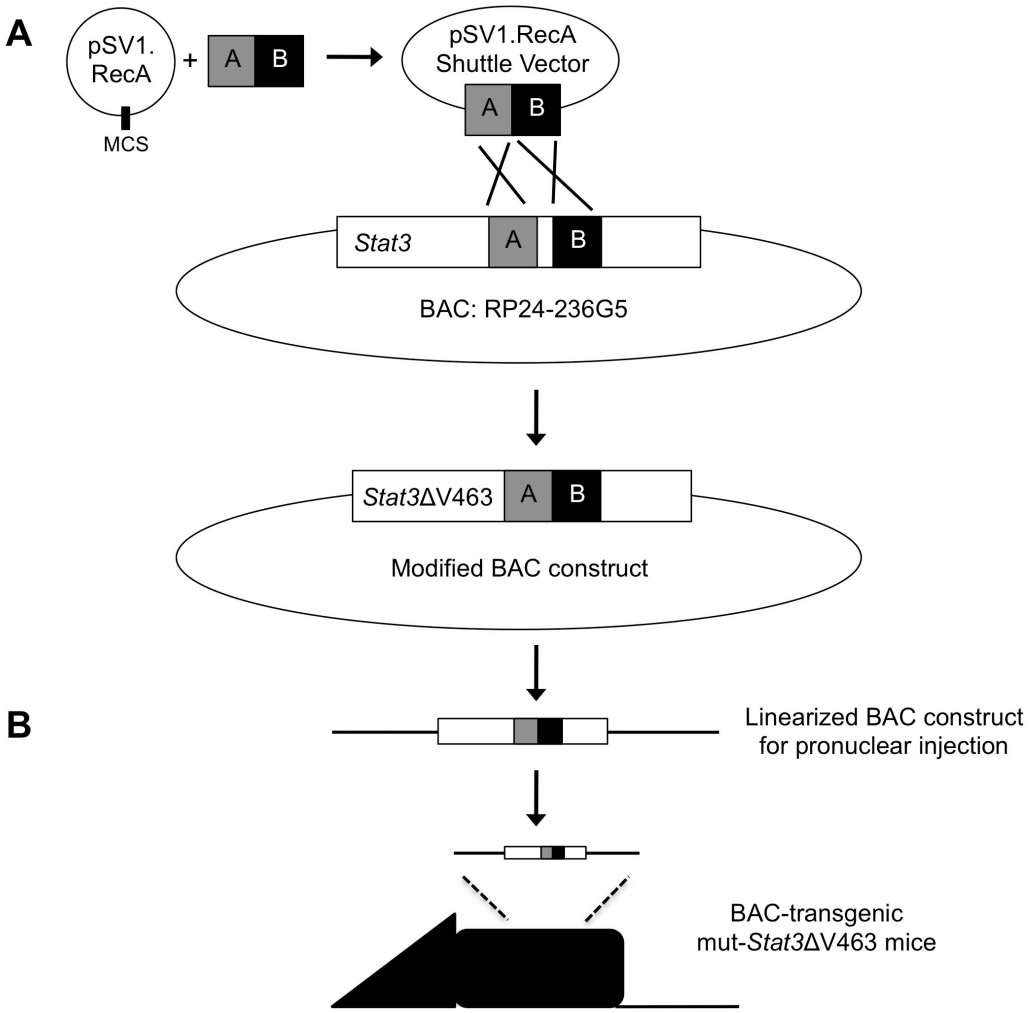

Figure 3.3. Strategy for targeted BAC deletion of V463 in *Stat3*

(A) The recombination cassette (A B) consisted of two ~500 bp segments (A and B) homologous to regions of *Stat3* located immediately up and downstream of V463 and the intronic region to be deleted in the final construct. The recombination cassette was ligated into the multiple cloning site (MCS) of the pSV1.RecA shuttle vector, which carried the bacterial recombinase RecA, a temperature-sensitive origin of replication, and a tetracycline resistance gene. The recombination cassette was transformed into bacteria containing BAC RP24-236G5, which carried the complete Stat3 gene, ~60 Kb regions up and downstream, and a chloramphenicol resistance gene. A multi-step process, altering both temperature and bacterial growth media (antibiotics), allowed for the selection of bacterial colonies that had undergone homologous recombination, inserting the mutated recombination cassette in BAC RP24-236G5 and the native *Stat3* sequence in the shuttle vector.

(B) The *Stat3ΔV463* modified BAC construct was purified, linearized to remove the chloramphenicol resistance gene and bacterial origin of replication, and pronuclear injected into C57BL/6 zygotes. This process resulted in transgenic mice that carried copies of mutant *Stat3ΔV463* in addition to their endogenous wild-type *Stat3* sequences.

3.2.2. Generation of the *Stat3*ΔV463 Recombination Cassette.

The first step in our targeting strategy was generation of the recombination cassette. The cassette carried both the desired *Stat3*ΔV463 modification and flanking regions of *Stat3* homology, to be used to target the mutation to BAC RP24-236G5. The originally published technique involved restriction digestion and cloning of target sequences into the shuttle vector (*374*). To reduce the number of cloning steps, we used the modified protocol introduced by Misoluvin and colleagues (*373*). Accordingly, multi-template PCR, starting from BAC RP24-236G5, was used to generate the recombination cassette (Figure 3.4.). In order to achieve deletion of both V463 (eighth amino acid residue encoded by exon 16) and intron 15, three PCR reactions were used. First, a region upstream of the deletion (containing intron 14 through exon 15) and a region downstream of the deletion (containing I464 of exon 16 through intron 17) were amplified from the unmodified RP24-236G5 using primers that created both external SalI cloning sites and 21 bp of internal homology between the two products (Figure 3.4.A). The two DNA products were subsequently used as a template for a second round of PCR using only two external primers (Figure 3.4.B) (*406*, *407*). This multi-template reaction yielded a product that consisted of the fused constituents. The 21 nucleotide sequence added by the primers of the first PCR reaction, and subsequently used to join the initial two PCR products, consisted of silent mutations for the first seven amino acid residues of exon 16 (T456-V462). Thus, the completed recombination cassette carried *Stat3* exons 15-17, with silent mutations incorporated into exon 16 and deletion of both V463 and intron 15 (Figure 3.4.B).

To avoid PCR-derived mutations during synthesis of the recombination cassette, the high fidelity thermostable polymerase KOD (Novagen) was used for a maximum of 30 cycles per reaction (*408*). PCR products were purified after each reaction by agarose gel electrophoresis. To avoid exposure of DNA to potentially damaging UV irradiation, crystal violet was used to visualize bands under ambient light. Small aliquots of the gel-purified PCR products were run on ethidium bromide (EtBr) containing agarose gels to verify their size and concentration (Figure 3.5.A).

Next, the recombination cassette was inserted into the pSV1.RecA shuttle vector, which carried a temperature sensitive origin of replication, tetracycline resistance gene, RecA and MCS with SalI restriction site (Figure 3.5.B). pSV1.RecA amplifies poorly when devoid of an insert so we grew up a pSV1.RecA containing a 2 Kb insert used in a previous BAC targeting strategy. pSV1.RecA was SalI digested overnight and treated with alkaline phosphatase. The linearized vector was purified by gel electrophoresis to remove the old insert. Complete removal of the insert was verified by running aliquots of both the uncut and SalI digested pSV1.RecA on an EtBr agarose gel (Figure 3.5.C). We had been sure to design the recombination cassette to contain no SalI sites other than those added by external primers HIES1 and HIES4 (Figure 3.4.), so SalI digestion of the synthesized recombination cassette yielded a single product. The digested recombination cassette was ligated into pSV1.RecA overnight and the ligation product was transformed

into *E. coli*. Transformants were grown on LB-tet plates overnight; individual colonies were screened for insertion of the recombination cassette using primers 116 and 117, which amplified across the SalI insertion site (Figure 3.5.B). PCR products were run on an EtBr agarose gel and positives selected by the presence of a ~1 Kb band, corresponding to the size of the recombination cassette (Figure 3.5.D). 66% of transformants screened contained the recombination cassette.

Four colonies competent for the recombination cassette were amplified in LB-tet media. The DNA was extracted and amplified using KOD and primers 116 and 117. The 1 Kb product was purified on a crystal violet agarose gel and submitted for DNA sequencing. Sequence files were aligned with WT *Stat3* (Figure 3.6.A). All sequenced colonies showed deletion of intron 15, silent mutations in exon 16, and deletion of the V463 codon. No other modifications were noted. The completed shuttle vector, with recombination cassette, could now be used for targeting of the *Stat3*ΔV463 mutation to BAC RP24-236G5.

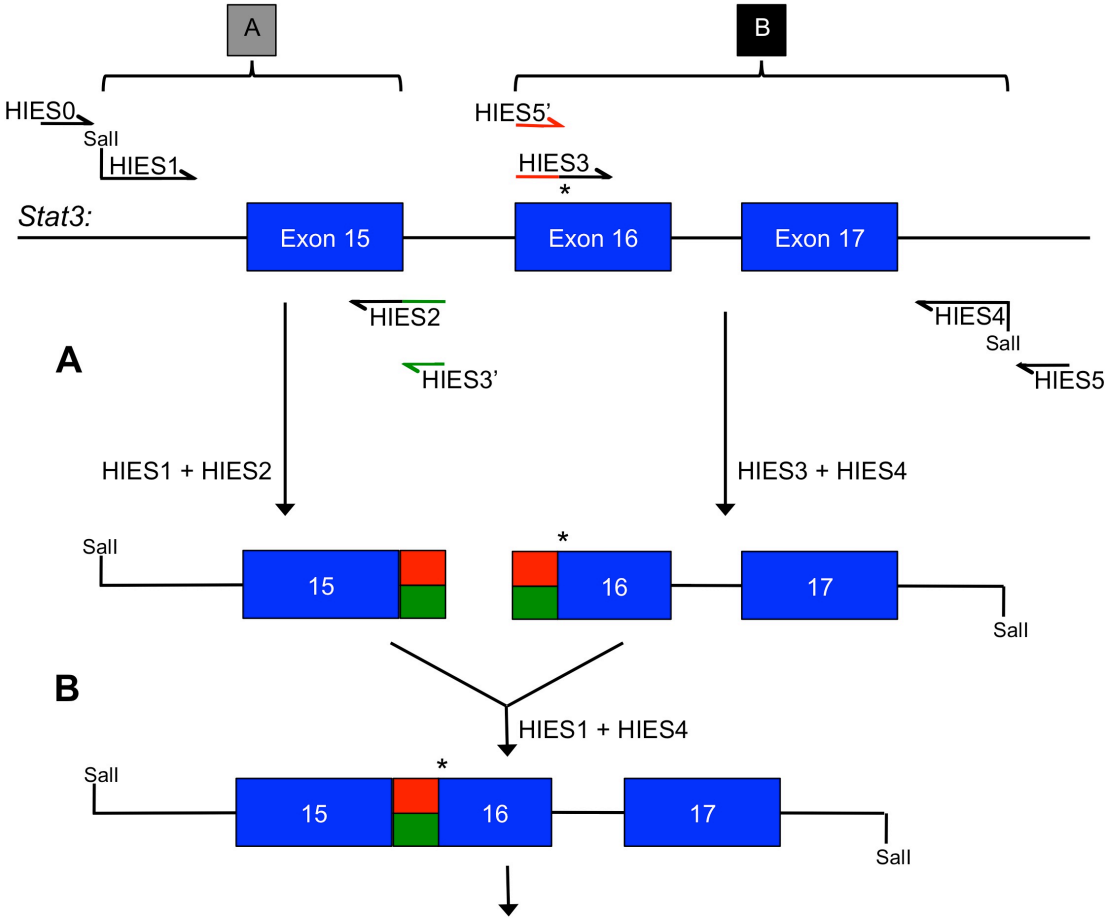

Figure 3.4. Strategy for construction of recombination cassette

(A) Segments A and B from Figure 3.3. were amplified from BAC RP24-236G5 using primer pairs: HIES1/ HIES2 and HIES3/HIES4, respectively. External primers HIES1 and HIES4 each consisted of ~20 nucleotides complimentary to either segment A or B and capped with a SalI restriction site (GTCGAC) and four non-annealling nucleotides. Primer HIES3 consisted of 24 nucleotides complimentary to exon 16 (encoding amino acids 464-471) fused to a 21 nucleotide non-annealing overhang (shown in red) that formed silent mutations for amino acids 456-462; the codon for valine 463 was omitted(*). Primer HIES2 consisted of 24 nucleotides complimentary to the terminal portion of exon 15 (encoding amino acids 447-455) and a 21 nucleotide sequence (shown in green) that was complimentary to the mutated sequence in HIES3 but not endogenous sequences.

(B) Multi-template PCR using HIES1 and HIES4 external primers with the PCR products from A resulted in the recombination cassette product which was SalI digested and ligated into the pSV1.RecA shuttle vector.

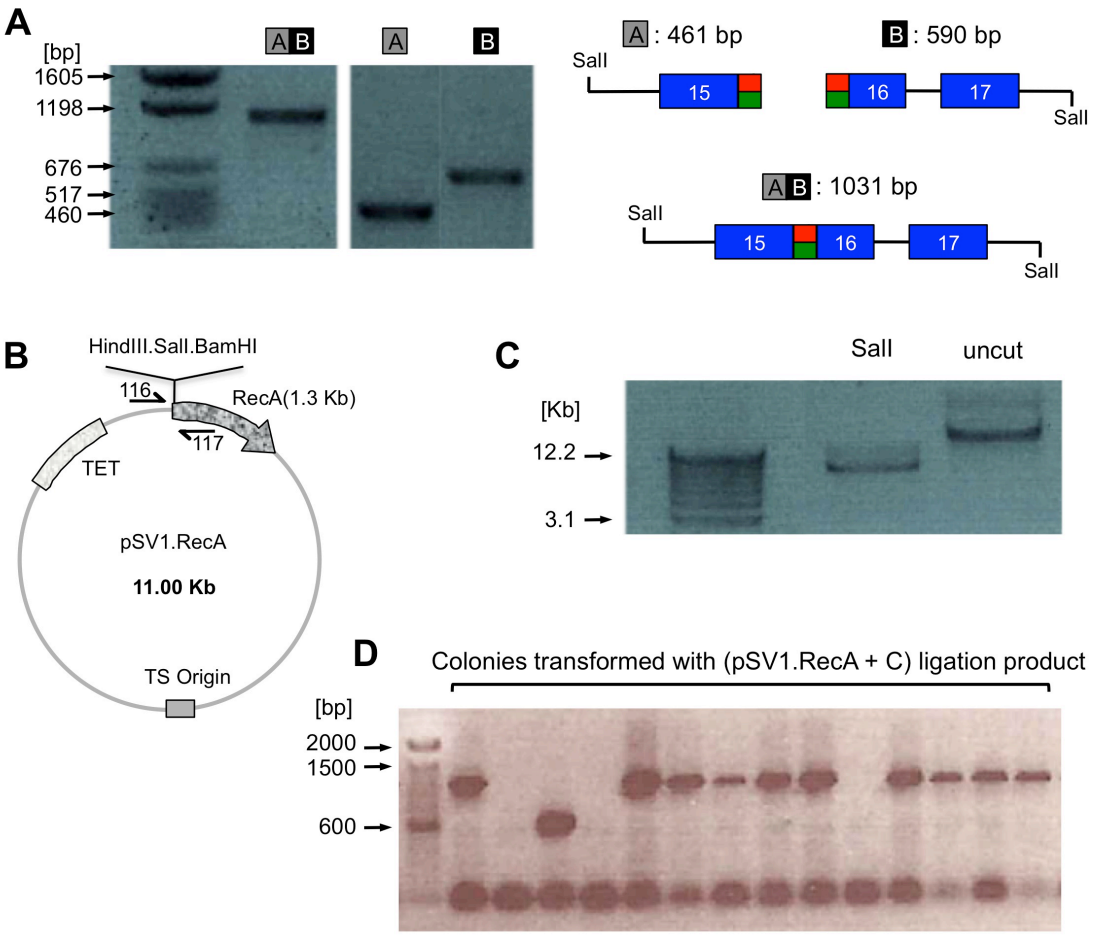

Figure 3.5. Generation of pSV1.RecA shuttle vector with recombination cassette

(A) Segments A, B, and A B were synthesized as described in Figure 3.4. PCR products were purified by running on a 1% agarose gel containing crystal violet [1 µg/mL] at each step. 10 ng each of the initial products were used in the multi-template PCR. Product sizes and concentrations were calculated from an ethidium bromide (EtBr) containing agarose gel (shown).

(B) A diagram of the pSV1.RecA shuttle vector containing a temperature sensitive origin of replication (TS), tetracycline resistance gene (TET), bacterial recombinase A (RecA) and MCS including a SalI restriction site. Primers 116 and 117 anneal just outside of the MCS and were used to test for insertion of the recombination cassette (D).

(C) A pSV1.RecA shuttle vector containing a SalI ligated 2 Kb insert from a previous study was SalI digested overnight and purified on a crystal violet agarose gel. Both the SalI digested and uncut pSV1.RecA were run on an EtBr agarose gel for quantitation (shown).

(D) Bacteria transformed with the ligation product of SalI digested A B and pSV1.RecA were grown overnight on tetracycline LB-agar plates. Colony PCR using primers 116 and 117 was used to select for colonies containing the 1 Kb recombination cassette. PCR products were run on an EtBr agarose gel (shown). 65 colonies of 98 screened contained the recombination cassette.



Figure 3.6. Sequencing of recombination cassette confirms mutation

(A) Four positive colonies from Figure 3.5.D were grown in LB-tet overnight. DNA was extracted and amplified using primers 116 and 117 and the high fidelity KOD DNA polymerase. The 1 Kb product was purified on a crystal violet agarose gel and submitted for DNA sequencing. Sequence files were aligned with endogenous *Stat3* using ClustalV software (higgins et al 1992) with minor manual adjustment. Recombination cassette sequences appear in black and *Stat3* in gray with exons 15-17 in blue. The mutated region of exon 16 in the recombination cassette is highlighted in red.

3.2.3. Homologous Recombination Leads to *Stat3*ΔV463 BAC Construct.

As previously described, the recombinant pSV1.RecA was transformed into competent BAC RP24-236G5 containing bacteria (*374*). pSV1.RecA carried a tetracycline resistance gene and the BAC carried a chloramphenicol resistance gene, so co-transformants were selected by growth on LB-chloro-tet plates at 30° C overnight (Figure 3.7.A).The first step of the homologous recombination process is referred to as co-integration. It occurs by crossing over between one of the homology arms of the recombination cassette and the target BAC. In our case, this resulted in the incorporation of pSV1.RecA into RP24-236G5 (Figure 3.7. B). We selected for this process by increasing the temperature to 45° C, thus rendering the pSV1.RecA temperature-sensitive origin of replication inactive. Since the tetracycline resistance gene was contained in the pSV1.RecA vector, colonies that put the tetracycline resistance gene under the control of the BAC origin of replication (still active at 45° C) through the process of co-integration, had a survival advantage when grown on LB-chloro-tet plates. 288 colonies selected by this process were screened by colony PCR for recombination at the left- or right-arm of homology. Primer pairs were specific for recombination at the left-arm: HIES0 (annealed outside of the recombination cassette in intron 14 of *Stat3*), HIES3' (annealed to the mutated portion of exon 16 within the recombination cassette) or right-arm: HIES5' (complement of HIES3'), HIES5 (annealed outside of the recombination cassette in intron 17 of *Stat3*) (diagrammed in Figures 3.4. and 3.7.). PCR products were run on an EtBr agarose gel and positives selected as having a bright, distinct band of the expected size (Figure 3.8.A). Recombination efficiency was 15% and 19% at the left- and

right-arm respectively.

The second step of the process is referred to as resolution. It occurs by a second homologous recombination event that occurs within the co-integrate. In our case, recombination of the remaining arm of homology looped out the pSV1.RecA shuttle vector. This yielded the desired BAC construct, with the *Stat3*∆V463 recombination cassette precisely integrated, and the free shuttle vector now carrying the unmodified exon 15-17 region of *Stat3* (Figure 3.7.C). We selected for resolution through addition of the lipophilic chelating agent, fusaric acid. Fusaric acid has been shown to be useful for selection of loss of tetracycline resistance in *E. coli* (*409*, *410*). Colonies selected by 2 days growth on LB-chloro-fusaric acid plates were screened for complete recombination/resolution by PCR. Primers annealing outside of the recombination cassette (HIES0 and HIES5) were used; the amplified products were run on an EtBr agarose gel (Figure 3.8.B). Efficiency of the second homologous recombination step was 60%. As HIES0 and HIES5 annealed to both WT *Stat3* and the *Stat3*∆V463 construct, we looked for the presence of both WT (2,224 bp) and mutant (1.061 bp) bands. No WT bands were detected. However, this did not rule out the possibility of bacteria carrying unmodified RP24-236G5, as the PCR extension times may have been insufficient to fully amplify the WT fragment.

To exclude any clones that carried either the unaltered BAC, or BACs that had undergone gross rearrangements of non-targeted regions, we isolated DNA from five independently modified BAC clones, as well as the original unmodified RP24-236G5, and analyzed by restriction digestion (Figure 3.9.). Isolated BAC DNA aliquots were digested overnight with BamHI, EcoRI, EcoRV, HindIII, or PstI and run at low voltage on 0.7% agarose gels. The unmodified and *Stat3*∆V463 BAC constructs provided at least one unique digestion product size per enyzme (Figure 3.9.A). Analysis of EcoRV (Figure 3.9.B) and HindIII (Figure 3.9.C) digests identified two clones with digestion products solely consistent with *Stat3*∆V463 mutation. Insufficient DNA to allow accurate analysis was extracted from a third clone, and the two remaining clones potentially carried unmodified BACs. Comparison of all bands with those expected from the DNA sequence, ruled out gross rearrangements of the non-targeted BAC regions (Figure 3.9.D). DNA extracted from the two colonies thought to carry only the *Stat3*∆V463 BAC construct was KOD amplified using primers HIES0 and HIES5 and submitted for sequencing. The sequencing results confirmed correct integration of the *Stat3*∆V463 recombination cassette (data not shown). Glycerol stocks of correctly recombined colonies were prepared.

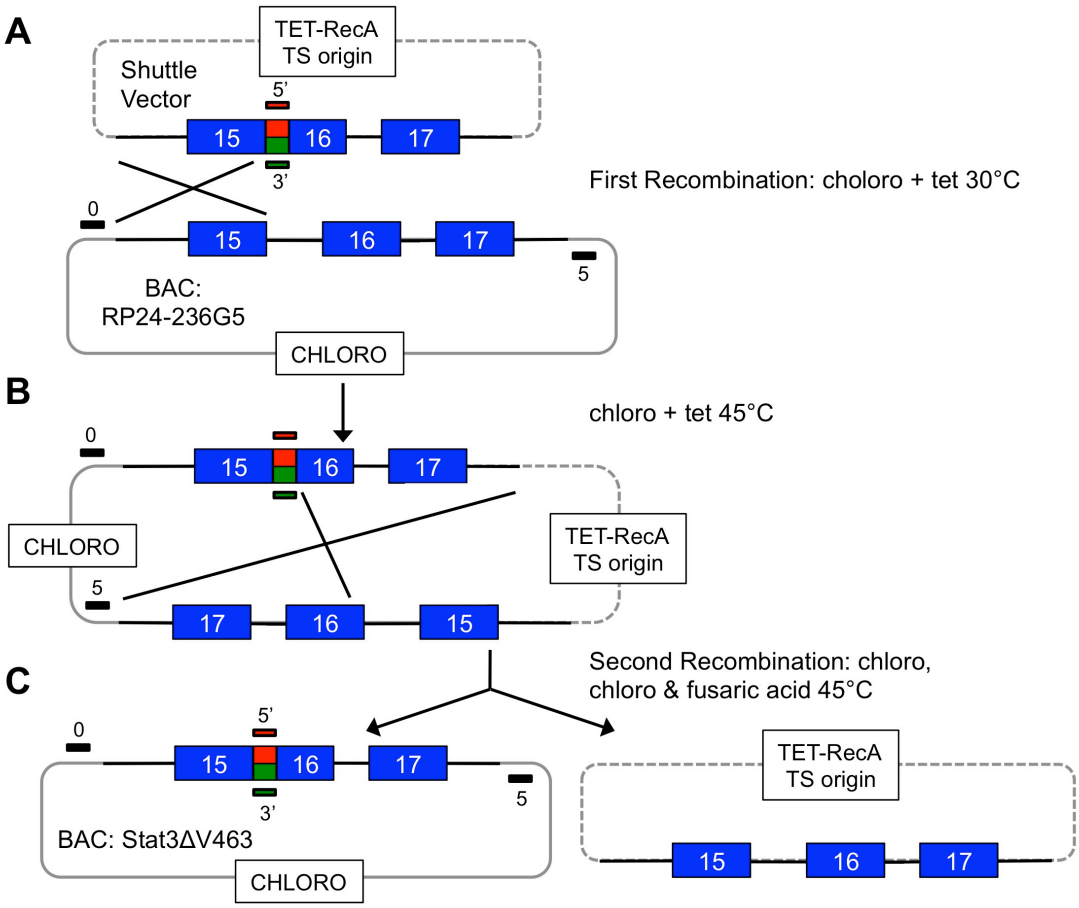

Figure 3.7. Strategy for recombination of mutant *Stat3* cassette with *Stat3* from BAC

(A) The temperature-sensitive pSV1.RecA, containing a sequenced recombination cassette, was transformed into bacteria containing BAC RP24-236G5 and selected by growth at 30°C on chloro+tet plates.

(B) Co-integrates were generated through a first homologous recombination step with either the exon 15 homology region (left: shown) or exons 16-17 homology region (right). Co-integrates were selected by growth at 45°C (pSV1.RecA transcriptional origin inactive) on chloro-tet plates. Colony PCR using primer pairs HIES0/HIES3' (recombination left) or HIES5'/HIES3 (recombination right) was used to screen for colonies with a single recombination.

(C) Positive colonies were grown at 45°C on chloro plates to allow a second homologous recombination event to occur. Colonies that deleted the tetracycline resistant pSV1.RecA shuttle vector were selected for on chloro-fusaric acid plates. Complete recombination was screened for by colony PCR using primer pair HIES0/HIES5.

As diagrammed in Figure 3.4., primers HIES0 and HIES5 anneal just outside the recombination cassette homology regions. HIES5' and HIES3' are complimentary and each anneal to the mutated region only of the recombination cassette.

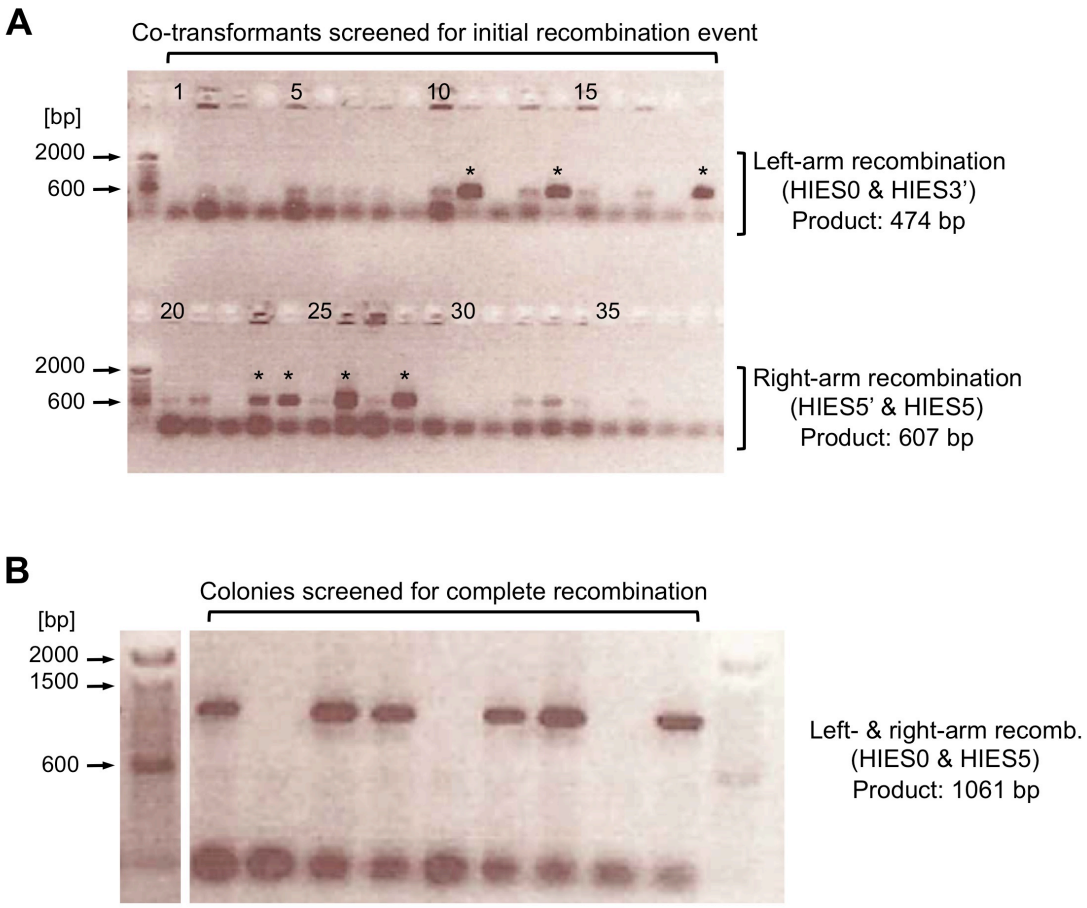

Figure 3.8. Generation of *Stat3*ΔV463 mutated BAC using homologous recombination

(A) Bacteria co-transformed with pSV1.RecA and BAC RP24-236G5 were grown for 24 hr at 30°C on chloro-tet plates; 14 colonies were re-plated on chloro-tet plates for 24 hr at 45°C and 288 colonies were screened for recombination by PCR. Half of the colonies were screened for recombination at the left-arm of homology and the other half for recombination at the right. PCR products were run on an EtBr agarose gel (shown) and positives selected as having a bright, distinct band of the expected size (*). Recombination efficiency was 15% and 19% at the left- and right-arm respectively.

(B) Colonies were grown for 5 hr at 45°C on chloro plates during the colony PCR analysis from (A). Twenty positive colonies (11 from left-arm and 8 from right-arm recombination) were streaked onto chloro-fusaric acid plates and grown for 48 hr. 96 colonies were screened for complete recombination by PCR, with products run on an EtBr agarose gel (shown). Recombination efficiency was 60%.

A

	HindIII	EcoRV
RP24-236G5 [Kb]	7.9	13.8
ΔV463 [Kb]	6.7	12.7

B

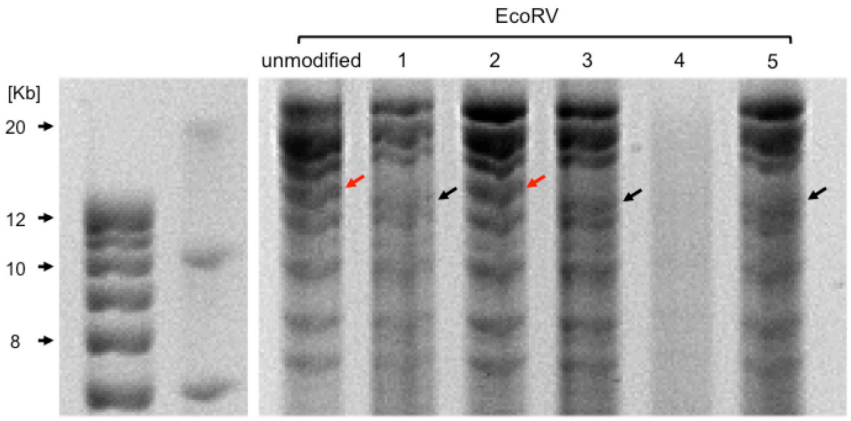

C

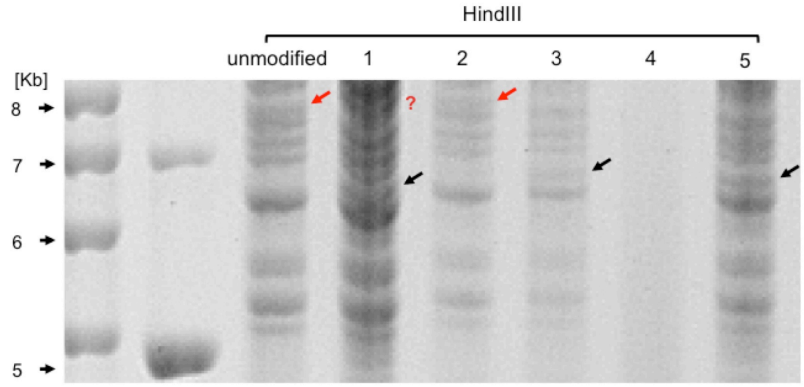

Figure 3.9. Verification of deletion in recombined colonies by restriction digestion

The unmodified BAC RP24-236G5 and 5 recombined colonies from Figure 3.8.B were grown overnight in LB-chloro, the DNA was extracted and analyzed by digestion with five restriction endonucleases: BamHI, EcoRI, EcoRV, HindIII, PstI.

(A) Table showing expected differences in restriction digest product sizes for EcoRV and HindIII treated RP24-236G5 and the *Stat3*ΔV463 modified BAC. Calculations from Lasergene (DNASTAR).

(B) DNA extracted from colonies 1-5, and the unmodified RP24-236G5 was digested overnight with EcoRV and run for 30 hr on an EtBr agarose gel. Black arrows mark bands unique to *Stat3*ΔV463 and red arrows mark bands unique to the unmodified BAC. Only a section of the gel is shown here; for the complete gel see (D).

(C) Same as (B) but with HindIII digestion.

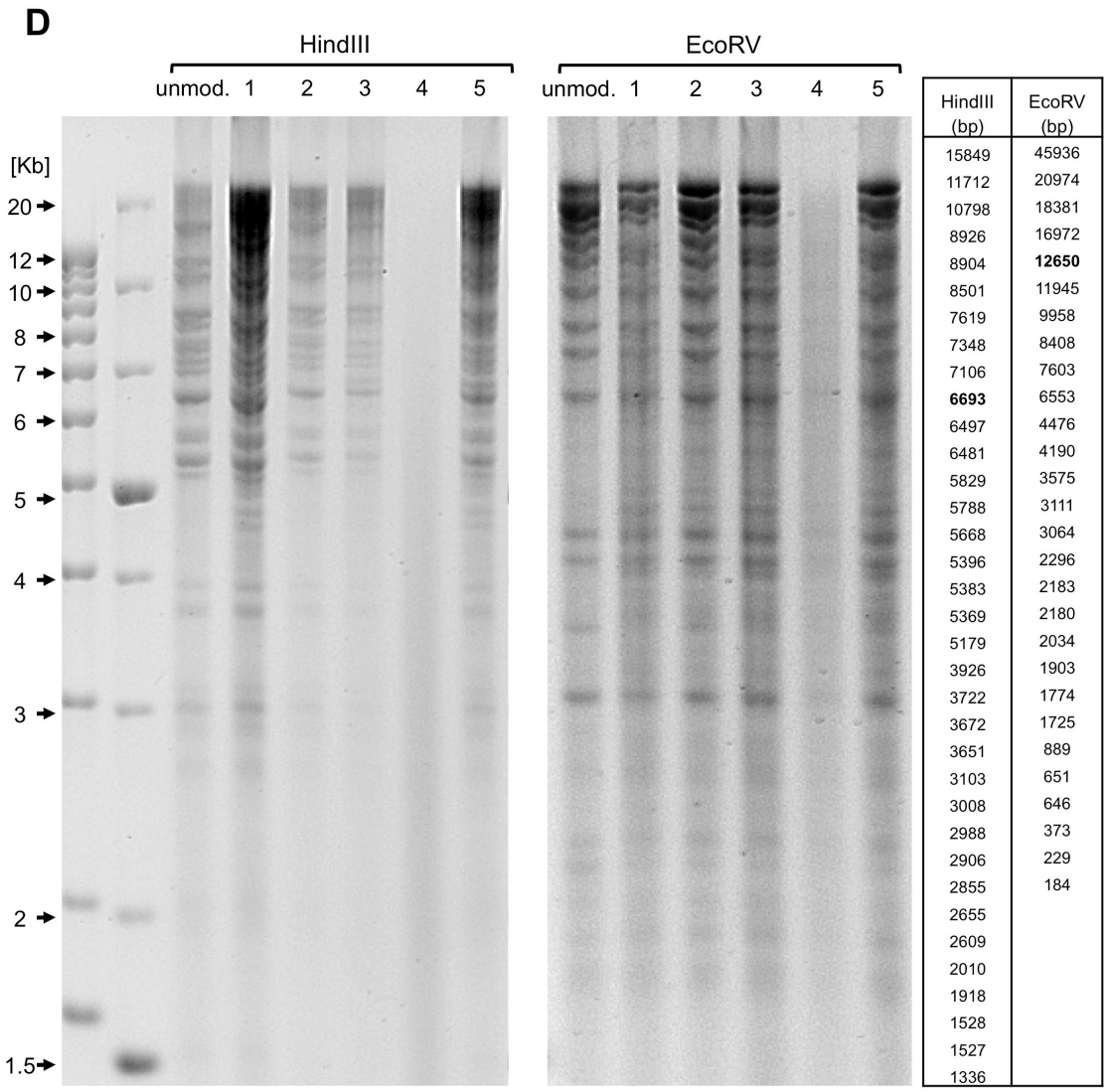

HindIII (bp)	EcoRV (bp)
15849	45936
11712	20974
10798	18381
8926	16972
8904	**12650**
8501	11945
7619	9958
7348	8408
7106	7603
6693	6553
6497	4476
6481	4190
5829	3575
5788	3111
5668	3064
5396	2296
5383	2183
5369	2180
5179	2034
3926	1903
3722	1774
3672	1725
3651	889
3103	651
3008	646
2988	373
2906	229
2855	184
2655	
2609	
2010	
1918	
1528	
1527	
1336	

Figure 3.9. Verification of deletion in recombined colonies by restriction digestion

The unmodified BAC RP24-236G5 and 5 recombined colonies from Figure 3.8.B were grown overnight in LB-chloro, the DNA was extracted and analyzed by digestion with five restriction endonucleases: BamHI, EcoRI, EcoRV, HindIII, PstI.

(D) DNA extracted from colonies 1-5 and the unmodified RP24-236G5 was digested overnight with HindIII and EcoRV and run for 30 hr on an EtBr agarose gel. The table on the right lists expected band sizes for the *Stat3*ΔV463 modified BAC with bands distinct from those expected for RP24-236G5 shown in bold.

3.2.4. Generation of *Stat3*ΔV463 BAC-Transgenic Mice.

BAC RP24-236GP was originally generated by cloning C57BL6/J genomic DNA into the pTARBAC1 vector (*411*); two NotI restriction sites flank this cloning site (*412*). Linear DNA fragments integrate five times more efficiently than circular fragments when injected into the male pronucleus of mouse zygotes (*413*). To linearize the *Stat3*ΔV463 BAC constructs, we took advantage of the NotI restriction sites flanking pTARBAC1 (Figure 3.10.A). No other NotI sites were present in the construct so digestion with NotI linearized the BAC in preparation for pronuclear injection. Thankfully, NotI digestion also removed the bacterial origin of replication and chloramphenicol resistance gene, which were cloned into pTARBAC1. Following overnight digestion with NotI, the linearized *Stat3*ΔV463 BAC constructs were purified by agarose gel electrophoresis and visualized with crystal violet. Complete digestion was verified by running aliquots on an EtBr agarose gel along with control, uncut samples (Figure 3.10.B).

The linearized 184 Kb *Stat3*ΔV463 BAC constructs were pronuclear injected into C57BL6 zygotes, and subsequently implanted in the oviduct of pseudo-pregnant recipients by Dr. Lionel Feigenbaum of the Laboratory Animal Sciences Program (NCI-Frederick, USA). 2 rounds of pronuclear injection and implantation netted 93 pups. Tail DNA was extracted from 3 week old pups and digested with PstI. PstI sites were situated just outside of the mutated portion of the *Stat3*ΔV463 construct (Figure 3.11.A). The PstI digestion products were analyzed by Southern blot. The complete recombination

cassette (Figure 3.4.B) was radiolabeled and used as a probe. The radiolabeled recombination cassette was able to hybridize with both WT *Stat3* (4.8 Kb) and mutant (3.6 Kb) PstI digest fragments (Figures 3.11.B and 3.11.C). Six founders (mice carrying the *Stat3*ΔV463 transgene) were identified by Southern blot. Comparison of the relative intensity of WT and mutant bands suggested that most founders carried only one copy of the transgene to two copies of endogenous *Stat3* (J10 and S5 from Figure 3.11.C). However, founders appearing to carry two (L1) or greater copy numbers (C6) of the mutant transgene were also identified (Figure 3.11.C).

Founder mice were viable and fertile. All mice carrying the *Stat3*ΔV463 mutation were bred to WT C57BL6 mates to prevent duplication of the randomly inserted transgene. Genotyping was performed using primer pairs HIES0/HIES3' or HIES5/HIES5', which annealed to the silent mutations incorporated into exon 16 of the mutant construct (Figure 3.4.). The transgene was transmitted in the expected Mendelian frequency. Again utilizing the silent mutations integrated into the mutant transgene, we designed primers that would specifically amplify either WT *Stat3* or *Stat3*ΔV463 mRNA (Figure 3.12.A). Expression levels of the two transcripts in resting $CD4^+$ T cells were assayed by RT-qPCR for both the L1 and C6 founder lines. Transgene expression levels correlated well with the Southern blot results in that *Stat3*ΔV463 was overexpressed relative to WT *Stat3* in cells from C6 mice, but expressed equally to WT *Stat3* in cells from founder line L1 (Figure 3.12.B). Equal expression of WT and mutant *Stat3* in L1 cells suggested that

the BAC construct carried all the regulatory regions necessary for endogenous-like control. Additionally, equal expression provided the desired one to one WT:mutant STAT3 ratio seen in AD-HIES patients. As a result, line L1 was denoted mut-*Stat3* and used for all subsequent experiments.

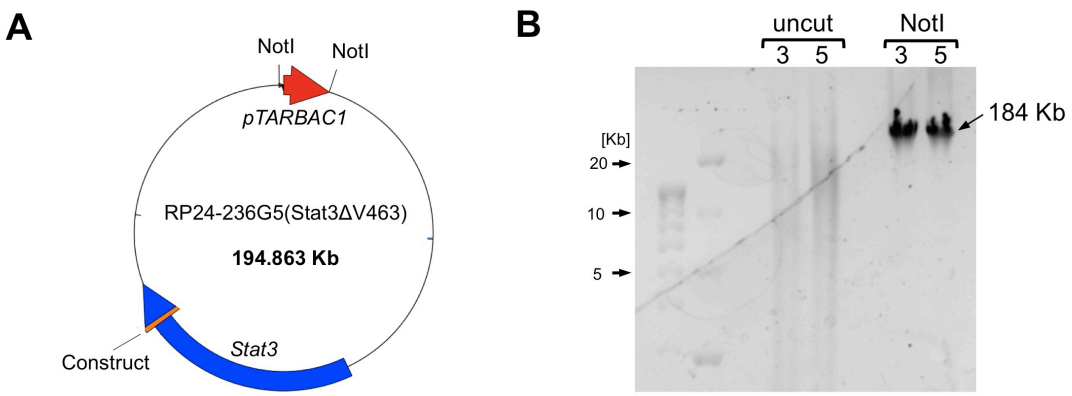

Figure 3.10. Linearization of the recombined BAC

Restriction analysis resulted in the selection of two BAC colonies carrying the *Stat3*ΔV463 mutation. These were linearized by digestion with NotI in preparation for pronuclear injection.

(A) Diagram of BAC RP24-236G5 carrying the *Stat3*ΔV463 mutation. The *Stat3* gene is shown in blue with the recombination cassette labeled in orange. NotI sites flank vector *pTARBAC1,* which contains the bacterial origin of replication and chloramphenicol resistance gene.

(B) DNA extracted from colonies 3 and 5 was digested overnight with NotI and run on an EtBr agarose gel along with undigested aliquots. Undigested bands consist of supercoils of the 195 Kb construct.

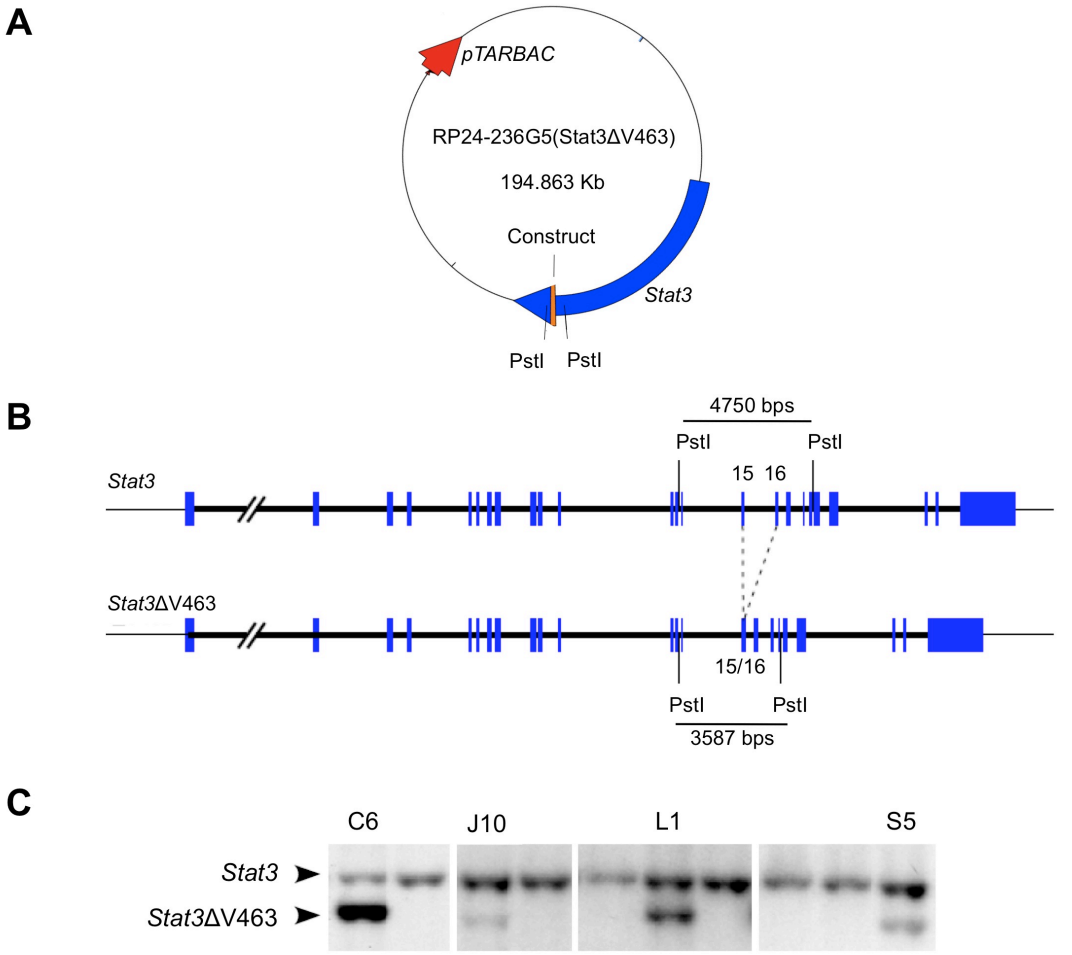

Figure 3.11. BAC-transgenic pups identified by Southern blot.

The linearized *Stat3*ΔV463 modified BAC was pronuclear injected into C57BL/6 zygotes which were subsequently implanted in the oviduct of pseudopregnant recipient mice. Pups were screened for integration of the BAC transgene by southern blot.

(A) Diagram of BAC RP24-236G5 carrying the *Stat3*ΔV463 mutation. The *Stat3* gene is shown in blue with the recombination cassette labeled in orange. PstI restriction sites flank the recombination cassette.

(B) Diagram comparing wild-type *Stat3* and *Stat3*ΔV463, with exons labeled in blue. Distance separating PstI restriction sites is labeled.

(C) Tail DNA was extracted from 3 week old pups and digested with PstI. A Southern blot was performed using the recombination cassette A B (Figure 3.5.) as a probe. The probe hybridized with both endogenous wild-type *Stat3* (upper band) and the *Stat3*ΔV463 transgene (lower band). Each column represents an individual mouse. Two rounds of pronuclear injection yielded 93 pups, 6 of which were positive for the transgene.

Pronuclear injection was performed by Dr. Lionel Feigenbaum (NCI, Frederick, USA).

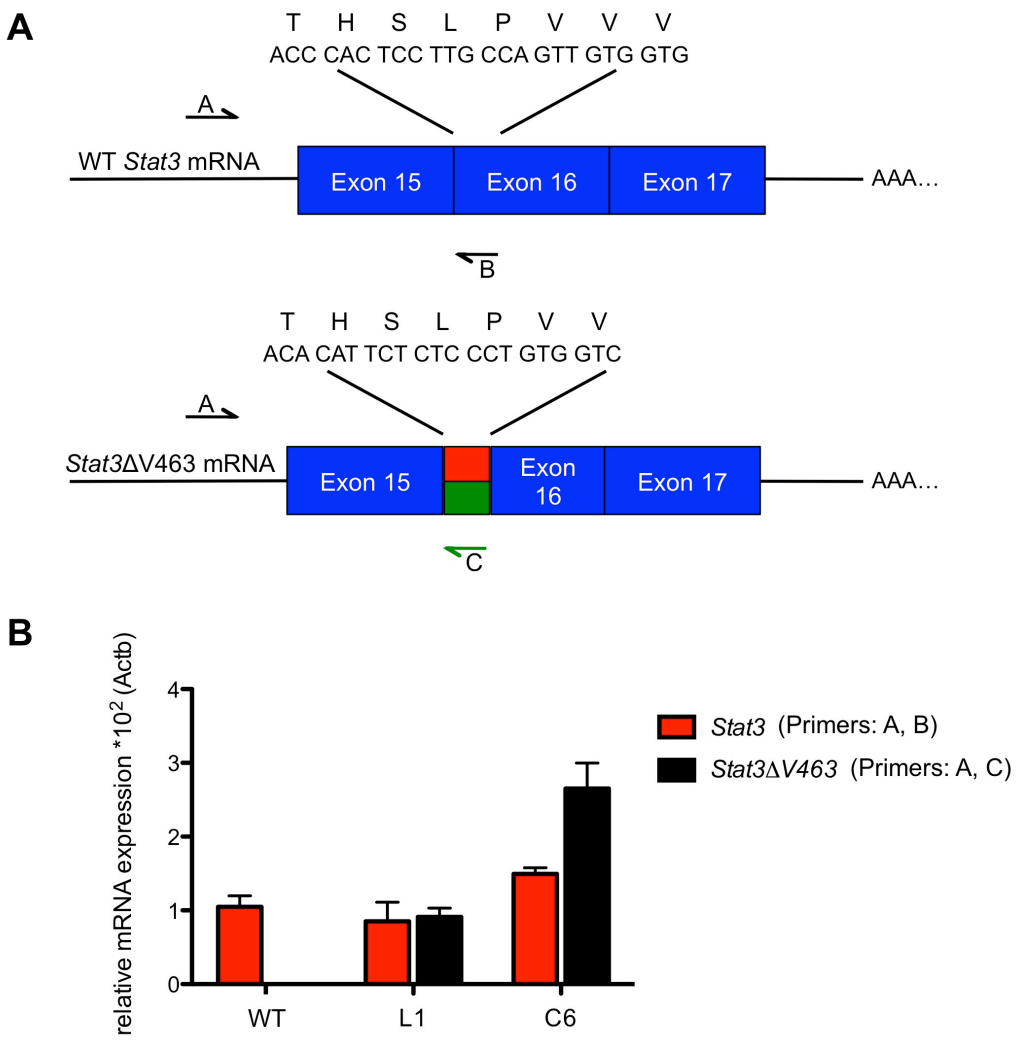

Figure 3.12. Expression of *Stat3*ΔV463 in transgenic mice assessed by qPCR.

(A) Diagram comparing spliced mRNA from WT and transgenic mice. Silent mutations incorporated into exon 16 of the *Stat3*ΔV463 construct (shown) were used to design primer pairs specific for the amplification of WT *Stat3* (A:B) and transgenic *Stat3*ΔV463 (A:C).

(B) RNA was extracted from MACS selected splenic B cells of WT and *Stat3*ΔV463 transgenic mice. Two *Stat3*ΔV463 lines, carrying different copy numbers of the transgene, were used. Expression levels of WT and mutant *Stat3* were assayed by RT-qPCR. Transcript levels were normalised to *Actb* and multiplied by a factor of 100. Bars represent the mean ±SEM.

Data represents the pooled results from two experiments, n=6/group. Statistical significance was determined using a Mann Whitney U Test. No comparisons reached statistical significance.

3.2.5. Mut-*Stat3* Mice Recapitulate Biochemical and Immunological AD-HIES Phenotype.

Having determined that the mutant *Stat3*ΔV463 construct was expressed in the BAC-transgenic mouse line, we next investigated its biochemical function. DNA-binding domain mutations of *STAT3* do not impair cytokine-dependent STAT3 phosphorylation in T cells (*75*). Accordingly, we found that IL-21 stimulation of T cells from WT C57BL6 and mut-*Stat3* mice resulted in equivalent levels of STAT3 Y705 phosphorylation by western blot (Figure 3.13.A). The kinetics of STAT3 phosphorylation was also unaffected by the presence of the *Stat3*ΔV463 transgene (Figure 3.13.A). Transgenic B cells also showed no defect in peak Y705 phosphorylation when cultured in the presence of IL-6, IL-10, or IL-21 (Figure 3.13.B). S727 phosphorylation, although less critical, is also thought to regulate STAT3 function (*8*, *414*). Unfortunately, the effect of dominant-negative *STAT3* mutations on serine phosphorylation has never been reported. However, we observed no differences in STAT3 S727 phosphorylation of activated WT and mut-*Stat3* T cells by FACS (data not shown).

Despite normal tyrosine phosphorylation, dominant-acting mutants in AD-HIES patient cells do inhibit STAT3 DNA binding (*75*). As shown in Figure 3.13.C, stimulation of control B cells with IL-6 induced a marked increase in STAT3 binding to a candidate DNA oligonucleotide. However, cytokine-dependent DNA binding activity in mut-*Stat3* B cells was substantially reduced (Figure 3.13.C). IL-6 treatment of mut-*Stat3* $CD4^+$ (Figure 3.13.D) and $CD11c^+$ (Figure 3.13.E) splenocytes also resulted in significantly reduced

DNA binding activity relative to WT. Collectively, these data strongly suggested that the *Stat3*ΔV463 construct worked in a dominant-negative fashion and was thus able to recapitulate the biochemical aspects of AD-HIES.

STAT3 is critical for production of the proinflammatory cytokine, IL-17A, in $CD4^+$ T cells (*218*, *381-383*). Consistent with this was the finding that AD-HIES patients have severely reduced numbers of IL-17A-producing T cells in the blood, partially explaining their immunodeficiency (*72*, *75-78*). To assess whether the biochemical abnormalities we observed in mut-*Stat3* mice had functional consequences, we next assessed the ability of WT and mut-*Stat3* circulating $CD4^+$ T cells to generate IL-17A. The percentage of IL-17A producing T cells in the blood of naïve mice is greatly reduced relative to that found in healthy human donors. As a result, we needed to push isolated $CD4^+$ cells towards IL-17A production by culturing in the presence of TGF-β1 and IL-6. As shown in Figure 3.14.A, $CD4^+$ T cells from the blood of WT mice were efficiently polarized to become IL-17A producers. In contrast, $CD4^+$ T cells isolated from mut-*Stat3* mice failed to produce significant IL-17A following differentiation *ex vivo*. To further explore the extent to which the BAC-transgenic model was able to mimic AD-HIES, we measured serum immunoglobulin (Ig) levels in unimmunized mice and found that IgE levels in mut-*Stat3* mice were six-fold higher than in WT littermate controls (Figure 3.14.B). Serum IgG1 levels were also significantly reduced in mut-*Stat3* mice, whereas the concentration of other isotypes was not different from controls

(Figure 3.14.B). Differences in IgG1 levels have not been reported for AD-HIES patients, suggesting some unique features of the mouse model. However, our data strongly supports the mut-*Stat3* mouse line as a useful tool, both for study of STAT3 function as a whole and AD-HIES pathogenesis in particular.

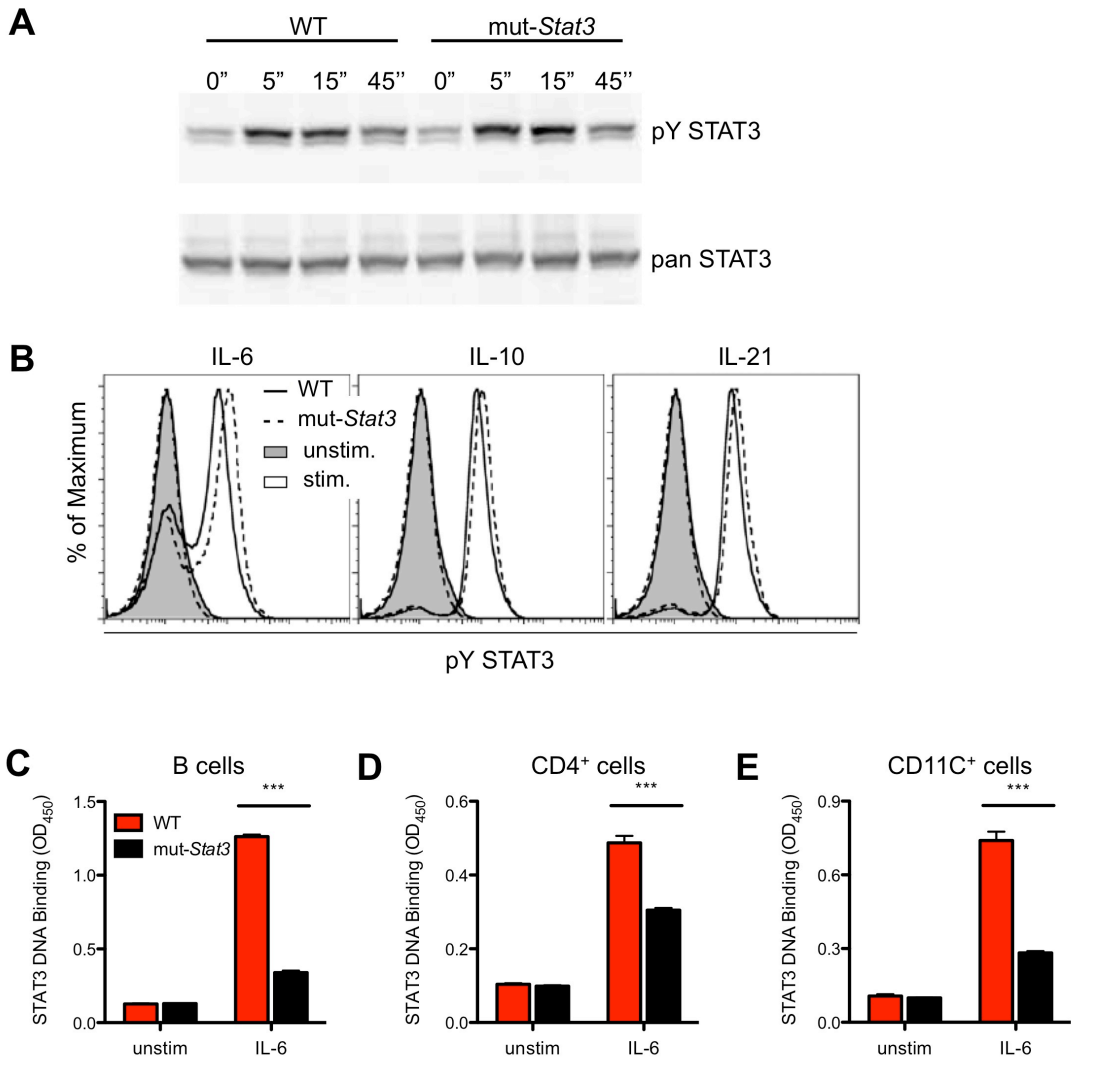

Figure 3.13. mut-Stat3 cells show normal STAT3 phosphorylation but aberrant DNA-binding.

(A) WT and mut-*Stat3* MACS sorted CD4$^+$ T cells were cultured in the presence or absence of 100 ng/mL IL-21 for 5-45 min. Cells were lysed and analyzed by western blot using pan- or anti-Y705 phosphorylated STAT3 antibodies. Data is representative of two independent experiments, n=3/group.

(B) Y705 phosphorylated STAT3 levels were monitored in WT (solid line) or mut-*Stat3* (dotted line) CD43$^-$ MACS sorted splenic B cells alone (shaded) or stimulated with 50 ng/mL IL-6, IL-10, or IL-21 for 30 min (unshaded). Data is representative of two independent experiments, n=6/group.

(C-E) STAT3 binding to a candidate oligonucleotide was quantified from cellular lysates using the TransAM STAT3 assay kit. MACS sorted CD43$^-$ B cells (C), CD4$^+$ T cells (D), and CD11C$^+$ cells (E) were unstimulated or stimulated with 50 ng/mL IL-6 for 15 min prior to lysis. Bars represent the mean ± SEM. Data is representative of 2 (C), 3 (D), or 1 (E) independent experiments, n=3 mice/group. Statistical significance was determined using a Mann Whitney U Test. *** $p \leq 0.001$.

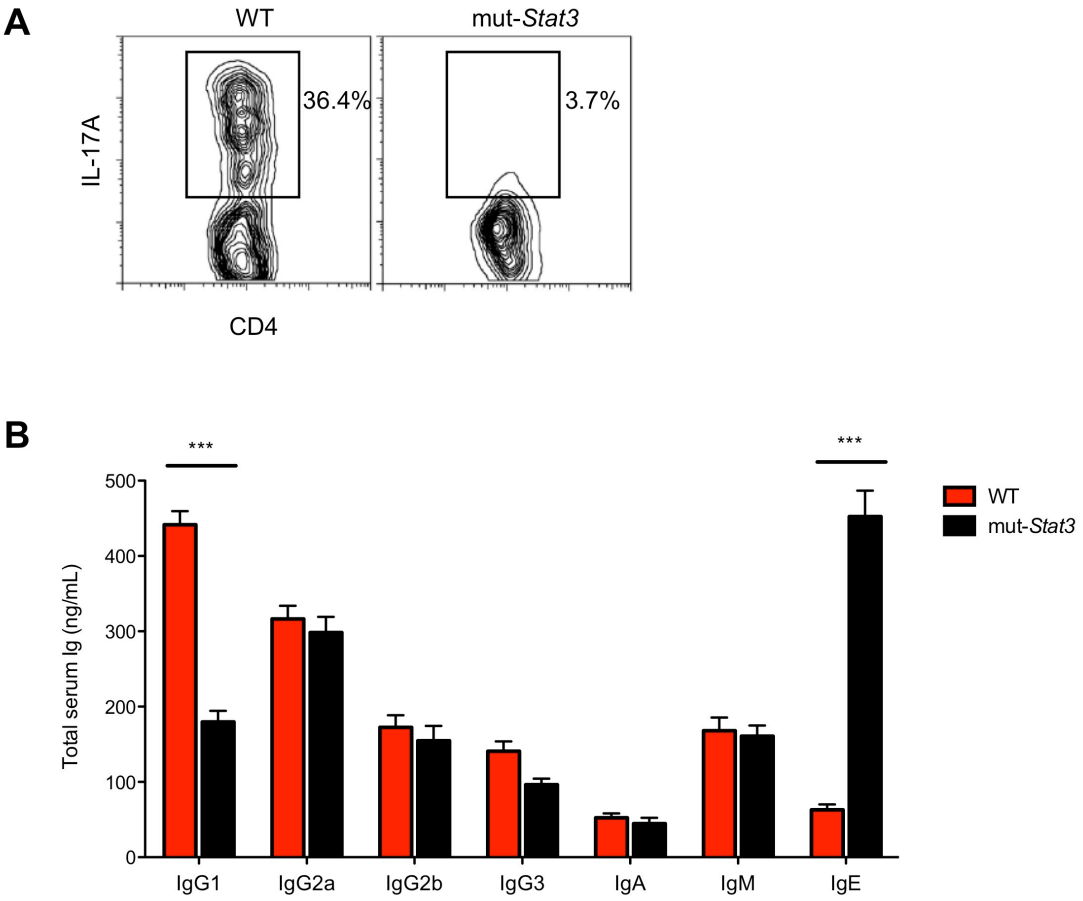

Figure 3.14. mut-*Stat3* mice recapitulate key aspects of HIES.

(A) Representative FACS plots showing IL-17A production from $CD4^+$ T cells MACS purified from blood and stimulated with anti-CD3, anti-CD28 antibodies, TGF-β1, and IL-6 for 70 hr. Data is representative of a single experiment, n=3/group.

(B) ELISA measurement of serum immunoglobulin levels from naïve WT and mut-*Stat3* mice aged 8-15 weeks. Bars represent the mean ± SEM, N=23.

Statistical significance was determined using a Mann Whitney U Test. * $p \leq 0.05$, ** $p \leq 0.01$, *** $p \leq 0.001$.

3.3. Discussion.

The importance of STAT proteins was evident from their initial discovery in Drosophila, where the introduction of a null *Stat* allele proved lethal (*415*-*417*). Mammals carry seven STAT proteins to drosophila's one, yet their functions are far from redundant. Indeed, S*tat3* is the only family member whose deletion results in complete embryonic lethality (*45*). Beyond playing a critical role in maintaining placental integrity, Cre-*loxP* mediated deletion (*418*) of *Stat3* from individual tissues has revealed striking roles for this transcription factor in a host of cellular compartments (*44*). As a result, the discovery of a group of patients with dominant-acting *STAT3* mutations was to some extent unanticipated (*71*). The finding immediately raised the question of whether the existence of such patients could be explained by incomplete impairment in STAT3 function or whether there were species-specific differences in the function of STAT3, as had been previously observed in another key cytokine signaling gene, *Jak3* (*419*-*423*). The high degree of homology between human and mouse STAT3 (99.87%) strongly suggested that introduction of patient-derived dominant-negative mutations into mice would yield similar biochemical defects. Therefore, we set out to create a mouse model of AD-HIES, in hopes that we could gain insight into both the mechanisms responsible for the clinical phenotype of this disease and, more broadly, the function of STAT3 at the organism level.

The BAC-transgenic system replicated the classical multisystem AD-HIES by expressing a patient-derived mutant allele that affected STAT3 DNA binding activity in a dominant negative fashion (*75*). In this context, our system stands

in contrast to models in which *Stat3* is fully deleted in the germline (*45*). Additionally, transgenic mice did not succumb to lethal autoimmune responses as had been previously reported for tissue specific deletions of *Stat3* (*53*, *56*). Thus, AD-HIES and our model are probably best characterized as resulting from impaired, but not abrogated, STAT3 function. Despite this, mut-*Stat3* $CD4^+$ T cells showed severe impairment in IL-17A production following *in vitro* differentiation, similar to that observed in *Stat3* deficient T cells (*218*, *383*). Similar results were reported following differentiation of AD-HIES patient T cells as well (*72*, *75*), suggesting that the intensity of a STAT3 signal has an effect on cytokine production from activated T cells. Further supporting the strength of our model, transgenic mice recapitulated another primary feature of AD-HIES, dysregulation of IgE.

Baseline immunoglobulin levels in mut-*Stat3* mice were consistent with the clinical phenotype of elevated IgE. However, IgE serum concentration in AD-HIES patients are typically a hundred times higher than those of normal individuals, whereas serum IgE in the mouse model averaged only a six-fold increase relative to WT. This difference is likely due to the short life and limited antigenic challenge encountered by specific pathogen free mice compared to humans. In agreement with this view, increased levels of IgE have been reported in mice raised under conventional conditions (*424*). Furthermore, serum IgE levels in mut-*Stat3* mice were comparable to those reported in other mouse models displaying elevated IgE (*425*).

AD-HIES associated mutations have now been identified in all regions of *STAT3* short of the small amino terminal domain (Figure 3.1.). However, most of the mutations identified in the nearly 300 patients described to date (*70-72*, *391-396*) have been focused in the DNA binding and SH2 domains. We selected to delete V463 of the DNA binding domain as it was one of the most prevalent mutations and has been associated with a severe clinical phenotype (*70*, *426*). In the future, it would be interesting to broaden our focus by comparing multiple mutation types present across different domains of STAT3. As the BAC-transgenic approach produced equivalent expression levels of mutant and endogenous WT *Stat3*, it could serve as an excellent template for the generation of further mutant *Stat3* mouse lines.

The molecular basis of the hypomorphic STAT3 activity observed in the different mutations is only beginning to be understood. Mutations in the DNA binding domain have consistently been shown to undergo normal Y705 phosphorylation following cytokine stimulation (*70-72*, *427*), whereas mutations in the SH2 domain have been reported to show reduced Y705 phosphorylation (*72*). A recent study proposes that the reduced phosphorylation of SH2 domain mutations may be due to conformational changes that prevent STAT3 docking to cytokine receptors such as gp130 (*427*). Additionally, they show that overexpressed SH2 mutant STAT3 proteins do not form dimers with WT STAT3 proteins, whereas DNA-binding mutants do (*427*). This suggests a novel mechanism to explain SH2 mutation dysfunction as one in which inactive STAT dimers are not formed. In such a system, expression of transgenic SH2 mutant STAT3 proteins might not be

sufficient to repress endogenous STAT3 activity. Therefore, gene knock in studies with the various mutations would also be greatly informative.

Our BAC-transgenic approach, nicely allowed us the opportunity to compare the effects of one versus several mutant gene copies. However, this also introduced confounding factors. For example, the presence of *Stat5a* in the *Stat3*ΔV463 BAC construct greatly complicated the system. Genes centrally located on BAC constructs are expressed more consistently *in vivo* than those found towards one end or the other (*428*). As such, we hoped that regulatory elements necessary for *Stat5a* expression from the BAC transgene would be absent due to its positioning. However, we observed ~1.5 fold increased expression of *Stat5a*, but not *Stat5b*, in mut-*Stat3* cells (data not shown). This strongly suggested that transgenic *Stat5a* was expressed in our system. Although the effect of transgenic *Stat5a* expression has not been reported, overexpression of *Stat5b* in mice resulted in increased $CD8^+$ T cell numbers (*429*). By comparison, mut-*Stat3* $CD8^+$ T cell numbers were comparable to WT (Figure 4.1.C). Another potential pitfall of the BAC-transgenic system is random insertion of the transgene. In an effort to minimize any potentially damaging gene disruptions, we have always maintained the colonies as heterozygous for the transgene by breeding to WT C57BL6 mates. Unfortunately, no *in situ* hybridization studies have been performed to determine the precise integration site.

Overall, our findings suggest that transgenic expression of the *Stat3*ΔV463 construct generated a very useful model of autosomal dominant HIES. Although there are several aspects of the HIES clinical phenotype that we have yet to explore in these mice, the reduced STAT3 DNA binding activity we observed across multiple cell types is very promising. The next chapter explores STAT3 function in the T and B cells of these mice, focusing particularly on gaining a mechanistic understanding of the hyper-IgE phenotype.

4. Chapter 4: Hypomorphic STAT3ΔV463 in T cell and B cell Biology.

4.1. Introduction.

As key mediators of cytokine signals, STATs play diverse and critical roles in the control of immune responses (*430*). Loss of *Stat3* in T cells has been associated with reduced $CD4^+$ T cell numbers in the periphery and reduced $CD8^+$ T cell numbers in the intestine (*219*). Similarly, *Stat3* deletion in the BM and early B cell progenitors resulted in reduced peripheral B cell numbers (*57*, *63*). However, AD-HIES patients exhibit normal peripheral B and T cell numbers (*431*). Discrepancies in mouse and human requirements for STAT mediated signals in lymphocyte development have been greatly publicized (*432-434*). Despite this, differences between AD-HIES and *Stat3* null cells may simply be attributable to the residual low level of STAT3 activity noted in AD-HIES.

STAT3 has also been shown to regulate T helper cell differentiation. Beyond being critical for the generation of Th17 cells (*218*, *241*, *381*, *383*, *435*, *436*), STAT3 activating cytokines have been shown to repress expression of the Treg specific transcription factor, Foxp3 (*208*, *243*, *437*). Additionally, *Stat3* deficient T cells produce lower levels of Th2 cytokines than WT following *in vitro* differentiation (*197*). STAT3 function also appears to be important for T cell-dependent terminal differentiation of antibody-secreting plasma cells (*62*). Long-lived plasma cells are formed during the germinal center reaction,

following interaction with Tfh cells (*438-441*). Reduced numbers of circulating $CD4^+$ cells carrying Tfh markers have recently been reported in AD-HIES patients (*442*). Collectively, these data highlight many potential lymphocyte abnormalities within a STAT3 null or hypomorphic environment. However, they provide little insight into why serum IgE might be increased in AD-HIES patients. Therefore, it was of interest to probe the effects of hypomorphic STAT3 activity on B and T cell responses, both *in vitro* and *in vivo*. Specifically, the *Stat3*ΔV463 mouse model was used to investigate a potential role for STAT3 in B cell CSR.

4.2. Results.

4.2.1. STAT3ΔV463's Effects in T Cell Homeostasis.

Previous studies in AD-HIES patients carrying STAT3 mutations or mice lacking STAT3 in T cells have reported no defects in lymphocyte development within the thymus (*59*, *60*, *385*). Consistent with this, we observed no difference in proportions of CD4 and CD8 SP or DP cells when comparing thymocytes of mut-*Stat3* and control (WT C57BL/6 littermates) mice (Figure 4.1.A). Reduced $CD4^+$ T cell numbers have been reported in the periphery of mice lacking STAT3 in T cells (*219*), but we observed no statistically significant change in either percentage or total number of T cells within the spleen (Figure 4.1.B and C). Therefore, despite a previously established role for STAT3 in peripheral T cell homeostasis, STAT3ΔV463 mutations did not affect peripheral T cell numbers. This was not surprising as STAT3 deficient T cells show only a modest decrease in $CD4^+$ T cell numbers (*219*), suggesting

that STAT3 plays only a contributory as opposed to absolute regulatory role in T cell proliferation and maintenance, and T cells carrying STAT3ΔV463 mutations have reduced, but not absent, STAT3 activity (Figure 3.13.D).

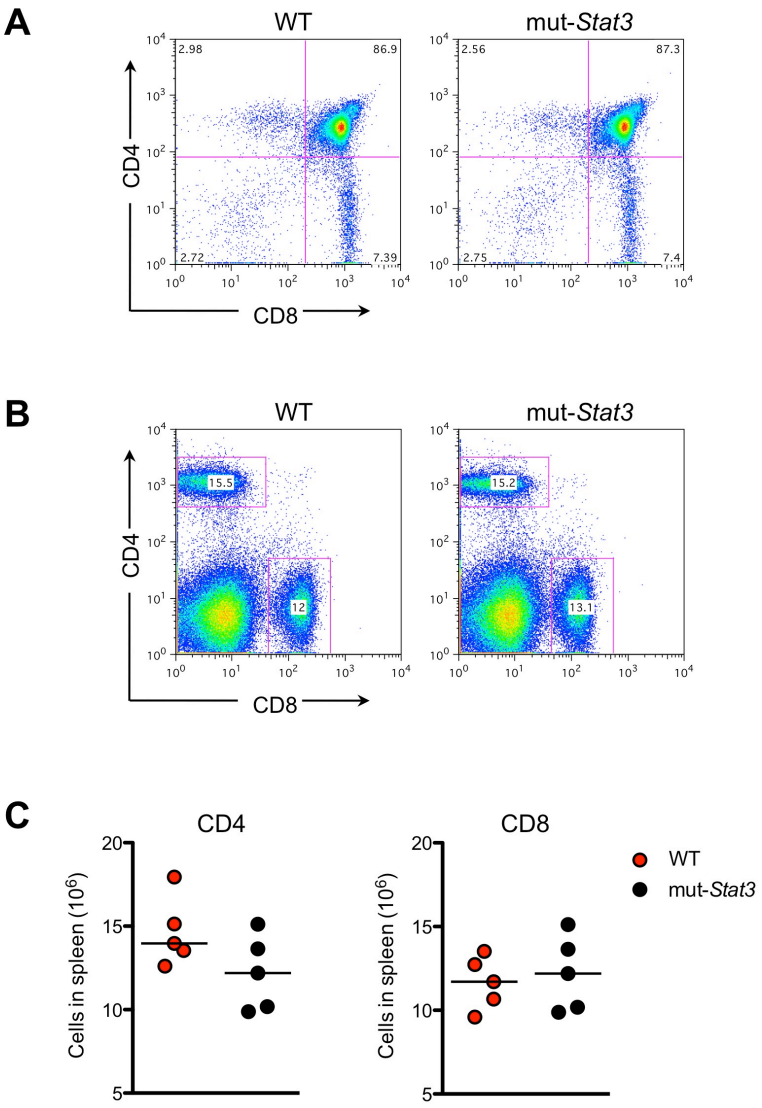

Figure 4.1. mut-*Stat3* mice exhibit normal thymocyte development and peripheral T cell numbers.

Thymi and spleens were harvested from 6-8 week old WT and mut-*Stat3* mice. Single cell suspensions were analyzed for surface marker expression by FACS.

(A) Representative FACS plots showing CD4/CD8 single- and double-positive thymocytes.

(B) Representative FACS plots showing CD4 and CD8 expression among splenocytes.

(C) Total number of $CD4^+TCR\beta^+$ and $CD8^+TCR\beta^+$ cells in spleens. Bars represent the mean and each point represents an individual mouse.

Data is representative of the pooled results of two independent experiments, totaling n=5/group. Statistical significance was determined using a Mann Whitney U Test. No comparisons yielded a statistically significant difference (C).

4.2.2. STAT3ΔV463's Effects in T Cell Differentiation.

STATs have been identified as key regulators in the differentiation of all known T helper cell subsets (*443*). Specifically, multiple murine studies have identified STAT3 as being critical for Th17 cell differentiation, both *in vitro* and *in vivo* (*218*, *241*, *381*, *383*, *435*, *436*). Fittingly, AD-HIES patients have severely reduced numbers of IL-17A producing memory T cells in the periphery and possess defects in IL-17A production following *in vitro* differentiation of naïve cells (*75*, *76*). Since Stat3ΔV463 could potentially affect multiple STAT signaling pathways through interaction with other STAT molecules, we decided to probe the ability of mut-*Stat3* T cells to differentiate into multiple subsets *in vitro*. In agreement with our previous findings, Th17 differentiation was strongly inhibited in mut-*Stat3* T cells (Figure 4.2.B). Interestingly, reduced IL-17A production in transgenic cells was accompanied by enhanced expression of the Treg lineage defining transcription factor Foxp3. In addition, increased numbers of $Foxp3^+$ cells were found in mut-*Stat3* cultures following iTreg induction. These findings support the notion that STAT3 and STAT5 play opposing roles in the differentiation of Th17 and Treg cells (*61*, *243*, *382*, *444*, *445*). Namely, hypomorphic STAT3 signaling releases the brake on STAT5 driven Foxp3 induction.

We also consistently identified increased numbers of IFN-γ^+ cells following Th1 differentiation (Figure 4.2.B). This is consistent with findings of increased IFN-γ production in the spleen and small intestine of mice with STAT3 deficient T cells (*219*, *241*). Conflicting results have been reported in AD-HIES

patient cells (*78*, *446*). A recent study has identified STAT3 as a driver of Th2 differentiation as well (*197*). However, we observed no differences in the production of the Th2 associated cytokine, IL-13, following *in vitro* activation of WT and mut-*Stat3* T cells (Figure 4.2.B). Unfortunately, Th2 differentiation under the treatment conditions was suboptimal so it is impossible to definitively rule out a Th2 differentiation defect in these cells. Thus, the presence of hypomorphic STAT3ΔV463 led to a deficiency in IL-17A but an increase in IFN-γ and Foxp3 expression in differentiated T cells.

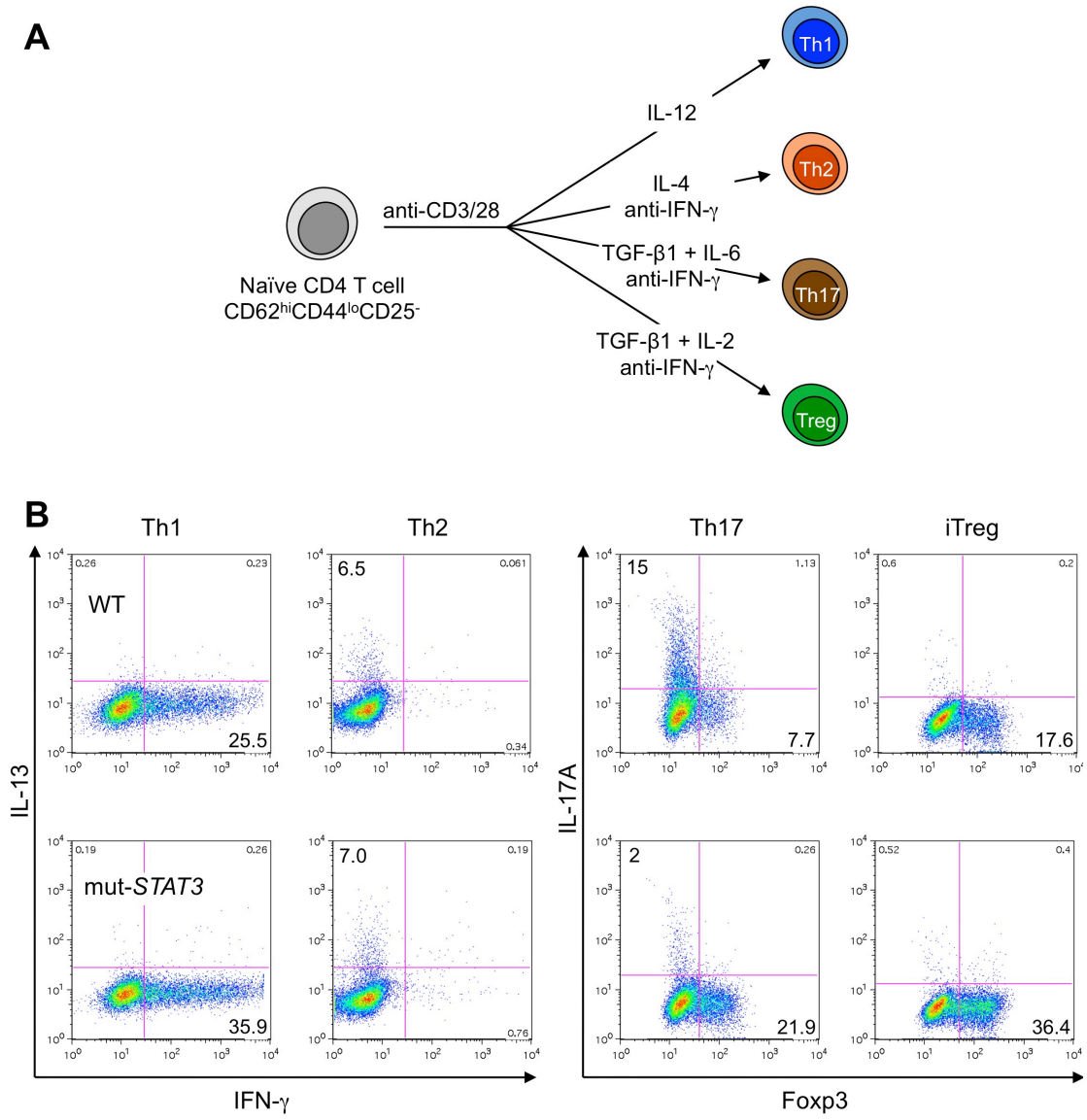

Figure 4.2. mut-*Stat3* mice exhibit abnormal *in vitro* CD4⁺ T cell differentiation.

Naïve CD4⁺ T cells (CD4⁺TCRβ⁺CD25⁻CD44^{lo}CD62^{hi}), were FACS sorted from spleens and lymph nodes of WT and mut-*Stat3* mice. Cells were differentiated for 70 hr as diagrammed in (A) and re-stimulated with PMA and Ionomycin in the presence of Brefeldin A for 2 hr. Expression of cytokines and transcription factors was determined by FACS.

(A) Diagram of treatment conditions used for differentiation of naïve CD4⁺ T cells.

(B) Representative FACS plots showing cytokine and transcription factor expression levels among WT (top row) and mut-*Stat3* (bottom row) CD4⁺ T cells.

Data is representative of 4 independent experiments, n=12/group.

4.2.3. STAT3ΔV463 Does Not Alter B Cell Development

In previous studies, both inducible deletion of STAT3 in the BM and conditional deletion of STAT3 in B cells resulted in a reduction in peripheral B cell numbers (*63*). Loss of peripheral B cells in the absence of STAT3 was attributed to fewer numbers of IL-7Rα^+ progenitor cells and a partial block at the pre-pro- to pro-B cell transition stage of B cell development (*63*). However, FACS analysis of the BM from steady state WT and mut-*Stat3* mice showed equivalent expression of the IL-7Rα on B220^{low} B cell progenitors (Figure 4.3A and B). Additionally, we looked for multiple cellular subsets from the B cell developmental pathway (diagrammed in Figure 4.4.A) and observed no statistically significant differences, in either percentages or absolute numbers, between the two groups (Figure 4.4.B).

Immature B cells leave the BM, passing through transitional type-1 and type-2 stages as they mature in the spleen, primarily developing into mature follicular B cells. Follicular B cells recirculate freely, homing to B cell follicles in secondary lymphoid organs such as the spleen. Also found in the spleen is a smaller, specialized population of naïve B cells that reside in the vicinity of the marginal sinus (*447*). These MZ B cells do not recirculate and are believed to act in conjunction with B1 B cells (that reside primarily in the peritoneum and at mucosal sites) in mounting T cell independent antibody responses (*216*, *448*, *449*). FACS analysis of splenocytes from WT and mut-*Stat3* mice yielded no differences in percentage of transitional, follicular, or MZ B cells (Figure 4.5.B). Analysis of peritoneal lavage extracts showed equivalent B1 cell

proportions in these mice as well (Figure 4.5.C). B cells with a mature follicular phenotype are also able to recirculate back to perisinusoidal areas of the BM (*450*). Consistent with our previous results, equivalent numbers of mature reciruclating cells were observed in the BM of these two groups (Figure 4.4.B). Therefore, these findings suggest that STAT3ΔV463 had no effect on B cell development, either within the BM, or the periphery. However, our analysis does not rule out improper organization or compartmentalization of these cellular subsets within secondary lymphoid organs. Immunohistochemistry (IHC) could be used to address this issue.

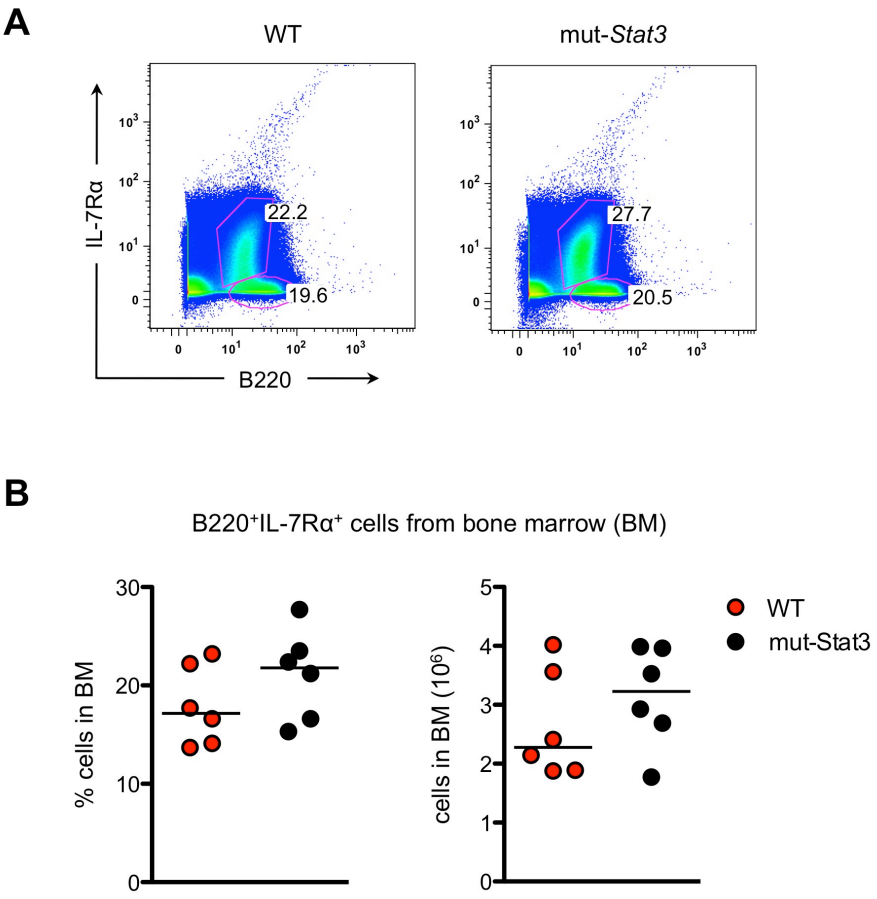

Figure 4.3. Normal IL-7Rα expression among B cell progenitors in the bone marrow of mut-*Stat3* mice.

Bone marrow was extracted from 6-8 week old WT and mut-*Stat3* mice. Expression of surface markers was determined by FACS.

(A) Representative FACS plots showing IL-7Rα expression among B220 low cells in bone marrow.

(B) Percent and total numbers of B220⁺IL-7Rα⁺ cells in bone marrow. Bars represent the mean and each point represents an individual mouse.

Data is representative of the pooled results from 2 independent experiments, totaling n=6/group. Statistical significance was determined using a Mann Whitney U Test. No comparisons yielded a statistically significant difference.

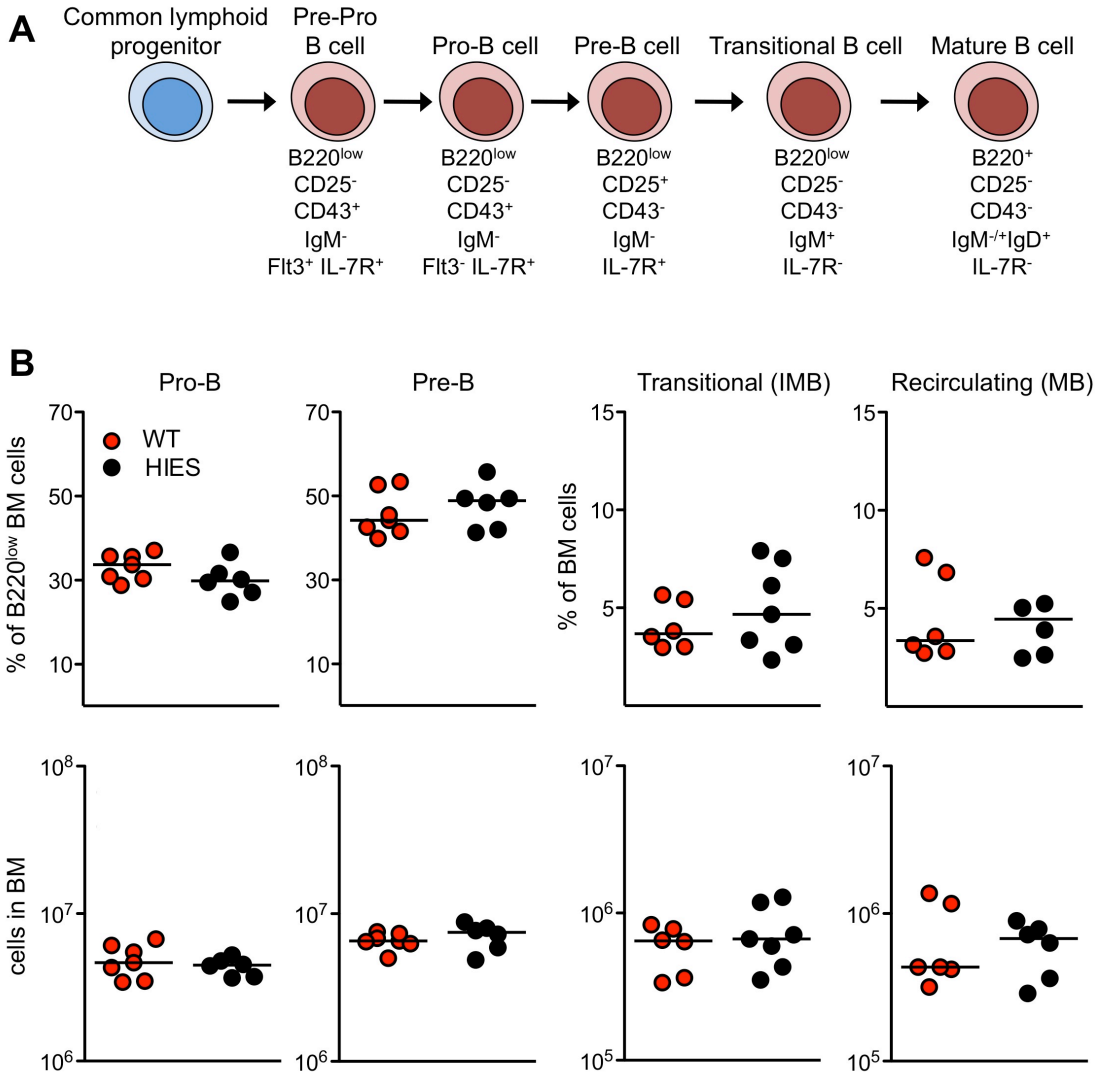

Figure 4.4. Normal B cell development in the bone marrow of mut-*Stat3* mice.

Bone marrow was extracted from 6-8 week old WT and mut-*Stat3* mice. Expression of surface markers was determined by FACS.

(A) Diagram depicting B cell development in the bone marrow with surface markers of the relevant stages listed below.

(B) Percent and total number of B cell subsets in bone marrow. B cell populations were defined by FACS as: pro-B ($B220^{low}CD25^{-}IgM^{-}$), pre-B ($B220^{low}CD25^{+}IgM^{-}$), transitional or immature-B ($B220^{low}CD25^{-}IgM^{hi}$), and recirculating ($B220^{hi}IgM^{+}$). Bars represent the mean and each point represents an individual mouse.

Data is representative of the pooled results from 2 independent experiments, totaling n=7/group. Statistical significance was determined using a Mann Whitney U Test. No comparisons yielded a statistically significant difference.

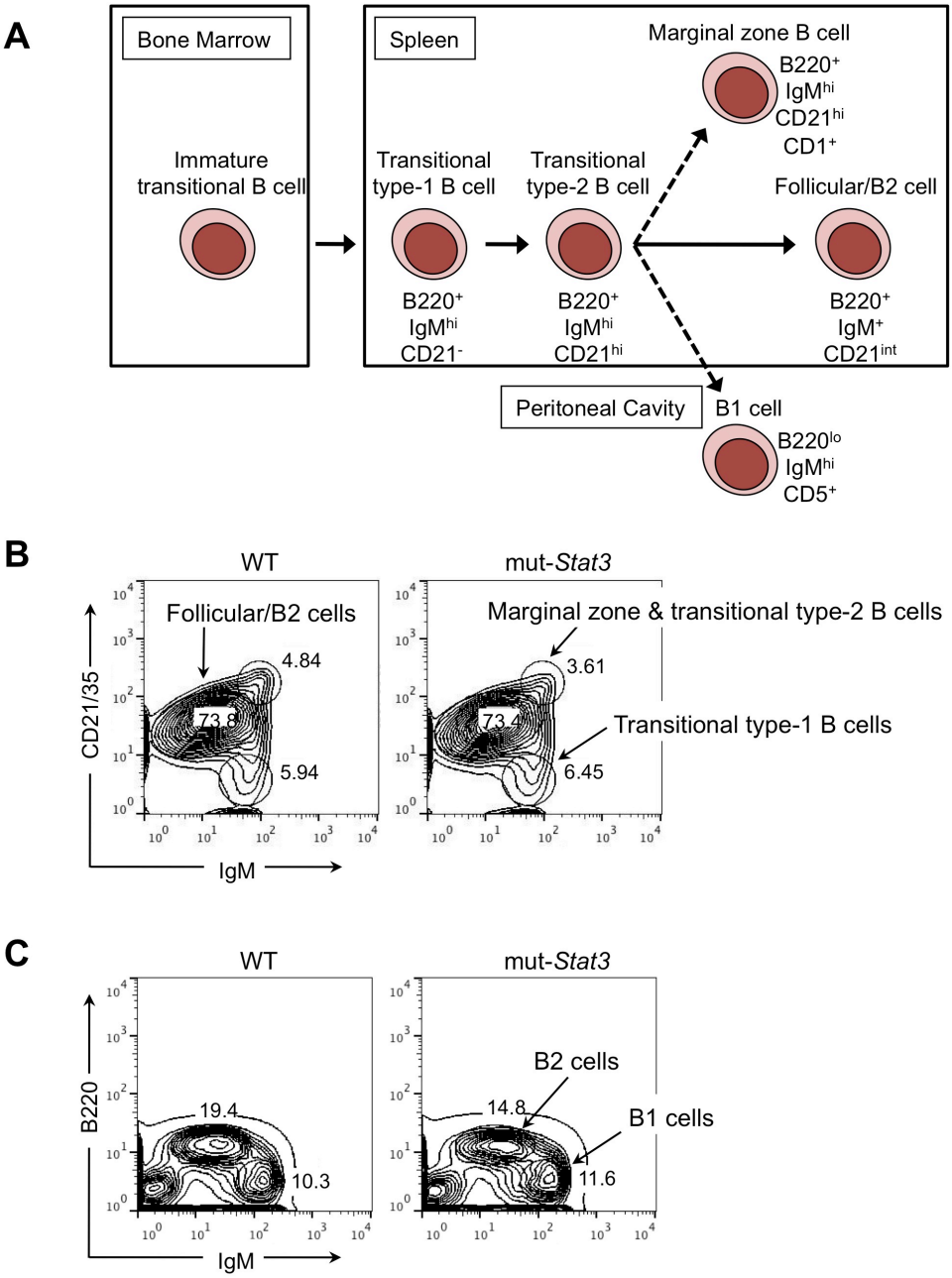

Figure 4.5. Peripheral B cell subsets intact in mut-*Stat3* mice.

Spleens and peritoneal cells were extracted from 6-8 week old WT and mut-*Stat3* mice. Expression of surface markers was determined by FACS.

(A) Diagram depicting B cell subsets found in the spleen and peritoneal cavity.

(B-C) Representative FACS plots with relevant B cell subsets gated from spleen (B) and peritoneal cavity (C). Data is representative of 2 independent experiments, n=7/group.

4.2.4. Interrogation of Germinal Center Responses in mut-*Stat3* Mice.

The transcriptional repressor Bcl6 is a master regulator of the germinal center response, controlling the differentiation of both GC B cells and Tfh cells (*101*, *174*, *284*, *451-453*). Recent data suggest the STAT3 activating cytokine IL-21 is an important inducer of Bcl6 in germinal center cells (*454*). Additionally, IL-17A has been reported as sufficient to drive germinal center formation under certain autoimmune conditions (*455*). Since mut-*Stat3* B and T cells showed reduced DNA-binding activity in response to IL-21 treatment (data not shown) and T cells showed reduced IL-17A production (Figure 4.2.B), we hypothesized that GC responses in mut-*Stat3* mice would be defective as well. Surprisingly, we observed no differences in the percent of cells positive for the GC B cell marker CD95 or the Tfh cell markers ICOS and CXCR5 in draining lymph nodes following acute immunization (Figure 4.6.B and C). This preliminary finding suggested that the primary players in GC responses are formed in mut-*Stat3* mice. However, we did not co-stain B cells for PNA, another important GC B cell marker, and the experimental set-up was inadequate to allow identification of antigen-specific responses only. We did not analyze tissue sections for proper organization of GCs by IHC so it is impossible to rule out abnormal GC responses in mut-*Stat3* mice.

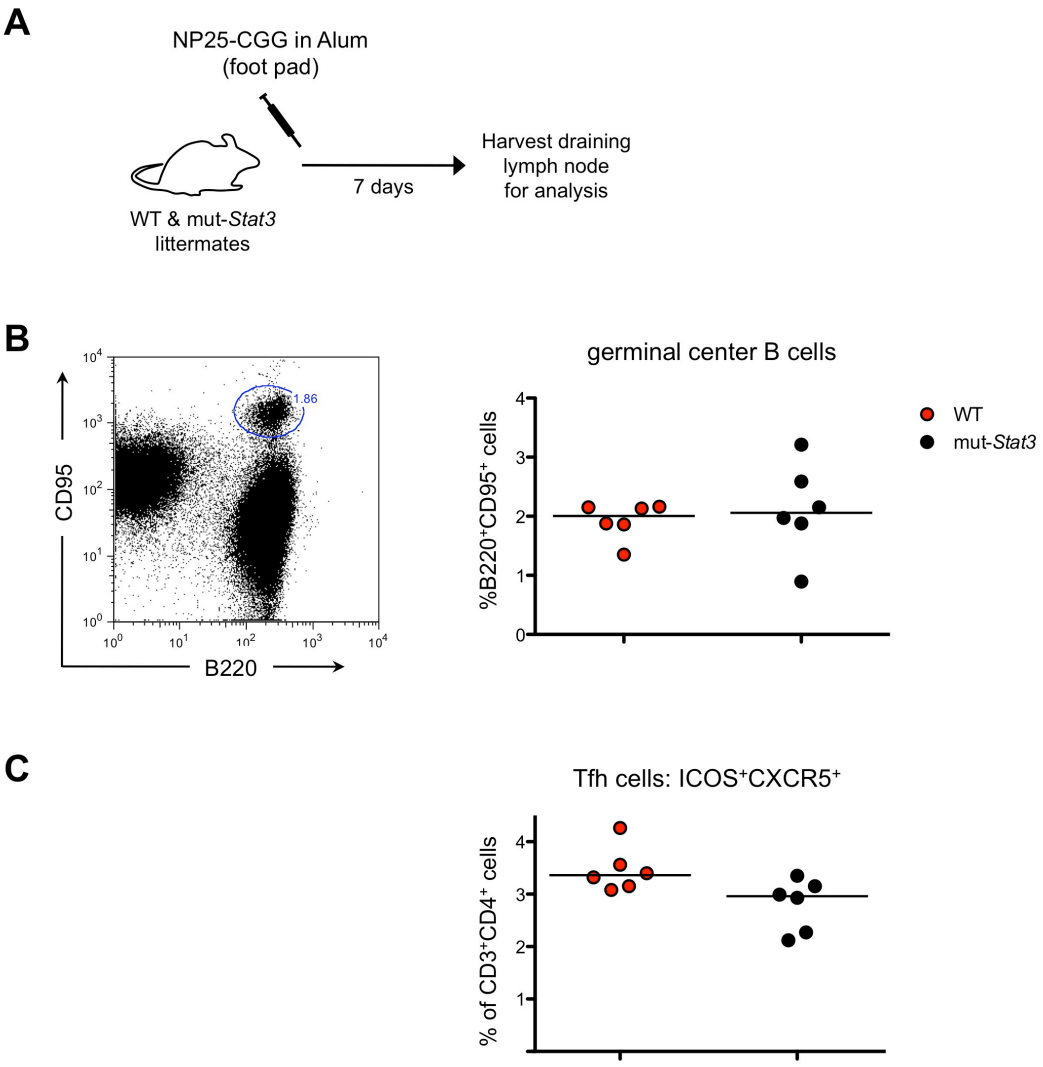

Figure 4.6. Germinal center B cells form normally following immunization in mut-*Stat3* mice.

C57BL/6 WT and mut-*Stat3* mice were injected in the hind foot pads with 100 µg NP25-CGG precipitated in Alum. Mice were sacrificed after 7 days. Single cell suspensions from the draining lymph nodes were stained and the expression of surface markers determined by FACS.

(A) Diagram depicting experimental strategy.

(B) Percent of germinal center B cells ($B220^+CD95^+$) in the draining lymph node of immunized mice. Representative FACS plot with gating strategy is shown on the left.

(C) Percent of Tfh cells ($ICOS^+CXCR5^+$) among $CD3^+CD4^+$ in the draining lymph node of immunized mice. Representative FACS plot with gating strategy is shown on the left.

Data represents the pooled results from 2 independent experiments, totaling n=6/group. Bars represent the mean and each point represents an individual mouse. Statistical significance was determined using a Mann Whitney U Test. No comparisons yielded a statistically significant difference.

4.2.5. Mut-*Stat3* Mice Mount IgE Skewed Antibody Response.

To begin to assess responses downstream of the GC and to test whether the observed hyper-IgE abnormality would also extend to the setting of neo-antigen stimulation, we immunized WT and mut-*Stat3* mice with a soluble antigen isolated from Schistosoma mansoni eggs (SEA), which induces a potent Th2- driven immune response (*456*). As shown in Figure 4.7.B., SEA-specific IgE production was greatly enhanced in mut-*Stat3* mice, whereas IgG1 production was reduced relative to controls, 21 days following immunization. IgG3 production was also blunted in mut-*Stat3* mice, but only low levels of this isotype were detected in the serum. Notably, in addition to dysregulation of IgE, impaired IgG responses postimmunization have been reported in both AD-HIES patients and mice with STAT3 deficient B cells (*62*, *457-460*). IgG2a and IgM SEA-specific responses were indistinguishable between the WT and mut-*Stat3* mice. In conclusion, these findings showed that the presence of STAT3ΔV463 did not preclude antigen specific antibody responses, but rather skewed these responses towards certain Ig isotypes. This suggested that STAT3ΔV463 may play a role in CSR.

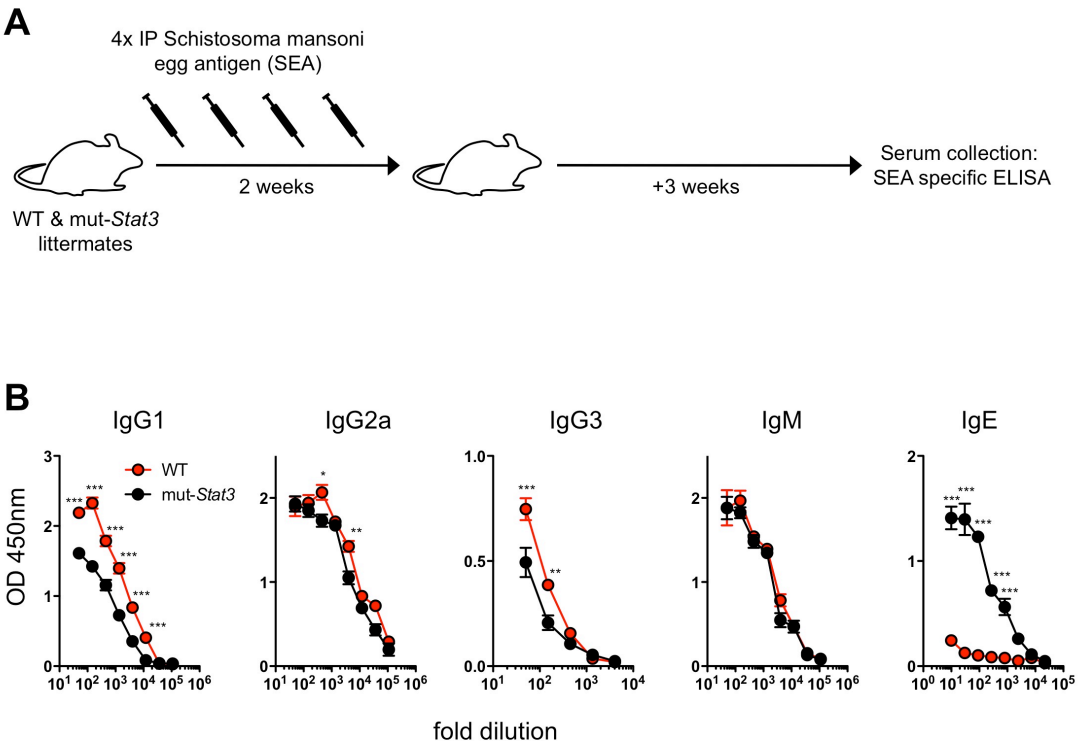

Figure 4.7. Skewed antigen-specific antibody responses in mut-*Stat3* mice.

The water souble Schistosoma mansoni egg antigen (SEA) was injected intraperitoneally (50 µg) into C57BL/6 WT and mut-*Stat3* mice 4 times over a 2 week period. Sera were collected and SEA specific immunoglobulin ELISAs run 3 weeks following the final injection.

(A) Diagram depicting experimental strategy.

(B) Serum (SEA)-specific immunoglobulins measured by ELISA. Data is presented as absolute absorbance of diluted serum sample at 450 nm vs $\log_{10}$ of the dilution factor. Each point represents the mean ±SEM, n=4/group.

Data is representative of 1 of 2 independent experiments. Statistical significance was determined using a repeated measure ANOVA followed by Bonferroni post-hoc test. * p≤0.05, ** p ≤ 0.01, *** p ≤ 0.001.

4.2.6. Intrinsic Defects in mut-*Stat3* B Cells Lead to Enhanced Igε CSR.

Elevated IgE levels are associated with a variety of conditions, but may or may not represent intrinsic B cell abnormalities (*461*). To investigate this in the HIES mouse model, we isolated mut-*Stat3* and WT B cells by CD43 depletion (> 85% purity), and activated them in culture for 72 hours in the presence of LPS+IL-4. Under these conditions B-lymphocytes undergo CSR from μ to γ1 and ε. Because B cells constitutively express the low-affinity IgE receptor, FcεRII, secreted IgE in these cultures interfered with accurate FACS analysis of surface IgE expression (*462*). As a result, ELISA measurement of secreted IgE in culture supernatants was used as a surrogate for μ-ε CSR. However, μ-γ1 CSR was measured by FACS analysis of IgG1 surface expression. Notably, *ex vivo* CSR levels mimicked serum profiles in that γ1 recombination was decreased, whereas secreted IgE was increased in mut-*Stat3* cultures relative to controls ($P < 0.0005$) (Figure 4.8.A). The increase in IgE levels *in vitro* was modest compared to those observed in the serum. B cells activated with LPS+IFN-γ or LPS+anti-δ-dextran undergo CSR to γ2a and γ3 respectively. As observed in the serum, we saw comparable IgG2a in WT and mut-*Stat3* B cell cultures. However, IgG3 CSR was significantly reduced in mut-*Stat3* B cell cultures compared to WT whereas no significant differences were detected in serum (compare Figure 4.8.A to 3.15.B).

To confirm that the increase in IgE levels by ELISA was representative of increased CSR, we determined the extent of μ-ε CSR at the DNA level in LPS+IL-4 cultures by digestion-circularization PCR (DC-PCR). This assay

quantifies the relative abundance of B-lymphocytes where deletional recombination between μ and ε has occurred (*463*, *464*). Amplification of μ-ε recombined DNA circles by DC-PCR was greater than 2-fold increased in mut-*Stat3* samples (Figure 4.8.B), indicating that isolated mut-*Stat3* B cells undergo more frequent μ-ε recombination than WT counterparts. Since the *in vitro* B cell cultures were not dependent on T cell help for CSR, these results argued that B cell intrinsic defects contribute to the serum isotype abnormalities noted in our mouse model of AD-HIES, including the eponymous elevated IgE levels.

CSR is closely associated with cell division (*123*, *126*) and loss of STAT3 has been linked to proliferative defects in multiple cell types (*72*, *465*). Therefore, we next explored whether B cells from mut-*Stat3* mice had altered proliferation *ex vivo* using CFSE labeling. FACS analysis of proliferative responses following *in vitro* activation with LPS and IL-4 revealed no significant differences between mut-*Stat3* and control B cells (Figure 4.9.A). This showed that CSR differences noted in mut-*Stat3* B cells could not simply be explained by increased or decreased cell divisions in this population.

CSR results from DNA deletion between highly repetitive switch (S) regions located upstream of Ig heavy chain constant (C_H) genes. Recombination is invariably preceded by germline transcription of the participating S-C_H domains. This phenomenon is believed to provide accessibility to the class-switch recombinase AID (*117*, *118*). A direct correlation between DNA

accessibility, germline transcription and CSR levels is well established (*139*, *466*). To determine whether the altered CSR observed in LPS+IL-4 activated mut-*Stat3* B cells was related to defects in transcription of Igγ1, Igε, or other genes, we used mRNA-Seq (*377*) to quantify gene expression in CSR-induced B cells. Notably, we detected a nearly three-fold increase in Sε-C_Hε transcripts in mut-*Stat3* B cells relative to control (Figure 4.9.B). In contrast, Sγ1-C_Hγ1 transcripts were comparable between the two samples (Figure 4.9.A). This suggested that increased transcription of the Igε locus promoted increased IgE CSR in mut-*Stat3* B cells.

Unfortunately, germline (pre-switch) transcripts and mature (post-switch) transcipts were indistinguishable in the mapped mRNA-Seq reads. Primer-pairs specific for pre-switch mRNAs were thus used to specifically measure germline transcripts in these cultures. Supporting the mRNA-Seq data, we observed increased germline transcription of the Igε locus and unaltered germline transcription of the Igγ1 locus in mut-*Stat3* B cells (Figure 4.10.A). Notably, we also measured increased mature Sμ-C_Hε transcripts (Figure 4.10.B), further supporting the IgE CSR bias. As a whole, transcriptional analysis provided strong evidence that the presence of STAT3ΔV463 in class-switching B cells leads to increased transcription of the Igε locus, and thus promotes subsequent increased IgE CSR. However, the data provided no evidence that reduced transcription of the Igγ1 locus could explain the reduced IgG1 surface expression observed in post-switch mut-*Stat3* B cells. Nonetheless, Ig_H class switching to downstream C_H genes (e.g., Cε) often

occurs through sequential CSR involving two downstream acceptor S regions (*467-470*). In particular, studies suggest that most switching to IgE involves an intermediate IgG1 class-switched state (*467-470*). Therefore, we hypothesize that reduced IgG1 surface expression in mut-*Stat3* B cells is due to enhanced subsequent switching of IgG1 B cells to IgE, rather than due to an intrinsic defect in IgG1 CSR itself.

Histone H3 pan-acetylation (H3Ac) and its lysine 4 trimethylation (H3K4me3) facilitate chromatin decondensation and promotes accessibility of regulatory proteins to transcribed genes (*471*). In the context of CSR, recent findings correlate levels of H3K4me3 with S-S recombination (*130*). To further characterize the Igε CSR defect, we performed ChIP-Seq (*377*) for H3K4me3 and H3Ac in mut-*Stat3* and WT B cells stimulated with LPS+IL-4. We found a direct correlation between Igε germline transcripts and H3K4me3, in that methylation was specifically increased (>2 fold) at the Igε locus in mut-*Stat3* B cells relative to control (Figure 4.11.A). There was not a significant difference in H3Ac between the two samples however (Figure 4.11.B). Collectively the data revealed an intrinsic bias of mut-*Stat3* B cells to undergo enhanced Igε H3K4me3, germline transcription, and CSR.

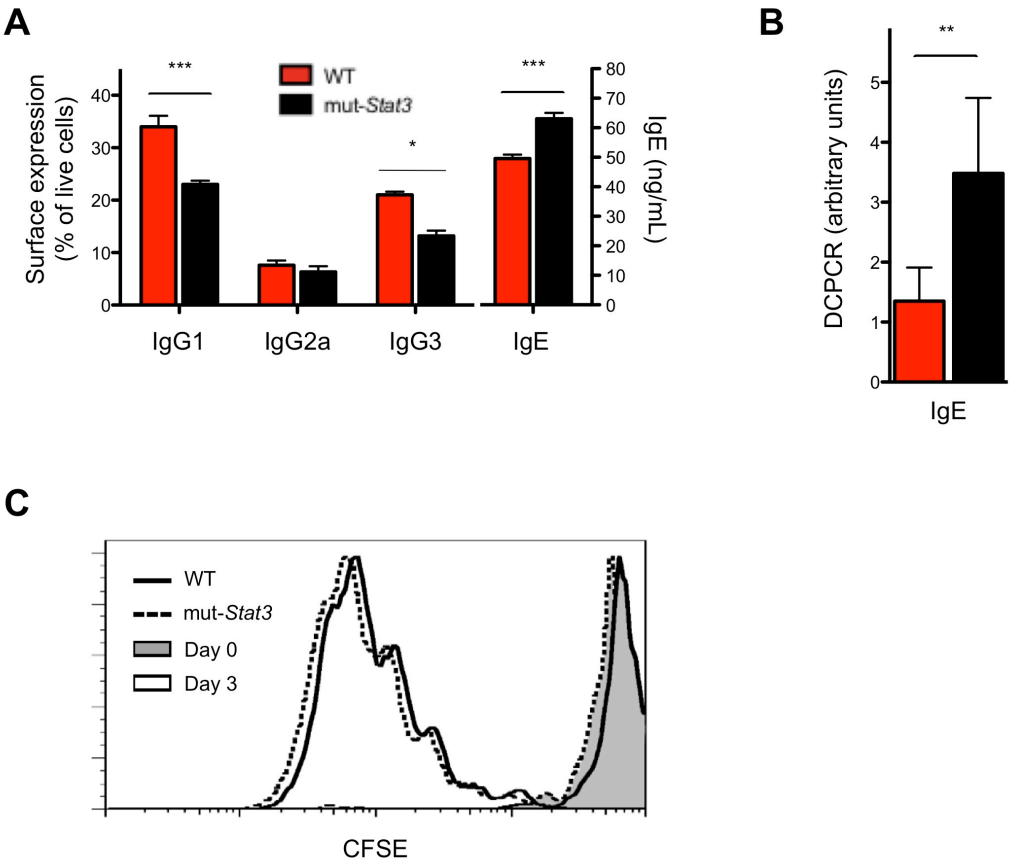

Figure 4.8. mut-*Stat3* B cells exhibit normal proliferation but altered CSR *in vitro*.

CD43$^-$ B cells were MACS selected from the spleens of C57BL/6 WT and mut-*Stat3* mice and activated *in vitro* with LPS and IL-4 for 72-96 hours (A: IFN-γ and anti-δ-dextran were supplemented for IL-4 in IgG2a and IgG3 switched cells respectively).

(A) Surface expression of IgG1, IgG2a and IgG3 were determined by FACS at 96 hours; IgE secretion was monitored by ELISA of culture supernatants. Bars represent the mean ±SEM, n=8/group.

(B) μ-ε CSR was assessed by DC-PCR on DNA extracted from activated B cells at 96 hours, Bars represent mean ±SEM, n=4/group.

(C) CFSE dilution was determined by FACS at 72 hours. Plot is gated on live B220$^+$ cells.

Data represents the pooled results from 2 (B) – 4 (A) independent experiments. (C) is representative of 4 independent experiments. Statistical significance was determined using a Mann Whitney U Test. * $p \leq 0.05$, ** $p \leq 0.01$, *** $p \leq 0.001$.

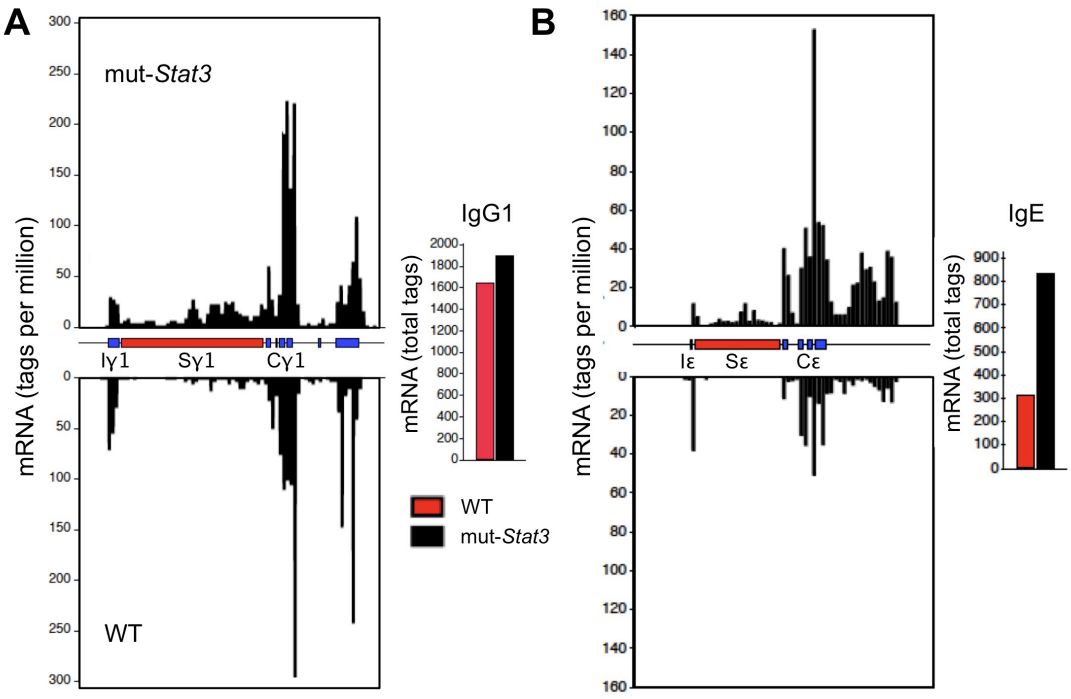

Figure 4.9. Altered transcription of the *Igε* locus in class-switching mut-*Stat3* B cells observed by mRNA-Seq.

CD43$^-$ B cells were MACS selected from the spleens of C57BL/6 WT and mut-*Stat3* mice and activated *in vitro* with LPS and IL-4 for 48 hours. mRNA was purified, fragmented and reverse transcribed. DNA fragments were amplified and sequenced using the Illumina Genome Analyzer II (Illumina).

(A) mRNA sequence tags (determined by mRNA-Seq) at the *Igγ1* locus in class-switching mut-*Stat3* (top) and WT (bottom) B cells. Bar graph depicts the absolute number of normalized tags, n=2 and 8 for mut-*Stat3* and WT respectively.

(B) mRNA sequence tags (determined by mRNA-Seq) at the *Igε* locus in class-switching mut-*Stat3* (top) and WT (bottom) B cells. Bar graph depicts the absolute number of normalized tags, n=2 and 8 for mut-*Stat3* and WT respectively.

Data is representative of 2 independent experiments. Alignment and pre-processing of the raw mRNA sequence reads was provided by Dr. Hong-wei Sun. Quantitation of sequence reads at individual genetic loci was carried out in R by Dr. Wolfgang Resch (NIH, Bethesda, USA).

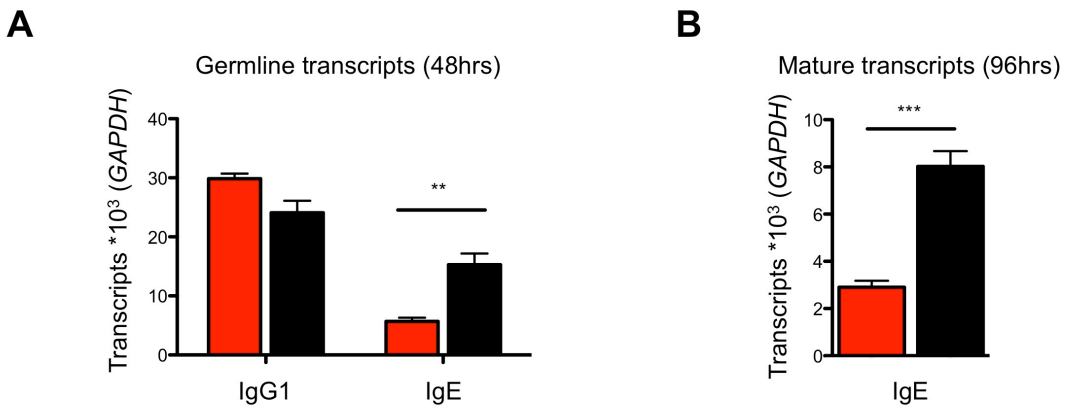

Figure 4.10. Increased *Igε* transcription from mRNA-Seq data confirmed by RT-qPCR.

CD43$^-$ B cells were MACS selected from the spleens of C57BL/6 WT and mut-*Stat3* mice and activated *in vitro* with LPS and IL-4 for 48-96 hours.

(A) Expression level of the germline (unswitched) *γ1* and *ε* loci were assayed by RT-qPCR on RNA extracted from B cells activated for 48 hours. Transcript levels were normalised to *GAPDH* and multiplied by a factor of 1000. Bars represent the mean ±SEM, n=4/group.

(B) Expression level of the mature (post-switch) *ε* locus was assayed by RT-qPCR on RNA extracted from B cells activated for 96 hours. Transcript levels were normalised to *GAPDH* and multiplied by a factor of 1000. Bars represent the mean ±SEM, n=4/group.

Data represents the pooled results from 2 independent experiments. Statistical significance was determined using a Mann Whitney U Test. * p≤0.05, ** p ≤ 0.01, *** p ≤ 0.001.

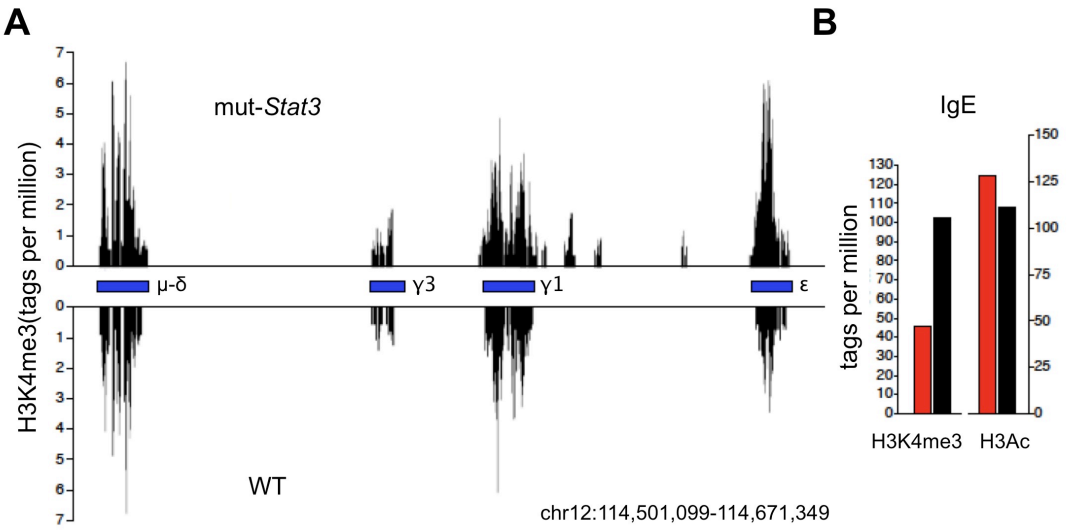

Figure 4.11. Marker of accessible chromatin structure, H3K4me3, increased at the *Igε* locus in class-switching mut-*Stat3* B cells.

CD43$^-$ B cells were MACS selected from the spleens of C57BL/6 WT and mut-*Stat3* mice and activated *in vitro* with LPS and IL-4 for 48 hours. Cells were lysed and treated with MNase to generate mononucleosome fractions. ChIP was performed using anti-H3K4me3 and –H3Ac antibodies, with subsequent sequencing completed on the Illumina Genome Analyzer II (Illumina).

(A) H3K4me3 ChIP-seq analysis, showing normalized sequence tags per million, plotted in 100 bp windows across the *Igh* locus in mut-*Stat3* (top) and WT (bottom) B cells, n=2/group.

(B) Bar graph depicts the absolute number of normalized tags identified across the *Igε* locus from both H3K4me3 and H3Ac ChIP-Seq, n=2/group.

Data is representative of 2 independent experiments. Alignment and pre-processing of the raw sequence reads was provided by Dr. Hong-wei Sun. Quantitation of sequence reads at individual genetic loci was carried out in R by Dr. Wolfgang Resch (NIH, Bethesda, USA).

4.2.7. Probing the Ability of mut-*Stat3* B Cells to Secrete Igs.

We noticed that differences in secreted IgE levels in culture were modest (20% increased) compared to those detected by DNA-recombination (nearly three-fold) (Figure 4.8.A and 4.8.B). This led us to speculate that STAT3ΔV463 might affect mut-*Stat3* B cells' ability to differentiate into antibody secreting cells, moreover, that STAT3 might be important for plasma cell differentiation, as previously proposed (*472*, *473*). Consistent with this idea, there was a two-fold reduction in the number of $CD138^{+}$ B cells in mut-*Stat3* cultures following *ex vivo* activation (Figure 4.12.A). However, although CD138 is a reliable marker for plasma cells and secreted antibodes are formed in culture, true plasma cells are not formed *in vitro*. Further strengthening our hypothesis, we observed reduced numbers of IgG1 secreting cells by ELISpot in the BM of mut-*Stat3* mice following immunization (Figure 4.12.B). We also identified STAT3 binding sites in the promoter region of transcriptional repressor and driver of plasma cell differentiation *Prdm1* or Blimp1 (Figure 4.12.C). However, transcription of the *Prdm1* locus was minimally reduced in the mRNA-Seq dataset for the mut-*Stat3* B cells relative to WT (Figure 4.12.C). Ultimately, these preliminary findings suggest reduced efficiency in plasma cell production from mut-*Stat3* B cells. However, the SEA immunization experiments demonstrated that antigen specific antibodies are secreted in the context of hypomorphic STAT3 signaling and the reduced numbers of antibody-secreting cells in the BM of mut-*Stat3* mice could be due to a trafficking defect. Also, plasma cell differentiation is highly dependent on GC formation, so any B cell intrinsic role for STAT3 in plasma cell differentiation is impossible to conclude from this series of experiments.

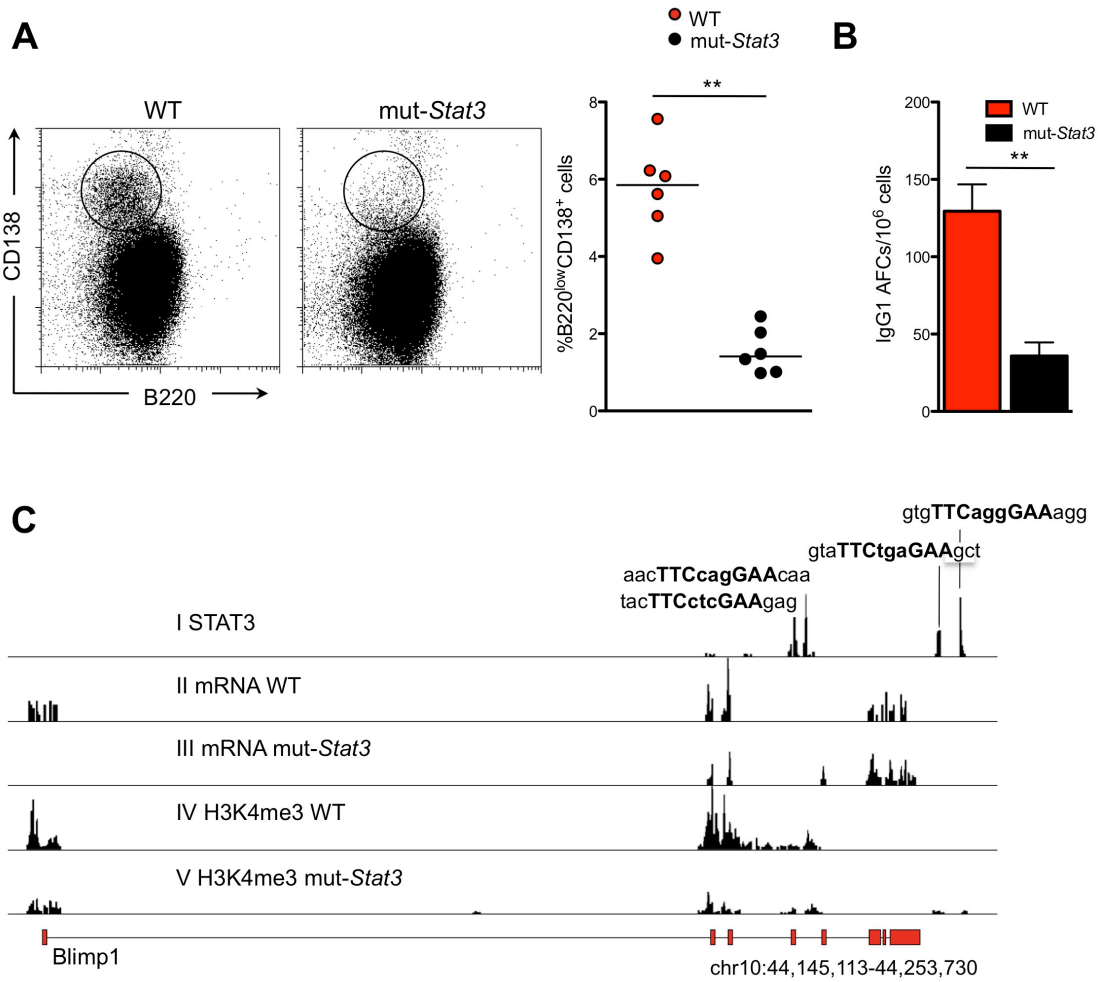

Figure 4.12. Investigation of plasma cell differentiation in mut-*Stat3* mice.

CD43$^-$ B cells were MACS selected from the spleens of C57BL/6 WT and mut-*Stat3* mice and activated *in vitro* with LPS and IL-4 for 48-96 hours (A and C). SEA was injected intraperitoneally (50 µg) into C57BL/6 WT and mut-*Stat3* mice 4 times over a 2 week period. Bone marrow was extracted 3 weeks later and analyzed by ELISpot (B).

(A) Surface expression of the plasma cell marker CD138 was determined by FACS at 96 hours. Representative FACS plot (left) and dot plot of cumulative data (right), Bars represent the mean and each point represents an individual mouse, n=6/group.

(B) IgG1 antibody forming cells (AFCs) were identified in the BM of SEA immunized mice by ELISpot. Bars represent mean ±SEM, n=6/group.

(C) Combined ChIP-Seq/mRNA-Seq analysis of the BLIMP1 (*Prdm1*) locus showing: STAT3 binding (lane I), mRNA and H3K4me3 in WT (lane II and IV) and mut-*Stat3* (lane III and V) cells. The location of *Prdm1* exons (red boxes) is depicted below. STAT3 consensus binding motifs are labeled (lane I).

Data is representative of 2 independent experiments. Statistical significance was determined using a Mann Whitney U Test. * p≤0.05, ** p ≤ 0.01, *** p ≤ 0.001.

4.2.8. STAT3 Regulates Expression of the Igε CSR Inhibitor Id2.

In response to IL-4 stimulation, STAT6 interacts with the Igε promoter and effects CSR to this isotype both *in vitro* and *in vivo* (*474*, *475*). Whether STAT3 plays a similar direct role in Igε CSR however has never been explored. Using ChIP-Seq, we mapped genomic occupancy of STAT6 and STAT3 in LPS+IL-4 stimulated B cells. The analyses uncovered 2,000 and 1,806 genes that recruited STAT6 and STAT3 respectively, with 853 of them recruiting both factors (Figure 4.13.A). To validate the specificity of the immunoprecipitation, we carried out unsupervised de novo searches for STAT binding consensus motifs. In agreement with a recent analysis of T lymphocytes (*476*), 85% of genes recruiting only STAT6 displayed the previously defined (*477*) STAT6 binding site: a TTC-GAA palindromic motif separated by a four base-pair spacer (Figure 4.13.B). In contrast, 95% of $STAT3^{+}STAT6^{-}$ genes carried the STAT3 binding site: a TTC-GAA motif separated by a three base-pair spacer (Figure 4.13.B). This single base-pair difference appears to provide specificity in targeting STATs to DNA, because few of the genes recruiting STAT3 or STAT6 displayed palindromic motifs with 4-bp or 3-bp spacers respectively (Figure 4.13.B). The data are thus consistent with the view that ChIP-Seq can reliably map STAT3 and STAT6 occupancy in the B cell genome.

We next investigated the Igε locus for STAT6/3 binding sites. We found prominent STAT6 recruitment at the Igε promoter (Figure 4.13.C), precisely at the location where a STAT6 palindromic binding motif (TTCccaaGAA) was

previously described (*474*, *475*). Conversely, we found no evidence of STAT3 binding to Igε (Figure 4.13C). Interestingly, when we expanded our focus to encompass the whole of the C_H regions, we identified comparable occupancy of the Igμ locus by both STAT3 and STAT6 and significant binding of the Igγ1 locus by STAT3, albeit less than STAT6 binding activity (Figure 4.13.C). This strongly suggested that STAT3 plays an active role in B cell CSR. For instance, STAT3 binding of the Igγ1 locus was strongest in a previously identified 3' regulatory region. Unfortunately, we did not further explore the precise function of STAT3 binding of Ig_H loci.

The ChIP-Seq data did convincingly suggest, however, that any role STAT3 played in regulation of the Igε locus was an indirect one. Therefore, we next looked for dysregulated genes in mutant cells, which might secondarily control IgE production. The mRNA-Seq analysis of *in vitro* cultures revealed 322 genes that displayed greater than 4 fold difference between WT and mut-*Stat3* B cells (Figure 4.14.A). Surprisingly, the majority of these genes were upregulated in mut-*Stat3* cells relative to control (Figure 4.14.A), suggesting STAT3 functions primarily as a negative regulator of gene expression in activated B cells. Although STATs are generally thought to act as transcriptional activators, recent reports of STAT occupancy leading to repression exist (*444*). Additionally, negative regulation of B cell gene expression by STAT3 may involve intermediate transcriptional repressors such as Blimp1. Well characterized STAT3 targets, such as the *Socs3* gene, were significantly different between WT and mut-*Stat3* cells (Figure 4.14.B).

By comparison, we found only minimal changes in the expression levels of most factors known to be involved in CSR (Figure 4.14.B). We did note, however, a dramatic down-regulation of Id2 (Figure 4.14.B). This transcriptional repressor was of particular interest because it antagonizes Igε recombination by heterodymerizing with E-box proteins (Pax5 and E2A) that directly regulate Igε transcription (*478*).

To confirm the defect in *Id2* gene expression, we stimulated mut-*Stat3* and control B cells with LPS and numerous STAT activating cytokines. Supporting the mRNA-Seq findings, treatment with either LPS alone or LPS+IL-4 resulted in reduced *Id2* transcription in mut-*Stat3* cells (Figure 4.14.C). Notably, *Id2* transcipts were particularly low when mutant cells were treated with IL-21 (Figure 4.14.C), which induces abundant STAT3 phosphorylation during B-lymphocyte stimulation (*446*, *479*). To determine whether STAT3 directly regulated *Id2* gene expression, we next examined the *Id2* locus for STAT3 binding motifs and/or direct STAT3 recruitment by ChIP-Seq. The Id2 basal promoter exhibited STAT3 occupancy in control B cells and this coincided with the presence of a STAT3 palindromic binding motif (TTCtcgGAA, Figure 4.15.A, lane I). However, we also noted very prominent binding of STAT3 (>5 fold) 93kb upstream of the *Id2* locus, at a phylogenetically conserved region that also harbors two distinct STAT3 binding motifs (Figure 4.15.A, lanes I and V). Because the closest gene flanking this element (other than *Id2*) is 1.2Mb away (not shown), we considered the possibility that this domain might represent an *Id2* enhancer element. The acetyltransferase and transcriptional

coactivator p300 has been shown to be a useful marker for transcriptional enhancers (*480*, *481*), therefore we next assessed by ChIP-Seq whether p300 was associated with this element in LPS+IL-4 stimulated B cells. We detected specific binding of p300 to the putative enhancer (Figure 4.15.A, lane II). Importantly, p300 recruitment coincided with a chromatin signature characteristic of transcriptional enhancers (*482*), i.e. abundant histone H3 monomethylated at lysine 4 (H3K4me1), but little H3K4me3 (Figure 4.15.A, lanes III and IV). Comparatively, the *Id2* gene was H3K4me3^{high}H3K4me1^{low}, as befits promoter-proximal regions (*482*) (Figure 4.15.A). Furthermore, RNA polymerase II ChIP-Seq in B cells showed abundant recruitment to both the *Id2* promoter and gene body, but minor recruitment to the putative enhancer (not shown). Altogether, these results implied that STAT3 directly regulates *Id2* transcription in B-lymphocytes by interacting with its basal promoter and potentially an upstream transcriptional enhancer. Unfortunately the *Id2* putative enhancer element was never confirmed by chromosome conformation capture (3C).

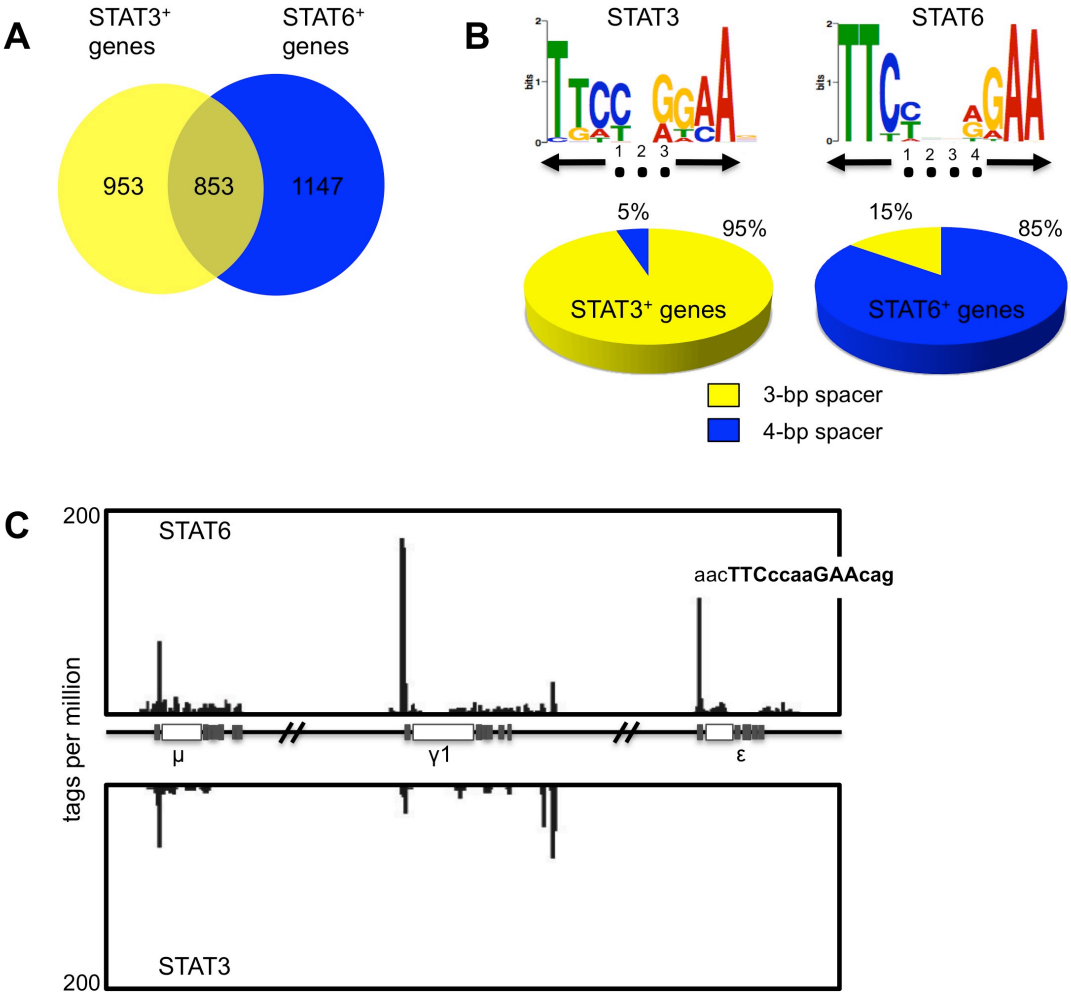

Figure 4.13. STAT3 and STAT6 genome-wide occupancy in activated B cells.

CD43$^-$ B cells were MACS selected from the spleens of C57BL/6 WT mice and activated *in vitro* with LPS and IL-4 for 48 hours. Cells were lysed, chemically cross-linked and sonicated to generate fractionated genomic DNA. ChIP was performed using anti-phospho-STAT3 and –phospho-STAT6 antibodies, with subsequent sequencing completed on the Illumina Genome Analyzer II (Illumina), n=2/group.

(A) Venn diagram showing the number of genes uniquely bound by STAT3, STAT6, or both in ChIP-seq analysis of activated B cells. STAT-bound genes were identified when at least one ChIP-Seq island was present within the gene domain, defined from 1 Kb upstream of the transcription start site to the transcription termination site.

(B) STAT3 and STAT6 consensus binding motifs were defined within sequence-tag islands obtained via STAT3- or STAT6-Seq respectively, using a parallel version of MEME82 (upper graphs). The percentage of genes recruiting STAT3 or STAT6 (from A) associated with a STAT binding motif carrying a 4 (blue) or 3 (yellow) bp spacer was calculated (lower pie charts).

(C) ChIP-Seq analysis, showing STAT6 (top) and STAT3 (bottom) recruitment, plotted in 100 bp windows across the *Igh* locus. STAT binding is represented in normalized sequence tags per million.

Alignment and pre-processing of the raw sequence reads was provided by Dr. Hong-wei Sun. The genome-wide comparison of STAT3 and STAT6 binding was carried out by Dr. Golnaz Vahedi (NIH).

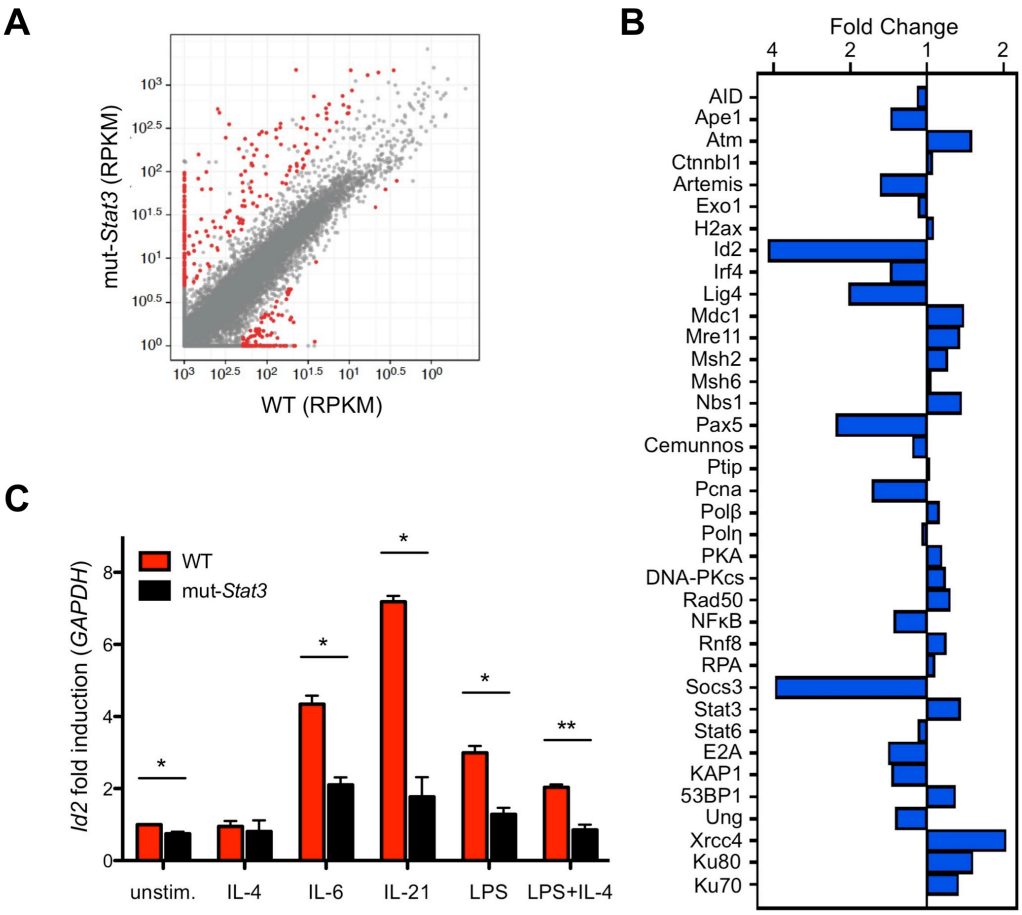

Figure 4.14. Expression of Id2, an Igε CSR inhibitor, is dysregulated in mut-*Stat3* B cells.

CD43$^-$ B cells were MACS selected from the spleens of C57BL/6 WT and mut-*Stat3* mice and activated *in vitro* with LPS and IL-4 for 48 hours (A-B) or with various cytokine mixtures for 12 hours (C). mRNA was extracted and used for down-stream processing.

(A) Scatter plot comparing gene expression in WT and mut-*Stat3* B cell mRNA-Seq datasets. Values are given as reads per kilobase of exon per million mapped reads (RPKM). Red dots denote 322 genes which display a greater than 4 fold change and more than 2 RPKM difference between the two datasets.

(B) mRNA expression fold changes between WT and mut-*Stat3* B cells, filtered for genes known to be involved in CSR. *Socs3*, a STAT3 target gene, is provided as a control.

(C) Expression level of *Id2* was assayed by RT-qPCR on RNA extracted from B cells activated for 12 hours. Transcript levels were normalised to *GAPDH* and bars represent the mean ±SEM relative to unstimulated cells, n=4/group.

Data is representative of 2 independent experiments. Statistical significance was determined using a Mann Whitney U Test. * p≤0.05, ** p ≤ 0.01, *** p ≤ 0.001. Alignment and pre-processing of the raw mRNA sequence reads was provided by Dr. Hong-wei Sun. Quantitation of sequence reads at individual genetic loci was carried out in R by Dr. Wolfgang Resch (NIH, Bethesda, USA).

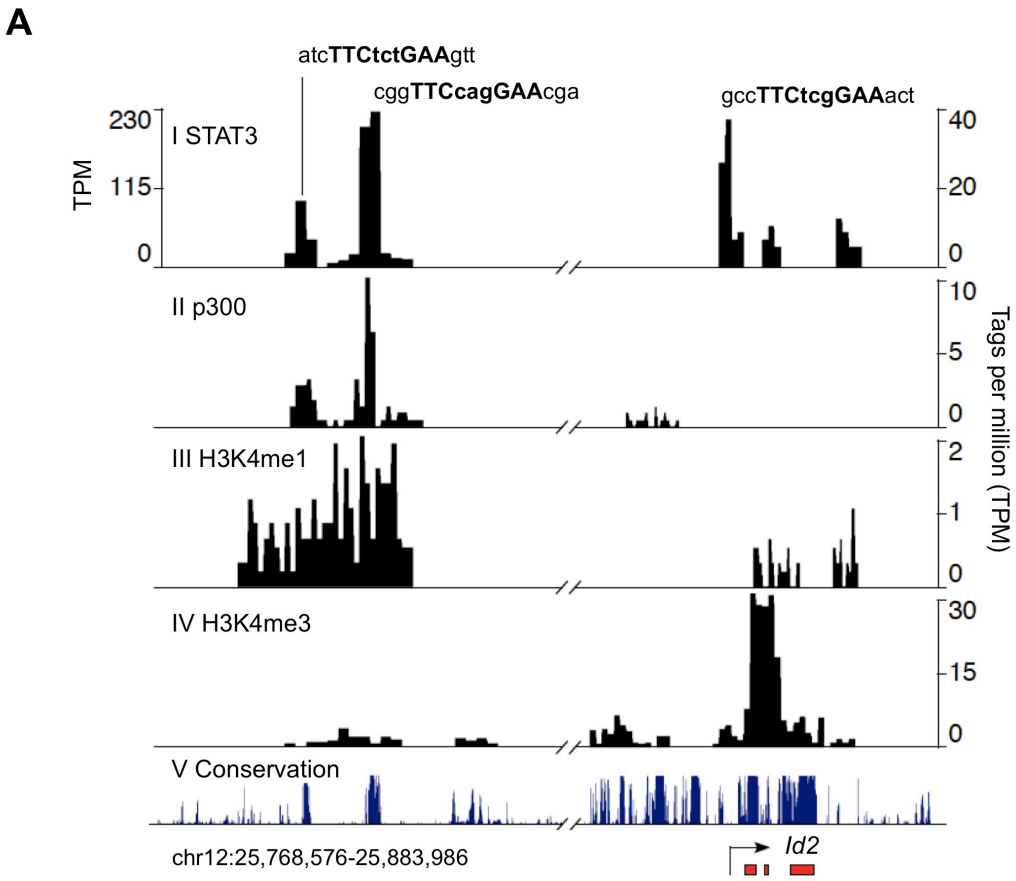

Figure 4.15. STAT3 binds both the *Id2* promoter and an upstream putative enhancer element.

CD43^{-} B cells were MACS selected from the spleens of C57BL/6 WT mice and activated *in vitro* with LPS and IL-4 for 48 hours. Cells were lysed and ChIP-Seq was performed using anti-phospho-STAT3, p300, H3K4me1 and H3K4me3 antibodies.

(A) ChIP-Seq analysis, showing STAT3 (lane I), p300 (lane II), H3K4me1 (lane III), H3K4me3 (lane IV), and phylogenetic conservation (lane V) profiles across a region spanning the *Id2* locus and a putative *Id2* enhancer element 93 Kb upstream in chromosome 12. The location of *Id2* exons (red boxes) is depicted below and the direction of transcription is indicated with an arrowhead. STAT3 consensus binding motifs are provided for both the *Id2* promoter and putative enhancer domains (lane I).

Data is representative of 2 (STAT3, H3K4me3) or 1 (p300, H3K4me1) independent experiments. Alignment and pre-processing of the raw sequence reads was provided by Dr. Hong-wei Sun. Quantitation of sequence reads at individual genetic loci was carried out by Dr. Wolfgang Resch and Dr. Golnaz Vahedi (NIH, Bethesda, USA).

4.2.9. Reconstitution of mut-*Stat3* B Cells with Id2 Restores IgE Regulation.

If the failure to induce Id2 was a relevant mechanism underlying the dysregulation of IgE in mut-*Stat3* mice, we hypothesized that restoration of its expression might reverse this abnormality. We therefore explored whether high Igε CSR in mut-*Stat3* B cells could be rescued by ectopic Id2 expression. To this end, mut-*Stat3* and control cells were activated in the presence of LPS+IL-4 and transduced with a retrovirus that expressed Id2 and GFP bicistronically, or GFP control only (Figure 4.16.A). As shown in Figure 4.16.B, following two rounds of transduction within the first 24 hours of culture, more than 80% of $CD19^+$ cells consistently expressed the GFP reporter 72 hours later. We found that expression of *Id2* uniformly inhibited CSR several-fold, likely due to Id2's reported inhibition of AID transcription upon overexpression (*483*). Despite Id2 reconstitution, however, μ-γ1 CSR remained statistically reduced in mut-*Stat3* B cells compared to WT (Figure 4.16.C). Id2 levels thus did not explain the reduced μ-γ1 CSR we observed in mut-*Stat3* mice. Conversely, ectopic Id2 expression eliminated the elevated IgE production in these cultures; cells infected with the control GFP empty vector maintained elevated IgE production (Figure 4.16.C). Importantly, Id2 reconstitution was accompanied by downregulation in Igε germline transcripts (Figure 4.16.D). Altogether, the data supported the notion that STAT3 modulates Igε CSR levels by direct regulation of Id2 expression in activated B cells and that failure to induce Id2 in mut-*Stat3* cells promoted the hyper-IgE phenotype observed. However, as retroviral reconstitution of Id2 likely led to non-physiologic levels of this important inhibitor of IgE CSR, this experiment does

not definitively prove that Id2 dysregulation is the sole factor leading to elevated IgE CSR in mut-*Stat3* B cells. Indeed, overexpression of Id2 could have inhibited Igε transcription in a dominant fashion.

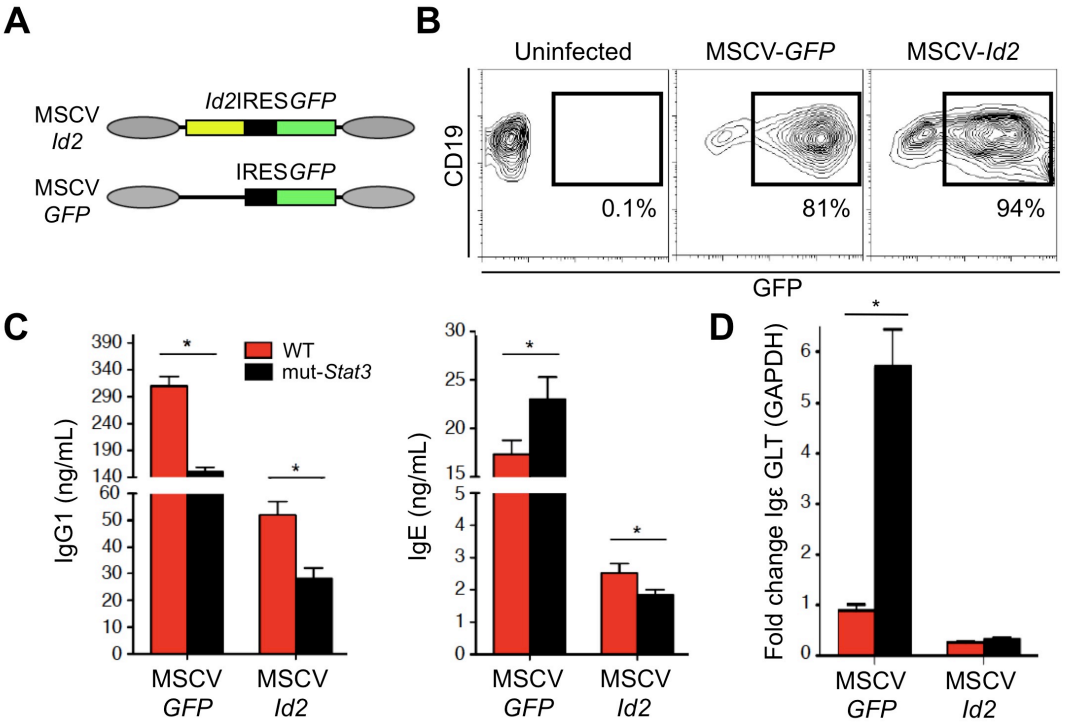

Figure 4.16. Reconstitution of mut-*Stat3* B cells with Id2 restores IgE regulation.

CD43$^-$ B cells were MACS selected from the spleens of C57BL/6 WT and mut-*Stat3* mice and activated *in vitro* with LPS and IL-4. Cells were transduced with either MSCV-Id2 or MSCV-GFP control retroviruses at 12 and 24 hours. RNA was extracted from cells at 72 hours and cell culture supernatants were analyzed by ELISA.

(A) Depiction of MSCV-Id2-IRES-GFP and MSCV-IRES-GFP retroviral vectors with *Id2* gene shown in yellow and *GFP* in green.

(B) Representative 72 hour FACS plots depicting the transduction efficiency of activated B cells with control (GFP) or Id2 retrovirus.

(C) IgG1 and IgE levels were assessed by ELISA from the cell culture supernatants of B cells infected with control (GFP) or Id2 retrovirus at 72 hours. Bars represent the mean ±SEM, n=4/group.

(D) Expression level of the germline (unswitched) Ig*ε* locus was assayed by RT-qPCR on RNA extracted from transduced B cells at 72 hours. Transcript levels were normalised to *GAPDH* and bars represent the mean ±SEM relative to unstimulated WT cells, n=4/group.

Data is representative of 2 independent experiments. Statistical significance was determined using a Mann Whitney U Test. * p≤0.05, ** p ≤ 0.01, *** p ≤ 0.001.

4.3. Discussion.

Despite STAT3's diverse functions related to growth, development and differentiation in a variety of tissues, previous reports indicated normal B and T cell numbers in AD-HIES patients (*394*, *426*, *484*). The *Stat3*ΔV463 mouse model recapitulated these findings, both supporting the strength of this model and suggesting that low levels of STAT3 activity are sufficient for normal B and T cell homeostasis. Previous studies looking at *Stat3* deficiency in B cells provided conflicting results. On the one hand, $CD19^{cre}$-mediated deletion of $Stat3^{flox/flox}$ alleles resulted in defective plasma cell terminal differentiation but otherwise normal B cell ontogeny (*62*). On the other hand, mice where $Stat3^{flox/flox}$ were conditionally ablated via Mx^{Cre} displayed developmental defects in early BM B cell progenitors (*63*). Peripheral *Stat3* deletion by Mx^{Cre} however was incomplete and no defects were reported in the mature B cell compartment of these mice (*63*). Notably, neither of the studies reported the full spectrum of AD-HIES B cell defects. These inconsistencies might be best explained by differences in the timing of *Stat3* deletion (*485*), as well as difficulties in deleting two floxed *Stat3* alleles (as opposed to more efficient deletion of a $Stat3^{flox/-}$ background). The AD-HIES transgenic mouse model however did not depend on either the timing or efficiency of Cre-recombinase activity, but recapitulated the AD-HIES phenotype by physiological expression of the human mutant *Stat3* allele in the entire organism.

Although hypomorphic STAT3 function appears sufficient to maintain total B and T cell numbers, several STAT3 activating cytokines have been reported to play critical roles in the generation of both B and T memory populations in

mice (*79*, *486-489*). Numerous infectious models have strengthened the STAT3-memory linkage by revealing that the STAT3-regulated transcription factors Blimp-1 (encoded by *Prdm1*) and Bcl6 (*Bcl6*), both of which tend to counter-regulate the other, are key players in the generation of effector and central memory CD8 T cells, respectively (*106-110*). Accordingly, reduced numbers of $CD27^{+}CD19^{+}$ B, $CD4^{+}$ and $CD8^{+}$ T memory cells have now been reported in AD-HIES patients and been associated with latent viral reactivation (*460*, *484*). Unfortunately, we have not explored either B or T memory cell production in our BAC-transgenic model. The ChIP-Seq data strongly supports a role for STAT3 in the regulation of Blimp-1 however, increasing the possibility of memory cell defects.

The $CD8^{+}$ T memory populations could be compared in LCMV infected mut-*Stat3* and WT littermate control mice. Further exploration of the B cell memory compartment will be indelibly linked to mut-*Stat3* mice's ability to form germinal centers, as this is the process by which antigen-specific B cells mature into both long-lived plasma cells and memory B cells (*490*). Bcl-6 deficient mice have an absence of germinal center B cells, yet are able to form short-lived antibody secreting cells (*101-103*). Meanwhile, genetic ablation of Blimp-1 in B cells prevented mature B cells from differentiating into either short-lived or long-lived plasma cells, without inhibiting germinal center formation (*92*). Coupling these data with our preliminary findings of normal germinal center B cell numbers but reduced plasma cell numbers in mut-*Stat3* mice, we propose that STAT3 is a potent regulator of Blimp-1 expression in B cells, but is more dispensable for Bcl-6. Intriguingly, Bcl-6 is frequently

overexpressed (*491-493*) in lymphomas and AD-HIES patients exhibit a high incidence of B cell lymphomas (*386*). As Blimp-1 potently represses Bcl-6 expression under normal physiological circumstances, a failure to induce Blimp-1 in AD-HIES B cells could contribute to their increased propensity to undergo unchecked expansion.

Bcl-6 has also been shown to be critical for the formation of Tfh cells (*174*, *453*). Our preliminary findings suggest that these cells are present in mut-*Stat3* mice. By comparison, a recent study found reduced Tfh cell numbers in AD-HIES patients, but this study was based strictly on circulating cells carrying Tfh-like markers (*442*). Clearly, further investigation is required. Our findings of increased IFN-γ and Foxp3 expression following *in vitro* T cell differentiation have also not been corroborated in AD-HIES. However, similar changes have been observed in *Stat3* deficient T cells *in vivo* (*219*). This study found no evidence for STAT3 binding to either the *Ifng* or *Foxp3* locus, suggesting an indirect role for STAT3 in regulation of these two factors (*219*). One possible explanation for increased IFN-γ production in a STAT3 null environment involves the SOCS family of feedback inhibitors. STAT3 activation induces SOCS3, which subsequently attenuates STAT3 signals. Likewise, STAT1 activation induces SOCS1, which attenuates STAT1 signals. Cells deficient in *Socs3*, show increased STAT3 and STAT1 phosphorylation following a STAT3 stimulus (IL-6) but normal STAT1 phosphorylation following a STAT1 stimulus (IFN-γ) (*494*). Alternatively, *Socs1* deficient cells show enhanced STAT1 and STAT3 phosphorylation following a STAT1

stimulus (IFN-γ), but normal phosphorylation following a STAT3 stimulus (IL-6) (*494*). This suggests cross-regulation of STAT1 and STAT3 signals via SOCS proteins. Socs3 is a well characterized STAT3 target and its expression was thus reduced in the mut-*Stat3* B cells. Decreased SOCS3 activity in mut-*Stat3* T cells could therefore lead to enhanced STAT1 signaling and subsequent IFN-γ production. STAT5 directly binds to the *Foxp3* locus and promotes its expression(*495*). The increased number of Foxp3^{+} cells in mut-*Stat3* cultures could thus be due to either a loss of STAT3 inhibition or enhanced STAT5 activity due to the additional *Stat5a* copy included in the transgene. As the additional *Stat5a* is not constitutively active this seems unlikely, but *Stat5a* deficient mice could be crossed with the mut-*Stat3* line in an effort to address this by normalizing expression levels.

IgE levels were increased in mut-*Stat3* B cell cultures compared to WT. In addition to IgE dysregulation, we also detected decreased IgG1 and IgG3 in mut-*Stat3* mice and cultures, which is consistent with the lower antigen specific IgG production observed in AD-HIES patients following immunization (*460*). While our data did not reveal a direct role of STAT3 in transcription and/or recombination of these isotypes, low levels of IgG in mut-*Stat3* mice might be explained by the inefficient terminal differentiation of AD-HIES B cells. In this context, several lines of evidence have previously linked STAT3 activity with the development of antibody secreting cells. Forced-expression of STAT3 in human B cells for instance, is sufficient to promote plasma cell differentiation (*472*), and transcription of *Prdm1*, the plasma cell master

regulator, depends on STAT3 (*473*). In agreement with these findings, we have observed reduced numbers of $CD138^+$ plasma cells both in immunized mut-*Stat3* mice and cell cultures. Furthermore, the ChIP-Seq analysis clearly showed binding of STAT3 to *Prdm1*, and mut-*Stat3* B cells displayed both reduced Blimp-1 transcription and H3K4me3 of Blimp1–associated chromatin. Our findings are thus consistent with the notion that STAT3 regulates multiple essential steps of bone marrow and peripheral B cell development.

In attempting to deduce how mutant STAT3 affects μ-ε CSR, we uncovered *Id2*, a factor known to downmodulate μ-ε switch recombination (*478*), as a primary target of STAT3. *Id2* was originally characterized as a TGF-1 inducible gene in B lymphocytes undergoing CSR (*478*), but these effects were minor compared to those we saw following STAT3 activation. Consistent with a direct role of STAT3 in *Id2* transcription, we have mapped STAT3 occupancy at the *Id2* promoter region and noted a more pronounced interaction at an upstream putative enhancer element. Our studies therefore call attention to STAT3 as a crucial regulator of *Id2* expression during B cell activation.

Like other E proteins, Id2 contains a helix-loop-helix moiety, but lacks an E-box DNA binding domain (*496*). As such, Id2 is believed to downmodulate Igε transcription by heterodymerizing with E2A and Pax5, and thus partially blocking their binding to Igε (*483*). In this context, our data argue STAT3 regulates recombination to Sε controlling the balance between E proteins at

the Igε promoter (Figure 4.17.). This balance in turn appears to define the extent of epigenetic reprogramming of the Igε locus, most particularly deposition of H3K4me3, which we found to be directly proportional to the frequency of μ-ε CSR. The essential role of this chromatin mark in effecting CSR was recently uncovered in B cells deficient for the H3K4 methyltransferase Ptip. Upon activation, these lymphocytes display a highly selective defect in Igγ1 and Igγ3 H3K4me3, germline transcription, and CSR (*130*). Ptip is likely to promote recombination via H3K4me3 by facilitating recruitment and/or stabilization of RNA polymerases, leading to AID accessibility. Intriguingly, Ptip was not required for μ-ε switching, suggesting a different methyltransferase promotes accessibility to Sε. The Sε methyltransferase our data propose, is likely recruited by E2A and/or PAX5 activity. In support of this view, global E2A occupancy in B-lymphocytes directly correlates with recruitment of H3K4 methylase activity to promoter-proximal sequences (*497*).

In conclusion, our studies identify a mechanism of hyper-IgE production in B cells expressing a AD-HIES-derived *Stat3* allele. The relevance of these findings to the human disease will be an important area for further investigation. Even if a similar mechanism is identified in AD-HIES, *STAT3* mutations do not account for all HIES patients. The applicability of our findings to related disorders such as AR-HIES, which has recently been linked to mutations in the Rho-Rac GTP-exchange factor Dock8, is uncertain (*74*). However, high levels of IgE are also the hallmark of numerous diseases, such

as Ommen syndrome, allergy, asthma, Comel-Netherton syndrome, eczema, Wiskott-Aldrich syndrome, atopy, and X-linked syndrome (*498*, *499*). By establishing a link between STAT3 and the regulation of Igε CSR, our findings could help in the design of novel therapeutics to treat disorders where IgE may play a pathogenic role.

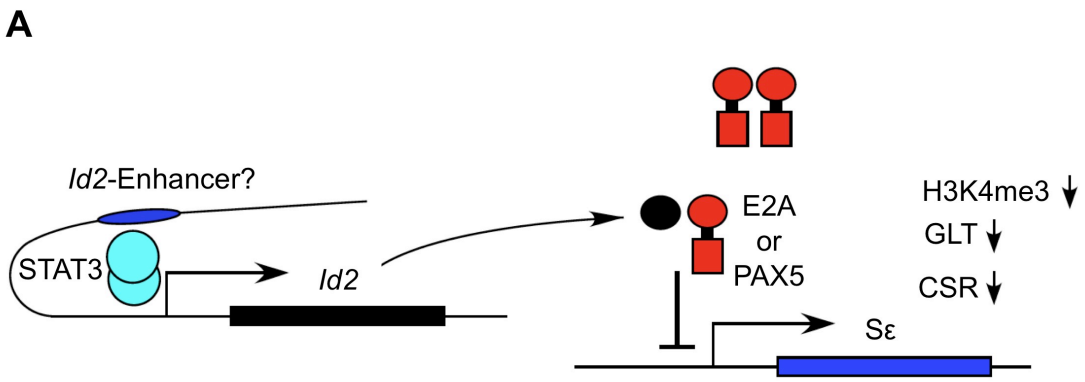

Figure 4.17. Proposed model of STAT3 regulation of IgE expression.

(A) STAT3 promotes *Id2* transcription in activated B cells through interaction with its promoter and potentially enhancer elements. Heterodimerization of ID2 with E2A and possibly PAX5 precludes their binding to the Igε basal promoter, leading to reduced active chromatin marks (H3K4me3), Igε germline transcription, AID accessibility, and, consequently, impaired IgE CSR. In cells expressing the dominant-negative STAT3ΔV463, *Id2* expression is decreased resulting in increased μ-ε CSR.

5. Chapter 5: Hypomorphic STAT3ΔV463 in Intestinal Immune Homeostasis.

5.1. Introduction.

As a key mediator of both pro- and anti-inflammatory cytokine signals, STAT3 plays important roles in the intestinal immune system, both at steady state and in the context of inflammation. STAT3 mediated IL-22 signaling into intestinal epithelial cells promotes would healing, and mice lacking STAT3 in their IECs show increased susceptibility to DSS-induced colitis (*49*). More strikingly, mice with STAT3 deficient neutrophils and macrophages develop a spontaneous colitis attributed to a loss of suppressive IL-10 signaling (*53*). Selective loss of STAT3 in Treg cells also leads to the development of fatal intestinal pathology (*294*). On the other hand, blockade of STAT3 activating cytokines like IL-6 and IL-23 is sufficient to prevent experimental colitis (*243*, *437*, *500-503*), suggesting that STAT3 is important in driving the inflammatory response as well as repressing it.

Genetic studies have identified both the *STAT3* and *JAK2* (upstream activator of STAT3) genes as susceptibility loci in crohn's disease (CD) and ulcerative colitis (UC) (*504*, *505*). Additionally, phosphorylated STAT3 levels are heightened in inflamed tissues from IBD patients relative to controls (*26*, *506*). However, STAT3's opposing pro- and anti-inflammatory actions make it difficult to discern if heightened STAT3 activity in the tissue is a cause or consequence of the pathology. As germline deletion of *Stat3* was

embryonically lethal (*45*), our *Stat3*ΔV463 mouse model provides us with a unique opportunity to explore the overall effect of STAT3 signaling within the intestine, both at steady state and in the context of inflammation.

Citrobacter rodentium is a naturally occurring A/E pathogen that infects the rodent gastrointestinal tract (*507*). Oral infection of immunocompetent mice with *C. rodentium* leads to a transient colonisation and inflammation that peaks after one week and is cleared in the ensuing two to three weeks (*508*). Bacterial colonization is limited to the intestinal mucosa with low bacterial burden in systemic organs. Infected mice exhibit mild signs of clinical disease and microscopically the mucosa presents crypt hyperplasia, goblet cell loss and mucosal infiltration of immune cells including T cells, macrophages and neutrophils. *C. rodentium* induces strong IL-17A responses from $CD4^+$ T cells (*209*) and the STAT3 activating cytokines IL-22 and IL-23 are necessary for bacterial clearance (*509*, *510*). Collectively, IECs, innate, and adaptive immune responses are all critical in host defense against this pathogen, making *C. rodentium* an ideal model to examine the importance of STAT3 function in multiple cell types of the intestinal immune system.

5.2. Results.

5.2.1. Steady-State Characterization of Intestinal Lymphoid Subsets in mut-*Stat3* Mice.

In contrast to previous reports of *Stat3* deletion in myeloid or Treg cells, hypomorphic STAT3 activity in mut-*Stat3* mice did not result in the development of spontaneous, fatal intestinal pathology. In fact, the total number of colonic lamina propria cells was indistinguishable between mut-*Stat3* and WT littermate control mice (Figure 5.1.A). The same was true of $CD4^+$ cells, suggesting a lack of spontaneous, underlying inflammation in this mouse model (Figure 5.1.B). Mice with a T cell specific deletion of *Stat3* are reported to have a reduction in percent and total number of $CD8^+$ T cells in the colonic lamina propria, despite normal $CD4^+$ numbers (*219*). A mechanism for this finding remains unknown and it will be of interest to examine $CD8^+$ T cell populations in mut-*Stat3* mice in the future.

As no gross pathological changes were observed, we next investigated whether the dominant-negative transgene would affect intestinal T cell subsets, as had been reported in mice with *Stat3* deficient T cells (*219*). FACS analysis of cytokine expression in mut-*Stat3* $CD4^+$ cells revealed an approximate 50% reduction in the percentage of IL-17A producing cells compared to WT (Figure 5.2.B). Notably, the MFI was also reduced at steady-state (Figure 5.2.B). Also consistent with the *in vitro* findings, we found an increased percentage of $Foxp3^+$ cells (Figure 5.2.B). No statistical difference in the percentage of IFN-γ producers was noted. As IL-17A production is completely extinguished in Stat3 deficient T cells, these data

reemphasized the reduced, but not absent, STAT3 activity in mut-*Stat3* cells.

In addition to classical lymphocytes, the colonic mucosa contains ILC populations. Beyond their role in lymphoid organogenesis, recent studies have highlighted the role of ILCs as immune effector cells (*333*, *511-513*). In particular, RORγt-dependent ILC populations are thought to contribute to IL-23-mediated mucosal host defence and immune pathology. RORγt-dependent ILCs are thought to consist of three cellular subsets: LTi-like cells (IL-17A and IL-22 producers), NK22s (IL-22 producers), and $CD4^{-}NKp46^{-}$ ILCs (IL-17A, IL-22 and IFN-γ producers). As these populations are all dependent on both STAT mediated cytokine signals and the transcription factor Id2 for survival, we were concerned that these cells might be deficient in mut-*Stat3* mice. To the contrary we found that all three populations were preserved in mut-*Stat3* mice (Figure 5.2.A). Functional characterization of ILC populations in mut-*Stat3* mice will be important for future studies as LTi-like cells are reported to be an essential source of host protective IL-22 in *C. rodentium* infection (*511*).

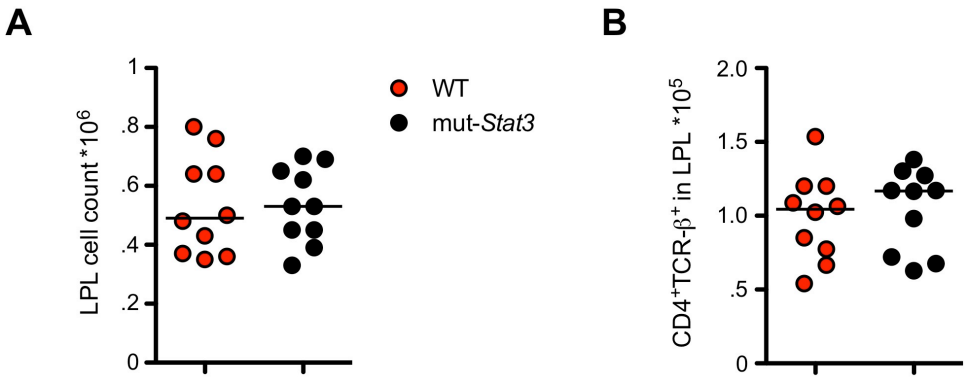

Figure 5.1. Steady-state comparison of WT and mut-*Stat3* colonic LPLs.

Cells were isolated from the colonic lamina propria of cohoused C57BL/6 WT and mut-*Stat3* mice. Expression of surface markers was determined by FACS.

(A) Total number of lymphocytes in the lamina propria of steady-state WT and mut-*Stat3* mice. Bars represent the mean and each point represents an individual mouse.

(B) Total number of $CD4^+TCR\text{-}\beta^+$ cells in the lamina propria of steady-state WT and mut-*Stat3* mice. Bars represent the mean and each point represents an individual mouse.

Data represents the pooled results of 2 independent experiments. Statistical significance was determined using a Mann Whitney U Test.

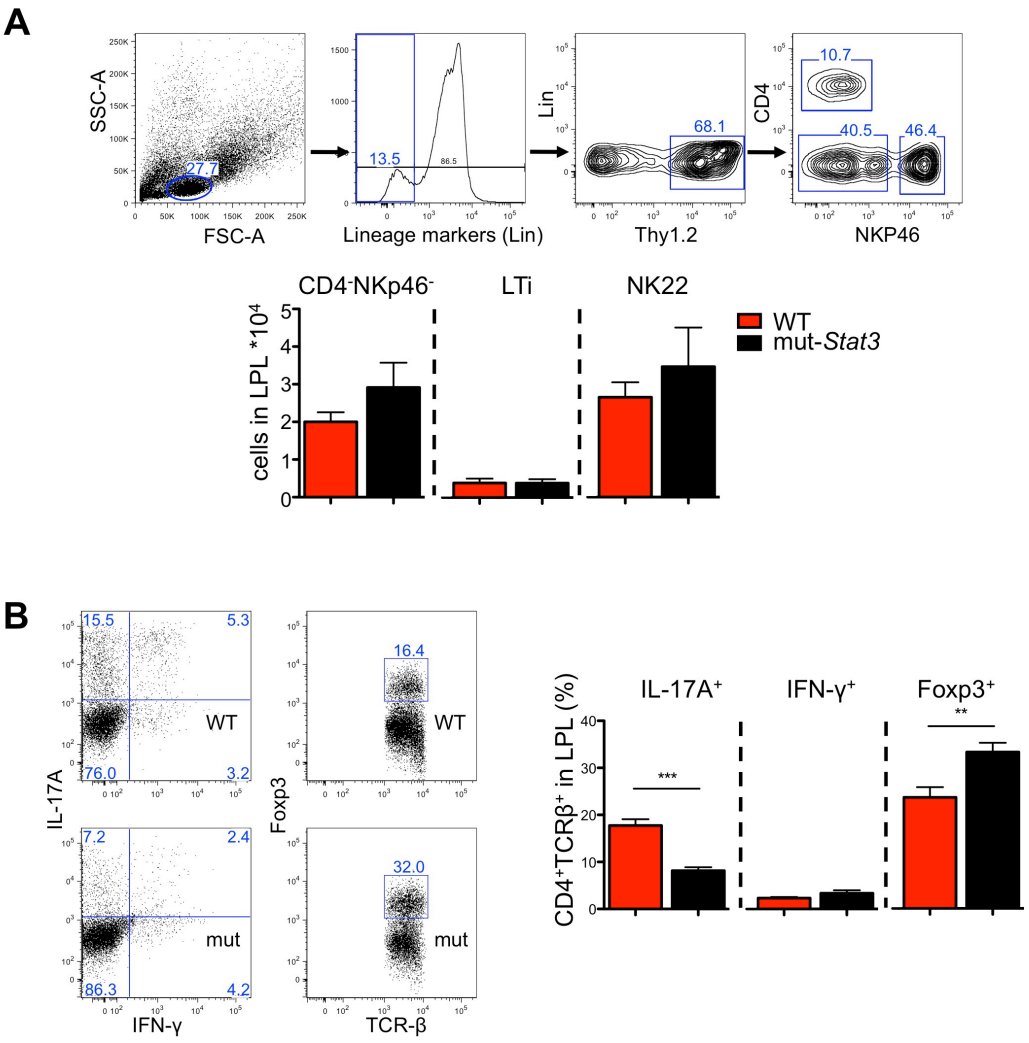

Figure 5.2. Steady-state comparison of WT and mut-*Stat3* innate lymphoid and CD4⁺ T cells.

Cells were isolated from the colonic lamina propria of cohoused C57BL/6 WT and mut-*Stat3* mice. Single cell suspensions were re-stimulated with PMA and Ionomycin in the presence of Brefeldin-A for 4 hours (B). Expression of surface markers and cytokines/transcription factors was determined by FACS.

(A) FACS plots demonstrating gating strategy for innate lymphoid subsets: (top). Total number of FACS defined populations in LPLs (below). CD4⁻NKp46⁻: Lineage⁻Thy1.2⁺CD4⁻NKp46⁻, LTi: Lineage⁻Thy1.2⁺CD4⁺NKp46⁻, NK22: Lineage⁻Thy1.2⁺CD4⁻NKp46⁺. Bars represent the mean ±SEM, n=4/group.

(B) Representative FACS plots showing IL-17A, IFN-γ and Foxp3 expression among viable WT and mut-Stat3 CD4⁺TCR-β⁺ cells (left). Summary of FACS data showing frequency of positive cells (right). Bars represent the mean ±SEM, n=10/group

Data is representative of 1 (A) or 2 (B) independent experiments. Statistical significance was determined using a Mann Whitney U Test. * p≤0.05, ** p ≤ 0.01, *** p ≤ 0.001.

5.2.2. Mut-*Stat3* Mice Show Increased Susceptibility to DSS Colitis.

Supplementation of drinking water in mice with low-molecular weight dextran sodium sulfate results in epithelial damage and a robust inflammatory response in the colon lasting several days (*360*). The acute phase of DSS-induced colitis is independent of B and T cells, as it occurs in SCID mice, suggesting this model is mediated by innate rather than adaptive immunity (*361*). STAT3 phosphorylation is elevated in the colon of DSS treated mice (*362*) and mice with *Stat3* deficient IECs are more susceptible (*49*). Administration of DSS to mut-*Stat3* mice yielded similar results, with rapid weight loss necessitating termination of all mice as a humane end-point by day 7 (Figure 5.3.A and 5.3.B). This strongly suggested that expression of the *Stat3*ΔV463 transgene resulted in epithelial and/or innate immune defects in the mut-*Stat3* mice.

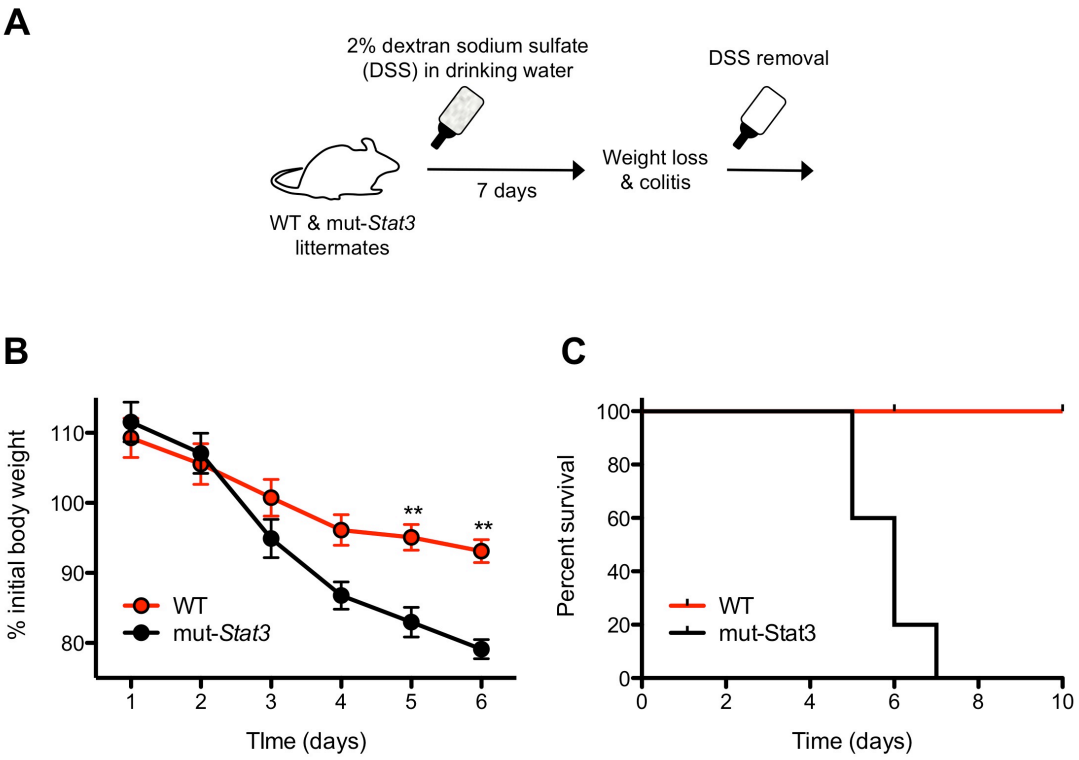

Figure 5.3. mut-*Stat3* mice show increased susceptibility to DSS colitis.

Cohoused C57BL/6 WT and mut-*Stat3* mice were administered 2% DSS in their drinking water for 7 days. Weight and body scores were monitored daily; mice were sacrificed after 20% weight loss.

(A) Schematic of experimental design.

(B) Weight loss during the course of the experiment shown as percentage of day 0 weight. Bars represent the mean ±SEM, n=10/group.

(C) Survival plot during the course of the experiment shown as a percentage.

Data represents the pooled results of 2 independent experiments. Statistical significance was determined using a repeated measure ANOVA followed by Bonferroni post-hoc test. * p≤0.05, ** p ≤ 0.01, *** p ≤ 0.001

5.2.3. Mut-*Stat3* Mice Show Increased Susceptibility to *C. rodentium.*

Having observed defects in both B and T lymphocyte function *in vitro*, as well as possible epithelial or innate immune defects in DSS colitis, we next turned to the question of whether mut-*Stat3* animals had impaired host defense against a bacterial pathogen. For this we orally infected animals with *C. rodentium* (Figure 5.4.A). As expected, WT mice developed mild signs of clinical disease but no weight loss (Figure 5.4.C). In contrast, mut-*Stat3* littermates developed a significant wasting disease from approximately one week post-infection (Figure 5.4.C). Rapid weight loss and/or severe clinical signs of disease led to the necessary sacrifice of more than half of the mut-*Stat3* mice within two weeks of infection (Figure 5.4.B). Remaining WT and mut-*Stat3* mice were sacrificed on day 14 and their cecums and distal colons were evaluated for histological changes (see methods). Histological analysis revealed significantly elevated inflammation in both the cecum and distal colon of mut-*Stat3* mice (Figure 5.4.D).

To investigate the possible systemic spread of *C. rodentium* in these mice, spleens and livers of sacrificed animals were harvested and analyzed for bacterial colonization and inflammatory infiltrates (see methods). As expected, the majority of WT spleens and livers showed little or no *C. rodentium* colonization. However, all mut-*Stat3* livers and the majority of spleens showed a significant *C. rodentium* burden (Figure 5.5.A). Corresponding with these findings, we noted increased splenic cell numbers in mut-*Stat3* mice (Figure 5.5.B). FACS analysis of splenocytes revealed a significant increase in the number of $CD11b^{+}Gr\text{-}1^{+}$ myeloid cells (neutrophils, monocytes, macrophages)

in mut-*Stat3* spleens relative to WT, suggesting an influx of these cells in response to the bacterial colonization (Figure 5.5.C). Collectively, these data showed a clear defect in the ability of *mut-Stat3* mice to contain *C. rodentium* infection within the intestine.

We also analyzed *C. rodentium* colonization at the site of infection. Both WT and mut-*Stat3* mice showed high bacterial loads in the gut relative to what was observed systemically. No significant difference was noted in *C. rodentium* colonization of the cecum between the two groups. However, colonization of the distal colon was slightly elevated in mut-*Stat3* mice (Figure 5.6.A). Corresponding with the increased inflammation noted histologically in mut-*Stat3* colons, the total LPL numbers were nearly two-fold increased in these mice (Figure 5.6.B). As observed in the spleen, FACS analysis of the LPLs uncovered a profound increase in $CD11b^{+}Gr\text{-}1^{+}$ cells in mut-*Stat3* colons (Figure 5.6.C). However, closer analysis of the $CD11b^{+}Gr\text{-}1^{int}$ cells by FSC and SSC revealed two distinct populations (Figure 5.6.C: dot plots). We hypothesized that the more granular population could be eosinophils and confirmed this by showing that they expressed Siglec-F, a sialic acid-binding Ig superfamily receptor selectively expressed on mouse eosinophils (*514-516*) (Figure 5.6.C: histogram). Notably, eosinophils were both the most prevalent and enhanced myeloid population in mut-*Stat3* colons (Figure 5.6.C). Little is known about the role of eosinophils in intestinal inflammation, although they are elevated in IBD (*517-519*). Depletion of this subset by injection of an anti-Siglec-F antibody prior to *C. rodentium* infection would be interesting to pursue in the future.

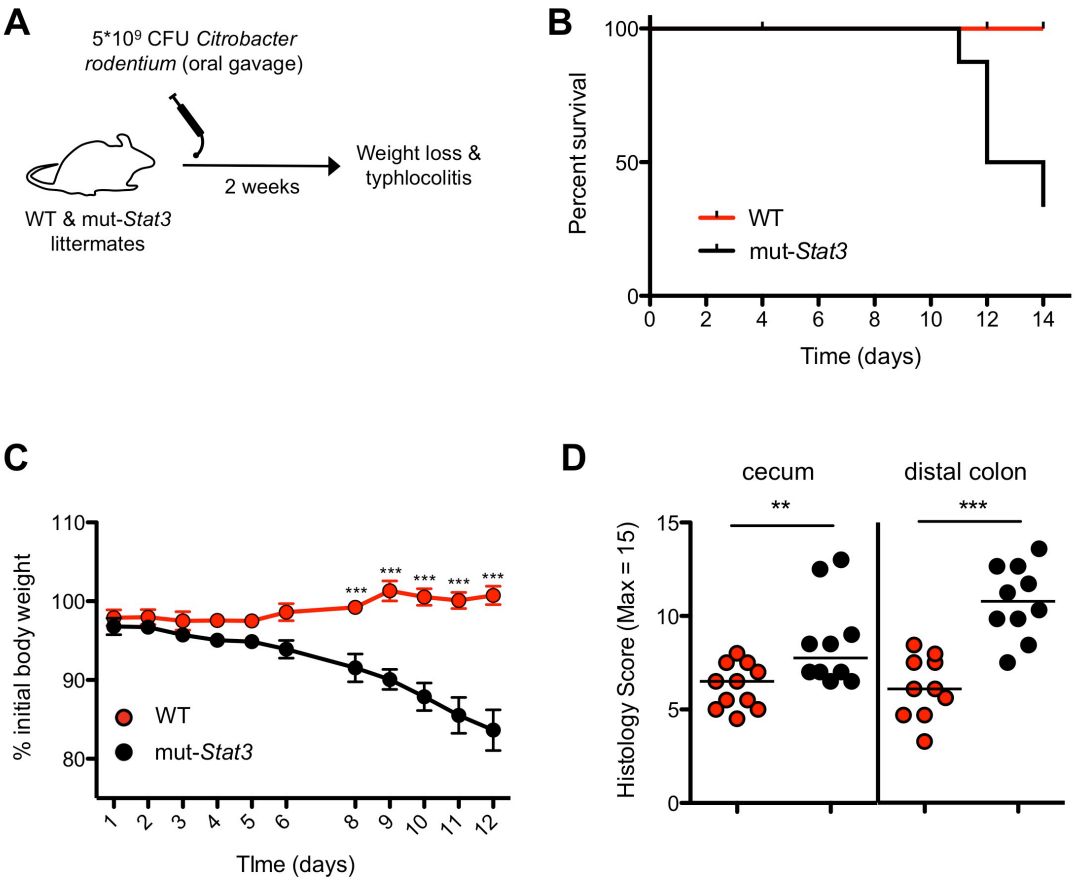

Figure 5.4. mut-*Stat3* mice show increased susceptibility to *Citrobacter rodentium* induced colitis.

Cohoused C57BL/6 WT and mut-*Stat3* mice were infected orally with 5*10^9 colony forming units (CFU) of *C. rodentium*. Weight and body scores were monitored daily. Mice were sacrificed when mut-*Stat3* mice developed clinical signs of disease (2 weeks) and assessed for intestinal inflammation.

(A) Schematic of experimental design.

(B) Survival plot during the course of the experiment shown as a percentage.

(C) Weight loss during the course of the experiment shown as percentage of day 0 weight. Bars represent the mean ±SEM.

(D) Histological analysis of inflammation from the cecum and distal colon. Bars represent the mean and each point represents an individual mouse.

Data represents the pooled results of 2 independent experiments (n=11 for WT, n=10 for mut-*Stat3*). Statistical significance was determined using a repeated measure ANOVA followed by Bonferroni post-hoc test (C) and Mann Whitney U Test (D). * p≤0.05, ** p ≤ 0.01, *** p ≤ 0.001.

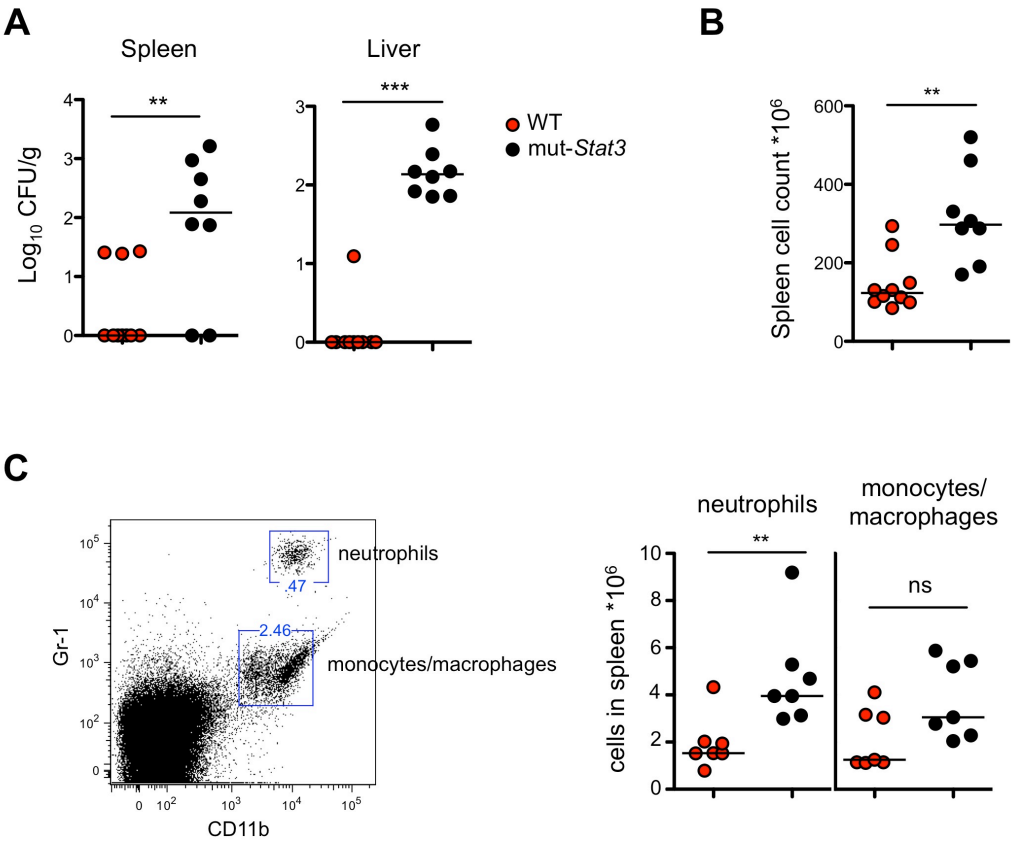

Figure 5.5. mut-*Stat3* mice show increased systemic bacterial dissemination following a 2 week infection with *Citrobacter rodentium*.

Cohoused C57BL/6 WT and mut-*Stat3* mice were infected orally with $5*10^9$ CFU of *C. rodentium*. Mice were sacrificed when mut-*Stat3* mice developed clinical signs of disease (2 weeks).

(A) Spleen and liver sections from infected mice were homogenized and *C. rodentium* colonization determined as CFU per mass. Bars represent the mean and each point represents an individual mouse.

(B) Total cell counts of RBC lysed spleens from infected mice. Bars represent the mean and each point represents an individual mouse.

(C) Representative FACS plot of infected spleens, gated on $CD11c^-$ viable cells defining $CD11b^+Gr\text{-}1^{hi}$ neutrophils and $CD11b^+Gr\text{-}1^{int}$ inflammatory monocytes/macrophages (left). Total number of FACS defined populations in infected spleens (right). Bars represent the mean and each point represents an individual mouse.

Data represents the pooled results of 2 independent experiments, totaling n=10 for WT and n=8 for mut-*Stat3*. Statistical significance was determined using a Mann Whitney U Test. * $p \leq 0.05$, ** $p \leq 0.01$, *** $p \leq 0.001$.

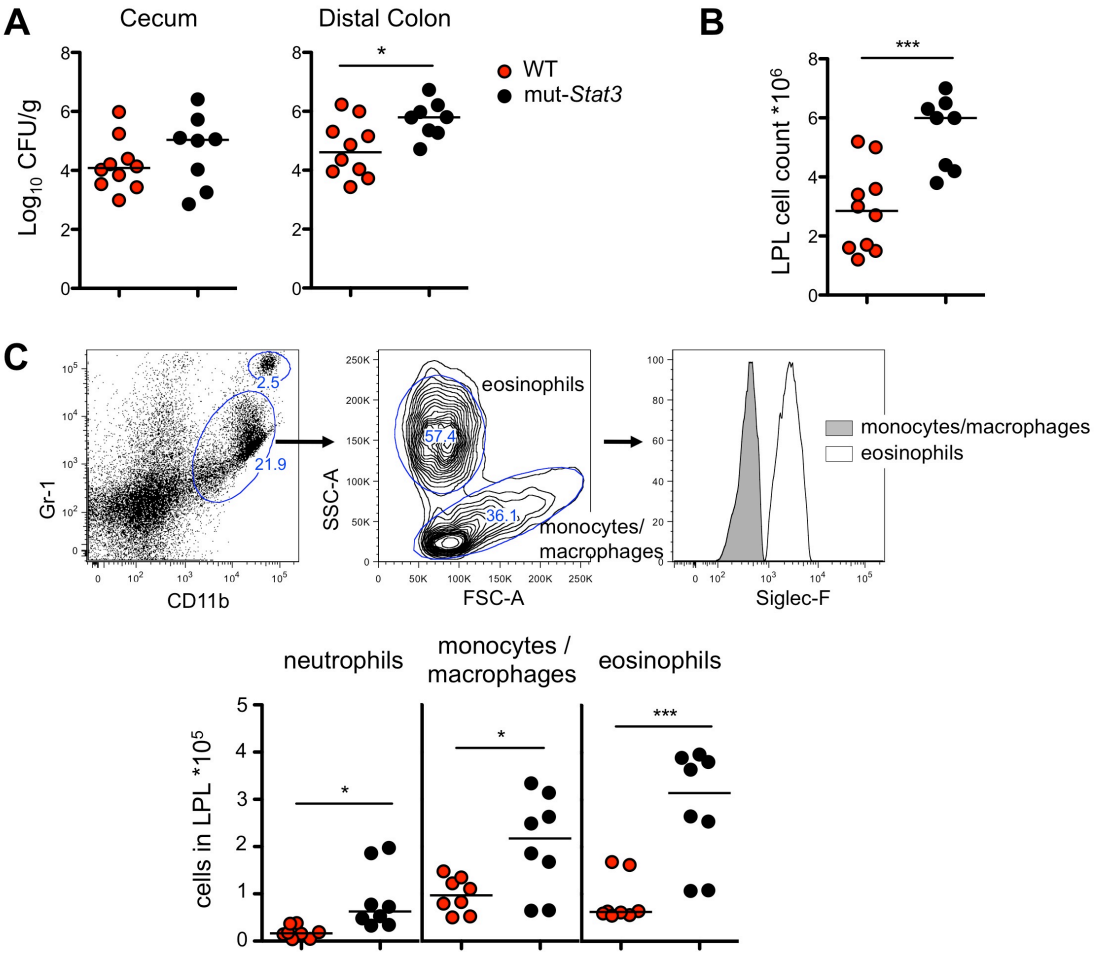

Figure 5.6. Increase in *C. rodentium* colonization and enhanced myeloid accumulation in colons of mut-*Stat3* mice at 2 weeks post infection.

Cohoused C57BL/6 WT and mut-*Stat3* mice were infected orally with $5*10^9$ CFU of *C. rodentium*. Mice were sacrificed when mut-*Stat3* mice developed clinical signs of disease (2 weeks).

(A) Cecum and distal colon sections from infected mice were homogenized and *C. rodentium* colonization determined as CFU per mass. Bars represent the mean and each point represents an individual mouse.

(B) Total number of lymphocytes in the lamina propria of infected WT and mut-*Stat3* mice. Bars represent the mean and each point represents an individual mouse.

(C) Representative FACS plots of LPLs, gated on $CD11c^-$ viable cells defining $CD11b^+Gr\text{-}1^{hi}$ neutrophils, $CD11b^+Gr\text{-}1^{int}Siglec\text{-}F^-$ monocytes/macrophages and $CD11b^+Gr\text{-}1^{int}Siglec\text{-}F^+$ eosinophils (top). Total number of FACS defined populations in LPLs (below). Bars represent the mean and each point represents an individual mouse.

Data represents the pooled results of 2 independent experiments, totaling n=10 for WT and n=8 for mut-*Stat3*. Statistical significance was determined using a Mann Whitney U Test. * $p \leq 0.05$, ** $p \leq 0.01$, *** $p \leq 0.001$.

5.2.4. Interrogation of the Adaptive Immune Response to *C. rodentium* in mut-*Stat3* Mice.

C. rodentium infection of immune-deficient mouse strains has established that $CD4^+$ T cells, B cells, and *C. rodentium*–specific antibody responses are all essential components for containment and clearance of this pathogen (*367*, *368*). Infection of mice with *C. rodentium* results in robust production of IL-17A, IL-17F, and IFN-γ in $CD4^+$ T cells (*209*, *520*). Additionally, T cells can be a major source of GM-CSF and TNF-α (*521*, *522*), which are both highly expressed in the colons of infected mice (*510*, *523*, *524*). IL-17A, IL-17F, IFN-γ and GM-CSF deficient mice have all been shown to be more susceptible to this A/E pathogen (*510*, *520*, *524*).

To compare the adaptive arm of *C. rodentium* immunity in WT and mut-*Stat3* mice, we orally infected animals as previously described and sacrificed them two weeks later. Serum was collected and isolated $CD4^+TCR\beta^+$ colonic LPLs were re-stimulated with PMA and Ionomycin and expression of intracellular cytokines or transcription factors assessed by FACS. As previously reported (*525*), we observed high percentages of WT $CD4^+$ cells producing IL-17A and/or IFN-γ following *C. rodentium* infection (Figures 5.7.B and 5.7.C). Notably, 40-50% of cells were GM-CSF^+ and/or TNF-α^+, suggesting that $CD4^+$ T cells are a significant source of these inflammatory mediators in *C. rodentium* infection (Figure 5.7.B). While similar percentages of GM-CSF, TNF-α, and IL-22 expressing cells were present in both populations, IL-17A and IL-17F producing cells were approximately 50% reduced in mut-*Stat3* mice (Figure 5.7.B). The percentage of IFN-γ producing cells was also skewed

in mut-*Stat3* mice (~ 20% increase) while the percentage of IL-13 producers was unaltered (Figure 5.7.C). IL-17A and IL-17F singly or doubly deficient mice have previously been shown to exhibit increased bacterial loads and colonic pathology compared to controls 14 days post-infection with *C. rodentium* (*520*), suggesting a possible host-protective defect in the adaptive immune response of mut-*Stat3* mice. However, this and other studies have clearly indicated non-T cells as a significant source of IL-17A/F production in *C. rodentium* infection, necessitating further analysis of total IL-17 production in the colons of infected mut-*Stat3* mice. How hypomorphic STAT3 activity affects ILC production of IL-17A and IL-17F will be of particular interest to pursue.

The increased percentage of IFN-γ producing colonic $CD4^+$s in infected mut-*Stat3* mice was different than what we had observed in steady state mice (Figure 5.2.B), but similar to what we had observed following *in vitro* differentiation with IL-12 (Figure 4.2.B). These data suggest that both cell-intrinsic and environmental alterations could contribute to increased IFN-γ production in mut-*Stat3* T cells. Additionally, IFN-γ production from $CD4^+$ T cells has been shown to be dispensable for *C. rodentium* clearance (*367*), bringing into question the effect of this elevated inflammatory mediator in the system. Notably, the percentage of $Foxp3^+$ and $IL\text{-}10^+$ cells were also dramatically increased in mut-*Stat3* mice compared to WT (Figure 5.7.D). Although $Foxp3^+$ cells were also elevated at steady state, the marked increase in these regulatory factors in *C. rodentium* infection could also be

resultant from the greater intestinal inflammation noted histologically in these mice (Figure 5.4.D).

In a previous study, CD4 or TCRβ deficient mice infected with *C. rodentium* died by 3 weeks post-infection. By comparison, $Rag2^{-/-}$ or B cell deficient mice died even quicker (2 weeks post-infection) (*526*). An independent study found that B cell deficient mice survived initial infection, only to succumb to severe gut inflammation at 6 weeks. The authors further showed that the host-protective function of B cells was independent of secretory IgA and IgM, as knockout mice cleared *C. rodentium* normally. Rather, the transfer of IgG antibodies from immune sera conferred protection (*368*).

To analyze the humoral immune response against *C. rodentium,* we collected serum from WT and mut-*Stat3* mice sacrificed 4, 9, and 14 days post infection (Figure 5.8.B); the serum concentration of multiple immunoglobulin isotypes were assessed by bead array or ELISA. As expected, very minimal serum differences were observed between mice sacrificed 4 or 9 days post infection (Figure 5.8.B). However, serum from mut-*Stat3* mice sacrificed 14 days post-infection showed elevated levels of all isotypes tested. IgG2b, IgG2c and IgE levels were elevated in WT (Figure 5.8.B). With the exception of IgG1, serum concentrations of all isotypes were statistically higher in mut-*Stat3* mice compared to WT at day 14, suggesting a strong humoral response in these mice (Figure 5.8.B). As mut-*Stat3* mice also showed higher bacterial burdens it is likely that the elevated humoral response was attributable to increased

antigenic challenge rather than intrinsic cellular defects. We also measured *C. rodentium* specific immunoglobulins in day 14 sera by ELISA. *C. rodentium* specific IgM levels were equivalent between WT and mut-*Stat3* mice, while IgG3 and IgA responses were slightly elevated in the mut-*Stat3* sera (Figure 5.8.C). Collectively, these data suggested that the humoral immune response to *C. rodentium* was intact in mut-*Stat3* animals.

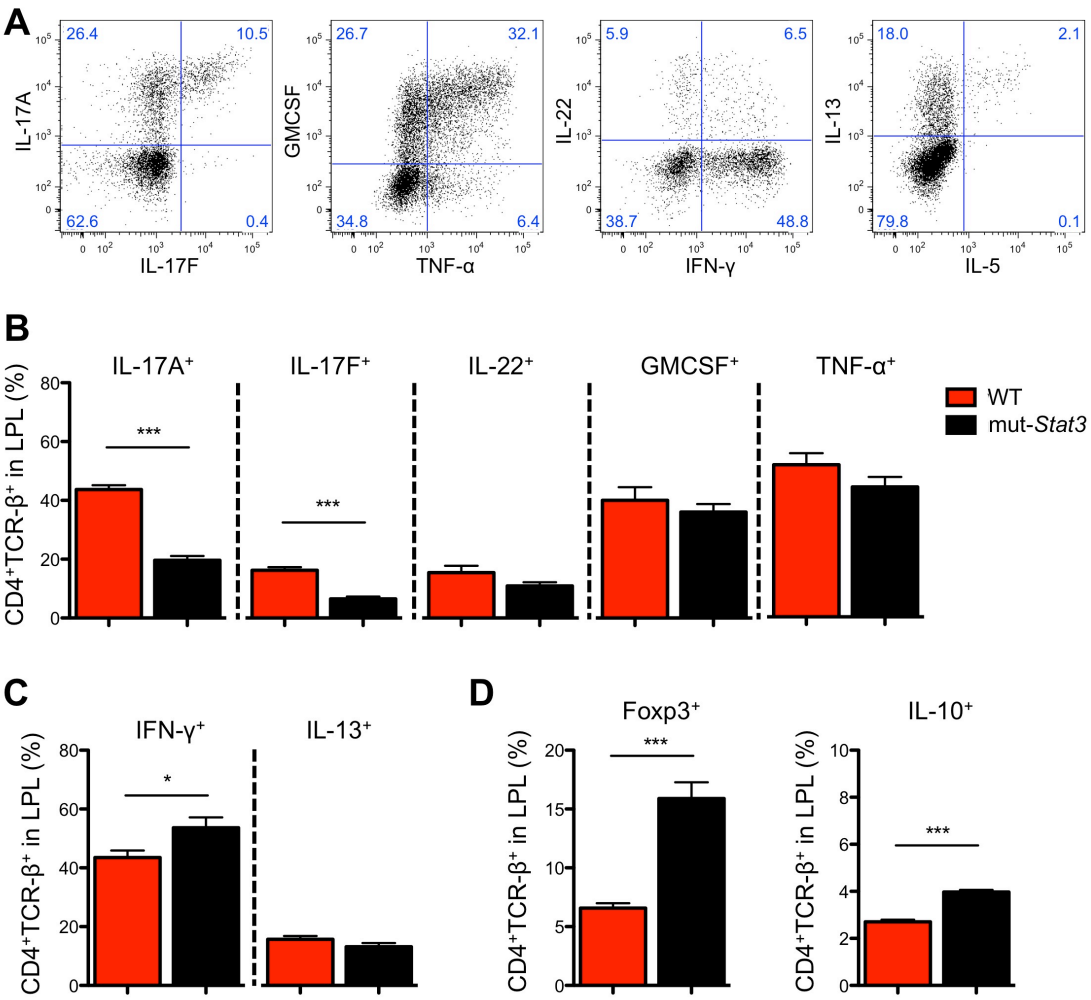

Figure 5.7. Analysis of cytokine and transcription factor expression from colonic CD4⁺ T cells at 2 weeks post *C. rodentium* infection.

Cohoused C57BL/6 WT and mut-*Stat3* mice were infected orally with $5*10^9$ CFU of *C. rodentium*. Mice were sacrificed when mut-*Stat3* mice developed clinical signs of disease (2 weeks) and cells were isolated from the colonic lamina propria. Single cell suspensions were re-stimulated with PMA and Ionomycin in the presence of Brefeldin-A for 4 hours. Expression of cytokines and transcriptions factors was determined by FACS.

(A) Representative FACS plots of viable $CD4^+TCR\text{-}\beta^+$ cells.

(B) Frequency of $IL\text{-}17A^+$, $IL\text{-}17F^+$, $IL\text{-}22^+$, $GMCSF^+$ and $TNF\text{-}\alpha^+$ cells in colon. Bars represent the mean ±SEM.

(C) Frequency of $IFN\text{-}\gamma^+$ and $IL\text{-}13^+$ cells in colon. Bars represent the mean ±SEM.

(D) Frequency of $Foxp3^+$ and $IL\text{-}10^+$ cells in colon. Bars represent the mean ±SEM.

Data is representative of 2 independent experiments, totaling n=8 for WT and n=6 for mut-*Stat3*. Statistical significance was determined using a Mann Whitney U Test. * $p \leq 0.05$, ** $p \leq 0.01$, *** $p \leq 0.001$.

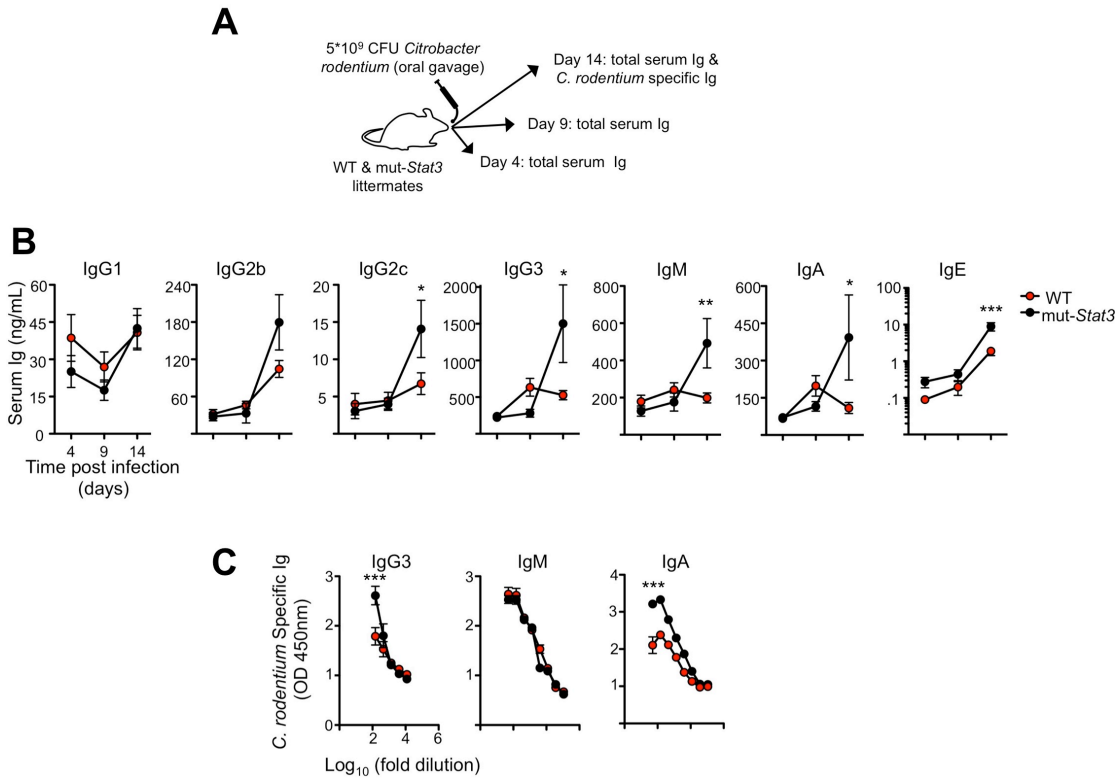

Figure 5.8. Mut-*Stat3* mice infected with *C. rodentium* mount a humoral immune response.

Cohoused C57BL/6 WT and mut-*Stat3* mice were infected orally with $5*10^9$ CFU of *C. rodentium*. Mice were sacrificed at days 4, 9 and 14. Sera were collected and antibody production analyzed by bead array and ELISA.

(A) Schematic of experimental design.

(B) Total serum immunoglobulin levels days 4, 9 and 14 post infection measured by bead array and ELISA. Each dot represents the mean ±SEM.

(C) Serum *C. rodentium*-specific immunoglobulins measured by ELISA. Data is presented as absolute absorbance of diluted serum sample at 450 nm vs $\log_{10}$ of the dilution factor. Each dot represents the mean ±SEM.

Data represents the cumulative results of 3 independent experiments, totaling n=25 for WT and n=21 for mut-*Stat3*. Statistical significance was determined using a Two-Way ANOVA followed by Bonferroni post-hoc test. * $p \leq 0.05$, ** $p \leq 0.01$, *** $p \leq 0.001$.

5.2.5. Reduced IL-22 and Antimicrobial Peptide Production in Early *C. rodentium* Infection of Mut-*Stat3* Mice.

IL-22 is indispensable for early host protection against *C. rodentium* infection (*329*, *509*, *512*). Loss of either IL-22 or its primary inducer, IL-23, results in dramatic weight loss, intestinal pathology, and death within two weeks of *C. rodentium* infection (*509*). IL-22 activates STAT3 (*527*) and has been shown to directly induce epithelial defense through the expression of anti-microbial peptides (AMPs), such as β-defensins (*237*), S100A7 (psoriasin), S100A8 (calgranulin A), S100A9 (calgranulin B) (*528*), RegIIIβ and RegIIIγ (*509*). IL-23p19 and IL-12/23p40 are drastically upregulated in the colon of *C. rodentium* infected mice, with expression peaking around day 4 (*509*). In order to probe for potential defects in the IL-23/IL-22 axis, we analyzed RNA extracted from cecum and distal colon tissue sections of WT and mut-*Stat3* littermates 4 days post-infection with *C. rodentium*. RT-qPCR analysis revealed equivalent expression of IL-23p19 and IL-12p35 in the two groups of mice, however IL-12/23p40 was significantly increased in mut-*Stat3* mice (Figure 5.9.A). Expression levels in the distal colon were lower than those observed in the cecum but followed the same trend (data not shown). As IL-23 was expressed in infected mut-*Stat3* mice, we next looked immediately downstream at IL-22 production. RT-qPCR analysis showed significant reductions in IL-22 expression in both the cecum and distal colon of mut-*Stat3* mice (Figure 5.9.B).

IL-22R is expressed predominantly on tissue epithelial cells (*237*), where its engagement induces AMP production (*237*, *509*, *529*, *530*). Further

supporting a potential defect in mut-*Stat3* epithelial host defence, expression levels of the secreted C-type lectins, RegIIIβ and RegIIIγ, were greater than 10 fold reduced in the cecum and 20 fold reduced in the distal colon of these mice relative to WT (Figure 5.10.B). Expression levels of the AMPs S100A8 and S100A9 were either equivalent across the two groups or marginally increased in mut-*Stat3* tissues by comparison (Figure 5.10.C). This later finding suggested that STAT3 mediated IL-22 signaling was more selective in induction of AMPs than originally proposed. Comparison of the original IL-22$^{-/-}$ in *C. rodentium* study with recent studies identifying IL-17C as another key player in epithelial host defense lends some support to this model (*509*, *531*, *532*). IL-17C binds to the IEC expressed receptor IL-17RE (*532*) and is upregulated in the colon following *C. rodentium* infection (*531*). *C. rodentium* infected IL-17RE deficient mice exhibit a very similar phenotype to IL-22 deficient mice, including reduced expression of AMPs in the colon. However, loss of RegIIIβ and RegIIIγ were not as dramatic as S100A8 and S100A9 in IL-17RE deficient mice (*531*). The opposite was found in IL-22$^{-/-}$s, in fact, S100 proteins were increased in IL-22$^{-/-}$ mice at early time points (*509*). Additionally, IL-17C was a much better inducer of S100A8 and S100A9 than RegIIIβ and RegIIIγ in IECs *in vitro* (*531*).

Therefore, our data suggest that hypomorphic STAT3 signaling in the intestine during acute *C. rodentium* infection leads to reduced IL-22 production, likely through loss of STAT3 mediated IL-23 signals. Reduced IL-22 signaling leads to reduced expression of the AMPs RegIIIβ and RegIIIγ.

Further analysis of the IL-17C/IL-17RE signaling pathway in mut-*Stat3* mice will be necessary, but the presence of S100A8 and S100A9 suggest that it is intact in these mice, suggesting only a partial defect in epithelial host defense.

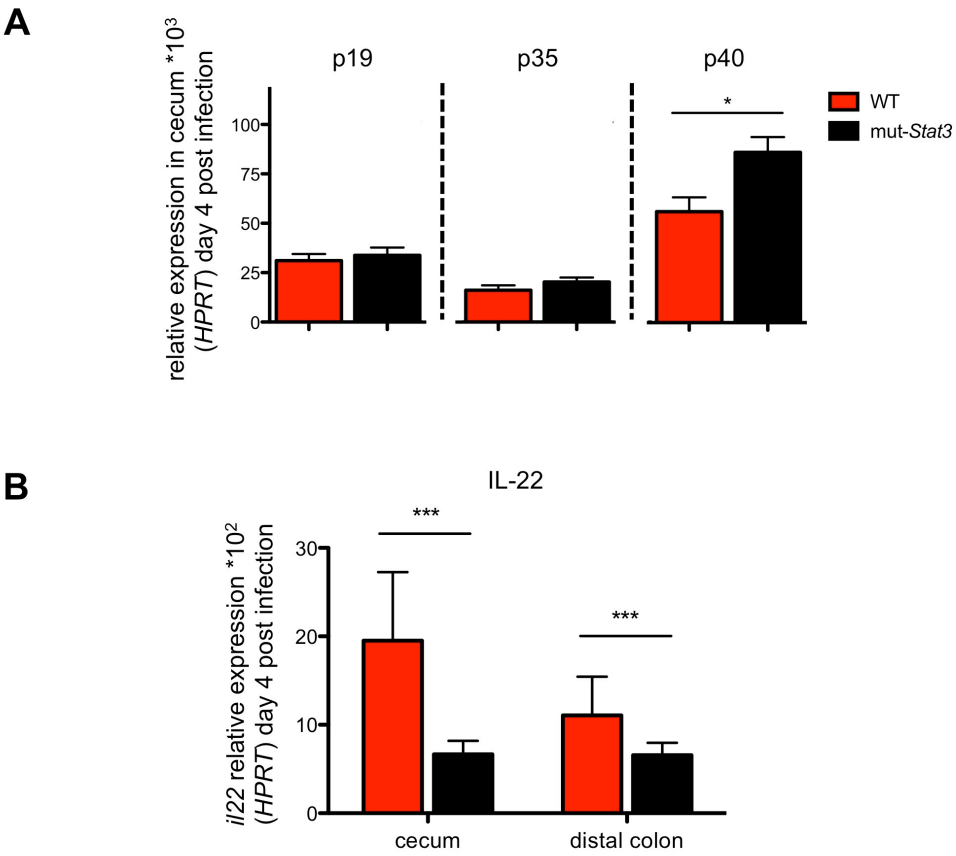

Figure 5.9. Reduced IL-22 expression despite intact IL-23 response in the colon following *C. rodentium* infection in mut-*Stat3* mice.

Cohoused C57BL/6 WT and mut-*Stat3* mice were infected orally with $5*10^9$ CFU of *C. rodentium*. Mice were sacrificed 4 days later and mRNA extracted from the cecum and colon.

(A) Expression level of the IL-12 and IL-23 subunits p19, p35 and p40 were assayed by RT-qPCR. Transcript levels were normalised to *HPRT* and multiplied by a factor of 1000. Bars represent the mean ±SEM, n=8/group.

(B) Expression level of the IL-22 was assayed by RT-qPCR. Transcript levels were normalised to *HPRT* and multiplied by a factor of 100. Bars represent the mean ±SEM, n=4/group.

Data is representative of 2 (A) or 1 (B) independent experiments. Statistical significance was determined using a Mann Whitney U Test. * $p \leq 0.05$, ** $p \leq 0.01$, *** $p \leq 0.001$.

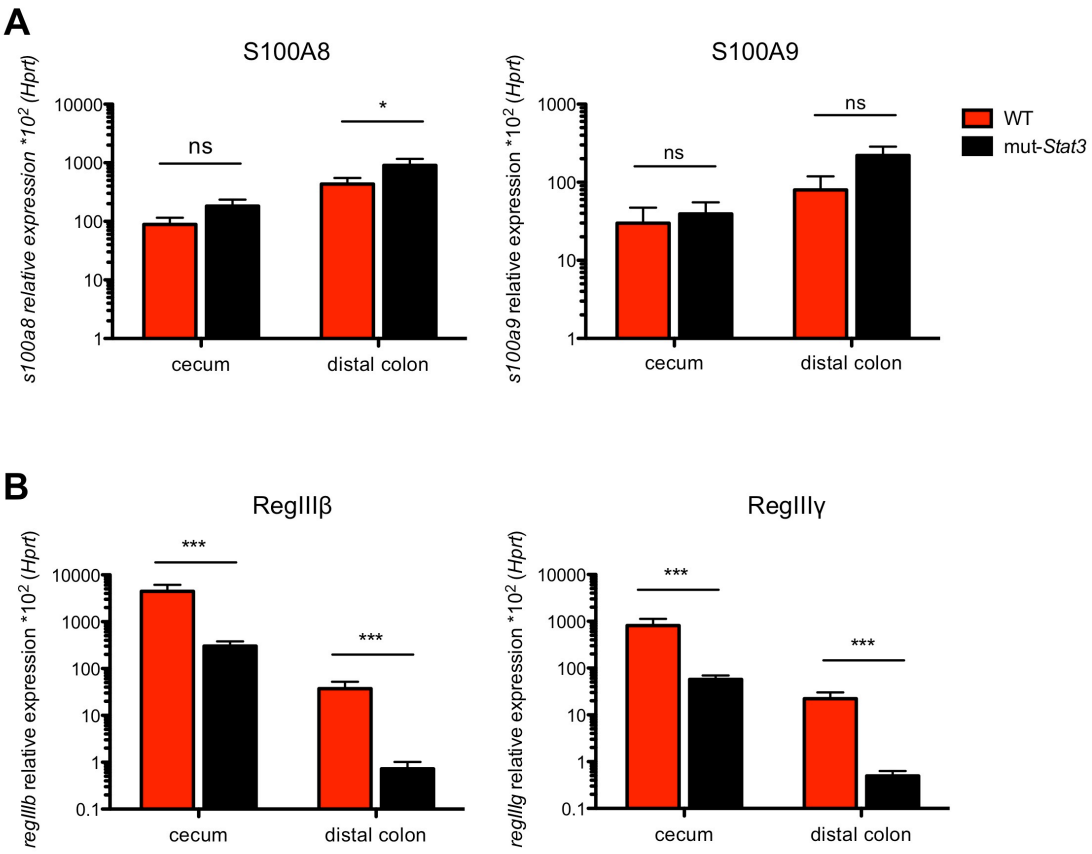

Figure 5.10. Reduced expression of RegIII family of antimicrobial peptides in mut-*Stat3* mice following *C. rodentium* infection.

Cohoused C57BL/6 WT and mut-*Stat3* mice were infected orally with $5*10^9$ CFU of *C. rodentium*. Mice were sacrificed 4 days later and mRNA extracted from the cecum and colon.

(A) Expression level of the antimicrobial peptides S100A8 and S100A9 were assayed by RT-qPCR. Transcript levels were normalised to *HPRT,* multiplied by a factor of 100 and plotted on a $\log_{10}$ scale. Bars represent the mean ±SEM.

(B) Expression level of the antimicrobial peptides RegIII-β and RegIII-γ were assayed by RT-qPCR. Transcript levels were normalised to *HPRT,* multiplied by a factor of 100 and plotted on a $\log_{10}$ scale. Bars represent the mean ±SEM.

Data is representative of 2 independent experiments, n=8/group. Statistical significance was determined using a Mann Whitney U Test. * $p \leq 0.05$, ** $p \leq 0.01$, *** $p \leq 0.001$.

5.2.6. Mut-*Stat3* Mice Exhibit Elevated Intestinal Pathology, Despite Declining *C. rodentium* Colonization, Post 1-week Infection.

Having observed both early (IL-22, AMPs) and late (IL-17, IFN-γ, IL-10) abnormalities in *C. rodentium* infected mut-*Stat3* mice, we were uncertain what was driving the severe intestinal pathology observed at two weeks post-infection. To determine if the increased pathology noted was simply resultant from a failure to control *C. rodentium* numbers, we compared bacterial colonization levels and histological scores of cecums and distal colons from WT and mut-*Stat3* mice sacrificed 4,9, or 14 days post-infection. In both WT and mut-*Stat3* tissues, *C. rodentium* levels peaked 9 days post-infection and dropped back to levels comparable to those observed at day 4, by day 14 (Figure 5.11.A). The same trend was observed in both the cecum and the distal colon, suggesting that resolution of bacterial infection had begun. This further substantiated a productive *C. rodentium*-specific humoral response in mut-*Stat3* mice as colonization of the intestine remains elevated in B cell, CD4, or Rag deficient mice (*368*, *526*). Histology scores in WT mice also peaked by day 9 post-infection and appeared moderately reduced by day 14 (Figure 5.11.B). In contrast, there was no evidence of resolving inflammation at day 14 in the mut-*Stat3* animals despite a resolving bacterial load (Figure 5.11.B).

In addition to driving AMP production, IL-22 is also an important promoter of IEC repair and wound-healing (*49*). STAT3 provides important pro-survival and anti-apoptotic signals to IECs (*533*, *534*). We hypothesized that impaired wound-healing in mut-*Stat3* epithelial cells might be responsible for the high

histology scores in the presence of a resolving *C. rodentium* infection. Closer examination of histology sections revealed that epithelial hyperplasia, goblet cell loss and epithelial integrity were similar in mut-*Stat3* colons at days 9 and 14 post-infection (Figure 5.12.A). Indicators of epithelial damage remained statistically unchanged in WT colon as well, although there was a trend towards reduced damage on day 14 (Figure 5.12.A). Further characterization of both epithelial proliferation by BrdU incorporation and apoptosis by immunohistochemistry will be required to assess the epithelial repair response in mut-*Stat3* mice. Notably however, despite unchanged epithelial pathology, we did observe a marked increase in mut-*Stat3* LPL numbers between days 9 and 14 (Figure 5.12.B). As *C. rodentium* colonization was on the decline at day 14, this finding was suggestive of a possible unchecked inflammatory response in mut-*Stat3* animals.

IL-10 is another key cytokine during the resolution phase of inflammation. IL-10 plays very important roles in inhibiting proinflammatory responses from both innate and adaptive immunity during infection. As such, it prevents lesions in tissues caused by exacerbated adaptive immune responses (*535*, *536*). STAT3 is necessary for IL-10 suppressive functions, with STAT3 deficiency in neutrophils and macrophages leading to Th1 skewing and the development of chronic enterocolitis (*53*). We reasoned that IL-10 suppressive functions may be blunted in the mut-*Stat3* mice, leading to residual inflammatory responses and tissue damage at day 14, despite a resolving infection. Notably, IFN-γ producing $CD4^+$ T cells were increased in number in the mut-*Stat3* LPL (Figure 5.12.C).

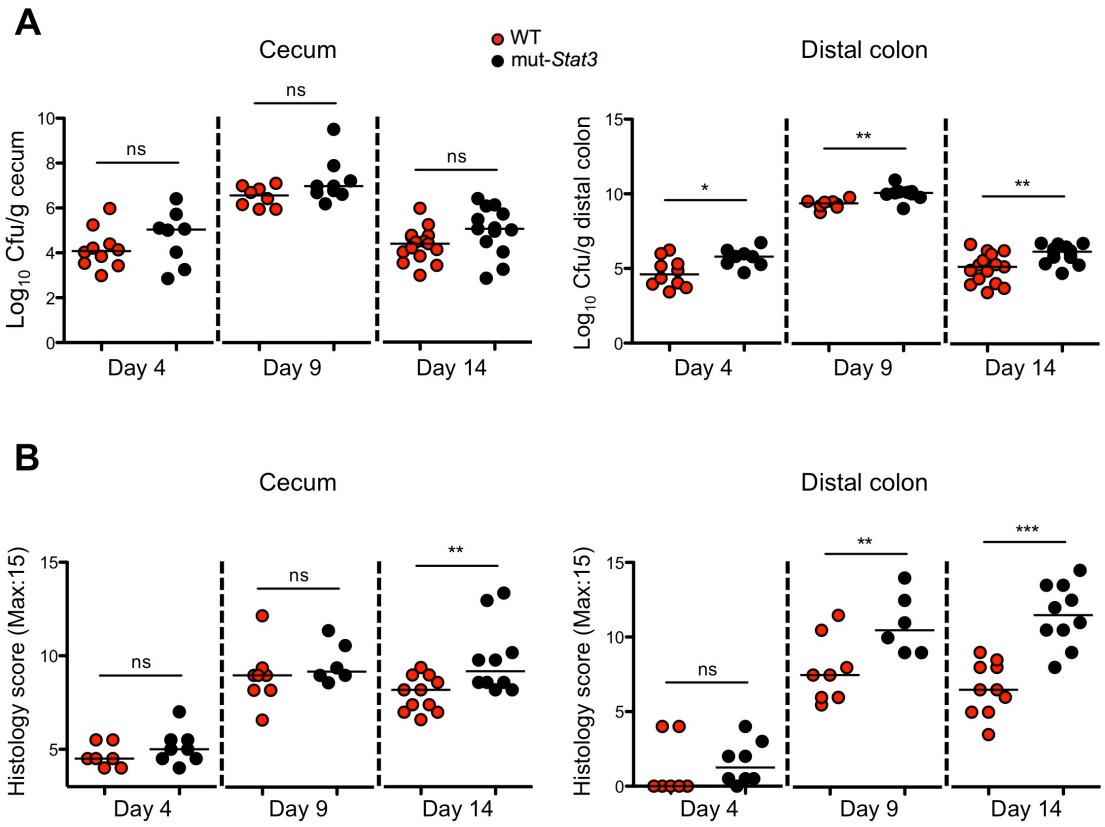

Figure 5.11. High levels of intestinal inflammation despite receding *C. rodentium* colonization in mut-*Stat3* mice at day 14.

Cohoused C57BL/6 WT and mut-*Stat3* mice were infected orally with $5*10^9$ CFU of *C. rodentium*. Mice were sacrificed at days 4, 9 and 14; *C. rodentium* colonization and intestinal inflammation were assessed.

(A) Cecum and distal colon sections from infected mice were homogenized and *C. rodentium* colonization determined as CFU per mass. Bars represent the mean and each point represents an individual mouse.

(B) Histological analysis of inflammation from the cecum and distal colon. Bars represent the mean and each point represents an individual mouse.

Data represents the cumulative results of 3 independent experiments, totaling n=32 for WT and n=28 for mut-*Stat3*. Statistical significance was determined using a Mann Whitney U Test. * p≤0.05, ** p ≤ 0.01, *** p ≤ 0.001.

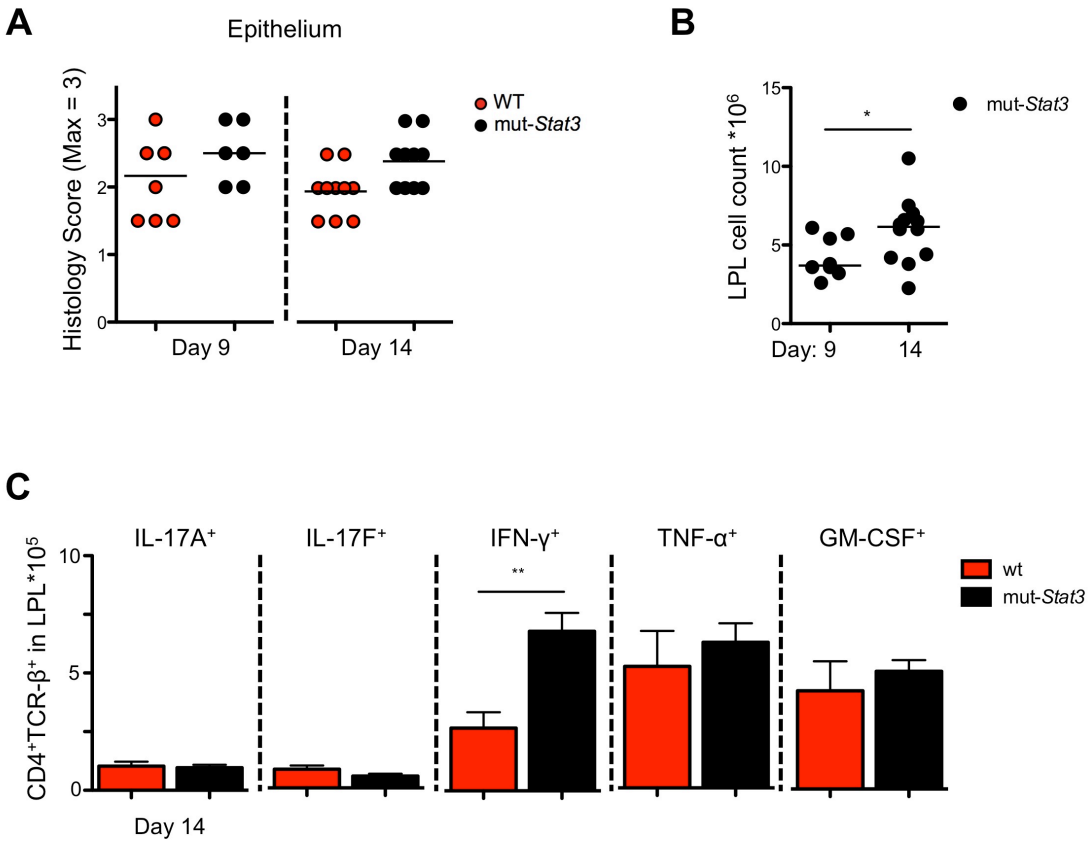

Figure 5.12. Day 14 residual colonic pathology in mut-*Stat3* animals is marked by increased LPL numbers and IFN-γ⁺ CD4 T cells.

Cohoused C57BL/6 WT and mut-*Stat3* mice were infected orally with $5*10^9$ CFU of *C. rodentium*; mice were sacrificed at days 9 and 14. Intestinal inflammation was assessed from tissue sections and cells were isolated from the colonic lamina propria. Single cell suspensions were re-stimulated with PMA and Ionomycin in the presence of Brefeldin-A for 4 hours. Cytokine expression was determined by FACS.

(A) Histological analysis of the epithelium from distal colon sections (see methods). Bars represent the mean and each point represents an individual mouse.

(B) Total number of lymphocytes in the lamina propria of infected mut-*Stat3* mice. Bars represent the mean and each point represents an individual mouse.

(C) Total number of IL-17A⁺, IL-17F⁺, IFN-γ⁺, TNF-α⁺, and GM-CSF⁺ CD4 T cells in the colon 14 days post-*C. rodentium* infection. Bars represent the mean ±SEM.

Data represents the cumulative results of 2 independent experiments, n=20 for WT and n=18 for mut-*Stat3* (A-B). Data is representative of 2 independent experiments, n=8 for WT and n=6 for mut-*Stat3* (C). Statistical significance was determined using a Mann Whitney U Test. * p≤0.05, ** p ≤ 0.01, *** p ≤ 0.001.

5.2.7. IL-10 Signals Dampened in mut-*Stat3* Mice.

A major function of the inhibitory response activated by IL-10 is to limit cytokine and chemokine production from dendritic cells and macrophages activated by agonists of TLRs, such as LPS and bacterial lipoproteins (*537-539*). Comparison of LPS and LPS+IL-10 treated cells is a well-characterized model for the investigation of IL-10 function (*540*). To investigate the effectiveness of IL-10 signaling in our model, $CD11c^+$ splenocytes were isolated from WT and mut-*Stat3* mice and stimulated with LPS or LPS+IL-10 for 24 hours. RNA was extracted and gene expression analyzed by microarray (Figure 5.13.A).

Comparison of the WT microarray datasets revealed approximately 300 genes that were greater than 2 fold different between LPS and LPS+IL-10 treated cells (Figure 5.13.B). The microarray datasets from all genotypes and treatment conditions were then filtered on these 300 "IL-10 responsive genes" and a two dimensional clustering analysis was performed (Figure 5.13.C). Consistent with previous studies, the majority of genes in the dataset were repressed following IL-10 treatment, but a small subset of genes were upregulated by IL-10 (Figure 5.13.C). Although subtle expression differences were detectable between LPS treated WT and mut-*Stat3* $CD11c^+$ cells, gene expression was markedly different between the two cell populations in LPS+IL-10 treated conditions (Figure 5.13.C). Both IL-10 repressed and activated genes showed moderate changes in expression between LPS and LPS+IL-10 treated mut-*Stat3* cells compared to WT. However, in general, genes repressed by IL-10 in WT were still repressed in mut-*Stat3* cells.

Therefore, this study provided solid evidence of reduced, but not absent, IL-10 responses in mut-*Stat3* cells.

IL-10 is produced in mice very rapidly after exposure to LPS (*541*, *542*) and plays a key role in the prevention of endotoxic shock (*543-545*). Both IL-10 deficient mice and mice injected with IL-10 neutralizing antibody show drastically increased sensitivity to endotoxic shock, with rapid death and elevated production of the proinflammatory cytokines IL-1β, IL-6, IL-12, TNF-α, and IFN-γ following low doses of LPS (*542*, *545*). To gain an assessment of IL-10 function *in vivo*, WT and mut-*Stat3* mice were IP injected with LPS and monitored for a 24 hour period (Figure 5.14.A). Serum samples were collected at 90 min post injection and analyzed for cytokine levels by bead array or ELISA. Whereas no death was observed in the WT mice, all mut-*Stat3* mice succumbed to endotoxic shock (Figure 5.14.B). Analysis of serum cytokines revealed elevated levels of both IL-12 and TNF-α in mut-*Stat3* mice, supporting a functional IL-10 defect in these animals.

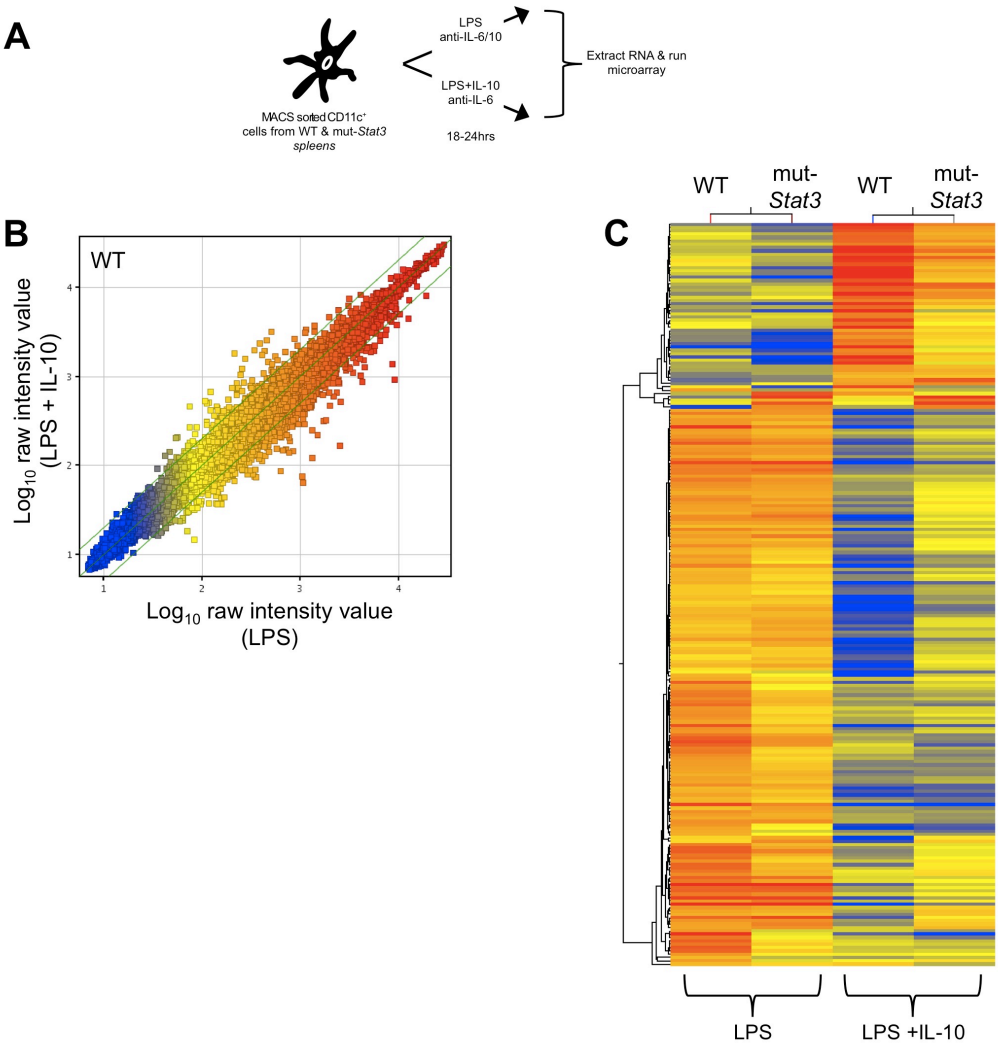

Figure 5.13. IL-10 gene signature blunted in CD11C⁺ mut-*Stat3* cells.

CD11c⁺ cells were MACS sorted from the spleens of C57BL/6 WT and mut-*Stat3* mice. Cells were stimulated with IFN-γ and IL-4, and either LPS, or LPS and IL-10 for 18-24 hours. RNA was extracted and gene expression analyzed by microarray (Affymetrix).

(A) Schematic of experimental design to compare WT and mut-*Stat3* IL-10 signatures.

(B) Scatter plot comparing averaged gene expression of LPS and LPS+IL-10 treated WT CD11c⁺ cells. 447 transcripts representing 317 unique genes showed a greater than 2 fold change (green line) in expression between conditions and were defined as IL-10 responsive genes.

(C) Two-dimensional cluster analysis (hierarchical, Pearson uncentered, average linkage, unsupervised) of the IL-10 responsive gene list from (B). Each row corresponds to a transcript and each column to the mean expression values of a sample.

Data represents the pooled results of 3 independent microarrays. This experiment was performed by A. Kotlyar and Dr. A. Laurence in the laboratory of J.J.O'Shea (NIH). Data analysis performed by S. Steward-Tharp.

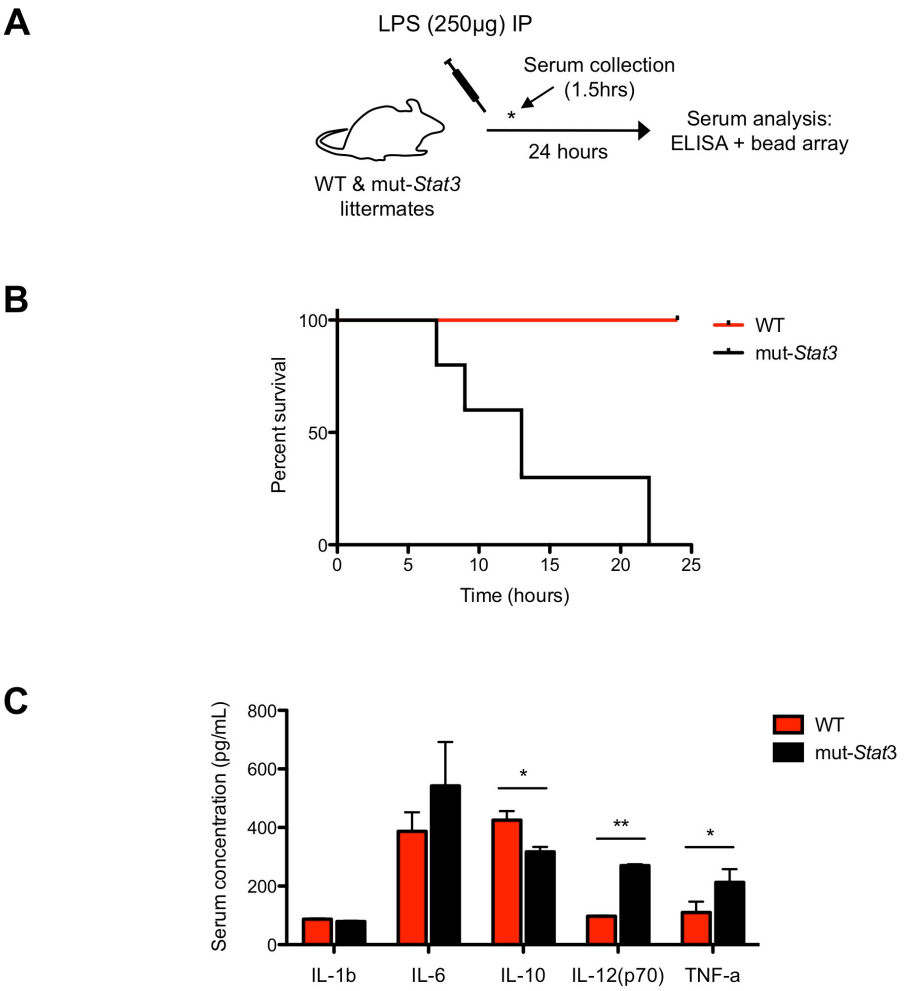

Figure 5.14. mut-*Stat3* mice show heightened sensitivity to endotoxic shock.

Cohoused C57BL/6 WT and mut-*Stat3* mice were IP injected with 250 µg LPS. Sera were collected after 90 minutes and analyzed for cytokine production by bead array and ELISA.

(A) Schematic of experimental design.

(B) Survival plot during the course of the experiment shown as a percentage.

(C) Serum cytokine levels 90 minutes post LPS injection measured by bead array and ELISA. Each bar represents the mean ±SEM.

Data represents the pooled results of 2 independent experiments n=10/group. Statistical significance was determined using a Mann Whitney U Test. * p≤0.05, ** p ≤ 0.01, *** p ≤ 0.001. This experiment was performed by A. Kotlyar and Dr. A. Laurence in the laboratory of J.J.O'Shea (NIH). Data analysis performed by S. Steward-Tharp.

5.2.8. Both Hematopoietic and Non-Hematopoietic Compartments Contribute to *C. rodentium* Phenotype of mut-*Stat3* Mice.

In response to *C. rodentium* infection, in mut-*Stat3* animals, we observed reduced production of host-protective factors of both epithelial (RegIIIβ, RegIIIγ) and hematopoietic (IL-17, IL-22) origin. Additionally, our data strongly supports reduced activity of STAT3 activating cytokines such as IL-10, which can potentially affect both compartments. To dissect the relative contributions of impaired STAT3 signaling within the hematopoietic and non-hematopoietic compartments we rescued lethally irradiated WT and mut-*Stat3* mice with WT and mut-*Stat3* BM (Figure 5.15.A). Eight weeks following transplantation animals were orally infected with *C. rodentium.* In accordance with our previous experiments, mut-*Stat3* mice transplanted with mut-*Stat3* BM lost significantly more weight than WT mice transplanted with WT BM. Interestingly, WT mice transplanted with mut-*Stat3* BM and mut-*Stat3* mice transplanted with WT BM both lost weight to a significantly greater extent that WT animals, suggesting that STAT3 function, both within the immune system and within the epithelial/stromal compartment, is critical in protection against *C. rodentium* infection (Figure 5.15.B). Notably, WT mice transplanted with mut-*Stat3* BM did not start to lose weight relative to WT controls until around day 9, whereas mice with mut-*Stat3* epithelia lost weight much earlier (Figure 5.15.B).

Further analysis revealed that infected mice transplanted with mut-*Stat3* BM had both an increased distal colon pathology and elevated percentages of IFN-γ producing $CD4^+$ T cells within the LPL, irrespective of the genotype of

the host animal (Figure 5.15.C and 5.16.B). As expected, mice transplanted with mut-*Stat3* BM also had reduced percentages of IL-17A and IL-17F producing $CD4^+$ T cells. By comparison, mut-*Stat3* hosts showed greatly diminished RegIIIγ expression in the colon, irrespective of the BM (Figure 5.16.A). Although statistical significance was not reached, mut-*Stat3* mice transplanted with WT BM showed a clear trend towards greater intestinal pathology (Figure 5.15.C).

Collectively, these data suggested that hypomorphic STAT3 activity within the epithelial and stromal compartment leads to reduced AMP production, early weight loss, and possibly increased intestinal pathology in *C. rodentium* infection. Meanwhile hypomorphic STAT3 activity within the hematopoietic compartment leads to abnormal cytokine production from T cells and delayed weight loss. We hypothesize that early defects in AMP production and epithelial responses lead to failed containment of *C. rodentium* and systemic dissemination of the bacteria, resulting in wasting disease. The trend towards increased intestinal pathology in mice with STAT3 defects in only non-hematopoietic cells could be attributable to impaired wound healing responses. Hypomorphic STAT3 signaling in the BM leads to weight loss at a later stage of infection, possibly associated with decreased IL-10 signaling and subsequent dysregulation of ongoing inflammatory responses such as IFN-γ. This suggests that STAT3 pro-inflammatory responses are either not required or remain sufficiently intact in mut-*Stat3* hematopoietic cells to contain *C. rodentium* infection, but that STAT3 regulatory responses within the BM may be insufficient to dampen residual inflammation.

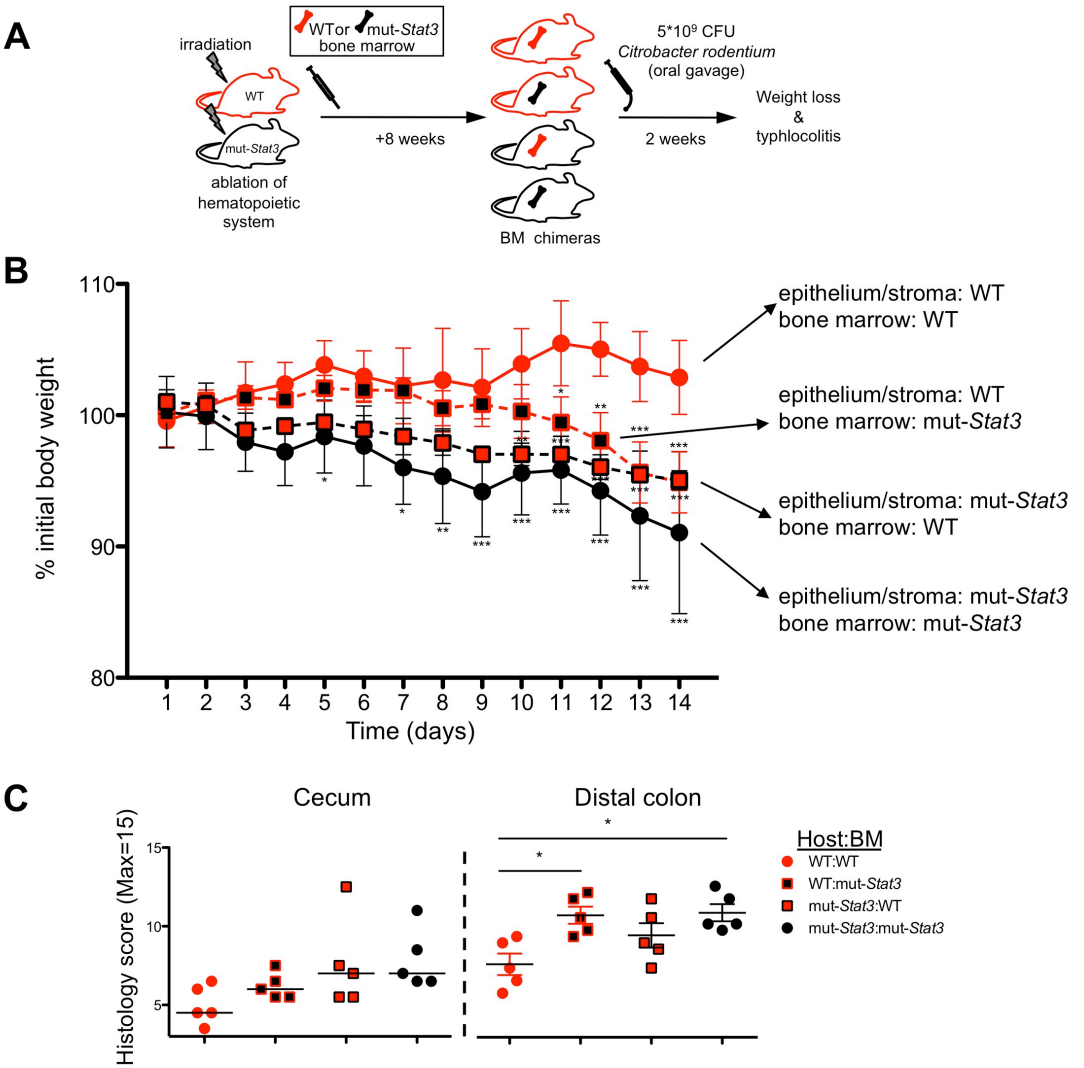

Figure 5.15. Both hematopoietic non-hematopoietic compartments contribute to increased susceptibility of mut-*Stat3* mice to *C. rodentium*.

Bone marrow chimeras were generated by lethal irradiation of C57BL/6 WT and mut-*Stat3* mice followed by i.v. injection of 10x10^6 WT or mut-*Stat3* bone marrow cells. Mice were allowed to rest for 8 weeks to allow re-constitution of the hematopoietic system. Re-constituted mice were infected orally with 5*10^9 CFU of *C. rodentium*. Mice were sacrificed at 2 weeks post infection and intestinal inflammation was assessed.

(A) Schematic of experimental design.

(B) Weight loss during the course of the experiment shown as percentage of day 0 weight. Bars represent the mean ±SEM.

(C) Histological analysis of inflammation from the cecum and distal colon. Bars represent the mean and each point represents an individual mouse.

Data is representative of a single experiment, n=5/group. Statistical significance was determined using a repeated measure ANOVA (B) and one-way ANOVA (C) followed by Bonferroni post-hoc test. * p≤0.05, ** p ≤ 0.01, *** p ≤ 0.001.

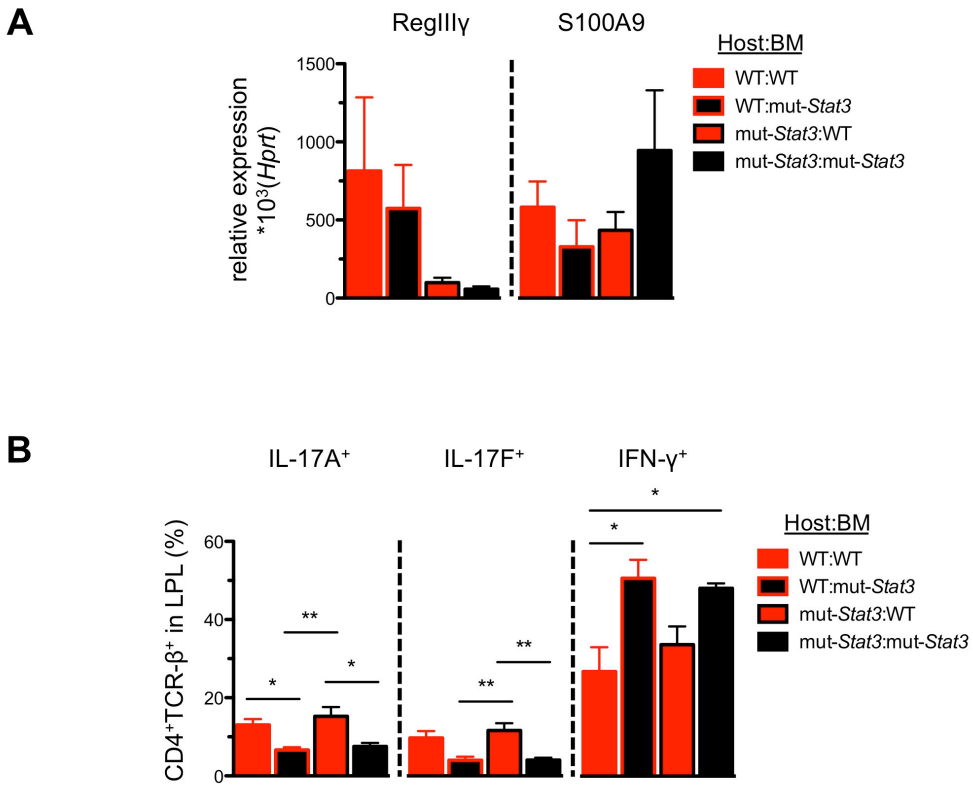

Figure 5.16. Both hematopoietic non-hematopoietic compartments contribute to increased susceptibility of mut-*Stat3* mice to *C. rodentium*.

Bone marrow chimeras were generated by lethal irradiation of C57BL/6 WT and mut-*Stat3* mice followed by i.v. injection of $10x10^6$ WT or mut-*Stat3* bone marrow cells. Mice were allowed to rest for 8 weeks to allow re-constitution of the hematopoietic system. Re-constituted mice were infected orally with $5*10^9$ CFU of *C. rodentium*. Mice were sacrificed at 2 weeks post infection, mRNA was extracted from the cecum, and cells were isolated from the colonic lamina propria. Single cell suspensions were re-stimulated with PMA and Ionomycin in the presence of Brefeldin-A for 4 hours. Expression of cytokines was determined by FACS.

(A) Expression level of the antimicrobial peptides RegIII-γ and S100A9 were assayed by RT-qPCR. Transcript levels were normalised to *HPRT* and multiplied by a factor of 1000. Bars represent the mean ±SEM.

(B) Frequency of IL-17A⁺, IL-17F⁺ and IFN-γ⁺ cells in colon. Bars represent the mean ±SEM.

Data is representative of a single experiment, n=5/group. Statistical significance was determined using a one-way ANOVA followed by Bonferroni post-hoc test. * $p \leq 0.05$, ** $p \leq 0.01$, *** $p \leq 0.001$.

5.3. Discussion.

The human IBDs are a heterogenous group of disorders characterized by chronic inflammation of the gastrointestinal tract. Genetic studies have identified *STAT3* as a susceptibility loci in CD and UC (*504*, *505*). However, tissue specific *Stat3* deletions in mice have revealed this transcription factor to mediate both protective (*49*, *53*, *294*) and pathological (*219*) processes within the intestinal tract, making STAT3's net role in either intestinal immune homeostasis or IBD difficult to discern. Our findings in the *Stat3*ΔV463 model of AD-HIES indicate that STAT3 plays predominantly a protective role at steady state. Hypomorphic STAT3 signaling resulted in independent defects in both hematopoietic and non-hematopoietic tissues that led to worse clinical disease in both an epithelial damage mediated model of acute colitis and following infection with the enteric pathogen *C. rodentium*. Specifically, STAT3 was important for IL-22 host-protective responses, both in expression of this IL-10 family member and in mediating its functionality such as induction of certain classes of AMPs from epithelial cells. As previously reported, STAT3 played a key role in the induction of IL-17A and IL-17F from T cells. Additionally, STAT3 was important for limiting inflammatory responses, possibly through IL-10 signaling. Hypomorphic STAT3 signaling did not lead to the development of spontaneous colitis. Thus, STAT3 is an important regulator of the intestinal immune response and its proper function is necessary for protection against acute colitis.

In the previous chapter, B and T cell development and peripheral numbers were shown to be normal in mut-*Stat3* mice despite hypomorphic STAT3

signaling. Here, we expanded our review of lymphocytes in mut-*Stat3* mice to ILCs, finding normal percentages of LTis, NK22s, and $CD4^{-}NKp46^{-}$s in LPL preparations. Id2 is essential for ILC formation (*546*, *547*), suggesting that the inhibition of this transcriptional repressor we observed in class-switching mut-*Stat3* B cells may not occur in early lymphoid progenitors. The finding of STAT3 binding primarily at the Id2 putative enhancer, rather than at the promoter, supports this hypothesis as recent data suggests that tissue specific expression of genes is regulated at the enhancer rather than the promoter level (*481*). By contrast, STAT3 potently binds the *Rorc* promoter (*219*) and is required for ROR-γt upregulation during Th cell differentiation (*218*). The ILC populations we analyzed are also ROR-γt dependant, suggesting that other factors may also regulate the *Rorc* locus in these cells.

We observed a severe phenotype in mut-*Stat3* mice treated with DSS. This finding was similar to what had previously been reported in mice with STAT3 deficient IECs (*49*). As phosphorylation of STAT3 in IECs is highly dependent on IL-22, and IL-$22^{-/-}$ mice also show a DSS phenotype indistinguishable from that observed in mut-*Stat3* mice (*49*), it is likely that the rapid weight loss we observed in DSS treated mut-*Stat3* mice was attributable to defects in IL-22 mediated STAT3 signaling within IECs. BM-chimeras should be generated to test this hypothesis, but our findings in *C. rodentium* infection clearly demonstrate that both IL-22 and IL-22 induced AMPs (RegIIIβ and RegIIIγ) have reduced expression in mut-*Stat3* tissues. Additionally, mice with mut-*Stat3* epithelia showed reduced expression of RegIIIγ regardless of whether

the hematopoietic compartment was of WT or mut-*Stat3* origin. IL-22 production has been demonstrated in numerous leukocyte populations (CD4, CD8, γδ T cells, NK cells, DCs, and various LTi-like subsets) (*215*, *216*, *548-551*), but never from non-hematopoietic cells. Therefore, our data suggest that STAT3 is less critical for IL-22 induction than function, and that hypomorphic STAT3 signaling leads to defects in both processes, resulting in impaired intestinal host defense.

We also observed reduced percentages of $CD4^+$ T cells producing IL-17 in the colonic LPL of mut-*Stat3* mice, both at steady state and during the course of *C. rodentium* infection. IL-17A and IL-17F deficient mice both exhibit higher *C. rodentium* colonization of the colon following infection (*520*), suggesting that reduced production of these cytokines in mut-*Stat3* mice could also contribute to impaired intestinal host defense. However, despite altered percentages, total numbers of IL-17A and IL-17F producing $CD4^+$ T cells were equivalent between WT and mut-*Stat3* mice during *C. rodentium* infection. Additionally, loss of IL-17RC, an essential receptor component for both IL-17A and IL-17F signaling (*552*), does not result in either greater weight loss or decreased survival following *C. rodentium* infection (*509*), suggesting a minimal role for loss of IL-17A or IL-17F in explaining the mut-*Stat3* phenotype.

Decreased IL-17A production from AD-HIES T cells has been linked with lower salivary AMP levels in these patients and is suggested to contribute to their increased predilection to develop oral and mucocutaneous candidiasis

(*553*). Additionally, low IL-17A and IL-22 production from AD-HIES T cells has been associated with failed protective responses from keratinocytes and bronchial epithelial cells, thus providing a possible explanation of AD-HIES patients' high incidence of cutaneous and sinopulmonary *Staphylococcal* infections (*78*). However, intestinal infections have not been reported in either increased incidence or severity in AD-HIES patients. This suggests potential discrepancies between the necessity of STAT3 for human and mouse IEC protective responses. For instance, IL-17C and IL-22 may serve more redundant roles in the human intestine than the current data suggests for mouse (*509*, *531*, *532*).

Our data also highlights potential problems in the resolution phase of *C. rodentium* infection. Despite epithelial and T cell defects during *C. rodentium infection*, mut-*Stat3* mice do mount a pathogen-specific humoral response that is likely to drive the receding bacterial colonization of the cecum and colon that we observed at 2 weeks post infection. Despite a resolving infection, inflammation of the colon remained elevated in mut-*Stat3* mice. This phenotype tracked with the mut-*Stat3* BM in the chimera experiment, suggesting a breakdown in immune regulation. Although various T-cell populations have anti-inflammatory functions, $Foxp3^+$ Treg cells and $Foxp3^-$ IL-10-secreting $CD4^+$ T cells are particularly important in the intestine (*554*).

A previous study in AD-HIES patients suggested that defects in IL-10 signaling could lead to failed generation of tolerogenic DCs and subsequent

reductions in iTreg numbers in these patients (*555*). However, we found no evidence of this in the intestine as mut-*Stat3* mice had slightly higher percentages of Foxp3$^+$ cells at steady state and a near 3-fold increase 2 weeks post *C. rodentium* infection. Mice that lack STAT3 specifically in Foxp3$^+$ Treg cells develop a spontaneous, IL-17A driven colitis (*294*). STAT3 deficient Tregs are capable of inhibiting *in vitro* T cell differentiation but show a selective impairment in regulation of IL-17A responses *in vivo* (*294*). The pathology noted in mut-*Stat3* animals post *C. rodentium* infection was associated with reduced IL-17A and increased IFN-γ responses, suggesting that reduced STAT3 activity within Tregs was unlikely to be the root cause. Instead we found that hypomorphic STAT3 signaling lead to clear inhibition of IL-10 responses in mut-*Stat3* cells. IL-10 controls chronic intestinal inflammation partly through direct anti-inflammatory effects on myeloid cells. Loss of this suppressive activity was evidenced by increased serum levels of pro-inflammatory cytokines following challenge of mut-*Stat3* mice with LPS.

Overall, these findings indicate that even a partial loss in STAT3 activity has very important repercussions in intestinal immune homeostasis. Not only does hypomorphic STAT3 signaling strongly inhibit protective IL-22 driven epithelial responses in acute colitis, but it also appears to hinder the resolution phase as well, likely due to a partial loss in IL-10 suppressive functions. In this manner, an immunodeficiency can lead to a subsequent pro-inflammatory state.

Obviously this has profound implications in the clinical management of AD-HIES patients. In fact, AD-HIES peripheral blood leukocytes stimulated with various microbial stimuli were reported to secrete elevated levels of a number of pro-inflammatory cytokines such as IFN-γ, TNF-α, and IL-12p70 (*70*, *556*, *557*). This suggests that the AD-HIES system may be tipped towards pro-inflammatory responses even at baseline. Little data exists on enterocolitis in AD-HIES patients but bacterial and fungal sinopulmonary infections are very common (*66*, *558*). Even when treated aggressively and promptly, these mucosal infections often progress to pneumatocele formation. Our data suggests that dysregulated local inflammation and resultant tissue destruction could well be the cause of this significant AD-HIES morbidity.

6. Chapter 6: General Discussion.

6.1. A BAC-Transgenic Approach for the AD-HIES Mouse Model.

The discovery of dominant-negative *STAT3* mutations in a majority of AD-HIES patients presented a unique opportunity for further understanding of both the pathogenesis of this disease and of the interplay of STAT3 function from various cell and tissue types (*70*, *71*). The aim of our initial experiments was to generate a mouse model of AD-HIES that could reproduce biochemical and clinical features of the disease. The data presented in this thesis suggest BAC-transgenic expression of mutant alleles as a useful targeting strategy for diseases caused by dominant-negative mutations. Despite increased total *Stat3* expression in the transgenic mice, the final ratio of the WT to mutant allele determined the net signaling defect. STATs are thought to remain latent in the cytoplasm until they are activated by JAKs downstream of extracellular ligands (*8*, *559*). As such, this additional layer of regulation likely contributed to the utility of our model. FACS analysis of STAT3 phosphorylation following cytokine stimulation of WT and mut-*Stat3* B cells yielded largely equivalent MFIs between the two groups, suggesting that JAK activity rather than cytoplasmic STAT3 availability was the limiting factor and that increased total STAT3 levels did not affect the net number of phosphorylated STAT3 dimers. Recent reports have suggested that STATs may also play roles in mediating gene expression in the absence of tyrosine phosphorylation (*560-564*). The mechanisms responsible for these actions are hypothesized to include interaction with other proteins and DNA elements. As

a result, we would expect that dominant-negative *STAT3* mutations from different regions of the protein could uniquely alter cytokine independent transcriptional responses. However, minimal useful correlations have arisen from comparison of different AD-HIES *STAT3* mutations with clinical phenotypes (*565*), lending little support to this hypothesis

Our study has also highlighted the utility of homologous recombination in *E. coli* for generation of mutated BAC constructs. The generation of the recombination cassette via a multi-template PCR approach, that integrated the desired sequence changes into the primers, eliminated the need for multiple cloning steps. Furthermore, the integration of silent mutations in the *Stat3*ΔV463 construct facilitated multiple processes, including: PCR screening for BACs carrying homologous integrants during recombination steps, genotyping, measurement of WT and mutant STAT3 expression levels *in vivo*. As a whole, our targeting strategy was quick, accurate and efficient, representing a significant improvement on the originally published methods (*374*). Since BAC RP24-236G5 showed expression patterns *in vivo* indistinguishable from endogenous *Stat3*, this vector would serve as an excellent starting point for the generation of further mouse strains carrying unique *Stat3* mutations. Mutations identified in the SH2 domain lead to defects in Y705 phosphorylation and have been suggested to be incapable of dimerizing with WT STAT3 (*72*, *427*). This suggests a novel mechanism for SH2 mutations' dysfunction, one in which inactive STAT dimers are not formed. In such a system, expression of transgenic SH2 mutant STAT3 proteins may prove insufficient to repress endogenous STAT3 activity.

However, inactive SH2 mutants may compete with WT STAT3 for binding to JAKs and thus block potential JAK phosphorylation of WT proteins. As our data suggests that JAK activation is the limiting factor, BAC-transgenic expression of SH2 mutants in this system would result in signaling defects similar to those we observed with DNA binding mutants. Regardless, modification of the BAC-targeting strategy to allow insertion of an SH2 mutation would be greatly informative.

Another advantage of the BAC-transgenic approach over a traditional knock-in was the generation of several mouse strains that expressed 1,2, or more copies of the mutant STAT3 construct. The data reported in this thesis was all generated using mice that expressed two copies of STAT3ΔV463. However, preliminary analysis of mice with a higher copy number of the mutant transgene has suggested a more severe phenotype, with both reduced litter sizes and long-term survival. Further characterization of these mice could provide important new insights into STAT3 function at steady state. Similarly, analysis of mice with only a single copy of the dominant-negative allele could help define the relative importance of STAT3 signaling in the different systems for which we have observed defects.

The primary shortcoming of the BAC-transgenic approach was that the parent BAC: RP24-236G5 included the *Stat5a* gene and transcriptional analysis suggested that it was expressed (~1.5 fold increased in transgenic cells). Studies in T cells and tumor cell lines have demonstrated that STAT3 and

STAT5(a/b) can have both complementary and opposing roles in transcriptional regulation (*444*, *566*, *567*). Similar to the STAT3 findings we did not observe an appreciable difference in STAT5 tyrosine phosphorylation levels between cytokine stimulated WT and mut-*Stat3* cells (data not shown). As elevated *Stat5a* expression levels did not alter STAT5 activation/tyrosine phosphorylation levels, we reasoned that the transgenic construct would have minimal direct effects on STAT5 signaling. However, these mice could be crossed onto a *Stat5a*$^{+/-}$ strain to normalize *Stat5a* expression levels.

Therefore, our BAC-transgenic mouse model of AD-HIES represents an important first step in furthering our understanding of both this disease and the interplay of STAT3 function from various cell types. BAC-recombineering proved both a robust and efficient approach in the generation of the model, which was able to reproduce both biochemical and clinical hallmarks of AD-HIES. However, the generation of more mice, using different AD-HIES mutations, will be key in gaining a greater understanding of the different patient subsets. Our data have demonstrated multiple functional abnormalities that arise in a hypomorphic STAT3 environment and cooperatively contribute to the AD-HIES phenotype. Further elucidation of the clinical relevance of specific defects will require mutant *Stat3* alleles that can be selectively expressed in different tissue types through use of the Cre-lox system.

6.2. STAT3ΔV463 in B Cell CSR and the Humoral Immune Response.

Antibody production is a key player in the adaptive immune response and is required for long-term immune protection. Antibody class, or isotype, is determined by the heavy chain constant (C_H) region, which determines the antibody's effector function. CD40 and/or TLR stimulation provides essential activation for B cells to undergo CSR. However, cytokines produced by Th and dendritic cells control CSR through the induction of GL transcripts. IL-4, IFN-γ, and TGF-β have all been shown to play important roles in determining isotype specificity in CSR (*139*, *470*, *568*, *569*). The transcriptional pathways controlling these cytokine effects have been defined, but the function of other cytokines produced within the germinal center, and the transcriptional pathways they activate, has not. Results from this thesis suggest a previously unrecognized role for STAT3 in regulating B cell CSR.

Hypomorphic STAT3 signaling resulted in reduced IgG1 and enhanced IgE CSR *in vitro*. Correspondingly, reduced serum IgG1 levels and elevated IgE levels were detected in mut-*Stat3* mice. As the *in vitro* system was independent of T cell function, these findings suggest a B cell-intrinsic role for STAT3 in CSR and provide a potential link between STAT3 dysfunction and AD-HIES. Curiously, a previous study reported reduced IgE secretion from AD-HIES patient B cells *in vitro* (*446*). Although puzzling these results do not exclude a potential bias of AD-HIES patient B cells to undergo preferential CSR to IgE. This is because the study only looked at IgE secretion and differences were only observed in the presence of IL-21, a STAT3 activating

cytokine known to promote Ig secretion (*570-574*). Indeed, the magnitude of the IgE CSR bias of mut-*Stat3* B cells was dramatically underestimated by measurement of secreted IgE levels in culture supernatants. This suggests that a more thorough investigation of CSR in AD-HIES B cells is merited.

Analysis of STAT3 binding in class-switching B cells by ChIP-Seq revealed significant binding of this trancription factor with the Ig heavy chain locus, providing further support for a role for STAT3 in regulating CSR. Interestingly, comparison of this dataset with ChIP-Seq analysis of STAT6, which is a well established driver of IgG1 and IgE CSR, revealed that nearly 50% of genes bound by STAT3 in activated B cells were also bound by STAT6. This suggested an interplay of STAT function in mediating B cell responses. Emerging evidence from analysis of STAT function in Th cell differentiation suggests that STATs work both cooperatively and in opposition with each other and with other transcription factors to ensure the desired balance between different cell fates and functions (*443*). As alternative lineages, each specified for particular effector functions, the different Th cell subsets are in many ways analogous to alternatively switched B cell populations. Closer analysis of STAT activity in B cells may well unravel a similar complex network of STAT signaling that controls CSR to the different isotypes. Complementary to this view, a recent study found that expression of T-bet and ROR-α, two transcription factors known to regulate Th cell differentiation downstream of STAT function (*180*, *188*, *189*, *219*, *575*), were respectively critical for maintaining IgG2a and IgA isotype specific memory B cells *in vivo* (*576*).

Another interesting insight from analysis of STAT3 and STAT6 binding to the Ig heavy chain locus was the complete absence of STAT3 binding at the Cε promoter region. Although a report of direct competition of STATs at a given locus does exist (*444*), STAT driven transcriptional repression is generally thought to be indirect. Fitting with this paradigm, we identified Id2, a transcriptional repressor of Igε, to be both a STAT3 target gene and to be downregulated in mut-*Stat3* B cells. Id2 is important in regulation of far more than just Igε transcription, which is exemplified by the finding that $Id2^{-/-}$ mice fail to develop peripheral lymph nodes (*547*). It is therefore unlikely that Id2 expression is uniformly reduced in all mut-*Stat3* cells. Id2 expression is also regulated by TGF-β (*577*, *578*) and STAT3 binding in B cells was primarily focused at an Id2 putative enhancer element that we identified, rather than at the promoter. Recent data suggests that tissue specific expression of genes is primarily regulated at enhancers (*481*). Thus, STAT3 regulation of Id2 in activated B cells may represent the exception rather than the norm.

Germinal center responses and plasma cell formation have not been fully investigated in the mut-*Stat3* model. Preliminary findings suggest that germinal centers are formed but plasma cell differentiation is inhibited in these mice. Regardless, mut-*Stat3* mice were able to mount *C. rodentium* specific humoral responses following infection with this intestinal pathogen, suggesting that defects in plasma cell formation are moderate at least. However, this does not rule out potential problems in affinity maturation or

memory B cell formation. There is an increasing body of evidence that suggests markedly reduced numbers of memory B cells in AD-HIES patients (*426*). It will be interesting to pursue potential roles for hypomorphic STAT3 in this process as well.

6.3. STAT3ΔV463 in Intestinal Immune Homeostasis.

The intestinal immune system is faced with the rigorous task of responding to pathogenic invaders while remaining tolerant towards harmless commensal microbes and dietary factors that are abundant in the intestinal lumen. As a result, a balance of inflammatory and regulatory immune responses within the intestine is key to ensuring health of the host. Results from this thesis suggest that STAT3 is a key driver of both host-protective inflammatory and regulatory responses. Hypomorphic STAT3 activity led to defects in IEC AMP production, T cell cytokine responses, and blunting of regulatory IL-10 responses. Collectively, these contributed to a striking phenotype following infection with the intestinal A/E pathogen *C. rodentium*.

Although a multitude of pro-inflammatory cytokines (IL-6, IL-21, IL-22, IL-23) signal via STAT3, our data clearly demonstrates that hypomorphic STAT3 signaling does not prevent the onset of intestinal inflammation. In fact, we observed markedly increased tissue damage and inflammatory infiltrates in mut-*Stat3* mice following infection with *C. rodentium*. Notably, the number of eosinophils and IFN-γ producing T cells were particularly elevated in mut-

Stat3 mice at the peak of inflammation. Although eosinophils are elevated in IBD and other forms of colonic inflammation, their role remains largely unknown (*579-582*). Similarly, the function of eosinophils in *C. rodentium* infection has not been explored. Eosinophilia is a common clinical feature of HIES (*385*) and is also associated with atopic diseases and elevated IgE levels. Closer examination of intestinal eosinophil numbers in mut-*Stat3* mice at steady-state will be necessary to determine if increased eosinophil numbers represent a unique marker of the mut-*Stat3* inflammatory response.

IFN-γ can be a potent driver of intestinal pathology. In addition to elevated numbers of IFN-γ producing T cells following *C. rodentium* infection, we have consistently identified increased numbers of IFN-γ^+ cells following Th1 differentiation of mut-*Stat3* mice *in vitro*. This is consistent with findings of increased IFN-γ production in the spleen and small intestine of mice with STAT3 deficient T cells (*219*, *241*) and suggest a T cell intrinsic role for STAT3 in inhibiting IFN-γ production. STAT3's inhibitory effects are unlikely to be direct as genome-wide analysis of STAT3 binding in T cells revealed no association of STAT3 with the *Ifng* locus (*219*). One possible explanation for increased IFN-γ production in a hypomorphic STAT3 environment is reduced expression of SOCS3 and subsequent increased STAT1 signaling activity (see Chapter 4 discussion). Loss of IL-10 signaling in myeloid cells leads to enhanced IL-12 secretion (*583*, *584*). Consistent with this, mut-*Stat3* CD11c$^+$ cells secrete approximately two-fold more IL-12 than WT when stimulated *in vitro* (Dr. Arian Laurence, personal communication). IL-12 induces expression

of IFN-γ in activated Th cells. Thus, the elevated numbers of IFN-γ producing T cells we observed in *C. rodentium* infected mut-*Stat3* mice is most likely attributable to both an intrinsic bias towards IFN-γ production and elevated IL-12 production from myeloid cells due to loss of IL-10 signaling. Interestingly, IFN-γ drives production of IL-12 from myeloid cells. Loss of IL-10 inhibition of this process in mut-*Stat3* mice could lead to a positive feedback loop, driving the intestinal inflammation we observed in late *C. rodentium* infection. Blockade of IFN-γ in mut-*Stat3* mice following *C. rodentium* infection will be an important next step towards understanding the role of IFN-γ in this system.

Our findings provide important new insight into IL-22 function within the intestine. Previous work has identified IL-22 as a major mediator of STAT3 phosphorylation in IECs (*49*) and a major driver of host protective AMP production and wound-repair processes (*49*, *509*). Intriguingly, our data suggests that STAT3 selectively regulates RegIIIβ and RegIIIγ production and that other mechanisms, perhaps IL-17C, are sufficient to induce production of additional AMPS. RegIIIγ$^{-/-}$ mice exhibit increased bacterial colonization of the small intestine epithelial surface and microbiota driven elevated IgA and IFN-γ responses (*585*). Reduced RegIII family production in mut-*Stat3* mice could thus lead to a breakdown in host-bacterial mutualism within the intestine and contribute to skewing of adaptive immune responses. Analysis of both the makeup and spatial localization of the microbiota in mut-*Stat3* mice could provide important insight into STAT3's role in both maintenance of the intestinal barrier and microbial colonization.

Th17 cells are an important component of the intestinal immune system and have been shown to contribute to protective immune responses against diverse bacterial and fungal infections (243, 452, 453, 594, 595, 724 LT). Introduction of dominant-negative STAT3ΔV463 resulted in a marked reduction in the percent of T cells producing IL-17A and IL-17F in the lamina propria. This suggested a host-protective defect as reduced production of classical Th17 cytokines has been associated with the increased susceptibility of AD-HIES patients to oral, cutaneous, and sinopulmonary infections (*78*, *553*). However, despite being present at a reduced frequency following infection with the intestinal A/E pathogen *C. rodentium*, the total number of IL-17A and IL-17F producing T cells was equivalent between WT and mut-*Stat3* mice. This suggested that despite profound defects in Th17 differentiation *in vitro*, hypomorphic STAT3 animals can mount a sizeable Th17 response in the face of an acute infection with a complex pathogen. Innate immune cells are becoming an increasingly appreciated reservoir of early host-protective IL-17 and further characterization of functional responses from these populations ($\gamma\delta$ T cells $CD3^+$ invariant natural killer T (iNKT) cells, ILCs, NK cells and myeloid cells) will be required to assess the net IL-17 defect in mut-*Stat3* mice (*215*, *586-591*).

Dysregulated, IL-23 driven Th17 cell responses are associated with pathology in a number of autoimmune diseases, including experimental colitis and IBD (439, 447, 450, 632, 638, 697). Our data suggests that hypomorphic STAT3

signaling would inhibit IL-17 dependent disease pathways but not necessarily all IL-23 driven pathologies. Indeed, T cell derived GM-CSF has been demonstrated to be an important mediator of EAE (*521*) and we saw equivalent numbers of GM-CSF$^+$ T cells in WT and mut-*Stat3* mice following *C. rodentium* infection. Additionally, STAT3 has previously been shown to have direct and cell-intrinsic functions in promoting T cell accumulation in an experimental model of colitis (*219*). The accumulation of IFN-γ^+ CD4 T cells in the lamina propria of *C. rodentium* infected mut-*Stat3* mice suggests that T cell proliferative capacity is intact, however co-transfer of WT and mut-*Stat3* cells into a lymphopenic environment could rule out any cell-intrinsic proliferative defects.

Regulatory T cells serve essential functions in suppressing inflammatory responses and promoting self-tolerance (488, 692). Therefore, it was notable that hypomorphic STAT3 signaling led to increased numbers of Foxp3$^+$ cells both *in vitro* and *in vivo*, at steady-state and disease. Both the commensal flora and dietary factors like retinoic acid are thought to modulate the balance of Treg and Th17 cells in the intestine (249, 253-255, 511, 594-597). Thus, perturbation of either of these in the hypomorphic STAT3 environment could lead to enhanced induction of Tregs. Additionally, IL-23 has been shown to inhibit intestinal Treg cell differentiation and STAT3 deficient T cells show a cell-intrinsic bias towards Treg conversion when transferred into a lymphopenic environment (*219*, *243*). Collectively then, both a cell-intrinsic bias and environmental factors may contribute to the increased number of Tregs we observed in mut-*Stat3* mice. Whether these mut-*Stat3* Tregs are

functional is yet to be determined, although studies using AD-HIES patient Tregs suggest that they will be (*555*). Selective deletion of STAT3 in Foxp3^{+} cells is reported to result in fatal enterocolitis due to an inability to regulate IL-17 driven responses (*294*). As IL-17 production is also curbed in mut-*Stat3* mice this seems an unlikely cause for the pathology we noted following *C. rodentium* infection.

All together, our data supports a key role for STAT3 in the maintenance of intestinal homeostasis and suggests that a partial loss of STAT3 signaling could lead to an increased susceptibility of AD-HIES patients to certain enteric pathogens. Additionally, hypomorphic STAT3 activity has the potential to result in protective inflammatory responses becoming pathogenic due to defects in IL-10 signaling. Reports of enterocolitis in AD-HIES patients are extremely limited, suggesting possible species-specific differences in intestinal host-defense. However, reduced IL-10 signaling could contribute to other AD-HIES morbidities, chiefly, pneumatocele formation secondary to bacterial and fungal pulmonary infections.

6.4. Conclusions.

Even as complexities of immune cell function continue to be unraveled, STAT mediated signaling events remain key regulators of the immune response. Unlike all other members of the *Stat* gene family, ablation of *Stat3* leads to embryonic lethality (*45*). Selective inactivation of *Stat3* in various adult mouse

tissues has led to many advances in our understanding of this transcription factor's function within the immune system (*44*). Nevertheless, as STAT3 appears to control seemingly conflicting pro- and anti-inflammatory pathways in different cell types, much is left to learn about STAT3 function at the organism level. The discovery of dominant-negative *STAT3* mutations in AD-HIES patients presented a unique opportunity for further understanding of both the pathogenesis of this disease and of the interplay of STAT3 function from various cell and tissue types (*70*, *71*).

From this work, STAT3 appears to regulate multiple aspects of both the innate and adaptive immune responses and as such contributes to immune homeostasis and host-protection. We identified a previously unrecognized role for STAT3 in B cell CSR that may contribute to the hyper-IgE phenotype noted in *STAT3*-mutated HIES patients. Additionally, our data supported previous findings of STAT3 being both a critical driver of IL-17 production and inhibitor of Foxp3 expression (*219*). As numerous studies have indicted that the Th17-Treg balance is critical for the maintenance of intestinal immune homeostasis, this finding may explain the relative lack of autoimmunity identified in AD-HIES patients, despite numerous reports of fatal enterocolitis following selective deletion of *Stat3* in specific cell types.

Our findings clearly demonstrate that potent pro-inflammatory responses can be formed in a hypomorphic STAT3 environment and may even contribute to pathology due to a partial loss of the immunoregulatory activity of IL-10. The

signaling of other IL-10 family members also appears to be blunted as we noted a profound reduction in certain IL-22 mediated host-protective responses within the intestine. These findings may be of particular clinical relevance as enhanced tissue damage and loss of normal lung architecture, secondary to bacterial and fungal pneumonia, is a significant source of morbidity and mortality in AD-HIES patients.

7. Bibliography

1. M. Gadina *et al.*, Signaling by type I and II cytokine receptors: ten years after, *Curr. Opin. Immunol.* **13**, 363–373 (2001).

2. W. J. Leonard, J. J. O'Shea, Jaks and STATs: biological implications, *Annu. Rev. Immunol.* **16**, 293–322 (1998).

3. J. E. Darnell, I. M. Kerr, G. R. Stark, Jak-STAT pathways and transcriptional activation in response to IFNs and other extracellular signaling proteins, *Science* **264**, 1415–1421 (1994).

4. J. N. Ihle, The Janus kinase family and signaling through members of the cytokine receptor superfamily, *Proc. Soc. Exp. Biol. Med.* **206**, 268–272 (1994).

5. M. Müller *et al.*, The protein tyrosine kinase JAK1 complements defects in interferon-alpha/beta and -gamma signal transduction, *Nature* **366**, 129–135 (1993).

6. S. A. Oakes *et al.*, Signaling via IL-2 and IL-4 in JAK3-deficient severe combined immunodeficiency lymphocytes: JAK3-dependent and independent pathways, *Immunity* **5**, 605–615 (1996).

7. H. B. Sadowski, K. Shuai, J. E. Darnell, M. Z. Gilman, A common nuclear signal transduction pathway activated by growth factor and cytokine receptors, *Science* **261**, 1739–1744 (1993).

8. D. E. Levy, J. E. Darnell, Stats: transcriptional control and biological impact, *Nat. Rev. Mol. Cell Biol.* **3**, 651–662 (2002).

9. N. Stahl *et al.*, Choice of STATs and other substrates specified by modular tyrosine-based motifs in cytokine receptors, *Science* **267**, 1349–1353 (1995).

10. A. C. Greenlund *et al.*, Stat recruitment by tyrosine-phosphorylated cytokine receptors: an ordered reversible affinity-driven process, *Immunity* **2**, 677–687 (1995).

11. K. Shuai *et al.*, Interferon activation of the transcription factor Stat91 involves dimerization through SH2-phosphotyrosyl peptide interactions, *Cell* **76**, 821–828 (1994).

12. K. M. McBride, G. Banninger, C. McDonald, N. C. Reich, Regulated nuclear import of the STAT1 transcription factor by direct binding of importin-alpha, *EMBO J.* **21**, 1754–1763 (2002).

13. H. M. Seidel *et al.*, Spacing of palindromic half sites as a determinant of selective STAT (signal transducers and activators of transcription) DNA binding and transcriptional activity, *Proc. Natl. Acad. Sci. U.S.A.* **92**, 3041–3045 (1995).

14. D. C. Look, M. R. Pelletier, R. M. Tidwell, W. T. Roswit, M. J. Holtzman, Stat1 depends on transcriptional synergy with Sp1, *J. Biol. Chem.* **270**, 30264–30267 (1995).

15. C. McDonald, N. C. Reich, Cooperation of the transcriptional coactivators CBP and p300 with Stat6, *J. Interferon Cytokine Res.* **19**, 711–722 (1999).

16. M. Paulson *et al.*, Stat protein transactivation domains recruit p300/CBP through widely divergent sequences, *J. Biol. Chem.* **274**, 25343–25349 (1999).

17. M. Snyder, W. He, J. J. Zhang, The DNA replication factor MCM5 is essential for Stat1-mediated transcriptional activation, *Proc. Natl. Acad. Sci. U.S.A.* **102**, 14539–14544 (2005).

18. X. Zhang, M. H. Wrzeszczynska, C. M. Horvath, J. E. Darnell, Interacting regions in Stat3 and c-Jun that participate in cooperative transcriptional activation, *Mol. Cell. Biol.* **19**, 7138–7146 (1999).

19. J. J. Schuringa, H. Timmer, D. Luttickhuizen, E. Vellenga, W. Kruijer, c-Jun and c-Fos cooperate with STAT3 in IL-6-induced transactivation of the IL-6 respone element (IRE), *Cytokine* **14**, 78–87 (2001).

20. K. A. Mowen *et al.*, Arginine methylation of STAT1 modulates IFNalpha/beta-induced transcription, *Cell* **104**, 731–741 (2001).

21. P. Shankaranarayanan, P. Chaitidis, H. Kühn, Acetylation by histone acetyltransferase CREB-binding protein/p300 of STAT6 is required for transcriptional activation of the 15-lipoxygenase-1 gene, *Journal of Biological …* (2001).

22. S. John, U. Vinkemeier, E. Soldaini, J. E. Darnell, W. J. Leonard, The significance of tetramerization in promoter recruitment by Stat5, *Mol. Cell. Biol.* **19**, 1910–1918 (1999).

23. M. Paulson, C. Press, E. Smith, N. Tanese, D. E. Levy, IFN-Stimulated transcription through a TBP-free acetyltransferase complex escapes viral shutoff, *Nat Cell Biol* **4**, 140–147 (2002).

24. H. Yu, D. Pardoll, R. Jove, STATs in cancer inflammation and immunity: a leading role for STAT3, *Nat. Rev. Cancer* **9**, 798–809 (2009).

25. E. B. Haura, J. Turkson, R. Jove, Mechanisms of disease: Insights into the emerging role of signal transducers and activators of transcription in cancer, *Nat Clin Pract Oncol* **2**, 315–324 (2005).

26. J. Mudter *et al.*, Activation pattern of signal transducers and activators of transcription (STAT) factors in inflammatory bowel diseases, *Am. J. Gastroenterol.* **100**, 64–72 (2005).

27. N. Aoki, T. Matsuda, A cytosolic protein-tyrosine phosphatase PTP1B specifically dephosphorylates and deactivates prolactin-activated STAT5a and STAT5b, *J. Biol. Chem.* **275**, 39718–39726 (2000).

28. S. J. Haque, P. Harbor, M. Tabrizi, T. Yi, B. R. Williams, Protein-tyrosine phosphatase Shp-1 is a negative regulator of IL-4- and IL-13-dependent signal transduction, *J. Biol. Chem.* **273**, 33893–33896 (1998).

29. K. Rakesh, D. K. Agrawal, Controlling cytokine signaling by constitutive inhibitors, *Biochem. Pharmacol.* **70**, 649–657 (2005).

30. F. Schaper *et al.*, Activation of the protein tyrosine phosphatase SHP2 via the interleukin-6 signal transducing receptor protein gp130 requires tyrosine kinase Jak1 and limits acute-phase protein expression, *Biochem. J.* **335 (Pt 3)**, 557–565 (1998).

31. T. Naka *et al.*, Structure and function of a new STAT-induced STAT inhibitor, *Nature* **387**, 924–929 (1997).

32. R. Starr *et al.*, A family of cytokine-inducible inhibitors of signalling, *Nature* **387**, 917–921 (1997).

33. T. A. Endo *et al.*, A new protein containing an SH2 domain that inhibits JAK kinases, *Nature* **387**, 921–924 (1997).

34. A. Yoshimura, T. Naka, M. Kubo, SOCS proteins, cytokine signalling and immune regulation, *Nat. Rev. Immunol.* **7**, 454–465 (2007).

35. T. Kamura *et al.*, VHL-box and SOCS-box domains determine binding specificity for Cul2-Rbx1 and Cul5-Rbx2 modules of ubiquitin ligases, *Genes Dev.* **18**, 3055–3065 (2004).

36. J. G. Zhang *et al.*, The conserved SOCS box motif in suppressors of cytokine signaling binds to elongins B and C and may couple bound proteins to proteasomal degradation, *Proc. Natl. Acad. Sci. U.S.A.* **96**, 2071–2076 (1999).

37. S. E. Nicholson *et al.*, Suppressor of cytokine signaling-3 preferentially binds to the SHP-2-binding site on the shared cytokine receptor subunit gp130, *Proc. Natl. Acad. Sci. U.S.A.* **97**, 6493–6498 (2000).

38. J. E. Fenner *et al.*, Suppressor of cytokine signaling 1 regulates the immune response to infection by a unique inhibition of type I interferon activity, *Nat Immunol* **7**, 33–39 (2006).

39. H. Sakamoto *et al.*, A Janus kinase inhibitor, JAB, is an interferon-gamma-inducible gene and confers resistance to interferons, *Blood* **92**, 1668–1676 (1998).

40. G. R. Stark, J. E. Darnell, The JAK-STAT pathway at twenty, *Immunity* **36**, 503–514 (2012).

41. S. Akira *et al.*, Molecular cloning of APRF, a novel IFN-stimulated gene factor 3 p91-related transcription factor involved in the gp130-mediated signaling pathway, *Cell* **77**, 63–71 (1994).

42. C. Lütticken *et al.*, Association of transcription factor APRF and protein kinase Jak1 with the interleukin-6 signal transducer gp130, *Science* **263**, 89–92 (1994).

43. Z. Zhong, Z. Wen, J. E. Darnell, Stat3: a STAT family member activated by tyrosine phosphorylation in response to epidermal growth factor and interleukin-6, *Science* **264**, 95–98 (1994).

44. D. E. Levy, C.-K. Lee, What does Stat3 do? *J. Clin. Invest.* **109**, 1143–1148 (2002).

45. K. Takeda *et al.*, Targeted disruption of the mouse Stat3 gene leads to early embryonic lethality, *Proc. Natl. Acad. Sci. U.S.A.* **94**, 3801–3804 (1997).

46. C. B. Ware *et al.*, Targeted disruption of the low-affinity leukemia inhibitory factor receptor gene causes placental, skeletal, neural and metabolic defects and results in perinatal death, *Development* **121**, 1283–1299 (1995).

47. S. Sano *et al.*, Keratinocyte-specific ablation of Stat3 exhibits impaired skin remodeling, but does not affect skin morphogenesis, *EMBO J.* **18**, 4657–4668 (1999).

48. R. S. Chapman *et al.*, Suppression of epithelial apoptosis and delayed mammary gland involution in mice with a conditional knockout of Stat3, *Genes Dev.* **13**, 2604–2616 (1999).

49. G. Pickert *et al.*, STAT3 links IL-22 signaling in intestinal epithelial cells to mucosal wound healing, *Journal of Experimental Medicine* **206**, 1465–1472 (2009).

50. D. J. Kim, J. M. Angel, S. Sano, J. DiGiovanni, Constitutive activation and targeted disruption of signal transducer and activator of transcription 3 (Stat3) in mouse epidermis reveal its critical role in UVB-induced skin carcinogenesis, *Oncogene* **28**, 950–960 (2009).

51. S. Sano, K. S. Chan, S. Carbajal, J. Clifford, M. Peavey, Stat3 links activated keratinocytes and immunocytes required for development of psoriasis in a novel transgenic mouse model, *Nat Med* (2004).

52. H. Yu, M. Kortylewski, D. Pardoll, Crosstalk between cancer and immune cells: role of STAT3 in the tumour microenvironment, *Nat. Rev. Immunol.* **7**, 41–51 (2007).

53. K. Takeda *et al.*, Enhanced Th1 activity and development of chronic enterocolitis in mice devoid of Stat3 in macrophages and neutrophils, *Immunity* **10**, 39–49 (1999).

54. D. J. Berg *et al.*, Enterocolitis and colon cancer in interleukin-10-deficient mice are associated with aberrant cytokine production and CD4(+) TH1-like responses, *J. Clin. Invest.* **98**, 1010–1020 (1996).

55. R. Kühn, J. Löhler, D. Rennick, K. Rajewsky, W. Müller, Interleukin-10-deficient mice develop chronic enterocolitis, *Cell* (1993).

56. T. Welte *et al.*, STAT3 deletion during hematopoiesis causes Crohn's disease-like pathogenesis and lethality: a critical role of STAT3 in innate immunity, *Proc. Natl. Acad. Sci. U.S.A.* **100**, 1879–1884 (2003).

57. C. K. Lee *et al.*, STAT3 is a negative regulator of granulopoiesis but is not required for G-CSF-dependent differentiation, *Immunity* **17**, 63–72 (2002).

58. S. Sano *et al.*, Stat3 in thymic epithelial cells is essential for postnatal maintenance of thymic architecture and thymocyte survival, *Immunity* **15**, 261–273 (2001).

59. K. Takeda *et al.*, Stat3 activation is responsible for IL-6-dependent T cell proliferation through preventing apoptosis: generation and characterization of T cell-specific Stat3-deficient mice, *J Immunol* **161**, 4652–4660 (1998).

60. H. Akaishi *et al.*, Defective IL-2-mediated IL-2 receptor alpha chain expression in Stat3-deficient T lymphocytes, *Int. Immunol.* **10**, 1747–1751 (1998).

61. L. Wei, A. Laurence, J. J. O'shea, New insights into the roles of Stat5a/b and Stat3 in T cell development and differentiation, *Semin. Cell Dev. Biol.* **19**, 394–400 (2008).

62. J. L. Fornek *et al.*, Critical role for Stat3 in T-dependent terminal differentiation of IgG B cells, *Blood* **107**, 1085–1091 (2006).

63. W. C. Chou, D. E. Levy, C.-K. Lee, STAT3 positively regulates an early step in B-cell development, *Blood* **108**, 3005–3011 (2006).

64. S. D. Davis, J. Schaller, R. J. Wedgwood, Job's Syndrome. Recurrent,' cold', staphylococcal abscesses, *Lancet* (1966).

65. R. H. Buckley, B. B. Wray, E. Z. Belmaker, Extreme hyperimmunoglobulinemia E and undue susceptibility to infection, *Pediatrics* **49**, 59–70 (1972).

66. R. H. Buckley, The hyper-IgE syndrome, *Clin Rev Allergy Immunol* (2001).

67. D. L. Domingo, A. F. Freeman, J. Davis, J. M. Puck, Novel intraoral phenotypes in hyperimmunoglobulin‐E syndrome, *Oral …* (2008).

68. J. C. Ling *et al.*, Coronary artery aneurysms in patients with hyper IgE recurrent infection syndrome, *Clin. Immunol.* **122**, 255–258 (2007).

69. T. Y. Young, D. Jerome, S. Gupta, Hyperimmunoglobulinemia E syndrome associated with coronary artery aneurysms: deficiency of central memory CD4+ T cells and expansion of effector …, *Annals of Allergy* (2007).

70. S. M. Holland *et al.*, STAT3 mutations in the hyper-IgE syndrome, *N Engl J Med* **357**, 1608–1619 (2007).

71. Y. Minegishi *et al.*, Dominant-negative mutations in the DNA-binding domain of STAT3 cause hyper-IgE syndrome, *Nature* **448**, 1058–1062 (2007).

72. E. D. Renner *et al.*, Novel signal transducer and activator of transcription 3 (STAT3) mutations, reduced TH17 cell numbers, and variably defective STAT3 phosphorylation in hyper-IgE syndrome, *Journal of Allergy and Clinical Immunology* **122**, 181–187 (2008).

73. Q. Zhang *et al.*, Combined immunodeficiency associated with DOCK8 mutations, *N Engl J Med* **361**, 2046–2055 (2009).

74. K. R. Engelhardt *et al.*, Large deletions and point mutations involving the dedicator of cytokinesis 8 (DOCK8) in the autosomal-recessive form of hyper-IgE syndrome, *Journal of Allergy and Clinical Immunology* **124**, 1289–1302.e4 (2009).

75. J. D. Milner *et al.*, Impaired T(H)17 cell differentiation in subjects with autosomal dominant hyper-IgE syndrome, *Nature* **452**, 773–776 (2008).

76. C. S. Ma *et al.*, Deficiency of Th17 cells in hyper IgE syndrome due to mutations in STAT3, *Journal of Experimental Medicine* **205**, 1551–1557 (2008).

77. L. de Beaucoudrey *et al.*, Mutations in STAT3 and IL12RB1 impair the development of human IL-17-producing T cells, *Journal of Experimental Medicine* **205**, 1543–1550 (2008).

78. Y. Minegishi *et al.*, Molecular explanation for the contradiction between systemic Th17 defect and localized bacterial infection in hyper-IgE syndrome, *Journal of Experimental Medicine* **206**, 1291–1301 (2009).

79. L. J. Mcheyzer-Williams, M. G. Mcheyzer-Williams, Antigen-specific memory B cell development, *Annu. Rev. Immunol.* **23**, 487–513 (2005).

80. X. Chen, F. Martin, K. A. Forbush, R. M. Perlmutter, J. F. Kearney, Evidence for selection of a population of multi-reactive B cells into the splenic marginal zone, *Int. Immunol.* **9**, 27–41 (1997).

81. A. M. Oliver, F. Martin, J. F. Kearney, IgMhighCD21high lymphocytes enriched in the splenic marginal zone generate effector cells more rapidly than the bulk of follicular B cells, *The Journal of Immunology* (1999).

82. F. Martin, A. M. Oliver, J. F. Kearney, Marginal zone and B1 B cells unite in the early response against T-independent blood-borne particulate antigens, *Immunity* **14**, 617–629 (2001).

83. K. Hayakawa *et al.*, Ly-1 B cells: functionally distinct lymphocytes that secrete IgM autoantibodies, *Proc. Natl. Acad. Sci. U.S.A.* **81**, 2494–2498 (1984).

84. A. F. Ochsenbein *et al.*, Control of early viral and bacterial distribution and disease by natural antibodies, *Science* **286**, 2156–2159 (1999).

85. N. Baumgarth *et al.*, B-1 and B-2 cell-derived immunoglobulin M antibodies are nonredundant components of the protective response to influenza virus infection, *J Exp Med* **192**, 271–280 (2000).

86. F. Ho, J. E. Lortan, I. C. MacLennan, M. Khan, Distinct short-lived and long-lived antibody-producing cell populations, *Eur. J. Immunol.* **16**, 1297–1301 (1986).

87. J. Jacob, R. Kassir, G. Kelsoe, In situ studies of the primary immune response to (4-hydroxy-3-nitrophenyl)acetyl. I. The architecture and dynamics of responding cell populations, *J Exp Med* **173**, 1165–1175 (1991).

88. M. G. McHeyzer-Williams, M. J. McLean, P. A. Lalor, G. J. Nossal, Antigen-driven B cell differentiation in vivo, *J Exp Med* **178**, 295–307 (1993).

89. M. C. Hsu, K.-M. Toellner, C. G. Vinuesa, I. C. M. Maclennan, B cell clones that sustain long-term plasmablast growth in T-independent extrafollicular antibody responses, *Proc. Natl. Acad. Sci. U.S.A.* **103**, 5905–5910 (2006).

90. D. Sze, K. M. Toellner, C. G. de Vinuesa, Intrinsic constraint on plasmablast growth and extrinsic limits of plasma cell survival, *The Journal of …* (2000).

91. C. A. Turner, D. H. Mack, M. M. Davis, Blimp-1, a novel zinc finger-containing protein that can drive the maturation of B lymphocytes into immunoglobulin-secreting cells, *Cell* **77**, 297–306 (1994).

92. M. Shapiro-Shelef *et al.*, Blimp-1 is required for the formation of immunoglobulin secreting plasma cells and pre-plasma memory B cells, *Immunity* **19**, 607–620 (2003).

93. A. Kallies *et al.*, Plasma cell ontogeny defined by quantitative changes in blimp-1 expression, *J Exp Med* **200**, 967–977 (2004).

94. A. L. Shaffer *et al.*, Blimp-1 orchestrates plasma cell differentiation by extinguishing the mature B cell gene expression program, *Immunity* **17**, 51–62 (2002).

95. M. Shapiro-Shelef, K. Calame, Regulation of plasma-cell development, *Nat. Rev. Immunol.* **5**, 230–242 (2005).

96. Y. Lin, K. Wong, K. Calame, Repression of c-myc transcription by Blimp-1, an inducer of terminal B cell differentiation, *Science* (1997).

97. I. C. MacLennan, Germinal centers, *Annu. Rev. Immunol.* **12**, 117–139 (1994).

98. J. M. Tuscano *et al.*, Bcl-x rather than Bcl-2 mediates CD40-dependent centrocyte survival in the germinal center, *Blood* **88**, 1359–1364 (1996).

99. X. Zhang *et al.*, Up-regulation of Bcl-xL expression protects CD40-activated human B cells from Fas-mediated apoptosis, *Cell. Immunol.* **173**, 149–154 (1996).

100. Y. Takahashi, H. Ohta, T. Takemori, Fas is required for clonal selection in germinal centers and the subsequent establishment of the memory B cell repertoire, *Immunity* **14**, 181–192 (2001).

101. A. L. Dent, A. L. Shaffer, X. Yu, D. Allman, L. M. Staudt, Control of inflammation, cytokine expression, and germinal center formation by BCL-6, *Science* (1997).

102. B. H. Ye *et al.*, The BCL-6 proto-oncogene controls germinal-centre formation and Th2-type inflammation, *Nat. Genet.* **16**, 161–170 (1997).

103. H. Toyama *et al.*, Memory B cells without somatic hypermutation are generated from Bcl6-deficient B cells, *Immunity* **17**, 329–339 (2002).

104. C. Tunyaplin *et al.*, Direct repression of prdm1 by Bcl-6 inhibits plasmacytic differentiation, *J Immunol* **173**, 1158–1165 (2004).

105. L. M. Mendez *et al.*, CtBP is an essential corepressor for BCL6 autoregulation, *Mol. Cell. Biol.* **28**, 2175–2186 (2008).

106. H. Ichii *et al.*, Role for Bcl-6 in the generation and maintenance of memory CD8+ T cells, *Nat Immunol* **3**, 558–563 (2002).

107. H. Ichii, A. Sakamoto, Y. Kuroda, T. Tokuhisa, Bcl6 acts as an amplifier for the generation and proliferative capacity of central memory CD8+ T cells, *J Immunol* **173**, 883–891 (2004).

108. A. Kallies, A. Xin, G. T. Belz, S. L. Nutt, Blimp-1 transcription factor is required for the differentiation of effector CD8(+) T cells and memory responses, *Immunity* **31**, 283–295 (2009).

109. R. L. Rutishauser *et al.*, Transcriptional repressor Blimp-1 promotes CD8(+) T cell terminal differentiation and represses the acquisition of central memory T cell properties, *Immunity* **31**, 296–308 (2009).

110. H. Shin *et al.*, A role for the transcriptional repressor Blimp-1 in CD8(+) T cell exhaustion during chronic viral infection, *Immunity* **31**, 309–320 (2009).

111. S. W. Martin, C. C. Goodnow, Burst-enhancing role of the IgG membrane tail as a molecular determinant of memory, *Nat Immunol* **3**, 182–188 (2002).

112. A. Waisman *et al.*, IgG1 B cell receptor signaling is inhibited by CD22 and promotes the development of B cells whose survival is less dependent on Ig alpha/beta, *J Exp Med* **204**, 747–758 (2007).

113. K. Horikawa *et al.*, Enhancement and suppression of signaling by the conserved tail of IgG memory-type B cell antigen receptors, *J Exp Med* **204**, 759–769 (2007).

114. W. Dunnick, G. Z. Hertz, L. Scappino, C. Gritzmacher, DNA sequences at immunoglobulin switch region recombination sites, *Nucleic Acids Res.* **21**, 365–372 (1993).

115. I. M. Min, L. R. Rothlein, C. E. Schrader, J. Stavnezer, E. Selsing, Shifts in targeting of class switch recombination sites in mice that lack mu switch region tandem repeats or Msh2, *J Exp Med* **201**, 1885–1890 (2005).

116. S. Reynaud *et al.*, Interallelic class switch recombination contributes significantly to class switching in mouse B cells, *J Immunol* **174**, 6176–6183 (2005).

117. M. Muramatsu *et al.*, Class switch recombination and hypermutation require activation-induced cytidine deaminase (AID), a potential RNA editing enzyme, *Cell* **102**, 553–563 (2000).

118. P. Revy *et al.*, Activation-induced cytidine deaminase (AID) deficiency causes the autosomal recessive form of the Hyper-IgM syndrome (HIGM2), *Cell* **102**, 565–575 (2000).

119. S. K. Petersen-Mahrt, R. S. Harris, M. S. Neuberger, AID mutates E. coli suggesting a DNA deamination mechanism for antibody diversification, *Nature* (2002).

120. J. Chaudhuri, M. Tian, C. Khuong, K. Chua, E. Pinaud, Transcription-targeted DNA deamination by the AID antibody diversification enzyme, *Nature* (2003).

121. S. K. Dickerson, E. Market, E. Besmer, F. N. Papavasiliou, AID mediates hypermutation by deaminating single stranded DNA, *J Exp Med* **197**, 1291–1296 (2003).

122. P. Pham, R. Bransteitter, J. Petruska, M. F. Goodman, Processive AID-catalysed cytosine deamination on single-stranded DNA simulates somatic hypermutation, *Nature* **424**, 103–107 (2003).

123. J. Hasbold, L. M. Corcoran, D. M. Tarlinton, S. G. Tangye, P. D. Hodgkin, Evidence from the generation of immunoglobulin G-secreting cells that stochastic mechanisms regulate lymphocyte differentiation, *Nat Immunol* **5**, 55–63 (2004).

124. P. D. Hodgkin, J. H. Lee, A. B. Lyons, B cell differentiation and isotype switching is related to division cycle number, *The Journal of experimental …* (1996).

125. M. N. McCall, P. D. Hodgkin, Switch recombination and germ-line transcription are division-regulated events in B lymphocytes, *Biochim. Biophys. Acta* **1447**, 43–50 (1999).

126. J. S. Rush, M. Liu, V. H. Odegard, S. Unniraman, D. G. Schatz, Expression of activation-induced cytidine deaminase is regulated by cell division, providing a mechanistic basis for division-linked class switch recombination, *Proc. Natl. Acad. Sci. U.S.A.* **102**, 13242–13247 (2005).

127. J. L. Workman, Nucleosome displacement in transcription, *Genes Dev.* (2006).

128. C. J. Woo, A. Martin, M. D. Scharff, Induction of somatic hypermutation is associated with modifications in immunoglobulin variable region chromatin, *Immunity* **19**, 479–489 (2003).

129. L. Wang, N. Whang, R. Wuerffel, AID-dependent histone acetylation is detected in immunoglobulin S regions, *The Journal of …* (2006).

130. J. A. Daniel *et al.*, PTIP promotes chromatin changes critical for immunoglobulin class switch recombination, *Science* **329**, 917–923 (2010).

131. K. Yu, F. Chedin, C.-L. Hsieh, T. E. Wilson, M. R. Lieber, R-loops at immunoglobulin class switch regions in the chromosomes of stimulated B cells, *Nat Immunol* **4**, 442–451 (2003).

132. J. Chaudhuri, F. W. Alt, Class-switch recombination: interplay of transcription, DNA deamination and DNA repair, *Nat. Rev. Immunol.* **4**, 541–552 (2004).

133. Y. Nambu *et al.*, Transcription-coupled events associating with immunoglobulin switch region chromatin, *Science* **302**, 2137–2140 (2003).

134. U. Basu *et al.*, The RNA exosome targets the AID cytidine deaminase to both strands of transcribed duplex DNA substrates, *Cell* **144**, 353–363 (2011).

135. D. Rajagopal *et al.*, Immunoglobulin switch mu sequence causes RNA polymerase II accumulation and reduces dA hypermutation, *Journal of Experimental Medicine* **206**, 1237–1244 (2009).

136. L. Wang, R. Wuerffel, S. Feldman, A. A. Khamlichi, A. L. Kenter, S region sequence, RNA polymerase II, and histone modifications create chromatin accessibility during class switch recombination, *Journal of Experimental Medicine* **206**, 1817–1830 (2009).

137. A. Yamane *et al.*, Deep-sequencing identification of the genomic targets of the cytidine deaminase AID and its cofactor RPA in B lymphocytes, *Nat Immunol* **12**, 62–69 (2011).

138. S. Fagarasan, S. Kawamoto, O. Kanagawa, K. Suzuki, Adaptive immune regulation in the gut: T cell-dependent and T cell-independent IgA synthesis, *Annu. Rev. Immunol.* **28**, 243–273 (2010).

139. J. Stavnezer, J. E. J. Guikema, C. E. Schrader, Mechanism and Regulation of Class Switch Recombination, *Annu. Rev. Immunol.* **26**, 261–292 (2008).

140. M. Sellars, B. Reina-San-Martin, P. Kastner, S. Chan, Ikaros controls isotype selection during immunoglobulin class switch recombination, *Journal of Experimental Medicine* **206**, 1073–1087 (2009).

141. E. C. Kim, C. R. Edmonston, X. Wu, A. Schaffer, P. Casali, The HoxC4 homeodomain protein mediates activation of the immunoglobulin heavy chain 3' hs1,2 enhancer in human B cells. Relevance to class switch DNA recombination, *J. Biol. Chem.* **279**, 42258–42269 (2004).

142. J. P. Manis, N. Van Der Stoep, M. Tian, Class switching in B cells lacking 3′ immunoglobulin heavy chain enhancers, *The Journal of …* (1998).

143. E. Pinaud, A. A. Khamlichi, C. Le Morvan, M. Drouet, Localization of the 3′ IgH locus elements that effect long-distance regulation of class switch recombination, *Immunity* (2001).

144. J. Chen, R. Lansford, V. Stewart, F. Young, F. W. Alt, RAG-2-deficient blastocyst complementation: an assay of gene function in lymphocyte development, *Proc. Natl. Acad. Sci. U.S.A.* **90**, 4528–4532 (1993).

145. E. Sakai, A. Bottaro, L. Davidson, B. P. Sleckman, F. W. Alt, Recombination and transcription of the endogenous Ig heavy chain locus is effected by the Ig heavy chain intronic enhancer core region in the absence of the matrix attachment regions, *Proc. Natl. Acad. Sci. U.S.A.* **96**, 1526–1531 (1999).

146. K. Cunningham, H. Ackerly, F. Alt, W. Dunnick, Potential regulatory elements for germline transcription in or near murine Sgamma1, *Int. Immunol.* **10**, 527–536 (1998).

147. K. Adams, H. Ackerly, K. Cunningham, W. Dunnick, A DNase I hypersensitive site near the murine gamma1 switch region contributes to insertion site independence of transgenes and modulates the amount of transcripts induced by CD40 ligation, *Int. Immunol.* **12**, 1705–1713 (2000).

148. S. R. Park, H. Zan, Z. Pal, J. Zhang, A. Al-Qahtani, HoxC4 binds to the promoter of the cytidine deaminase AID gene to induce AID expression, class-switch DNA recombination and somatic hypermutation, *Nature* (2009).

149. T. H. Tran *et al.*, B cell-specific and stimulation-responsive enhancers derepress Aicda by overcoming the effects of silencers, *Nat Immunol* **11**, 148–154 (2010).

150. S. Pauklin, I. V. Sernández, G. Bachmann, A. R. Ramiro, S. K. Petersen-Mahrt, Estrogen directly activates AID transcription and function, *Journal of Experimental Medicine* **206**, 99–111 (2009).

151. T. Mai *et al.*, Estrogen receptors bind to and activate the HOXC4/HoxC4 promoter to potentiate HoxC4-mediated activation-induced cytosine deaminase induction, immunoglobulin class switch DNA recombination, and somatic hypermutation, *Journal of Biological Chemistry* **285**, 37797–37810 (2010).

152. E. J. Pone *et al.*, BCR-signalling synergizes with TLR-signalling for induction of AID and immunoglobulin class-switching through the non-canonical NF-κB pathway, *Nat Commun* **3**, 767 (2012).

153. M. Kondo, I. L. Weissman, K. Akashi, Identification of clonogenic common lymphoid progenitors in mouse bone marrow, *Cell* **91**, 661–672 (1997).

154. H. Han *et al.*, Inducible gene knockout of transcription factor recombination signal binding protein-J reveals its essential role in T versus B lineage decision, *Int. Immunol.* **14**, 637–645 (2002).

155. F. Radtke *et al.*, Deficient T cell fate specification in mice with an induced inactivation of Notch1, *Immunity* **10**, 547–558 (1999).

156. K. Tanigaki *et al.*, Regulation of alphabeta/gammadelta T cell lineage commitment and peripheral T cell responses by Notch/RBP-J signaling, *Immunity* **20**, 611–622 (2004).

157. C. N. Ting, M. C. Olson, K. P. Barton, J. M. Leiden, Transcription factor GATA-3 is required for development of the T-cell lineage, *Nature* **384**, 474–478 (1996).

158. E. Robey, B. J. Fowlkes, Selective events in T cell development, *Annu. Rev. Immunol.* (1994).

159. R. Ceredig, T. Rolink, A positive look at double-negative thymocytes, *Nat. Rev. Immunol.* (2002).

160. E. C. Dudley, H. T. Petrie, L. M. Shah, M. J. Owen, A. C. Hayday, T cell receptor beta chain gene rearrangement and selection during thymocyte development in adult mice, *Immunity* **1**, 83–93 (1994).

161. Q. Hu *et al.*, Specific recognition of thymic self-peptides induces the positive selection of cytotoxic T lymphocytes, *Immunity* **7**, 221–231 (1997).

162. T. K. Starr, S. C. Jameson, K. A. Hogquist, P OSITIVE ANDN EGATIVES ELECTION OFT C ELLS, *Annu. Rev. Immunol.* **21**, 139–176 (2003).

163. J. L. Gowans, The recirculation of lymphocytes from blood to lymph in the rat, *J. Physiol. (Lond.)* **146**, 54–69 (1959).

164. A. H. Sharpe, Mechanisms of costimulation, *Immunol Rev* **229**, 5–11 (2009).

165. C. S. Hsieh *et al.*, Development of TH1 CD4+ T cells through IL-12 produced by Listeria-induced macrophages, *Science* **260**, 547–549 (1993).

166. T. R. Mosmann, R. L. Coffman, TH1 and TH2 cells: different patterns of lymphokine secretion lead to different functional properties, *Annu. Rev. Immunol.* **7**, 145–173 (1989).

167. S. L. Swain, A. D. Weinberg, M. English, G. Huston, IL-4 directs the development of Th2-like helper effectors, *J Immunol* **145**, 3796–3806 (1990).

168. D. H. Zhang, L. Cohn, P. Ray, K. Bottomly, A. Ray, Transcription factor GATA-3 is differentially expressed in murine Th1 and Th2 cells and controls Th2-specific expression of the interleukin-5 gene, *J. Biol. Chem.* **272**, 21597–21603 (1997).

169. W. Zheng, R. A. Flavell, The transcription factor GATA-3 is necessary and sufficient for Th2 cytokine gene expression in CD4 T cells, *Cell* **89**, 587–596 (1997).

170. I. I. Ivanov *et al.*, The orphan nuclear receptor RORgammat directs the differentiation program of proinflammatory IL-17+ T helper cells, *Cell* **126**, 1121–1133 (2006).

171. S. Aggarwal, N. Ghilardi, M.-H. Xie, F. J. De Sauvage, A. L. Gurney, Interleukin-23 promotes a distinct CD4 T cell activation state characterized by the production of interleukin-17, *J. Biol. Chem.* **278**, 1910–1914 (2003).

172. L. E. Harrington *et al.*, Interleukin 17-producing CD4+ effector T cells develop via a lineage distinct from the T helper type 1 and 2 lineages, *Nat Immunol* **6**, 1123–1132 (2005).

173. J. D. Fontenot, M. A. Gavin, A. Y. Rudensky, Foxp3 programs the development and function of CD4+CD25+ regulatory T cells, *Nat Immunol* **4**, 330–336 (2003).

174. R. I. Nurieva *et al.*, Bcl6 mediates the development of T follicular helper cells, *Science* **325**, 1001–1005 (2009).

175. R. I. Nurieva, Y. Chung, D. Hwang, X. O. Yang, H. S. Kang, Generation of follicular helper T cells is mediated by IL-21 but independent of TH1, TH2 or TH17 lineages, *Immunity* (2008).

176. R. P. Bucy *et al.*, Heterogeneity of single cell cytokine gene expression in clonal T cell populations, *J Exp Med* **180**, 1251–1262 (1994).

177. R. P. Bucy *et al.*, Single cell analysis of cytokine gene coexpression during CD4+ T-cell phenotype development, *Proc. Natl. Acad. Sci. U.S.A.* **92**, 7565–7569 (1995).

178. L. Zhou, M. M. W. Chong, D. R. Littman, Plasticity of CD4+ T cell lineage differentiation, *Immunity* **30**, 646–655 (2009).

179. J. Zhu, H. Yamane, W. E. Paul, Differentiation of effector CD4 T cell populations (*), *Annu. Rev. Immunol.* **28**, 445–489 (2010).

180. S. J. Szabo *et al.*, A novel transcription factor, T-bet, directs Th1 lineage commitment, *Cell* **100**, 655–669 (2000).

181. A. A. Lighvani *et al.*, T-bet is rapidly induced by interferon-gamma in lymphoid and myeloid cells, *Proc. Natl. Acad. Sci. U.S.A.* **98**, 15137–15142 (2001).

182. A. Takeda *et al.*, Cutting edge: role of IL-27/WSX-1 signaling for induction of T-bet through activation of STAT1 during initial Th1 commitment, *J Immunol* **170**, 4886–4890 (2003).

183. A. C. Mullen *et al.*, Hlx is induced by and genetically interacts with T-bet to promote heritable T(H)1 gene induction, *Nat Immunol* **3**, 652–658 (2002).

184. A. C. Mullen *et al.*, Role of T-bet in commitment of TH1 cells before IL-12-dependent selection, *Science* **292**, 1907–1910 (2001).

185. S. Agarwal, A. Rao, Modulation of chromatin structure regulates cytokine gene expression during T cell differentiation, *Immunity* **9**, 765–775 (1998).

186. J. L. Grogan *et al.*, Basal chromatin modification at the IL-4 gene in helper T cells, *J Immunol* **171**, 6672–6679 (2003).

187. E.-S. Hwang, S. J. Szabo, P. L. Schwartzberg, L. H. Glimcher, T helper cell fate specified by kinase-mediated interaction of T-bet with GATA-3, *Science* **307**, 430–433 (2005).

188. M. Afkarian, J. R. Sedy, J. Yang, N. G. Jacobson, T-bet is a STAT 1-induced regulator of IL-12 R expression in naive CD 4+ T cells, *Nature* (2002).

189. S. J. Szabo *et al.*, Distinct effects of T-bet in TH1 lineage commitment and IFN-gamma production in CD4 and CD8 T cells, *Science* **295**, 338–342 (2002).

190. W. E. Thierfelder *et al.*, Requirement for Stat4 in interleukin-12-mediated responses of natural killer and T cells, *Nature* **382**, 171–174 (1996).

191. Y. Suzuki, J. S. Remington, The effect of anti-IFN-gamma antibody on the protective effect of Lyt-2+ immune T cells against toxoplasmosis in mice, *J Immunol* **144**, 1954–1956 (1990).

192. M. H. Kaplan, Y. L. Sun, T. Hoey, M. J. Grusby, Impaired IL-12 responses and enhanced development of Th2 cells in Stat4-deficient mice, *Nature* **382**, 174–177 (1996).

193. E. Pearce, A. W. Cheever, R. L. Coffman, Role of Cytokines and CD4+ T-Cell Subsets in the Regulation of Parasite Immunity and Disease, *Immunological …* (1989).

194. S. Trembleau *et al.*, Interleukin 12 administration induces T helper type 1 cells and accelerates autoimmune diabetes in NOD mice, *J Exp Med* **181**, 817–821 (1995).

195. F. Powrie *et al.*, Inhibition of Th1 responses prevents inflammatory bowel disease in scid mice reconstituted with CD45RBhi CD4+ T cells, *Immunity* **1**, 553–562 (1994).

196. M. F. Neurath *et al.*, The transcription factor T-bet regulates mucosal T cell activation in experimental colitis and Crohn's disease, *J Exp Med* **195**, 1129–1143 (2002).

197. G. L. Stritesky *et al.*, The transcription factor STAT3 is required for T helper 2 cell development, *Immunity* **34**, 39–49 (2011).

198. W. Ouyang *et al.*, Inhibition of Th1 development mediated by GATA-3 through an IL-4-independent mechanism, *Immunity* **9**, 745–755 (1998).

199. Q. Yu *et al.*, T cell factor 1 initiates the T helper type 2 fate by inducing the transcription factor GATA-3 and repressing interferon-gamma, *Nat Immunol* **10**, 992–999 (2009).

200. R. M. Anthony, L. I. Rutitzky, J. F. Urban, M. J. Stadecker, W. C. Gause, Protective immune mechanisms in helminth infection, *Nat. Rev. Immunol.* **7**, 975–987 (2007).

201. D. T. Umetsu, J. J. McIntire, O. Akbari, C. Macaubas, Asthma: an epidemic of dysregulated immunity, *Nature* (2002).

202. M. Veldhoen *et al.*, Transforming growth factor-beta “reprograms” the differentiation of T helper 2 cells and promotes an interleukin 9-producing subset, *Nat Immunol* **9**, 1341–1346 (2008).

203. V. Dardalhon *et al.*, IL-4 inhibits TGF-beta-induced Foxp3+ T cells and, together with TGF-beta, generates IL-9+ IL-10+ Foxp3(-) effector T cells, *Nat Immunol* **9**, 1347–1355 (2008).

204. V. Staudt *et al.*, Interferon-regulatory factor 4 is essential for the developmental program of T helper 9 cells, *Immunity* **33**, 192–202 (2010).

205. D. R. Littman, A. Y. Rudensky, Th17 and regulatory T cells in mediating and restraining inflammation, *Cell* (2010).

206. M. Veldhoen, R. J. Hocking, R. A. Flavell, B. Stockinger, Signals mediated by transforming growth factor-beta initiate autoimmune encephalomyelitis, but chronic inflammation is needed to sustain disease, *Nat Immunol* **7**, 1151–1156 (2006).

207. M. Veldhoen, R. J. Hocking, C. J. Atkins, R. M. Locksley, B. Stockinger, TGFbeta in the context of an inflammatory cytokine milieu supports de novo differentiation of IL-17-producing T cells, *Immunity* **24**, 179–189 (2006).

208. E. Bettelli *et al.*, Reciprocal developmental pathways for the generation of pathogenic effector TH17 and regulatory T cells, *Nature* **441**, 235–238 (2006).

209. P. Mangan, L. Harrington, D. O'Quinn, W. Helms, Transforming growth factor-β induces development of the TH17 lineage, *Nature* (2006).

210. K. Ghoreschi *et al.*, Generation of pathogenic T(H)17 cells in the absence of TGF-β signalling, *Nature* **467**, 967–971 (2010).

211. Y. Chung *et al.*, Critical regulation of early Th17 cell differentiation by interleukin-1 signaling, *Immunity* **30**, 576–587 (2009).

212. C. Sutton, C. Brereton, B. Keogh, K. H. G. Mills, E. C. Lavelle, A crucial role for interleukin (IL)-1 in the induction of IL-17-producing T cells that mediate autoimmune encephalomyelitis, *J Exp Med* **203**, 1685–1691 (2006).

213. M. J. Mcgeachy *et al.*, The interleukin 23 receptor is essential for the terminal differentiation of interleukin 17-producing effector T helper cells in vivo, *Nat Immunol* **10**, 314–324 (2009).

214. L. Zhou *et al.*, IL-6 programs T(H)-17 cell differentiation by promoting sequential engagement of the IL-21 and IL-23 pathways, *Nat Immunol* **8**, 967–974 (2007).

215. C. E. Sutton *et al.*, Interleukin-1 and IL-23 induce innate IL-17 production from gammadelta T cells, amplifying Th17 responses and autoimmunity, *Immunity* **31**, 331–341 (2009).

216. B. Martin, K. Hirota, D. J. Cua, B. Stockinger, M. Veldhoen, Interleukin-17-producing gammadelta T cells selectively expand in response to pathogen products and environmental signals, *Immunity* **31**, 321–330 (2009).

217. X. O. Yang *et al.*, Molecular antagonism and plasticity of regulatory and inflammatory T cell programs, *Immunity* **29**, 44–56 (2008).

218. X. O. Yang *et al.*, STAT3 regulates cytokine-mediated generation of inflammatory helper T cells, *J. Biol. Chem.* **282**, 9358–9363 (2007).

219. L. Durant *et al.*, Diverse targets of the transcription factor STAT3 contribute to T cell pathogenicity and homeostasis, *Immunity* **32**, 605–615 (2010).

220. A. Brüstle *et al.*, The development of inflammatory T(H)-17 cells requires interferon-regulatory factor 4, *Nat Immunol* **8**, 958–966 (2007).

221. B. U. Schraml *et al.*, The AP-1 transcription factor Batf controls T(H)17 differentiation, *Nature* **460**, 405–409 (2009).

222. F. J. Quintana *et al.*, Control of T(reg) and T(H)17 cell differentiation by the aryl hydrocarbon receptor, *Nature* **453**, 65–71 (2008).

223. M. Veldhoen *et al.*, The aryl hydrocarbon receptor links TH17-cell-mediated autoimmunity to environmental toxins, *Nature* **453**, 106–109 (2008).

224. H. R. Conti *et al.*, Th17 cells and IL-17 receptor signaling are essential for mucosal host defense against oral candidiasis, *Journal of Experimental Medicine* **206**, 299–311 (2009).

225. X. L. Rudner, K. I. Happel, E. A. Young, J. E. Shellito, Interleukin-23 (IL-23)-IL-17 cytokine axis in murine Pneumocystis carinii infection, *Infection and Immunity* **75**, 3055–3061 (2007).

226. S. A. Khader *et al.*, IL-23 and IL-17 in the establishment of protective pulmonary CD4+ T cell responses after vaccination and during Mycobacterium tuberculosis challenge, *Nat Immunol* **8**, 369–377 (2007).

227. H. Hoshino *et al.*, Increased elastase and myeloperoxidase activity associated with neutrophil recruitment by IL-17 in airways in vivo, *J. Allergy Clin. Immunol.* **105**, 143–149 (2000).

228. M. Laan, Z. H. Cui, H. Hoshino, J. Lötvall, Neutrophil recruitment by human IL-17 via CXC chemokine release in the airways, *The Journal of …* (1999).

229. P. Ye *et al.*, Requirement of interleukin 17 receptor signaling for lung CXC chemokine and granulocyte colony-stimulating factor expression, neutrophil recruitment, and host defense, *J Exp Med* **194**, 519–527 (2001).

230. F. Fossiez *et al.*, T cell interleukin-17 induces stromal cells to produce proinflammatory and hematopoietic cytokines, *J Exp Med* **183**, 2593–2603 (1996).

231. C. Albanesi, A. Cavani, G. Girolomoni, IL-17 is produced by nickel-specific T lymphocytes and regulates ICAM-1 expression and chemokine production in human keratinocytes: synergistic or antagonist effects with IFN-gamma and TNF-alpha, *J Immunol* **162**, 494–502 (1999).

232. D. V. Jovanovic *et al.*, IL-17 stimulates the production and expression of proinflammatory cytokines, IL-beta and TNF-alpha, by human macrophages, *J Immunol* **160**, 3513–3521 (1998).

233. S. Kotake *et al.*, IL-17 in synovial fluids from patients with rheumatoid arthritis is a potent stimulator of osteoclastogenesis, *J. Clin. Invest.* **103**, 1345–1352 (1999).

234. M. B. Teunissen, C. W. Koomen, R. de Waal-Malefyt, E. A. Wierenga, J. D. Bos, Interleukin-17 and interferon-gamma synergize in the enhancement of proinflammatory cytokine production by human keratinocytes, *J. Invest. Dermatol.* **111**, 645–649 (1998).

235. M. Numasaki *et al.*, Interleukin-17 promotes angiogenesis and tumor growth, *Blood* **101**, 2620–2627 (2003).

236. T. Starnes *et al.*, Cutting edge: IL-17F, a novel cytokine selectively expressed in activated T cells and monocytes, regulates angiogenesis and endothelial cell cytokine production, *J Immunol* **167**, 4137–4140 (2001).

237. K. Wolk *et al.*, IL-22 increases the innate immunity of tissues, *Immunity* **21**, 241–254 (2004).

238. S. Radaeva, R. Sun, H.-N. Pan, F. Hong, B. Gao, Interleukin 22 (IL-22) plays a protective role in T cell-mediated murine hepatitis: IL-22 is a survival factor for hepatocytes via STAT3 activation, *Hepatology* **39**, 1332–1342 (2004).

239. S. C. Liang *et al.*, Interleukin (IL)-22 and IL-17 are coexpressed by Th17 cells and cooperatively enhance expression of antimicrobial peptides, *J Exp Med* **203**, 2271–2279 (2006).

240. T. Korn, E. Bettelli, M. Oukka, IL-17 and Th17 Cells, *Annual review of …* (2009).

241. T. J. Harris *et al.*, Cutting edge: An in vivo requirement for STAT3 signaling in TH17 development and TH17-dependent autoimmunity, *J Immunol* **179**, 4313–4317 (2007).

242. D. Yen *et al.*, IL-23 is essential for T cell-mediated colitis and promotes inflammation via IL-17 and IL-6, *J. Clin. Invest.* **116**, 1310–1316 (2006).

243. P. P. Ahern *et al.*, Interleukin-23 drives intestinal inflammation through direct activity on T cells, *Immunity* **33**, 279–288 (2010).

244. A. Amadi-Obi *et al.*, TH17 cells contribute to uveitis and scleritis and are expanded by IL-2 and inhibited by IL-27/STAT1, *Nat Med* **13**, 711–718 (2007).

245. S. Z. Josefowicz, A. Rudensky, Control of regulatory T cell lineage commitment and maintenance, *Immunity* **30**, 616–625 (2009).

246. Y. Nishizuka, T. Sakakura, Thymus and reproduction: sex-linked dysgenesia of the gonad after neonatal thymectomy in mice, *Science* **166**, 753–755 (1969).

247. M. Asano, M. Toda, N. Sakaguchi, S. Sakaguchi, Autoimmune disease as a consequence of developmental abnormality of a T cell subpopulation, *J Exp Med* **184**, 387–396 (1996).

248. A. Bonomo *et al.*, Pathogenesis of post-thymectomy autoimmunity. Role of syngeneic MLR-reactive T cells, *J Immunol* **154**, 6602–6611 (1995).

249. F. Powrie, M. W. Leach, S. Mauze, L. B. Caddle, R. L. Coffman, Phenotypically distinct subsets of CD4+ T cells induce or protect from chronic intestinal inflammation in C. B-17 scid mice, *Int. Immunol.* **5**, 1461–1471 (1993).

250. F. Powrie, D. Mason, Subsets of rat CD4+ T cells defined by their differential expression of variants of the CD45 antigen: developmental relationships and in vitro and in vivo functions, *Curr. Top. Microbiol. Immunol.* **159**, 79–96 (1990).

251. P. J. Morrissey, K. Charrier, S. Braddy, D. Liggitt, J. D. Watson, CD4+ T cells that express high levels of CD45RB induce wasting disease when transferred into congenic severe combined immunodeficient mice. Disease development is prevented by cotransfer of purified CD4+ T cells, *J Exp Med* **178**, 237–244 (1993).

252. C. L. Bennett *et al.*, The immune dysregulation, polyendocrinopathy, enteropathy, X-linked syndrome (IPEX) is caused by mutations of FOXP3, *Nat. Genet.* **27**, 20–21 (2001).

253. M. E. Brunkow *et al.*, Disruption of a new forkhead/winged-helix protein, scurfin, results in the fatal lymphoproliferative disorder of the scurfy mouse, *Nat. Genet.* **27**, 68–73 (2001).

254. R. S. Wildin *et al.*, X-linked neonatal diabetes mellitus, enteropathy and endocrinopathy syndrome is the human equivalent of mouse scurfy, *Nat. Genet.* **27**, 18–20 (2001).

255. T. A. Chatila *et al.*, JM2, encoding a fork head-related protein, is mutated in X-linked autoimmunity-allergic disregulation syndrome, *J. Clin. Invest.* **106**, R75–81 (2000).

256. C.-W. J. Lio, C.-S. Hsieh, A two-step process for thymic regulatory T cell development, *Immunity* **28**, 100–111 (2008).

257. M. A. Burchill, J. Yang, C. Vogtenhuber, B. R. Blazar, M. A. Farrar, IL-2 receptor beta-dependent STAT5 activation is required for the development of Foxp3+ regulatory T cells, *J Immunol* **178**, 280–290 (2007).

258. J. D. Fontenot, J. P. Rasmussen, M. A. Gavin, A. Y. Rudensky, A function for interleukin 2 in Foxp3-expressing regulatory T cells, *Nat Immunol* **6**, 1142–1151 (2005).

259. M. A. Burchill, J. Yang, K. B. Vang, M. A. Farrar, Interleukin-2 receptor signaling in regulatory T cell development and homeostasis, *Immunol. Lett.* **114**, 1–8 (2007).

260. B. Salomon *et al.*, B7/CD28 costimulation is essential for the homeostasis of the CD4+CD25+ immunoregulatory T cells that control autoimmune diabetes, *Immunity* **12**, 431–440 (2000).

261. K. B. Vang *et al.*, IL-2, -7, and -15, but not thymic stromal lymphopoeitin, redundantly govern CD4+Foxp3+ regulatory T cell development, *The Journal of Immunology* **181**, 3285–3290 (2008).

262. M. Feuerer, J. A. Hill, D. Mathis, C. Benoist, Foxp3+ regulatory T cells: differentiation, specification, subphenotypes, *Nat Immunol* **10**, 689–695 (2009).

263. Y. Y. Wan, R. A. Flavell, Regulatory T-cell functions are subverted and converted owing to attenuated Foxp3 expression, *Nature* (2007).

264. L. M. Williams, A. Y. Rudensky, Maintenance of the Foxp3-dependent developmental program in mature regulatory T cells requires continued expression of Foxp3, *Nat Immunol* **8**, 277–284 (2007).

265. E. M. Shevach, Mechanisms of foxp3+ T regulatory cell-mediated suppression, *Immunity* **30**, 636–645 (2009).

266. C. E. Tadokoro *et al.*, Regulatory T cells inhibit stable contacts between CD4+ T cells and dendritic cells in vivo, *J Exp Med* **203**, 505–511 (2006).

267. Q. Tang *et al.*, Visualizing regulatory T cell control of autoimmune responses in nonobese diabetic mice, *Nat Immunol* **7**, 83–92 (2006).

268. K. Wing *et al.*, CTLA-4 control over Foxp3+ regulatory T cell function, *Science* **322**, 271–275 (2008).

269. X. Yu *et al.*, The surface protein TIGIT suppresses T cell activation by promoting the generation of mature immunoregulatory dendritic cells, *Nat Immunol* **10**, 48–57 (2009).

270. Y. P. Rubtsov *et al.*, Regulatory T cell-derived interleukin-10 limits inflammation at environmental interfaces, *Immunity* **28**, 546–558 (2008).

271. L. W. Collison *et al.*, IL-35-mediated induction of a potent regulatory T cell population, *Nat Immunol* **11**, 1093–1101 (2010).

272. S. Deaglio *et al.*, Adenosine generation catalyzed by CD39 and CD73 expressed on regulatory T cells mediates immune suppression, *J Exp Med* **204**, 1257–1265 (2007).

273. P. Pandiyan, L. Zheng, S. Ishihara, J. Reed, M. J. Lenardo, CD4+CD25+Foxp3+ regulatory T cells induce cytokine deprivation-mediated apoptosis of effector CD4+ T cells, *Nat Immunol* **8**, 1353–1362 (2007).

274. D. Jankovic *et al.*, Conventional T-bet(+)Foxp3(-) Th1 cells are the major source of host-protective regulatory IL-10 during intracellular protozoan infection, *J Exp Med* **204**, 273–283 (2007).

275. C. L. Maynard *et al.*, Regulatory T cells expressing interleukin 10 develop from Foxp3+ and Foxp3- precursor cells in the absence of interleukin 10, *Nat Immunol* **8**, 931–941 (2007).

276. M. C. Kullberg, D. Jankovic, P. L. Gorelick, Bacteria-triggered CD4+ T regulatory cells suppress Helicobacter hepaticus–induced colitis, *The Journal of …* (2002).

277. D. Yu, C. G. Vinuesa, The elusive identity of T follicular helper cells, *Trends in Immunology* (2010).

278. R. Forster, T. Emrich, E. Kremmer, M. Lipp, Expression of the G-protein--coupled receptor BLR1 defines mature, recirculating B cells and a subset of T-helper memory cells, *Blood* (1994).

279. S. Crotty, Follicular Helper CD4 T Cells (Tfh), *Annu. Rev. Immunol.* (2011).

280. P. Schaerli *et al.*, CXC chemokine receptor 5 expression defines follicular homing T cells with B cell helper function, *J Exp Med* **192**, 1553–1562 (2000).

281. D. Breitfeld *et al.*, Follicular B helper T cells express CXC chemokine receptor 5, localize to B cell follicles, and support immunoglobulin production, *J Exp Med* **192**, 1545–1552 (2000).

282. C. H. Kim *et al.*, Subspecialization of CXCR5+ T cells: B helper activity is focused in a germinal center-localized subset of CXCR5+ T cells, *J Exp Med* **193**, 1373–1381 (2001).

283. N. Fazilleau, L. J. Mcheyzer-Williams, H. Rosen, M. G. Mcheyzer-Williams, The function of follicular helper T cells is regulated by the strength of T cell antigen receptor binding, *Nat Immunol* **10**, 375–384 (2009).

284. A. C. Poholek *et al.*, In vivo regulation of Bcl6 and T follicular helper cell development, *The Journal of Immunology* **185**, 313–326 (2010).

285. S. Nakayamada *et al.*, Early Th1 cell differentiation is marked by a Tfh cell-like transition, *Immunity* **35**, 919–931 (2011).

286. J. J. O'shea, W. E. Paul, Mechanisms underlying lineage commitment and plasticity of helper CD4+ T cells, *Science* **327**, 1098–1102 (2010).

287. Z. Chen, C. M. Tato, L. Muul, A. Laurence, J. J. O'shea, Distinct regulation of interleukin-17 in human T helper lymphocytes, *Arthritis Rheum.* **56**, 2936–2946 (2007).

288. N. Hayashi *et al.*, T helper 1 cells stimulated with ovalbumin and IL-18 induce airway hyperresponsiveness and lung fibrosis by IFN-gamma and IL-13 production, *Proc. Natl. Acad. Sci. U.S.A.* **104**, 14765–14770 (2007).

289. M. Löhning *et al.*, Long-lived virus-reactive memory T cells generated from purified cytokine-secreting T helper type 1 and type 2 effectors, *Journal of Experimental Medicine* **205**, 53–61 (2008).

290. M. A. Koch *et al.*, The transcription factor T-bet controls regulatory T cell homeostasis and function during type 1 inflammation, *Nat Immunol* **10**, 595–602 (2009).

291. Y. Wang, M. A. Su, Y. Y. Wan, An essential role of the transcription factor GATA-3 for the function of regulatory T cells, *Immunity* **35**, 337–348 (2011).

292. Y. Zheng *et al.*, Regulatory T-cell suppressor program co-opts transcription factor IRF4 to control T(H)2 responses, *Nature* **458**, 351–356 (2009).

293. Y. Chung *et al.*, Follicular regulatory T cells expressing Foxp3 and Bcl-6 suppress germinal center reactions, *Nat Med* **17**, 983–988 (2011).

294. A. Chaudhry *et al.*, CD4+ Regulatory T Cells Control TH17 Responses in a Stat3-Dependent Manner, *Science* **326**, 986–991 (2009).

295. R. Nurieva, G. J. Martinez, S. Rawal, Y. H. Wang, Follicular regulatory T (Tfr) cells with dual Foxp3 and Bcl6 expression suppress germinal center reactions, *Nature* (2011).

296. X. Zhou *et al.*, Instability of the transcription factor Foxp3 leads to the generation of pathogenic memory T cells in vivo, *Nat Immunol* **10**, 1000–1007 (2009).

297. L. Xu, A. Kitani, I. Fuss, W. Strober, Cutting edge: regulatory T cells induce CD4+CD25-Foxp3- T cells or are self-induced to become Th17 cells in the absence of exogenous TGF-beta, *J Immunol* **178**, 6725–6729 (2007).

298. M. Tsuji *et al.*, Preferential generation of follicular B helper T cells from Foxp3+ T cells in gut Peyer's patches, *Science* **323**, 1488–1492 (2009).

299. G. Wei *et al.*, Global mapping of H3K4me3 and H3K27me3 reveals specificity and plasticity in lineage fate determination of differentiating CD4+ T cells, *Immunity* **30**, 155–167 (2009).

300. Y. K. Lee, R. Mukasa, R. D. Hatton, C. T. Weaver, Developmental plasticity of Th17 and Treg cells, *Curr. Opin. Immunol.* (2009).

301. M. C. Kullberg *et al.*, IL-23 plays a key role in Helicobacter hepaticus-induced T cell-dependent colitis, *J Exp Med* **203**, 2485–2494 (2006).

302. S. Hue *et al.*, Interleukin-23 drives innate and T cell-mediated intestinal inflammation, *J Exp Med* **203**, 2473–2483 (2006).

303. L. Cosmi *et al.*, Human interleukin 17-producing cells originate from a CD161+CD4+ T cell precursor, *Journal of Experimental Medicine* **205**, 1903–1916 (2008).

304. H. Kebir *et al.*, Preferential recruitment of interferon-gamma-expressing TH17 cells in multiple sclerosis, *Ann. Neurol.* **66**, 390–402 (2009).

305. A. N. Hegazy *et al.*, Interferons direct Th2 cell reprogramming to generate a stable GATA-3(+)T-bet(+) cell subset with combined Th2 and Th1 cell functions, *Immunity* **32**, 116–128 (2010).

306. D. Artis, Epithelial-cell recognition of commensal bacteria and maintenance of immune homeostasis in the gut, *Nat. Rev. Immunol.* **8**, 411–420 (2008).

307. A. M. Mowat, Anatomical basis of tolerance and immunity to intestinal antigens, *Nat. Rev. Immunol.* **3**, 331–341 (2003).

308. G. Eberl, Inducible lymphoid tissues in the adult gut: recapitulation of a fetal developmental pathway? *Nat. Rev. Immunol.* **5**, 413–420 (2005).

309. A. J. Macpherson, T. Uhr, Induction of protective IgA by intestinal dendritic cells carrying commensal bacteria, *Science* **303**, 1662–1665 (2004).

310. W. S. Garrett, J. I. Gordon, L. H. Glimcher, Homeostasis and inflammation in the intestine, *Cell* **140**, 859–870 (2010).

311. T. Sato *et al.*, Single Lgr5 stem cells build crypt-villus structures in vitro without a mesenchymal niche, *Nature* **459**, 262–265 (2009).

312. M. E. V. Johansson *et al.*, The inner of the two Muc2 mucin-dependent mucus layers in colon is devoid of bacteria, *Proceedings of the National Academy of Sciences* **105**, 15064–15069 (2008).

313. A. J. Ouellette, Paneth cells and innate mucosal immunity, *Curr. Opin. Gastroenterol.* **26**, 547–553 (2010).

314. S. Vaishnava, C. L. Behrendt, A. S. Ismail, in (2008).

315. L. A. Blackshaw, S. J. H. Brookes, D. Grundy, M. Schemann, Sensory transmission in the gastrointestinal tract, *Neurogastroenterol. Motil.* **19**, 1–19 (2007).

316. J. M. Kyd, A. W. Cripps, Functional differences between M cells and enterocytes in sampling luminal antigens, *Vaccine* **26**, 6221–6224 (2008).

317. C. Pearson, H. H. Uhlig, F. Powrie, Lymphoid microenvironments and innate lymphoid cells in the gut, *Trends in Immunology* **33**, 289–296 (2012).

318. H. Spits, T. Cupedo, Innate Lymphoid Cells: Emerging Insights in Development, Lineage Relationships, and Function, *Annu. Rev. Immunol.* **30**, 647–675 (2012).

319. R. E. Mebius *et al.*, The fetal liver counterpart of adult common lymphoid progenitors gives rise to all lymphoid lineages, CD45+CD4+CD3- cells, as well as macrophages, *J Immunol* **166**, 6593–6601 (2001).

320. H. Yoshida *et al.*, Expression of alpha(4)beta(7) integrin defines a distinct pathway of lymphoid progenitors committed to T cells, fetal intestinal lymphotoxin producer, NK, and dendritic cells, *J Immunol* **167**, 2511–2521 (2001).

321. R. E. Mebius, Organogenesis of lymphoid tissues, *Nat. Rev. Immunol.* **3**, 292–303 (2003).

322. T. Cupedo, N. K. Crellin, N. Papazian, E. J. Rombouts, Human fetal lymphoid tissue–inducer cells are interleukin 17–producing precursors to RORC+ CD127+ natural killer–like cells, *Nature* (2008).

323. S. Schmutz *et al.*, Cutting edge: IL-7 regulates the peripheral pool of adult ROR gamma+ lymphoid tissue inducer cells, *The Journal of Immunology* **183**, 2217–2221 (2009).

324. D. Bouskra *et al.*, Lymphoid tissue genesis induced by commensals through NOD1 regulates intestinal homeostasis, *Nature* **456**, 507–510 (2008).

325. E. Scandella *et al.*, Restoration of lymphoid organ integrity through the interaction of lymphoid tissue-inducer cells with stroma of the T cell zone, *Nat Immunol* **9**, 667–675 (2008).

326. G. Sonnenberg, L. Fouser, Border patrol: regulation of immunity, inflammation and tissue homeostasis at barrier surfaces by IL-22, *Nat Immunol* (2011).

327. M. Tsuji *et al.*, Requirement for lymphoid tissue-inducer cells in isolated follicle formation and T cell-independent immunoglobulin A generation in the gut, *Immunity* **29**, 261–271 (2008).

328. N. Satoh-Takayama *et al.*, IL-7 and IL-15 independently program the differentiation of intestinal CD3-NKp46+ cell subsets from Id2-dependent precursors, *Journal of Experimental Medicine* **207**, 273–280 (2010).

329. M. Cella *et al.*, A human natural killer cell subset provides an innate source of IL-22 for mucosal immunity, *Nature* **457**, 722–725 (2009).

330. C. Luci *et al.*, Influence of the transcription factor RORgammat on the development of NKp46+ cell populations in gut and skin, *Nat Immunol* **10**, 75–82 (2009).

331. S. L. Sanos *et al.*, RORgammat and commensal microflora are required for the differentiation of mucosal interleukin 22-producing NKp46+ cells, *Nat Immunol* **10**, 83–91 (2009).

332. H. Spits, J. P. Di Santo, The expanding family of innate lymphoid cells: regulators and effectors of immunity and tissue remodeling, *Nat Immunol* **12**, 21–27 (2011).

333. S. Buonocore *et al.*, Innate lymphoid cells drive interleukin-23-dependent innate intestinal pathology, *Nature* **464**, 1371–1375 (2010).

334. K. Moro *et al.*, Innate production of T(H)2 cytokines by adipose tissue-associated c-Kit(+)Sca-1(+) lymphoid cells, *Nature* **463**, 540–544 (2010).

335. A. E. Price *et al.*, Systemically dispersed innate IL-13-expressing cells in type 2 immunity, *Proceedings of the National Academy of Sciences* **107**, 11489–11494 (2010).

336. S. A. Saenz *et al.*, IL25 elicits a multipotent progenitor cell population that promotes T(H)2 cytokine responses, *Nature* **464**, 1362–1366 (2010).

337. D. R. Neill *et al.*, Nuocytes represent a new innate effector leukocyte that mediates type-2 immunity, *Nature* **464**, 1367–1370 (2010).

338. D. R. Neill, A. N. J. McKenzie, Nuocytes and beyond: new insights into helminth expulsion, *Trends Parasitol.* **27**, 214–221 (2011).

339. M. Bogunovic *et al.*, Origin of the lamina propria dendritic cell network, *Immunity* **31**, 513–525 (2009).

340. C. Varol, E. Zigmond, S. Jung, Securing the immune tightrope: mononuclear phagocytes in the intestinal lamina propria, *Nat. Rev. Immunol.* (2010).

341. I. Gütgemann, A. M. Fahrer, J. D. Altman, M. M. Davis, Induction of rapid T cell activation and tolerance by systemic presentation of an orally administered antigen, *Immunity* (1998).

342. H. Kobayashi *et al.*, In situ demonstration of dendritic cell migration from rat intestine to mesenteric lymph nodes: relationships to maturation and role of chemokines, *J. Leukoc. Biol.* **75**, 434–442 (2004).

343. O. Schulz *et al.*, Intestinal CD103+, but not CX3CR1+, antigen sampling cells migrate in lymph and serve classical dendritic cell functions, *Journal of Experimental Medicine* **206**, 3101–3114 (2009).

344. J. L. Coombes, F. Powrie, Dendritic cells in intestinal immune regulation, *Nat. Rev. Immunol.* **8**, 435–446 (2008).

345. C.-M. Sun *et al.*, Small intestine lamina propria dendritic cells promote de novo generation of Foxp3 T reg cells via retinoic acid, *J Exp Med* **204**, 1775–1785 (2007).

346. J. L. Coombes *et al.*, A functionally specialized population of mucosal CD103+ DCs induces Foxp3+ regulatory T cells via a TGF-beta and retinoic acid-dependent mechanism, *J Exp Med* **204**, 1757–1764 (2007).

347. U. Hadis *et al.*, Intestinal tolerance requires gut homing and expansion of FoxP3+ regulatory T cells in the lamina propria, *Immunity* **34**, 237–246 (2011).

348. M. Murai, O. Turovskaya, G. Kim, R. Madan, C. L. Karp, Interleukin 10 acts on regulatory T cells to maintain expression of the transcription factor Foxp3 and suppressive function in mice with colitis, *Nature* (2009).

349. R. D. Newberry, W. F. Stenson, R. G. Lorenz, Cyclooxygenase-2-dependent arachidonic acid metabolites are essential modulators of the intestinal immune response to dietary antigen, *Nat Med* **5**, 900–906 (1999).

350. M. Rimoldi, M. Chieppa, V. Salucci, F. Avogadri, Intestinal immune homeostasis is regulated by the crosstalk between epithelial cells and dendritic cells, *Nature* (2005).

351. R. M. Salazar-Gonzalez *et al.*, CCR6-mediated dendritic cell activation of pathogen-specific T cells in Peyer's patches, *Immunity* **24**, 623–632 (2006).

352. T. L. Denning, Y.-C. Wang, S. R. Patel, I. R. Williams, B. Pulendran, Lamina propria macrophages and dendritic cells differentially induce regulatory and interleukin 17-producing T cell responses, *Nat Immunol* **8**, 1086–1094 (2007).

353. K. Atarashi *et al.*, ATP drives lamina propria T(H)17 cell differentiation, *Nature* **455**, 808–812 (2008).

354. S. Laffont, K. R. R. Siddiqui, F. Powrie, Intestinal inflammation abrogates the tolerogenic properties of MLN CD103+ dendritic cells, *Eur. J. Immunol.* **40**, 1877–1883 (2010).

355. M. C. Kullberg *et al.*, Helicobacter hepaticus triggers colitis in specific-pathogen-free interleukin-10 (IL-10)-deficient mice through an IL-12- and gamma interferon-dependent mechanism, *Infection and Immunity* **66**, 5157–5166 (1998).

356. L. Gorelik, R. A. Flavell, Abrogation of TGFβ signaling in T cells leads to spontaneous T cell differentiation and autoimmune disease, *Immunity* (2000).

357. F. Powrie, J. Carlino, M. W. Leach, S. Mauze, R. L. Coffman, A critical role for transforming growth factor-beta but not interleukin 4 in the suppression of T helper type 1-mediated colitis by CD45RB(low) CD4+ T cells, *J Exp Med* **183**, 2669–2674 (1996).

358. K. J. Maloy, F. Powrie, Intestinal homeostasis and its breakdown in inflammatory bowel disease, *Nature* **474**, 298–306 (2011).

359. S. Kitajima, S. Takuma, M. Morimoto, Changes in colonic mucosal permeability in mouse colitis induced with dextran sulfate sodium, *Exp. Anim.* **48**, 137–143 (1999).

360. I. Okayasu *et al.*, A novel method in the induction of reliable experimental acute and chronic ulcerative colitis in mice, *Gastroenterology* **98**, 694–702 (1990).

361. L. A. Dieleman *et al.*, Dextran sulfate sodium-induced colitis occurs in severe combined immunodeficient mice, *Gastroenterology* **107**, 1643–1652 (1994).

362. A. Suzuki *et al.*, CIS3/SOCS3/SSI3 plays a negative regulatory role in STAT3 activation and intestinal inflammation, *J Exp Med* **193**, 471–481 (2001).

363. R. Mundy, F. Girard, A. J. FitzGerald, G. Frankel, Comparison of colonization dynamics and pathology of mice infected with enteropathogenic Escherichia coli, enterohaemorrhagic E. coli and Citrobacter rodentium, *FEMS Microbiol. Lett.* **265**, 126–132 (2006).

364. D. B. Schauer, S. Falkow, Attaching and effacing locus of a Citrobacter freundii biotype that causes transmissible murine colonic hyperplasia, *Infection and Immunity* **61**, 2486–2492 (1993).

365. A. Takahashi *et al.*, Production of beta-defensin-2 by human colonic epithelial cells induced by Salmonella enteritidis flagella filament structural protein, *FEBS Lett.* **508**, 484–488 (2001).

366. T. T. MacDonald, G. Monteleone, Immunity, inflammation, and allergy in the gut, *Science* **307**, 1920–1925 (2005).

367. L. Bry, M. Brigl, M. B. Brenner, CD4+-T-Cell Effector Functions and Costimulatory Requirements Essential for Surviving Mucosal Infection with Citrobacter rodentium, *Infection and Immunity* **74**, 673–681 (2005).

368. C. Maaser *et al.*, Clearance of Citrobacter rodentium requires B cells but not secretory immunoglobulin A (IgA) or IgM antibodies, *Infection and Immunity* **72**, 3315–3324 (2004).

369. S. Sawa *et al.*, RORγt(+) innate lymphoid cells regulate intestinal homeostasis by integrating negative signals from the symbiotic microbiota, *Nat Immunol* (2011), doi:10.1038/ni.2002.

370. A. V. Tumanov *et al.*, Lymphotoxin controls the IL-22 protection pathway in gut innate lymphoid cells during mucosal pathogen challenge, *Cell Host Microbe* **10**, 44–53 (2011).

371. J. Qiu *et al.*, The Aryl Hydrocarbon Receptor Regulates Gut Immunity through Modulation of Innate Lymphoid Cells, *Immunity* **36**, 92–104 (2012).

372. N. Ota *et al.*, IL-22 bridges the lymphotoxin pathway with the maintenance of colonic lymphoid structures during infection with Citrobacter rodentium, *Nat Immunol* **12**, 941–948 (2011).

373. Z. Misulovin, X. W. Yang, W. Yu, N. Heintz, E. Meffre, A rapid method for targeted modification and screening of recombinant bacterial artificial chromosome, *J. Immunol. Methods* **257**, 99–105 (2001).

374. X. W. Yang, P. Model, N. Heintz, Homologous recombination based modification in Escherichia coli and germline transmission in transgenic mice of a bacterial artificial chromosome, *Nat. Biotechnol.* **15**, 859–865 (1997).

375. M. Ji *et al.*, Id2 intrinsically regulates lymphoid and erythroid development via interaction with different target proteins, *Blood* **112**, 1068–1077 (2008).

376. D. Jankovic *et al.*, Schistosome-infected IL-4 receptor knockout (KO) mice, in contrast to IL-4 KO mice, fail to develop granulomatous pathology while maintaining the same lymphokine expression profile, *J Immunol* **163**, 337–342 (1999).

377. S. Kuchen *et al.*, Regulation of microRNA expression and abundance during lymphopoiesis, *Immunity* **32**, 828–839 (2010).

378. C. Trapnell, L. Pachter, S. L. Salzberg, TopHat: discovering splice junctions with RNA-Seq, *Bioinformatics* **25**, 1105–1111 (2009).

379. T. Hirano, K. Ishihara, M. Hibi, Roles of STAT3 in mediating the cell growth, differentiation and survival signals relayed through the IL-6 family of cytokine receptors, *Oncogene* **19**, 2548–2556 (2000).

380. C. Schindler, J. E. Darnell, Transcriptional responses to polypeptide ligands: the JAK-STAT pathway, *Annu. Rev. Biochem.* **64**, 621–651 (1995).

381. Z. Chen *et al.*, Selective regulatory function of Socs3 in the formation of IL-17-secreting T cells, *Proc. Natl. Acad. Sci. U.S.A.* **103**, 8137–8142 (2006).

382. A. Laurence *et al.*, Interleukin-2 signaling via STAT5 constrains T helper 17 cell generation, *Immunity* **26**, 371–381 (2007).

383. A. N. Mathur *et al.*, Stat3 and Stat4 direct development of IL-17-secreting Th cells, *J Immunol* **178**, 4901–4907 (2007).

384. Y. Laouar, T. Welte, X.-Y. Fu, R. A. Flavell, STAT3 is required for Flt3L-dependent dendritic cell differentiation, *Immunity* **19**, 903–912 (2003).

385. J. Heimall, A. Freeman, S. M. Holland, Pathogenesis of hyper IgE syndrome, *Clin Rev Allergy Immunol* **38**, 32–38 (2010).

386. G. D. Leonard *et al.*, Non-Hodgkin“s lymphoma in Job”s syndrome: a case report and literature review, *Leuk. Lymphoma* **45**, 2521–2525 (2004).

387. E.-O. Glocker *et al.*, A homozygous CARD9 mutation in a family with susceptibility to fungal infections, *N Engl J Med* **361**, 1727–1735 (2009).

388. B. Ferwerda *et al.*, Human dectin-1 deficiency and mucocutaneous fungal infections, *N Engl J Med* **361**, 1760–1767 (2009).

389. D. Pociask, T. Reinhart, F. McAllister, J. Edeal, IL-22 mediates mucosal host defense against Gram-negative bacterial pneumonia, *Nat Med* (2008).

390. K. I. Happel *et al.*, Divergent roles of IL-23 and IL-12 in host defense against Klebsiella pneumoniae, *J Exp Med* **202**, 761–769 (2005).

391. H. Jiao *et al.*, Novel and recurrent STAT3 mutations in hyper-IgE syndrome patients from different ethnic groups, *Mol. Immunol.* **46**, 202–206 (2008).

392. H.-J. Kim, J.-H. Kim, Y. K. Shin, S.-I. Lee, K.-M. Ahn, A novel mutation in the linker domain of the signal transducer and activator of transcription 3 gene, p.Lys531Glu, in hyper-IgE syndrome, *J. Allergy Clin. Immunol.* **123**, 956–958 (2009).

393. A. E. Powers *et al.*, Coccidioides immitis meningitis in a patient with hyperimmunoglobulin E syndrome due to a novel mutation in signal transducer and activator of transcription, *Pediatr. Infect. Dis. J.* **28**, 664–666 (2009).

394. L. F. S. MD *et al.*, Diagnostic approach to the hyper-IgE syndromes: Immunologic and clinical key findings to differentiate hyper-IgE syndromes from atopic dermatitis, *Journal of Allergy and Clinical Immunology* **126**, 611–617.e1 (2010).

395. C. W. MSc *et al.*, Mutations in STAT3 and diagnostic guidelines for hyper-IgE syndrome, *Journal of Allergy and Clinical Immunology* **125**, 424–432.e8 (2010).

396. L. Xie, X. Hu, Y. Li, W. Zhang, L. Chen, Hyper-IgE syndrome with STAT3 mutation: a case report in Mainland China, *Clin. Dev. Immunol.* **2010**, 289873 (2010).

397. X. W. Yang, C. Wynder, M. L. Doughty, N. Heintz, BAC-mediated gene-dosage analysis reveals a role for Zipro1 (Ru49/Zfp38) in progenitor cell proliferation in cerebellum and skin, *Nat. Genet.* **22**, 327–335 (1999).

398. Y. Zhang, F. Buchholz, J. P. Muyrers, A. F. Stewart, A new logic for DNA engineering using recombination in Escherichia coli, *Nat. Genet.* **20**, 123–128 (1998).

399. J. P. Muyrers, Y. Zhang, G. Testa, A. F. Stewart, Rapid modification of bacterial artificial chromosomes by ET-recombination, *Nucleic Acids Res.* **27**, 1555–1557 (1999).

400. J. P. Muyrers *et al.*, Point mutation of bacterial artificial chromosomes by ET recombination, *EMBO Rep.* **1**, 239–243 (2000).

401. W. Yu *et al.*, Coordinate regulation of RAG1 and RAG2 by cell type-specific DNA elements 5' of RAG2, *Science* **285**, 1080–1084 (1999).

402. W. Yu *et al.*, Continued RAG expression in late stages of B cell development and no apparent re-induction after immunization, *Nature* **400**, 682–687 (1999).

403. H. Nagaoka, G. Gonzalez-Aseguinolaza, M. Tsuji, M. C. Nussenzweig, Immunization and infection change the number of recombination activating gene (RAG)-expressing B cells in the periphery by altering immature lymphocyte production, *J Exp Med* **191**, 2113–2120 (2000).

404. M. Lalioti, J. Heath, A new method for generating point mutations in bacterial artificial chromosomes by homologous recombination in Escherichia coli, *Nucleic Acids Res.* **29**, E14 (2001).

405. Y. Wang, D. E. Levy, Comparative evolutionary genomics of the STAT family of transcription factors, *JAK-STAT* **1**, 23–33 (2012).

406. R. M. Horton, H. D. Hunt, S. N. Ho, J. K. Pullen, L. R. Pease, Engineering hybrid genes without the use of restriction enzymes: gene splicing by overlap extension, *Gene* **77**, 61–68 (1989).

407. R. M. Horton, Z. L. Cai, S. N. Ho, L. R. Pease, Gene splicing by overlap extension: tailor-made genes using the polymerase chain reaction, *BioTechniques* **8**, 528–535 (1990).

408. M. Takagi *et al.*, Characterization of DNA polymerase from Pyrococcus sp. strain KOD1 and its application to PCR, *Appl. Environ. Microbiol.* **63**, 4504–4510 (1997).

409. B. R. Bochner, H. C. Huang, G. L. Schieven, B. N. Ames, Positive selection for loss of tetracycline resistance, *J. Bacteriol.* **143**, 926–933 (1980).

410. S. R. Maloy, W. D. Nunn, Selection for loss of tetracycline resistance by Escherichia coli, *J. Bacteriol.* **145**, 1110–1111 (1981).

411. K. Osoegawa *et al.*, An improved approach for construction of bacterial artificial chromosome libraries, *Genomics* **52**, 1–8 (1998).

412. C. Zeng *et al.*, Large-Insert BAC/YAC Libraries for Selective Re-isolation of Genomic Regions by Homologous Recombination in Yeast, *Genomics* **77**, 27–34 (2001).

413. R. L. Brinster, H. Y. Chen, M. E. Trumbauer, M. K. Yagle, R. D. Palmiter, Factors affecting the efficiency of introducing foreign DNA into mice by microinjecting eggs, *Proc. Natl. Acad. Sci. U.S.A.* **82**, 4438–4442 (1985).

414. T. Decker, P. Kovarik, Serine phosphorylation of STATs, *Oncogene* **19**, 2628–2637 (2000).

415. R. Yan, S. Small, C. Desplan, C. R. Dearolf, J. E. Darnell, Identification of a Stat gene that functions in Drosophila development, *Cell* **84**, 421–430 (1996).

416. X. S. Hou, M. B. Melnick, N. Perrimon, Marelle acts downstream of the Drosophila HOP/JAK kinase and encodes a protein similar to the mammalian STATs, *Cell* **84**, 411–419 (1996).

417. H. Luo, J. E. Darnell Jr, C. R. Dearolf, in (1996).

418. S. Akira, Roles of STAT3 defined by tissue-specific gene targeting, *Oncogene* **19**, 2607–2611 (2000).

419. T. Nosaka *et al.*, Defective lymphoid development in mice lacking Jak3, *Science* **270**, 800–802 (1995).

420. S. Y. Park *et al.*, Developmental defects of lymphoid cells in Jak3 kinase-deficient mice, *Immunity* **3**, 771–782 (1995).

421. D. C. Thomis, C. B. Gurniak, E. Tivol, A. H. Sharpe, L. J. Berg, Defects in B lymphocyte maturation and T lymphocyte activation in mice lacking Jak3, *Science* **270**, 794–797 (1995).

422. P. Macchi *et al.*, Mutations of Jak-3 gene in patients with autosomal severe combined immune deficiency (SCID), *Nature* **377**, 65–68 (1995).

423. S. M. Russell *et al.*, Mutation of Jak3 in a patient with SCID: essential role of Jak3 in lymphoid development, *Science* **270**, 797–800 (1995).

424. H. Matsuda *et al.*, Development of atopic dermatitis-like skin lesion with IgE hyperproduction in NC/Nga mice, *Int. Immunol.* **9**, 461–466 (1997).

425. N. Charles *et al.*, Lyn kinase controls basophil GATA-3 transcription factor expression and induction of Th2 cell differentiation, *Immunity* **30**, 533–543 (2009).

426. M.-O. Chandesris *et al.*, Autosomal Dominant STAT3 Deficiency and Hyper-IgE Syndrome, *Medicine* **91**, e1–e19 (2012).

427. J. He *et al.*, STAT3 mutations correlated with hyper-IgE syndrome lead to blockage of IL-6/STAT3 signalling pathway, *J Biosci* **37**, 243–257 (2012).

428. N. Heintz, BAC to the future: the use of bac transgenic mice for neuroscience research, *Nature Reviews Neuroscience* **2**, 861–870 (2001).

429. J. Kelly *et al.*, A role for Stat5 in CD8+ T cell homeostasis, *J Immunol* **170**, 210–217 (2003).

430. J. J. O'shea, R. Plenge, JAK and STAT Signaling Molecules in Immunoregulation and Immune-Mediated Disease, *Immunity* **36**, 542–550 (2012).

431. C. Speckmann *et al.*, Reduced memory B cells in patients with hyper IgE syndrome, *Clin. Immunol.* **129**, 448–454 (2008).

432. J. J. Peschon *et al.*, Early lymphocyte expansion is severely impaired in interleukin 7 receptor-deficient mice, *J Exp Med* **180**, 1955–1960 (1994).

433. C. M. Roifman, J. Zhang, D. Chitayat, N. Sharfe, A partial deficiency of interleukin-7R alpha is sufficient to abrogate T-cell development and cause severe combined immunodeficiency, *Blood* **96**, 2803–2807 (2000).

434. W. J. Leonard, Cytokines and immunodeficiency diseases, *Nat. Rev. Immunol.* (2001).

435. X. Liu, Y. S. Lee, C.-R. Yu, C. E. Egwuagu, Loss of STAT3 in CD4+ T cells prevents development of experimental autoimmune diseases, *J Immunol* **180**, 6070–6076 (2008).

436. M. Nishihara *et al.*, IL-6-gp130-STAT3 in T cells directs the development of IL-17+ Th with a minimum effect on that of Treg in the steady state, *Int. Immunol.* **19**, 695–702 (2007).

437. A. Izcue *et al.*, Interleukin-23 restrains regulatory T cell activity to drive T cell-dependent colitis, *Immunity* **28**, 559–570 (2008).

438. C. D. C. Allen, T. Okada, J. G. Cyster, Germinal-center organization and cellular dynamics, *Immunity* **27**, 190–202 (2007).

439. K. L. Good-Jacobson, M. J. Shlomchik, Plasticity and heterogeneity in the generation of memory B cells and long-lived plasma cells: the influence of germinal center interactions and dynamics, *The Journal of Immunology* **185**, 3117–3125 (2010).

440. A. E. Hauser, S. M. Kerfoot, A. M. Haberman, Cellular choreography in the germinal center: new visions from in vivo imaging, *Semin Immunopathol* **32**, 239–255 (2010).

441. C. D. C. Allen, T. Okada, H. L. Tang, J. G. Cyster, Imaging of germinal center selection events during affinity maturation, *Science* **315**, 528–531 (2007).

442. C. S. Ma *et al.*, Functional STAT3 deficiency compromises the generation of human T follicular helper cells, *Blood* **119**, 3997–4008 (2012).

443. J. J. O'shea, R. Lahesmaa, G. Vahedi, A. Laurence, Y. Kanno, Genomic views of STAT function in CD4+ T helper cell differentiation, *Nat. Rev. Immunol.* **11**, 239–250 (2011).

444. X.-P. Yang *et al.*, Opposing regulation of the locus encoding IL-17 through direct, reciprocal actions of STAT3 and STAT5, *Nat Immunol* **12**, 247–254 (2011).

445. T. Korn *et al.*, IL-6 controls Th17 immunity in vivo by inhibiting the conversion of conventional T cells into Foxp3+ regulatory T cells, *Proceedings of the National Academy of Sciences* **105**, 18460–18465 (2008).

446. D. T. Avery *et al.*, STAT3 is required for IL-21-induced secretion of IgE from human naive B cells, *Blood* **112**, 1784–1793 (2008).

447. G. Kraal, Cells in the marginal zone of the spleen, *Int. Rev. Cytol.* **132**, 31–74 (1992).

448. F. Martin, J. F. Kearney, B‐cell subsets and the mature preimmune repertoire. Marginal zone and B1 B cells as part of a “natural immune memory,” *Immunol Rev* (2000).

449. S. Pillai, A. Cariappa, S. T. Moran, Marginal zone B cells, *Annu. Rev. Immunol.* **23**, 161–196 (2005).

450. A. Cariappa *et al.*, Perisinusoidal B cells in the bone marrow participate in T-independent responses to blood-borne microbes, *Immunity* **23**, 397–407 (2005).

451. S. Crotty, R. J. Johnston, S. P. Schoenberger, Effectors and memories: Bcl-6 and Blimp-1 in T and B lymphocyte differentiation, *Nat Immunol* **11**, 114–120 (2010).

452. R. J. Johnston *et al.*, Bcl6 and Blimp-1 are reciprocal and antagonistic regulators of T follicular helper cell differentiation, *Science* **325**, 1006–1010 (2009).

453. D. Yu *et al.*, The transcriptional repressor Bcl-6 directs T follicular helper cell lineage commitment, *Immunity* **31**, 457–468 (2009).

454. M. A. Linterman *et al.*, IL-21 acts directly on B cells to regulate Bcl-6 expression and germinal center responses, *Journal of Experimental Medicine* **207**, 353–363 (2010).

455. H.-C. Hsu *et al.*, Interleukin 17–producing T helper cells and interleukin 17 orchestrate autoreactive germinal center development in autoimmune BXD2 mice, *Nat Immunol* **9**, 166–175 (2007).

456. D. Jankovic, S. Steinfelder, M. C. Kullberg, A. Sher, Mechanisms underlying helminth- induced Th2 polarization: default, negative or positive pathways? *Chem Immunol Allergy* **90**, 65–81 (2006).

457. S. C. Dreskin, P. K. Goldsmith, J. I. Gallin, Immunoglobulins in the hyperimmunoglobulin E and recurrent infection (Job's) syndrome. Deficiency of anti-Staphylococcus aureus immunoglobulin A, *J. Clin. Invest.* **75**, 26–34 (1985).

458. D. Y. Leung, D. M. Ambrosino, R. D. Arbeit, J. L. Newton, R. S. Geha, Impaired antibody responses in the hyperimmunoglobulin E syndrome, *J. Allergy Clin. Immunol.* **81**, 1082–1087 (1988).

459. K. A. Sheerin, R. H. Buckley, Antibody responses to protein, polysaccharide, and phi X174 antigens in the hyperimmunoglobulinemia E (hyper-IgE) syndrome, *J. Allergy Clin. Immunol.* **87**, 803–811 (1991).

460. D. T. Avery *et al.*, B cell-intrinsic signaling through IL-21 receptor and STAT3 is required for establishing long-lived antibody responses in humans, *Journal of Experimental Medicine* **207**, 155–171 (2010).

461. E. Ozcan, L. D. Notarangelo, R. S. Geha, Primary immune deficiencies with aberrant IgE production, *J. Allergy Clin. Immunol.* **122**, 1054–62–quiz 1063–4 (2008).

462. I. M. Katona, J. F. Urban, I. Scher, C. Kanellopoulos-Langevin, F. D. Finkelman, Induction of an IgE response in mice by Nippostrongylus brasiliensis: characterization of lymphoid cells with intracytoplasmic or surface IgE, *J Immunol* **130**, 350–356 (1983).

463. T. Yamada, D. Zhu, A. Saxon, K. Zhang, CD45 controls interleukin-4-mediated IgE class switch recombination in human B cells through its function as a Janus kinase phosphatase, *J. Biol. Chem.* **277**, 28830–28835 (2002).

464. C. C. Chu, W. E. Paul, E. E. Max, Quantitation of immunoglobulin mu-gamma 1 heavy chain switch region recombination by a digestion-circularization polymerase chain reaction method, *Proc. Natl. Acad. Sci. U.S.A.* **89**, 6978–6982 (1992).

465. R. Spolski, W. J. Leonard, Interleukin-21: basic biology and implications for cancer and autoimmunity, *Annu. Rev. Immunol.* **26**, 57–79 (2008).

466. J. P. Manis, M. Tian, F. W. Alt, Mechanism and control of class-switch recombination, *Trends in Immunology* **23**, 31–39 (2002).

467. L. Du *et al.*, Involvement of Artemis in nonhomologous end-joining during immunoglobulin class switch recombination, *Journal of Experimental Medicine* **205**, 3031–3040 (2008).

468. R. Mandler, F. D. Finkelman, A. D. Levine, C. M. Snapper, IL-4 induction of IgE class switching by lipopolysaccharide-activated murine B cells occurs predominantly through sequential switching, *J Immunol* **150**, 407–418 (1993).

469. F. C. Mills, M. P. Mitchell, N. Harindranath, E. E. Max, Human Ig S gamma regions and their participation in sequential switching to IgE, *J Immunol* **155**, 3021–3036 (1995).

470. C. M. Snapper, F. D. Finkelman, D. Stefany, D. H. Conrad, W. E. Paul, IL-4 induces co-expression of intrinsic membrane IgG1 and IgE by murine B cells stimulated with lipopolysaccharide, *J Immunol* **141**, 489–498 (1988).

471. B. Li, M. Carey, J. L. Workman, The role of chromatin during transcription, *Cell* **128**, 707–719 (2007).

472. S. A. Diehl *et al.*, STAT3-mediated up-regulation of BLIMP1 Is coordinated with BCL6 down-regulation to control human plasma cell differentiation, *J Immunol* **180**, 4805–4815 (2008).

473. R. Reljic, S. D. Wagner, L. J. Peakman, D. T. Fearon, Suppression of Signal Transducer and Activator of Transcription 3-Dependent B Lymphocyte Terminal Differentiation by Bcl-6, *Journal of Experimental Medicine* **192**, 1841–1848 (2000).

474. S. Delphin, J. Stavnezer, Characterization of an interleukin 4 (IL-4) responsive region in the immunoglobulin heavy chain germline epsilon promoter: regulation by NF-IL-4, a C/EBP family member and NF-kappa B/p50, *J Exp Med* **181**, 181–192 (1995).

475. L. A. Linehan, W. D. Warren, P. A. Thompson, M. J. Grusby, M. T. Berton, STAT6 is required for IL-4-induced germline Ig gene transcription and switch recombination, *J Immunol* **161**, 302–310 (1998).

476. L. Wei *et al.*, Discrete roles of STAT4 and STAT6 transcription factors in tuning epigenetic modifications and transcription during T helper cell differentiation, *Immunity* **32**, 840–851 (2010).

477. T. Decker, P. Kovarik, A. Meinke, GAS elements: a few nucleotides with a major impact on cytokine-induced gene expression, *J. Interferon Cytokine Res.* **17**, 121–134 (1997).

478. M. Sugai *et al.*, Essential role of Id2 in negative regulation of IgE class switching, *Nat Immunol* **4**, 25–30 (2003).

479. W. J. Leonard, R. Spolski, Interleukin-21: a modulator of lymphoid proliferation, apoptosis and differentiation, *Nat. Rev. Immunol.* **5**, 688–698 (2005).

480. A. Visel *et al.*, ChIP-seq accurately predicts tissue-specific activity of enhancers, *Nature* **457**, 854–858 (2009).

481. N. D. Heintzman *et al.*, Histone modifications at human enhancers reflect global cell-type-specific gene expression, *Nature* **459**, 108–112 (2009).

482. T.-K. Kim *et al.*, Widespread transcription at neuronal activity-regulated enhancers, *Nature* **465**, 182–187 (2010).

483. H. Gonda *et al.*, The balance between Pax5 and Id2 activities is the key to AID gene expression, *J Exp Med* **198**, 1427–1437 (2003).

484. A. M. Siegel *et al.*, A Critical Role for STAT3 Transcription Factor Signaling in the Development and Maintenance of Human T Cell Memory, *Immunity* **35**, 806–818 (2011).

485. M. Schmidt-Supprian, K. Rajewsky, Vagaries of conditional gene targeting, *Nat Immunol* **8**, 665–668 (2007).

486. H. Elsaesser, K. Sauer, D. G. Brooks, IL-21 is required to control chronic viral infection, *Science* **324**, 1569–1572 (2009).

487. A. Fröhlich *et al.*, IL-21R on T cells is critical for sustained functionality and control of chronic viral infection, *Science* **324**, 1576–1580 (2009).

488. J. S. Yi, M. Du, A. J. Zajac, A vital role for interleukin-21 in the control of a chronic viral infection, *Science* **324**, 1572–1576 (2009).

489. K. E. Foulds, M. J. Rotte, R. A. Seder, IL-10 is required for optimal CD8 T cell memory following Listeria monocytogenes infection, *J Immunol* **177**, 2565–2574 (2006).

490. S. G. Tangye, D. M. Tarlinton, Memory B cells: effectors of long-lived immune responses, *Eur. J. Immunol.* **39**, 2065–2075 (2009).

491. B. W. Baron *et al.*, Identification of the gene associated with the recurring chromosomal translocations t(3;14)(q27;q32) and t(3;22)(q27;q11) in B-cell lymphomas, *Proc. Natl. Acad. Sci. U.S.A.* **90**, 5262–5266 (1993).

492. J. P. Kerckaert *et al.*, LAZ3, a novel zinc-finger encoding gene, is disrupted by recurring chromosome 3q27 translocations in human lymphomas, *Nat. Genet.* **5**, 66–70 (1993).

493. B. H. Ye, P. H. Rao, R. S. Chaganti, R. Dalla-Favera, Cloning of bcl-6, the locus involved in chromosome translocations affecting band 3q27 in B-cell lymphoma, *Cancer research* (1993).

494. B. A. Croker, D. L. Krebs, J. G. Zhang, S. Wormald, SOCS3 negatively regulates IL-6 signaling in vivo, *Nature* (2003).

495. Z. Yao *et al.*, Nonredundant roles for Stat5a/b in directly regulating Foxp3, *Blood* **109**, 4368–4375 (2007).

496. M. W. Quong, W. J. Romanow, C. Murre, E protein function in lymphocyte development, *Annu. Rev. Immunol.* **20**, 301–322 (2002).

497. Y. C. Lin *et al.*, A global network of transcription factors, involving E2A, EBF1 and Foxo1, that orchestrates B cell fate, *Nat Immunol* **11**, 635–643 (2010).

498. B. Grimbacher, B. H. Belohradsky, S. M. Holland, Immunoglobulin E in primary immunodeficiency diseases, *Allergy* (2002).

499. R. S. Geha, H. H. Jabara, S. R. Brodeur, The regulation of immunoglobulin E class-switch recombination, *Nature Reviews …* (2003).

500. R. Atreya *et al.*, Blockade of interleukin 6 trans signaling suppresses T-cell resistance against apoptosis in chronic intestinal inflammation: evidence in crohn disease and experimental colitis in vivo, *Nat Med* **6**, 583–588 (2000).

501. P. P. Ahern, A. Izcue, K. J. Maloy, F. Powrie, The interleukin-23 axis in intestinal inflammation, *Immunol Rev* **226**, 147–159 (2008).

502. C. O. Elson *et al.*, Monoclonal anti-interleukin 23 reverses active colitis in a T cell-mediated model in mice, *Gastroenterology* **132**, 2359–2370 (2007).

503. D. Noguchi *et al.*, Blocking of IL-6 signaling pathway prevents CD4+ T cell-mediated colitis in a T(h)17-independent manner, *Int. Immunol.* **19**, 1431–1440 (2007).

504. J. C. Barrett *et al.*, Genome-wide association defines more than 30 distinct susceptibility loci for Crohn's disease, *Nat. Genet.* **40**, 955–962 (2008).

505. D. P. B. McGovern *et al.*, Genome-wide association identifies multiple ulcerative colitis susceptibility loci, *Nat. Genet.* **42**, 332–337 (2010).

506. A. Musso *et al.*, Signal transducers and activators of transcription 3 signaling pathway: an essential mediator of inflammatory bowel disease and other forms of intestinal inflammation, *Inflamm Bowel Dis* **11**, 91–98 (2005).

507. D. Borenshtein, M. E. McBee, D. B. Schauer, Utility of the Citrobacter rodentium infection model in laboratory mice, *Curr. Opin. Gastroenterol.* **24**, 32–37 (2008).

508. R. Mundy, T. T. MacDonald, G. Dougan, G. Frankel, S. Wiles, Citrobacter rodentium of mice and man, *Cell. Microbiol.* **7**, 1697–1706 (2005).

509. Y. Zheng *et al.*, Interleukin-22 mediates early host defense against attaching and effacing bacterial pathogens, *Nat Med* **14**, 282–289 (2008).

510. C. P. Simmons *et al.*, Impaired resistance and enhanced pathology during infection with a noninvasive, attaching-effacing enteric bacterial pathogen, Citrobacter rodentium, in mice lacking IL-12 or IFN-gamma, *J Immunol* **168**, 1804–1812 (2002).

511. G. F. Sonnenberg, L. A. Monticelli, M. M. Elloso, L. A. Fouser, D. Artis, CD4(+) lymphoid tissue-inducer cells promote innate immunity in the gut, *Immunity* **34**, 122–134 (2011).

512. N. Satoh-Takayama *et al.*, Microbial Flora Drives Interleukin 22 Production in Intestinal NKp46+ Cells that Provide Innate Mucosal Immune Defense, *Immunity* **29**, 958–970 (2008).

513. N. Satoh-Takayama *et al.*, The natural cytotoxicity receptor NKp46 is dispensable for IL-22-mediated innate intestinal immune defense against Citrobacter rodentium, *The Journal of Immunology* **183**, 6579–6587 (2009).

514. M. Zhang *et al.*, Defining the in vivo function of Siglec-F, a CD33-related Siglec expressed on mouse eosinophils, *Blood* **109**, 4280–4287 (2007).

515. H. Tateno, P. R. Crocker, J. C. Paulson, Mouse Siglec-F and human Siglec-8 are functionally convergent paralogs that are selectively expressed on eosinophils and recognize 6'-sulfo-sialyl Lewis X as a preferred glycan ligand, *Glycobiology* **15**, 1125–1135 (2005).

516. H. Aizawa *et al.*, Molecular analysis of human Siglec-8 orthologs relevant to mouse eosinophils: identification of mouse orthologs of Siglec-5 (mSiglec-F) and Siglec-10 (mSiglec-G), *Genomics* **82**, 521–530 (2003).

517. T. Hakala, J. P. Mecklin, M. Forss, H. Järvinen, P. Lehtovirta, Endometrial carcinoma in the cancer family syndrome, *Cancer* **68**, 1656–1659 (1991).

518. G. Marra, C. R. Boland, Hereditary nonpolyposis colorectal cancer: the syndrome, the genes, and historical perspectives, *J. Natl. Cancer Inst.* **87**, 1114–1125 (1995).

519. M. Aarnio, J. P. Mecklin, L. A. Aaltonen, M. Nyström-Lahti, H. J. Järvinen, Life-time risk of different cancers in hereditary non-polyposis colorectal cancer (HNPCC) syndrome, *Int. J. Cancer* **64**, 430–433 (1995).

520. H. Ishigame *et al.*, Differential roles of interleukin-17A and -17F in host defense against mucoepithelial bacterial infection and allergic responses, *Immunity* **30**, 108–119 (2009).

521. M. El-Behi *et al.*, The encephalitogenicity of T(H)17 cells is dependent on IL-1- and IL-23-induced production of the cytokine GM-CSF, *Nat Immunol* **12**, 568–575 (2011).

522. L. Codarri *et al.*, RORγt drives production of the cytokine GM-CSF in helper T cells, which is essential for the effector phase of autoimmune neuroinflammation, *Nat Immunol* **12**, 560–567 (2011).

523. N. S. Gonçalves *et al.*, Critical role for tumor necrosis factor alpha in controlling the number of lumenal pathogenic bacteria and immunopathology in infectious colitis, *Infection and Immunity* **69**, 6651–6659 (2001).

524. Y. Hirata, L. Egea, S. M. Dann, L. Eckmann, M. F. Kagnoff, GM-CSF-facilitated dendritic cell recruitment and survival govern the intestinal mucosal response to a mouse enteric bacterial pathogen, *Cell Host Microbe* **7**, 151–163 (2010).

525. P. R. Mangan *et al.*, Transforming growth factor-beta induces development of the T(H)17 lineage, *Nature* **441**, 231–234 (2006).

526. C. P. Simmons *et al.*, Central Role for B Lymphocytes and CD4+ T Cells in Immunity to Infection by the Attaching and Effacing Pathogen Citrobacter rodentium, *Infection and Immunity* **71**, 5077–5086 (2003).

527. H. Pan, F. Hong, S. Radaeva, B. Gao, Hydrodynamic gene delivery of interleukin-22 protects the mouse liver from concanavalin A-, carbon tetrachloride-, and Fas ligand-induced injury via activation of STAT3, *Cell. Mol. Immunol.* **1**, 43–49 (2004).

528. K. Wolk *et al.*, IL-22 regulates the expression of genes responsible for antimicrobial defense, cellular differentiation, and mobility in keratinocytes: a potential role in psoriasis, *Eur. J. Immunol.* **36**, 1309–1323 (2006).

529. S. M. Sa *et al.*, The effects of IL-20 subfamily cytokines on reconstituted human epidermis suggest potential roles in cutaneous innate defense and pathogenic adaptive immunity in psoriasis, *J Immunol* **178**, 2229–2240 (2007).

530. Y. Zheng *et al.*, Interleukin-22, a T(H)17 cytokine, mediates IL-23-induced dermal inflammation and acanthosis, *Nature* **445**, 648–651 (2007).

531. X. Song *et al.*, IL-17RE is the functional receptor for IL-17C and mediates mucosal immunity to infection with intestinal pathogens, *Nat Immunol* **12**, 1151–1158 (2011).

532. V. Ramirez-Carrozzi *et al.*, IL-17C regulates the innate immune function of epithelial cells in an autocrine manner, *Nat Immunol* **12**, 1159–1166 (2011).

533. J. Bollrath *et al.*, gp130-Mediated Stat3 Activation in Enterocytes Regulates Cell Survival and Cell-Cycle Progression during Colitis-Associated Tumorigenesis, *Cancer Cell* **15**, 91–102 (2009).

534. S. Grivennikov *et al.*, IL-6 and Stat3 Are Required for Survival of Intestinal Epithelial Cells and Development of Colitis-Associated Cancer, *Cancer Cell* **15**, 103–113 (2009).

535. J.-L. Mege, S. Meghari, A. Honstettre, C. Capo, D. Raoult, The two faces of interleukin 10 in human infectious diseases, *Lancet Infect Dis* **6**, 557–569 (2006).

536. C. M. Filippi, M. G. von Herrath, IL-10 and the resolution of infections, *J. Pathol.* **214**, 224–230 (2008).

537. C. Bogdan, Y. Vodovotz, C. Nathan, Macrophage deactivation by interleukin 10, *J Exp Med* **174**, 1549–1555 (1991).

538. C. Bogdan, J. Paik, Y. Vodovotz, C. Nathan, Contrasting mechanisms for suppression of macrophage cytokine release by transforming growth factor-beta and interleukin-10, *J. Biol. Chem.* **267**, 23301–23308 (1992).

539. D. F. Fiorentino *et al.*, IL-10 acts on the antigen-presenting cell to inhibit cytokine production by Th1 cells, *J Immunol* **146**, 3444–3451 (1991).

540. R. Lang, D. Patel, J. J. Morris, R. L. Rutschman, P. J. Murray, Shaping gene expression in activated and resting primary macrophages by IL-10, *J Immunol* **169**, 2253–2263 (2002).

541. P. Durez *et al.*, In vivo induction of interleukin 10 by anti-CD3 monoclonal antibody or bacterial lipopolysaccharide: differential modulation by cyclosporin A, *J Exp Med* **177**, 551–555 (1993).

542. A. Marchant *et al.*, Interleukin-10 controls interferon-gamma and tumor necrosis factor production during experimental endotoxemia, *Eur. J. Immunol.* **24**, 1167–1171 (1994).

543. M. Howard, T. Muchamuel, S. Andrade, S. Menon, Interleukin 10 protects mice from lethal endotoxemia, *J Exp Med* **177**, 1205–1208 (1993).

544. C. Gérard *et al.*, Interleukin 10 reduces the release of tumor necrosis factor and prevents lethality in experimental endotoxemia, *J Exp Med* **177**, 547–550 (1993).

545. D. J. Berg *et al.*, Interleukin-10 is a central regulator of the response to LPS in murine models of endotoxic shock and the Shwartzman reaction but not endotoxin tolerance, *J. Clin. Invest.* **96**, 2339–2347 (1995).

546. M. D. Boos, Y. Yokota, G. Eberl, B. L. Kee, Mature natural killer cell and lymphoid tissue-inducing cell development requires Id2-mediated suppression of E protein activity, *J Exp Med* **204**, 1119–1130 (2007).

547. Y. Yokota *et al.*, Development of peripheral lymphoid organs and natural killer cells depends on the helix-loop-helix inhibitor Id2, *Nature* **397**, 702–706 (1999).

548. W. Ouyang, J. K. Kolls, Y. Zheng, The biological functions of T helper 17 cell effector cytokines in inflammation, *Immunity* **28**, 454–467 (2008).

549. M. Colonna, Interleukin-22-producing natural killer cells and lymphoid tissue inducer-like cells in mucosal immunity, *Immunity* **31**, 15–23 (2009).

550. H. Takatori *et al.*, Lymphoid tissue inducer-like cells are an innate source of IL-17 and IL-22, *Journal of Experimental Medicine* **206**, 35–41 (2009).

551. T. Cupedo *et al.*, Human fetal lymphoid tissue-inducer cells are interleukin 17-producing precursors to RORC+ CD127+ natural killer-like cells, *Nat Immunol* **10**, 66–74 (2009).

552. Y. Hu *et al.*, IL-17RC is required for IL-17A- and IL-17F-dependent signaling and the pathogenesis of experimental autoimmune encephalomyelitis, *The Journal of Immunology* **184**, 4307–4316 (2010).

553. H. R. Conti *et al.*, New mechanism of oral immunity to mucosal candidiasis in hyper-IgE syndrome, *Mucosal Immunology* **4**, 448–455 (2011).

554. A. Izcue, J. L. Coombes, F. Powrie, Regulatory lymphocytes and intestinal inflammation, *Annu. Rev. Immunol.* **27**, 313–338 (2009).

555. M. Saito *et al.*, Defective IL-10 signaling in hyper-IgE syndrome results in impaired generation of tolerogenic dendritic cells and induced regulatory T cells, *Journal of Experimental Medicine*, 1–15 (2011).

556. T. R. Hawn *et al.*, Hyper-IgE syndrome is not associated with defects in several candidate toll-like receptor pathway genes, *Hum. Immunol.* **66**, 842–847 (2005).

557. M. Yeganeh *et al.*, Toll-like receptor stimulation induces higher TNF-alpha secretion in peripheral blood mononuclear cells from patients with hyper IgE syndrome, *Int. Arch. Allergy Immunol.* **146**, 190–194 (2008).

558. B. Grimbacher *et al.*, Hyper-IgE syndrome with recurrent infections--an autosomal dominant multisystem disorder, *N Engl J Med* **340**, 692–702 (1999).

559. J. E. Darnell, STATs and gene regulation, *Science* **277**, 1630–1635 (1997).

560. M. Chatterjee-Kishore, F. van Den Akker, G. R. Stark, Adenovirus E1A down-regulates LMP2 transcription by interfering with the binding of stat1 to IRF1, *J. Biol. Chem.* **275**, 20406–20411 (2000).

561. M. Chatterjee-Kishore, R. Kishore, D. J. Hicklin, F. M. Marincola, S. Ferrone, Different requirements for signal transducer and activator of transcription 1alpha and interferon regulatory factor 1 in the regulation of low molecular mass polypeptide 2 and transporter associated with antigen processing 1 gene expression, *J. Biol. Chem.* **273**, 16177–16183 (1998).

562. J. Yang *et al.*, Unphosphorylated STAT3 accumulates in response to IL-6 and activates transcription by binding to NFkappaB, *Genes Dev.* **21**, 1396–1408 (2007).

563. X. Cui *et al.*, Unphosphorylated STAT6 contributes to constitutive cyclooxygenase-2 expression in human non-small cell lung cancer, *Oncogene* **26**, 4253–4260 (2007).

564. J. Yang, G. R. Stark, Roles of unphosphorylated STATs in signaling, *Cell Res.* **18**, 443–451 (2008).

565. J. Heimall *et al.*, Paucity of genotype-phenotype correlations in STAT3 mutation positive Hyper IgE Syndrome (HIES), *Clin. Immunol.* **139**, 75–84 (2011).

566. S. R. Walker *et al.*, Reciprocal effects of STAT5 and STAT3 in breast cancer, *Mol. Cancer Res.* **7**, 966–976 (2009).

567. E. Iavnilovitch, B. Groner, I. Barash, Overexpression and forced activation of stat5 in mammary gland of transgenic mice promotes cellular proliferation, enhances differentiation, and delays postlactational apoptosis, *Mol. Cancer Res.* **1**, 32–47 (2002).

568. B. B. Cazac, J. Roes, TGF-beta receptor controls B cell responsiveness and induction of IgA in vivo, *Immunity* **13**, 443–451 (2000).

569. Z. Xu, H. Zan, E. J. Pone, T. Mai, P. Casali, Immunoglobulin class-switch DNA recombination: induction, targeting and beyond, *Nat. Rev. Immunol.* **12**, 517–531 (2012).

570. K. Ozaki *et al.*, Regulation of B cell differentiation and plasma cell generation by IL-21, a novel inducer of Blimp-1 and Bcl-6, *J Immunol* **173**, 5361–5371 (2004).

571. R. Ettinger *et al.*, IL-21 induces differentiation of human naive and memory B cells into antibody-secreting plasma cells, *J Immunol* **175**, 7867–7879 (2005).

572. S. Kuchen *et al.*, Essential role of IL-21 in B cell activation, expansion, and plasma cell generation during CD4+ T cell-B cell collaboration, *J Immunol* **179**, 5886–5896 (2007).

573. I. L. King, K. Mohrs, M. Mohrs, A nonredundant role for IL-21 receptor signaling in plasma cell differentiation and protective type 2 immunity against gastrointestinal helminth infection, *The Journal of Immunology* **185**, 6138–6145 (2010).

574. D. Zotos *et al.*, IL-21 regulates germinal center B cell differentiation and proliferation through a B cell-intrinsic mechanism, *Journal of Experimental Medicine* **207**, 365–378 (2010).

575. X. O. Yang *et al.*, T helper 17 lineage differentiation is programmed by orphan nuclear receptors ROR alpha and ROR gamma, *Immunity* **28**, 29–39 (2008).

576. N. S. Wang *et al.*, Divergent transcriptional programming of class specific B cell memory by T-bet and RORα, *Nat Immunol* **13**, 604–611 (2012).

577. C. Hacker *et al.*, Transcriptional profiling identifies Id2 function in dendritic cell development, *Nat Immunol* **4**, 380–386 (2003).

578. Y. Cao *et al.*, TGF-beta repression of Id2 induces apoptosis in gut epithelial cells, *Oncogene* **28**, 1089–1098 (2009).

579. S. C. Bischoff *et al.*, Quantitative assessment of intestinal eosinophils and mast cells in inflammatory bowel disease, *Histopathology* **28**, 1–13 (1996).

580. A. T. P. Carvalho *et al.*, Immunohistochemical study of intestinal eosinophils in inflammatory bowel disease, *J. Clin. Gastroenterol.* **36**, 120–125 (2003).

581. S. Dubucquoi *et al.*, Activated eosinophils and interleukin 5 expression in early recurrence of Crohn's disease, *Gut* **37**, 242–246 (1995).

582. L. Stevceva *et al.*, Eosinophilia is attenuated in experimental colitis induced in IL-5 deficient mice, *Genes Immun.* **1**, 213–218 (2000).

583. R. T. Gazzinelli *et al.*, … IL-10, mice acutely infected with Toxoplasma gondii succumb to a lethal immune response dependent on CD4+ T cells and accompanied by overproduction of IL-12, …, (1996).

584. G. Trinchieri, Interleukin-12 and the regulation of innate resistance and adaptive immunity, *Nat. Rev. Immunol.* **3**, 133–146 (2003).

585. S. Vaishnava *et al.*, The Antibacterial Lectin RegIII{gamma} Promotes the Spatial Segregation of Microbiota and Host in the Intestine, *Science Signaling* **334**, 255–183 (2011).

586. C. L. Roark *et al.*, Exacerbation of collagen-induced arthritis by oligoclonal, IL-17-producing gamma delta T cells, *J Immunol* **179**, 5576 5583 (2007).

587. Y. Ito *et al.*, Gamma/delta T cells are the predominant source of interleukin-17 in affected joints in collagen-induced arthritis, but not in rheumatoid arthritis, *Arthritis Rheum.* **60**, 2294–2303 (2009).

588. E. Lockhart, A. M. Green, J. L. Flynn, IL-17 production is dominated by gammadelta T cells rather than CD4 T cells during Mycobacterium tuberculosis infection, *J Immunol* **177**, 4662–4669 (2006).

589. K. D. C. Jensen *et al.*, Thymic selection determines gammadelta T cell effector fate: antigen-naive cells make interleukin-17 and antigen experienced cells make interferon gamma, *Immunity* **29**, 90–100 (2008).

590. M.L. Michel *et al.*, Identification of an IL-17-producing NK1.1(neg) iNKT cell population involved in airway neutrophilia, *J Exp Med* **204**, 995–1001 (2007).

591. S. T. Passos *et al.*, IL-6 promotes NK cell production of IL-17 during toxoplasmosis, *The Journal of Immunology* **184**, 1776–1783 (2010).